UNIVERSITY OF
BIRMINGHAM

COMBUSTION AND EMISSIONS OF AN AUTOMOTIVE DIESEL ENGINE USING BIODIESEL FUELS UNDER STEADY AND START CONDITIONS

by

DAI LIU

A thesis submitted to
The University of Birmingham
for the degree of
DOCTOR OF PHILOSOPHY

October 2014
School of Mechanical Engineering
The University of Birmingham

ABSTRACT

Biodiesels are promising alternative fuels and have been proved to reduce the smoke and THC emissions by many researchers. They can help to reduce the greenhouse gas (CO_2) in atmosphere since they are derived from vegetable oil or animal fat. The demands of biodiesel are increasing all over the world due to the concerning of running out of the crude oil. In Europe, biodiesel has already been blended in conventional diesel with 5.75% by volume selling in petrol stations. It is believed that this blend ratio will be increased due to more stringent emission regulation. Various feedstocks of biodiesel have been used in different countries and regions, determined by the local economy, climate and other reasons. The blend ratio of biodiesel in petrol station is also varies depending on the local government. Therefore, more calibration works have been done for the car manufacturers doing global business. In first part this research, the combustion characteristics and emissions of using biodiesels from different feedstocks with different blend ratio was studied by experimental works. Statistical analysis provided a way to find out the correlation between emissions and fuel properties. Then, a smoke index, containing Reynolds Number of fuel spray, cetane number and gross heat value of combustion, was created and showed a significant linear relationship with the smoke emissions. The effects of engine loads and EGR rates on the relationship were also discussed and modelled by Matlab fitting tools. The second part of this research was focused on the cold start with using biodiesel blends. The tests were conducted in a wide range of the temperatures (from -20°C to 90°C). Results showed that the methyl ester biodiesel reduced the PM during the acceleration period of the start while increased the PM during idle period at 20°C conditions. However, when the engine coolant was increased to 90°C before start, using of biodiesel decreased the PM and THC all the time. As ambient temperature decreased to

minus degree, using of biodiesel shows an increased emissions of PM and THC, which might due to the incomplete combustion caused by the increased viscosity at low temperature. The chemical compositions of particle emissions with using biodiesel blends at cold start were identified by a 2D-GC/MS and the results also confirmed this trend. Although the emissions of Polycyclic Aromatic Hydrocarbon (PAH) were decreased by using biodiesel blend, huge amount of n-alkanes were emitted due to large portion of incomplete combustion of biodiesel at -7°C condition.

LIST of ABBREVIATIONS

AC	Alternating Current
AFR	Air Fuel Ratio
BMEP	Brake Mean Effective Pressure
BSFC	Brake Specific Fuel Consumption
CAD	Crank Angle Degree
CI	Compression Ignition
CLD	Chemi-luminescence detection
CO	Carbon Monoxide
CO_2	Carbon Dioxide
COV	Coefficient of Variance
DOC	Diesel Oxidation Catalyst
ECU	Electric Control Unit
EGR	Exhaust Gas Recirculation
FA	Fatty Acid
FAME	Fatty Acid Methyl Ester
FID	Flame Ionization Detector
FSN	Filtered Smoke Number
FTP75	Federal Test Procedure
GC	Gas Chromatograph
GHV	Gross Heat Value
HC	Hydrocarbon
HEV	Hybrid Electric Vehicle
HVO	Hydrogenated Vegetable Oil
JME	Jatropha Methyl Ester
MFB	Mass Fraction Burn
NEDC	New European Drive Cycle
NIST	National Institute of Standards and Technology
NO	Nitric Oxide
NO_x	Nitrogen Dioxide

NVOF	Non-volatile Organic Fraction
PAH	Polycyclic Aromatic Hydrocarbons
PM	Particulate Matter
RME	Rapeseed Oil Methyl Ester
RoHR	Rate of Heat Release
RPM	Round Per Minute
RV	Reference Value
SI	Spark Ignition
SME	Soybean Oil Methyl Ester
SOC	Start of Combustion
SOF	Soluble Organic Fraction
SOI	Start of Injection
SVOC	Semi-Volatile Organic Carbon
TESD	Thermal Energy Storage Device
TME	Tallow Methyl Ester
TOFMS	Fast time-of-flight mass spectrometers
UVOME	Used Vegetable Oil Methyl Ester
VGT	Variable Geometric Turbocharger

ACKNOWLEDGEMENT

I would like to give my great thanks to my supervisor Professor Hongming Xu for his guidance and encouragement throughout my study. I thank my co-supervisor Dr. Karl Dearn, as well as Professor Akbar Ghafourian for their helpful suggestions.

I acknowledge the support of theEuropean Regional Development Fund and Advantage West Midlandfor the test facilities.

I would also like to express my appreciation to the industrial partners, Jaguar/Land Rover and Shell, for their support in progress of SERVE (Flex-diesel Engines with Sustainable Bio-fuels for Clean and Efficient On- and Off- Road vehicle Engines) project and other projects. Special thanks to Thomas Gardiner from JLR and David Korinec from AVL for their technical and facility support.

I appreciate the help in 2D-GCMS from Dr Mohammed Salim Alam in School of Environmental Science at the University of Birmingham.

I am also grateful to Dr Nik Rosli Abdullah, Dr Yanfei Li, Dr Xiao Ma, Dr He Ma, Dr Fan Zhang, Dr Arumugam Sakunthalai Ramadhas for their generous help and support.

Special thanks should give to my friends and colleagues at the University of Birmingham: Thomas Lattimore, Chongming Wang, Changzhao Jiang, Wentao Wang, JianYi Tian, Cheng Tan, Haichun Ding and Ziman Wang for their great support in my studying and living.

Finally, I would like to express my sincere gratitude to my parents for their unconditional support and encouragement.

TABLE OF CONTENTS

LIST OF FIGURES

LIST OF TABLES

LIST OF PUBLICATIONS

1. **Liu, D.**, Ghafourian, A., and Xu, H., "Phenomenology of EGR in a Light Duty Diesel Engine Fuelled with Hydrogenated Vegetable Oil (HVO), Used Vegetable Oil Methyl Ester (UVOME) and Their Blends," SAE Technical Paper 2013-01-1688, 2013, doi:10.4271/2013-01-1688.
2. **Liu, D.**, Xu, H., Tian, J., Tan, C. et al., "Cold and Warm Start Characteristics using HVO and RME Blends in a V6 Diesel Engine," *SAE Int. J. Fuels Lubr.* 6(2):478-485, 2013, doi:10.4271/2013-01-1306.
3. **Liu, D.**, Xu, H. and Sakunthalai, R.A., "Effects of Biodiesel Feedstock on the Emissions from a Modern Light Duty Engine," SAE Technical Paper 2014-01-1394, 2014.
4. Sakunthalai, R.A., Xu, H., **Liu, D.** and Tian, J., "Cold Start of Diesel Engines and its Control Strategies" International Journal of Green Energy, accepted at Feb, 2014.
5. Tan, C., Xu, H., Shuai, S., Ghafourian, A., **Liu D.** and Tian, J., "Investigation on Transient Emissions of a Turbocharged Diesel Engine Fuelled by HVO Blends," *SAE Int. J. Engines* 6(2):1046-1058, 2013, doi:10.4271/2013-01-1307.
6. Tian, J., Xu, H., Ghafourian, A., **Liu, D.** et al., "Transient Emissions Characteristics of a Turbocharged Engine Fuelled by Biodiesel Blends," *SAE Int. J. Fuels Lubr.* 6(2):457-465, 2013, doi:10.4271/2013-01-1302.
7. **Liu, D.**, Xu, H. Sakunthalai, R.A. and Tian, J., "Investigation on the performance of a diesel oxidation catalyst during cold start and warm start at low temperature conditions," SAE 2014 International Powertrain, Fuels & Lubricants Meeting, 2014-01-2712.
8. Sakunthalai, R.A., Xu, H., **Liu, D.** and Tian, J., "Impact of cold ambient conditions on cold start and idle emissions from diesel engines," SAE 2014 International Powertrain, Fuels & Lubricants Meeting, 2014-01-2715.
9. Tian, J., Xu, H., Ghafourian, A., **Liu, D.** and Tan, C., "Low temperature effects on a modern turbocharged diesel engine running under the NEDC," SAE 2014 International Powertrain, Fuels & Lubricants Meeting, 2014-01-2713.
10. "Characteristics of PM Emissions of an Automotive Diesel Engine Under Cold Start and transient conditions," **D. Liu**, H. Xu, R.A. Sakunthalai and J. Tian, Cambridge Particle Meeting, University of Cambridge, May 2013

Chaper 1. NTRODUCTION

Diesel vehicles are gaining an ever increasing market share due to their increased availability, high fuel efficiency and power output. With the development of advanced diesel engine technologies, such as high pressure common rail direct injection, split injection strategy, exhaust gas recirculation and turbocharging, vehicle manufacturers are able to produce smaller sized lighter diesel engines with higher power and lower emissions. However, the pollutant emissions of diesel engines are still a problem. The supply of mineral diesel fuel is also a concern for the future of diesel engine development. It appears necessary to focus on fuels which are renewable and which provide equivalent performance with reduced emissions, like bio-fuels. Biodiesel, as one of the types of bio-fuel, is an alternative fuel that can be directly used in any un-modified diesel engine. Biodiesel is beneficial to the carbon balance of the environment since it is made from renewable sources, such as vegetable oil and animal fat. Researchers have also shown that biodiesel reduces the particulate emission significantly(Ramadhas 2011). Although there are some disadvantages of biodiesel, such as high cost and low production volumes, biodiesel is still one of the promising alternative fuels to solve energy and environmental issues in the future.

1.1. BACKGROUND

The following sections provide the introduction of the main topics in this thesis including an overview of emission regulations and their control methods, diesel engine operation, biodiesel as an alternative fuel and diesel engine cold start issues.

1.1.1. Overview of Emission Regulations and Control Methods

The main problem for diesel engine emissions is the trade-off between nitrogen oxides (NO_x) and particulate matter (PM). NO_x is the combination of nitric oxide (NO) and nitrogen dioxide(NO_2). In the diesel engine, NO_2 can be 10-30% of the total NO_x emissions. Their formation is highly related to the combustion temperature. The higher the combustion temperature, the more NO is formed (Heywood 1998). PM is characterized by carbon mixtures which contain around 18,000 organic compounds with high molecular weight (Beatrice et al. 2002). They are mainly formed by the oxidation and/or pyrolysis of fuel molecules in fuel rich zones of the injected fuel spray (Heywood 1998). PM emissions are also related to combustion temperatures. High temperature at the end of combustion enhances the soot oxidation which reduces the PM emissions. However, high temperature during the injection period results in fuel pyrolysis which increases the PM emissions. PM emitted from engines is typically presented in two distinct types, nucleation mode and accumulation mode. Most researchers suggest that nucleation mode particulates consist of volatile materials, which means that they cannot be easily measured in an accurate way (Eastwood 2008). Accumulation particulates normally have a larger size and mass since they are formed from particle coagulation and aggregation (Eastwood 2008;Heywood 1998). The number of particles that may combine ranges from tens, through to hundreds, and even thousands, which results in variation of particulate size and mass (Eastwood 2008).

Emissions of unburned hydrocarbon (HC) and CO are also regulated by the European Commission. The formation of HC emissions in diesel engines under normal operating conditions mainly results from two sources: (1) the fuel mixing is leaner than that obtained during lean combustion during the ignition delay period; (2) fuel mixes slowly or insufficiently with air due to the fuel leaving the injector nozzle at low velocity or excess fuel

being injected into the cylinder (Heywood 1998). CO emissions are highly related to the fuel/air equivalence ratio. Diesel engines always emit low CO emissions due to the lean stoichiometry (Heywood 1998).

The evolutions of the European Union emission legislations for the light duty diesel engine from EUROI to the future EURO VI are shown in table 1.1 below.

Table 1.1 European Union emission standards for diesel engines of a light commercial vehicle

Tier	year	CO	HC	$HC+NO_x$	NOx	PM	PN
		g/km					#/km
Euro 1[a]	1992.07	2.72 (3.16)	-	0.97 (1.13)	-	0.14 (0.18)	-
Euro 2, IDI	1996.01	1.0	-	0.7	-	0.08	-
Euro 2, DI	1996.01[b]	1.0	-	0.9	-	0.10	-
Euro 3	2000.01	0.64	-	0.56	0.50	0.05	-
Euro 4	2005.01	0.50	-	0.30	0.25	0.025	-
Euro 5A	2009.09[c]	0.50	-	0.23	0.18	0.005[e]	-
Euro 5B	2011.09[d]	0.50	-	0.23	0.18	0.005[e]	6.0×10^{11}
Euro 6	2014.09	0.50	-	0.17	0.08	0.005[e]	6.0×10^{11}

From www.dieselnet.com and the Directive 1999/96/EC (2000)

a. Values in brackets are conformity of production (COP) limits
b. Until 1999.09.30 (after that date DI engines must meet the IDI limits)
c. 2011.01 for all models
d. 2013.01 for all models
e. 0.0045 g/km using the PMP measurement procedure

1.1.2. 4-stroke Diesel Engine Operation

The engine's power is obtained from the chemical energy of the fuel by combustion in the engine cylinders. Diesel engines always produce high power due to its high compression ratio. A complete 4-stroke engine cycle can be divided into four events: intake, compression, power and expansion. During the intake stroke, only air is inducted into the cylinder. For engines equipped with turbocharging systems, the intake air is compressed to allow engines to operate

at higher compression ratios and to improve the power output. The air inlet then flows into the combustion chamber through the intake valve and is compressed to a very high temperature during the compression stroke. The fuel injection occurs at the end of the compression stroke or at the start of the power stroke. The high pressure jet of fuel atomises to small droplets and evaporates, instantly mixing with the high temperature air. As the fuel and air mixes to give a combustible air/fuel mixture, spontaneous auto-ignition of the mixture occurs, initiating the combustion. The initial combustion can occur from several regions concurrently unlike in the spark ignition (SI) engine, where the initial combustion occurs at the spark plug. The combustion transforms chemical energy to heat energy, which increases the in-cylinder pressure instantly. The expanding gases force the piston downward to rotate the crankshaft and power the entire engine. The engine power is controlled by the quantity of fuel injection into the combustion chamber. Lastly, the residual gas is removed via the exhaust valves during the expansion stroke.

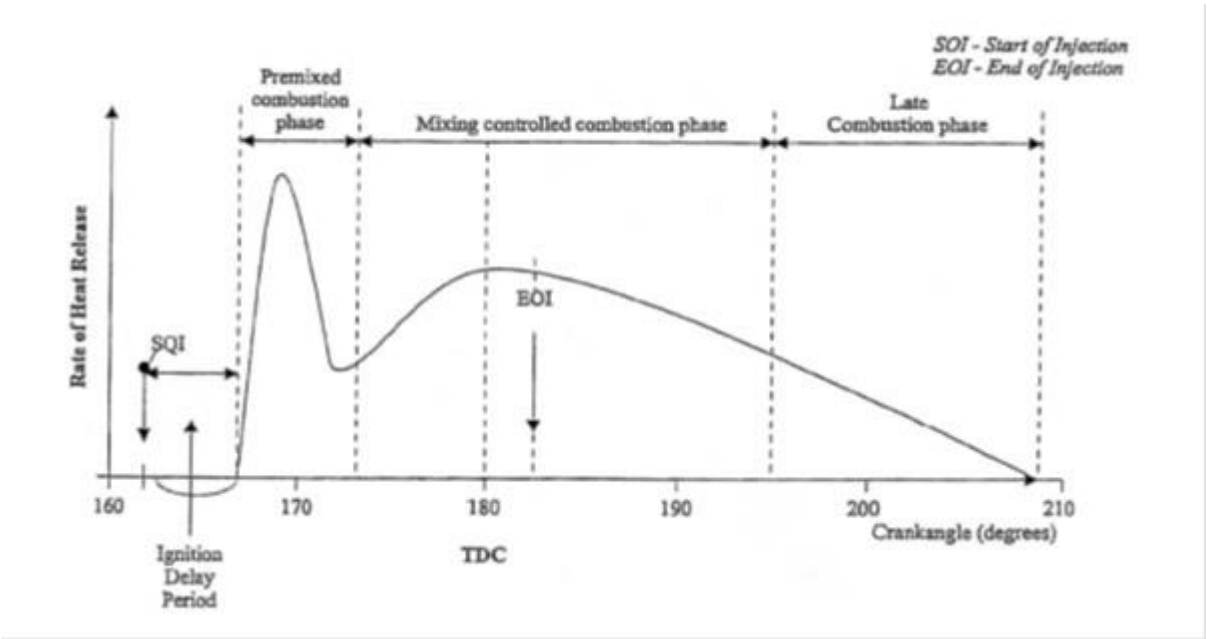

Figure 1.1:Typical diagram of the rate of heat release for a diesel engine.

From:http://petrolsmell.com/2012/07/02/combustion-in-ic-ci-engines/ (2010)

The rate of heat release (RoHR) quantifies the rate at which energy is transferred to the charged air by fuel combustion. A typical diagram of RoHR for a diesel engine with only one fuel injection per engine cycle is provided in Figure 1.1. The diagram will differ from engines which employ multi-injection strategies. It can be seen that the start of combustion (SOC) is several crank angle degree (CAD) later than the start of injection (SOI). This period between SOC and SOI is called the ignition delay which is the time required for the fuel to atomise, vaporise and forma combustible air/fuel mixture. At the end of the ignition delay period, the air/fuel mixture reaches the combustible ratio and temperature resulting in the fuel spontaneously burning and a rapid increase of ROHR and pressure. The combustion occurs wherever the air/fuel mixture reaches the combustible ratio, and this is known as premixed combustion. The premixed combustion phase occurs only within a few CADs until the premixed fuel/air mixture formed during the ignition delay has been consumed. After that, the heat-release rate is controlled by the formation rate of the flammable air/fuel mixture, which is called the mixed controlled combustion phase or the diffusion combustion phase. The burning rate is controlled by the initial fuel vapour and air mixing process. After this, the combustion continues with a low rate of heat release during the expansion stroke. This is caused by several reasons. Firstly, there is a small fraction of the residual fuel which may not yet have burned. Secondly, a fraction of the fuel energy is still contained in soot and fuel-rich combustion products which can still be released. Thirdly, the non-uniform cylinder charge and mixing during this period promotes complete combustion and produces less-dissociated product gases. Lastly, the in-cylinder temperature falls during the expansion stroke which results in slower kinetics of the final burnout processes.

1.1.3. Biodiesel as an Alternative Fuel

Due to the ever-rising price of crude oil and environmental concerns, various alternative fuels are being considered as a substitute to petroleum fuels. Renewable fuels have received a lot of attention due to their contributions in reducing environmental pollutants and their relatively low carbon cycle impact. Biomass generated fuels; such as alcohols, vegetable oils and their derivatives are promising renewable engine fuels. Biodiesel, derived from vegetable oil by transesterification and produced in the form of ethyl or methyl esters, is gaining more attention since its use does not require any hardware modification on conventional diesel engines. Meanwhile, the average molecule size of species in biodiesel is similar to those in mineral diesel and it can be blended into mineral diesel in any blend ratio. In Europe, biodiesel has already been blended into mineral diesel; 5.75% in volume at pump stations since 2010. It is anticipated that the blending ratio will increase to 20% by 2020. The oxygen content and sulphur free nature of biodiesel can reduce the particulates emission, which is always a significant problem for diesel engines. The use of biodiesel can also improve the durability of diesel engines because of its higher viscosity which results in better lubrication than mineral diesel. Biodiesel can biodegrade like sugar, making it less toxic compared with mineral diesel. Its high flash point also leads to safer handling and transportation.

1.1.4. Cold Start in Diesel Engines

Diesel engines are the versatile power sources for passenger cars and commercial vehicles but the cold start and idle stability of diesel engines are still not controlled very well. The auto-ignition of the diesel engine combustion depends upon the temperature at the end of the compression stroke. The first several cycles of the cold start are always difficult to be auto-ignited due to the low ambient temperatures, lack of lubrication and air blow-by from the

piston ring. When the ambient temperature decreases to a very low level, it will further aggravate the cold start problems, including misfire, rigid contact between moving parts, increases of frictional losses, idle instability and high emissions. The issue of cold start emissions becomes urgent since the engine test procedure has been amended by the European Union to synchronize sampling of the exhaust gas with the engine cranking start, thereby eliminating the 40 sec warm-up period which had existed previously. Furthermore, the European Union has also implemented the emissions of transient drive cycles at -7°C for passenger cars. The emissions of cold start occur because of incomplete combustion due to the low compression temperature and low air/fuel ratio. They can be affected by engine design and operating factors, including ambient temperature (Henein et al. 1992; Bielaczyc and Merkisz 1998; Han et al. 2001), fuel injection strategies (Henein, 1992; Han, 2000;Brown, 2007), fuel properties (Hara et al. 1999),(Heywood 1998), cranking speed (Han, Naeim Henein, & Bryzik 2000), compression ratio(Mohr and Urlaub 1994), lubricants and by some other control strategies, like EGR (Peng et al. 2008).

1.2. OBJECTIVES AND APPROACHES

In this research investigation, a light-duty turbocharged, modernV6 diesel engine equipped with a common rail injection system and EGR cooling system was tested. The main purpose was to correlate the fuel properties of biodiesel blends to their emissions at steady state conditions and also to investigate the chemical profiles of PM with using biodiesel blends. The objectives related to the research are listed below:

- To commission the diesel engine test rig for steady and transient operation studies

- To determine engine performance and emissions during combustion when using diesel-biodiesel blends (i.e. 0, 10, 30 and 60% biodiesel by volume) at standard steady state engine test points.
- To study the effect of EGR rate on engine performance and emissions when using diesel-biodiesel blends at steady state conditions.
- To investigate the correlations between fuel properties and engine emissions based on the results of various biodiesel feedstocks at different engine loads and EGR rates.
- To create a model to predict engine smoke emissions based on fuel properties and engine conditions.
- To study the engine performance and emissions at cold start with ambient temperature varying from 20°C to -20°C when fuelled with conventional diesel, winter diesel and diesel-biodiesel blends.
- To investigate the chemical characteristics of particulates emissions at cold start with using biodiesel fuel by 2D-GCMS.

1.3. THESIS OUTLINE

This research work was initiated by recent interest in the modern engine flexibility of using biodiesels produced from various feedstocks. The investigation started at steady state conditions and then transferred to transient engine tests. The present work is detailed in the following chapters. Chapter 1 gives a brief introduction about vehicle emission regulations, engine combustion characteristics and emissions. In addition, the background of biodiesel and the issues involved in engine cold start are also emphasised. In chapter 2, biodiesel properties

and the performance of the biodiesels are reviewed. Engine performance and emissions at cold start were also investigated. Chapter 3 presents the experimental setup of the two engine test cells, with the emission equipment and other additional control systems. This chapter also explains the experiment procedures, the data collection and analysis. Chapter 4 presents the engine combustion characteristics and emissions when fuelled with various biodiesels at steady state conditions. There were two purposes for the tests: 1. to study the engine performance and emissions when fuelled different biodiesels without any modification to the engine hardware and ECU control system; 2. based on the first test sequences, changes to the EGR rate were made to investigate the combined effect of EGR and biodiesel use. Chapter 5 investigated the relationship between fuel properties and engine emissions by statistical analysis. A smoke index was created to predict the smoke emissions when fuel properties, engine loads and EGR rates were changed. In chapter 6, the combustion characteristics and emissions were investigated at 20°C cold start and warm start. Two different biodiesels were blended in the mineral diesel to study the biodiesel effects on engine start. Chapter 7 studied the engine performance and emissions during cold start with the ambient temperature varied from -20°C to 20°C. Since the conventional mineral diesel would block the fuel line at -20°C due to its high CFPP, winter diesel and biodiesel-winter diesel blends were compared at the low temperature cold start. Chapter 8 identified the chemical compounds of the semi-volatile organic carbon (SVOC) in particle emissions by a 2D-GC/MS. The contributions of different organic species to particle emissions were different with using biodiesel blends. . Chapter 9 summarizes the results and findings from chapter 4 to chapter 8, and gives some recommendations for future work.

Chaper 2. LITERATURE REVIEW

2.1. EMISSIONS OF DIESEL ENGINE

2.1.1. NOx Emissions

Nitric oxide (NO) and nitrogen dioxide (NO_2) are always produced together in the engine combustion chamber as NO_x emissions. Normally, NO forms the majority of the NO_x emissions and it is also oxidized to form the NO_2. The principal source of NO is the reaction between oxygen and nitrogen from the atmospheric air. However, if the fuel contains a high portion of nitrogen, increased NO formation will occur. The mechanism of NO formation has been explained by Zeldovich (1975)and Lavoie et al. (1970) as below:

$$O + N_2 = NO + N \quad (2.1)$$

$$N + O_2 = NO + O \quad (2.2)$$

$$N + OH = NO + H \quad (2.3)$$

The first two reactions 2.1 and 2.2 were suggested by Zeldovich and the third one 2.3 was added by Lavoie et al.

Chemical equilibrium considerations show that the combustion of gases at typical flame temperatures would not result in high NO_2 emissions. However, the engine experiments show that the $NO_2$was 10-30% of the total NO_x emissions. A plausible principal for the NO/NO_2 conversion is given as below (Merryman and Levy 1975):

$$NO + HO_2 \rightarrow NO_2 + OH \quad (2.4)$$

$$NO_2 + O \rightarrow NO + O_2 \quad (2.5)$$

In the normal flame, the NO_2 formed in the reaction 2.4 would convert back to NO unless the NO_2 is quenched by mixing with cooler fluid or by contact with the surface of the cylinder wall and piston. This explains the NO_2 formation in the engines and also the higher NO_2/NO ratio at low load in diesel engines.

The total NO_x emissions are highly related to the in-cylinder temperatures during fuel combustion (Liam Lidstone et al. 2007). However, lean air/fuel ratio could also decrease the NO_x emissions due to the combustion temperature drop (Benajes et al. 2004). The injection timing and pressure could affect the NO_x emissions. Late injection timing always reduced the NO_x emissions because of the low combustion temperatures (Ueki and Miura 1999). High injection pressure has been applied in most of the current diesel engines which results in shorter ignition delay and better atomization and vaporization. This has resulted in either higher NO_x emissions (Bhusnoor et al. 2007)or lower NO_x emissions (Dhananjaya et al. 2008;Özer Can et al. 2004)which has depended on the fuel-air mixing during the ignition delay period.

2.1.2. Total Hydrocarbons

Total hydrocarbons (THCs) are formed due to incomplete combustion of the fuel (Dhananjaya, Mohanan, & Sudhir 2008). In the diesel engine, poor fuel/air mixing, either over-rich or over-lean is considered as the main reason for THC formation. In the over-rich regions, incomplete combustion occurs due to lack of oxygen. In the over-lean mixtures, as the equivalence ratio is lower than the lean combustion limit, the fuel/air mixture can only be oxidized by relatively slow thermal-oxidation reactions which will be incomplete. In addition, the flame quenching on the cylinder wall, and fuel impingement caused by the piston crown and cylinder wall are

other significant contributors to the THC emissions. Meanwhile, if misfire occurs in some operating cycles, the THC emissions will increase dramatically. However, the misfires are unlikely to occur in current well controlled engines, unless the engine is started at low ambient temperature conditions.

2.1.3. Carbon Monoxide

Carbon monoxide (CO) emissions are poisonous and affected by the fuel/air equivalence ratio. Either too lean or too rich fuel/air mixing produces the CO emissions (Kook et al. 2005;Kook et al. 2006;Opat et al. 2007). In the lean mixture regions, the increase of CO emissions is caused by incomplete combustion due to low temperatures. In the rich mixture regions, the lack of oxygen leads to partial oxidation of fuels which increases the CO emissions.

2.1.4. Particulate Matter

The particulate matter of diesel engines is a compound including soot, sulphuric acid and other condensed substances. The PM structure is illustrated schematically in figure 2.1. The particle emissions are generally the result of three processes: soot formation, soot oxidation and adsorption/condensation of hydrocarbons. The soot formation mainly occurs in the rich fuel zones of the fuel spray during the diffusion combustion phase. The high temperature of rich fuel zones leads to hydrocarbon fuel pyrolysis and an increase in the precursors of soot in the flame. The precursors of soot rapidly grow to bigger particles by dehydrogenation, coagulation and aggregation. The soot oxidation occurs after the soot formation process in the lean fuel zones and also after the late combustion phase. It is reported that over 90% of soot formed during combustion is oxidised before the gas is exhausted (Heywood 1998). The final process, adsorption and condensation, occur after the gases have been exhausted from the cylinder, when the exhaust temperature drops.

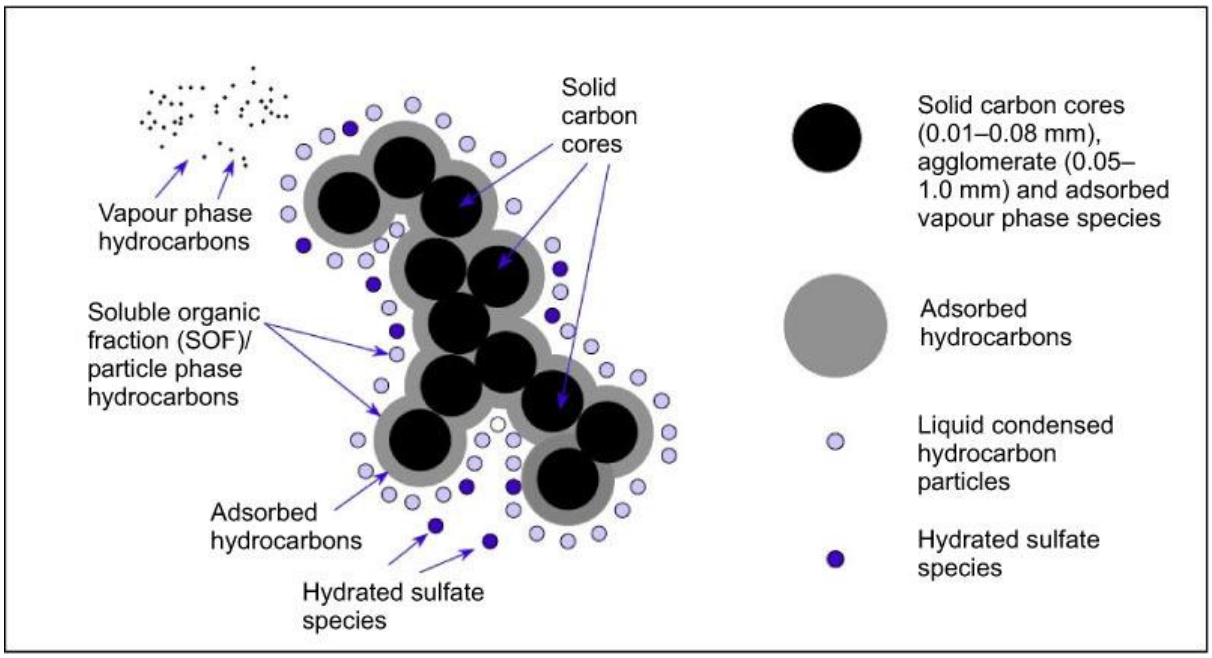

Figure 2.1: Schematic structure of diesel particulate matter (PM) formed during combustion of atomised fuel droplets. (Martyn V.Twigg 2009)

Chemical compositions of diesel engine particulates are normally defined by the analytical tools with four fractions: Carbonaceous Fraction (also defined as Elemental Carbon), Ash Fraction, Organic Fraction (also defined as Organic Carbon) and Sulphate Fraction.(Eastwood 2008). Pierson et al. (Pierson and Brachaczek 1982) studied of vehicle emissions in the Allegheny and Tuscarora Mountain Tunnels and reported that the carbon (elemental and organic) comprised around 80% component of the total PM, while only 5% of PM mass was sulphate and 10% of PM mass was inorganic material and/or ash from fuel and engine oil. The results also agreed by(Geller et al. 2005). Further separating the elemental and organic carbon identified that the elemental carbon was 50-70% of the total carbon component in diesel engines emissions.

Lots of research works have been done on organic carbon, especially the Polycyclic aromatic hydrocarbons (PAHs). This is because of their designation as hazardous air pollutants and they can also be used to trace the source of particulates. (Schauer et al. 1999)examined the PM emissions from two medium duty diesel trucks. They quantified over 100 compounds

including *n*-alkanes, *n*-alkanoic acids, benzoic acids, benzaldehydes, PAHs, oxy-PAHs, steranes, pentacyclic triterpanes, and azanapthalenes. These compounds originate from unburned fuel and lube oil components, their partially oxidized products, intermediate production of combustion and metallic ash from fuel, engine oil and additives.

The organic carbons of PM emissions are impacted by many factors. Three most common factors are reviewed below:

1. Engine load effect. Some researchers indicated that the organic carbons was reduced with the engine load increase while the elemental carbon showed the opposite trends.((Shi et al. 2000;Zielinska et al. 2004). Diesel combustion includes premixed and diffusion phases. Higher speed and load reduced the premixing time and emphasized the diffusion combustion, which resulted in higher elemental carbon levels.
2. Ambient temperature effect. Chemical speciation, including PAHs, hopanes and steranes, was analysed by Zielinska et al. (Zielinska et al, 2004)on a diesel vehicle at ambient temperature of -1°C and 25°C. The total PM emissions at -1°C condition was more than doubled at 25°C, mainly due to the increasing of organic carbon emissions. The semivolatile PAH was also increased, partially due to the higher partitioning of semivolatile compounds to the particle phase at lower temperature. Small change of hopane and sterane was observed at -1°C suggested a minor effect of ambient temperature on diesel engine oil consumption. The higher organic carbon was observed in the cooled exhaust PM accompanying by much more diverse compositions of PAH species comparing while less PAH species were observed in PM from the hot exhaust (Jana Moldanová et al. 2009).

3. Fuel property effect. Using of oxygenated fuels, such as biodiesels, always reduces the PM emissions. (Buchholz et al. 2004) labelled biofuels with ^{14}C and blended with conventional diesel fuel. They observed that carbon-oxygen bond remained intact during combustion and formed to CO2 in the end while the carbon-carbon double bond implicated in soot formation. Meanwhile, the carbon in ethanol was tended to form non-volatile organic fraction (NVOF) due to the tendency of ethanol to produce acetylene and other soot precursors during combustion. Meanwhile, the PAHs emissions were observed a significant correlation with the PAHs content in fuel. (Westerholm and Li 1994)also found that reductions of PAHs in fuel could decrease the PAHs in the emissions.

2.2. EXHAUST GAS RECIRCULATION (EGR)

2.2.1. Exhaust Gas Recirculation (EGR) Applications in Internal Combustion Engines

Exhaust Gas Recirculation (EGR) is an effective technique to reduce the NO_x emissions for both gasoline and diesel engines. By introducing a certain fraction of exhaust gases into the intake manifold via an EGR control valve, the high specific heat capacity of the exhaust gases reduces the combustion temperature and consequently reduces the NO_x emissions. However, the method of EGR application is quite different for gasoline and diesel engines. For gasoline engines, the mass of charged fresh air is kept constant due to the required power outputs, requiring the throttle to be opened more with EGR addition. For the diesel engine, the EGR replaces part of the charged fresh air and the total mass of charged air is kept constant. This replacement reduces the oxygen availability for combustion, but does not affect the engine power output significantly since the diesel engine combustion is always lean. The reduced

oxygen availability is also a reason for the reduction of NO_x emissions in diesel engines, with EGR addition.

The recycled exhaust gases can be extracted from the exhaust manifold or from the exhaust pipe after the catalysts. The gases from the exhaust manifold are hotter and contain much more NO_x, THC, CO and PM emissions compared with the gases after the catalysts. The higher temperature of EGR reduces the ignition delay and consequently reduces the fuel burned in the premixed combustion(Desantes et al. 2000). Meanwhile, the extra pollutant emissions of gases from the exhaust manifold may contribute to the increases of pollutant emissions(Beatrice et al. 2008).However, the low exhaust pressure after the catalysts limits the EGR levels which can be achieved and it also leads to difficulties in EGR rate control at high loads.

2.2.2. Effects of Exhaust Gas Recirculation (EGR) on Engine Performance and Emissions

EGR is an established method to reduce NO_x emissions in the internal combustion engine. The effect of NO_x reduction is more significant as the engine load increases. Experimental results indicate that the reduction of NO_x emissions is mainly caused by the dilution effect rather than the chemical or thermal effects (Ladommatos et al. 1998). Some researchers injected CO_2 into the intake manifold to simulate the EGR effects on the NO_x emissions {Nikolic, 2007; Cinar, 2004 }. Their results showed that the NO_x emissions decreased as the amount of CO_2 injected increased. Some studies (Buchwald et al. 2004; Tanaka et al. 2002;Zhang 1999) found that the EGR technique could be used to control the combustion quality and engine noise since the prolonged ignition delay prevented rapid combustion and reduced the peak combustion pressure and temperature.

However there are obvious drawbacks to the application of EGR. Many researchers found that EGR application would normally result in high PM emission, increased specific brake fuel consumption and degradation of lubrication oil and engine durability (Chuepeng et al. 2007; Dober et al. 2008; Horn et al. 2007; Benajes et al. 2007; Jacobs et al. 2003; Kawano et al. 2007). Other experimental results confirmed that an increased EGR rate caused increases in engine wear rate especially on the piston ring and cylinder liner because of the higher soot and sulphuric acid particles from the recycled exhaust gases (Dennis et al. 1999;Marques et al. 2007;Myung-whan et al. 2000). The high particle content in the cylinder forms an abrasive surface which then removes the lubricant film causing high wear rate on the surfaces (Dennis, Garner, & Taylor 1999; Ishiki et al. 2000; Jacobs, Assanis, & Filipi 2003; Li et al. 2002).

The EGR technique can also be used to reduce the soot and NO_x simultaneously. Soot is formed due to the high combustion temperature in the fuel rich regions. When at high EGR rate was applied, the prolonged ignition delay provided sufficient time for fuel evaporation and mixing with air which reduced the fuel rich regions. Meanwhile, the high EGR rate reduced the combustion temperature and the low temperature combustion significantly reduced the soot formation even in fuel rich regions (Akihama et al. 2001).Figure 2.2 shows the soot and NO_x formation at different combustion temperatures which indicates that the simultaneous reduction in soot and NO_x can be achieved by controlling the combustion at lower temperatures. Experimental results also showed that the smoke emissions were initially increased and then decreased with the increase of EGR rate in engines operating with common rail injection systems(Akihama et al 2001;Wagner et al. 2003). The EGR technique combined with injection timing strategy or new fuels (blended diesel and gasoline) can achieve other advanced combustion technologies such as homogeneous charge compression ignition (HCCI) and premixed charge compression ignition (PCCI) maintaining the soot and

NO_x at very low levels (Zhang et al. 2014; Horibe and Ishiyama 2009; Kimura et al. 2001; Horibe et al. 2009).Both of the combustion technologies depend upon sufficient fuel/air mixing during the ignition delay period.

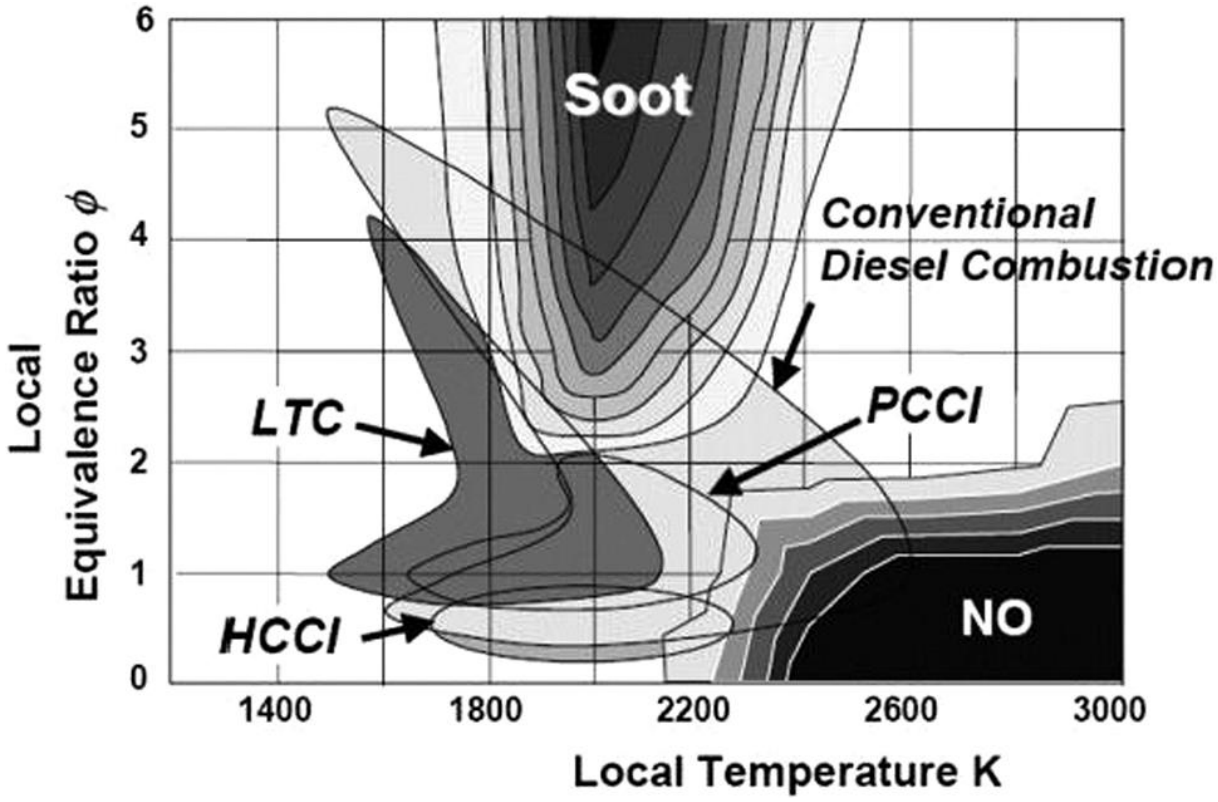

Figure 2.2. Combustion temperature affects the trade-off of soot and NOx emissions(Valentin Soloiu et al. 2013)

2.3. BIODIESEL AS AN ALTERNATIVE FUEL

2.3.1. **Biodiesel Production and Standardisation**

Biodiesel, defined by ASTM, compromises the mono-alkyl esters of long chain fatty acids derived from natural lipid feedstock, such as vegetable oils and animal fats. Pure vegetable oils and animal fats are not suitable for direct use in a diesel engine because their large molecule sizes produce high carbon deposits and cause pour point problems(Graboski and McCormick 1998). They can also result in other engine problems, for example long-term

engine deposits, injector plugging and lubrication oil gelling (Kalam and Masjuki 2005). To avoid those problems, some methods were used to reduce the large molecule size of vegetable oils and animal fats. The most common method of which is the transesterification reaction, by which the triglyceride in vegetable oil or animal fat is reacted with alcohols (methanol in figure 2.3), in the presence of a catalyst, to produce fatty acid methyl esters (FAME). The reaction process is simply shown in figure 2.3.

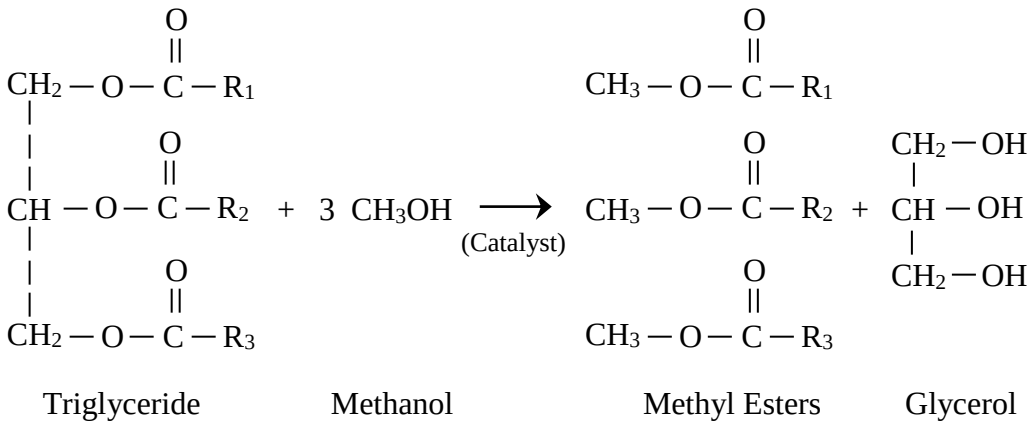

Figure 2.3 Transesterification reaction(Schmidt K and Van Gerpen JH 1996)(Van Gerpen et al., 2004)

It is popular to classify various biodiesels as "1st generation" and "2nd generation". In fact, there is no legal meaning or definition for the generations. Normally, the "1st generation" biodiesel refers to biodiesels derived from commonly used and edible feedstocks with well-established techniques, like the transesterification reaction mentioned above. Most biodiesels we are using today are classified as 1st generation biodiesel. The "2nd generation" biodiesel normally refers to the biodiesels converted from non-food or waste feedstocks, or produced via advanced conversion technologies (or both). Examples of the non-food feedstocks are jatropha and used vegetable oil. An example for the advanced conversion technique is hydrogenated vegetable oil (HVO). However, the definition for the generations is still not

precise. To avoid any misunderstanding, this work will not use the term of 1st generation and 2nd generation biodiesels.

Table 2.1 Some requirements and test methods for FAME

Property	Test method	Min. limit	Max. limit	Unit
Viscosity @ 40°C	EN ISO 3104	3.50	5.00	mm^2/s
Flash point	EN ISO 3679	120	-	°C
Sulphur content	EN ISO 20846/84	-	10.0	mg/kg
Carbon residue (on 10% distillation residue)	EN ISO 10370	-	0.30	% (m/m)
Cetane number	EN ISO 5165	51.0	-	
Sulphated ash content	ISO 3987	-	0.02	% (m/m)
Oxidation stability, 110°C	EN 14112	6.0	-	Hours
Acid value	EN 14104	-	0.50	mg KOH/g
Free glycerol	EN 14105/06	-	0.02	% (m/m)
Total glycerol	EN 14105	-	0.25	% (m/m)

To maintain the engine durability and reliability, the European committee released the European Standard EN 14214 which regulated the specifications of biodiesel production and their test methods. Table 2.1 displayed some requirements and test methods of the standard. Neat biodiesel, either used as an automotive fuel or blended with conventional diesel, is required to meet this standard. Biodiesel is produced in a pure form labelled as B100 or neat biodiesel and may be blended with conventional diesel fuel. The biodiesel blends are designated as BXX, where XX represents the blend ratio of biodiesel measured by volume.

2.3.2. Biodiesel Compositions and Profiles

Biodiesel can be produced by transesterification from various feedstocks, including oil-rich crops, animal fat and algal lipids. At present, different feedstocks are used in different regions.

In the US, the dominant feedstocks are soybean oil. In Europe, the dominant feedstocks are rapeseed oil and in Southeast Asia, palm oil dominates the market(Anon 2008;Curt Robbins et al. 2009). Recently, animal oil (especially beef tallow) and used vegetable oil (also called, used cooking oil or yellow grease) represents a significantly increasing biodiesel market in many regions and locations.

Numerous fatty acid (FA) species are produced while vegetable oils and animal fats are converted by transesterification. However, for a particular biodiesel, only several FA species generally dominate the compositions of FA derived by vegetable oils and animal fats. The commonly seen FA species in biodiesels are listed in table 2.2 with their common names, formal names, molecular formulas, weights and structures. The abbreviation consists of two parts and is separated by a colon symbol; the first part represents the carbon chain length of the FA molecule and the second part refers to the number of double bonds in the FA molecules. Among those FA species listed in the table 2.2, the dominant FAs in biodiesels are Palmitic acid (16:0), Stearic acid (18:0), Oleic acid (18:1), Linoleic acid (18:2) and Linolenic acid (18:3), which are highlighted in grey in the table.

Table 2.2 The common species in methyl ester biodiesel fuels(S.Kent Hoekman et al. 2012)

Common Name	Formal Name	CAS. No.	Abbreviation	Molecular Formula	Molecular Weight	Molecular Structure
Lauric acid	Dodecanoic acid	143-07-7	12:0	$C_{12}H_{24}O_2$	200.32	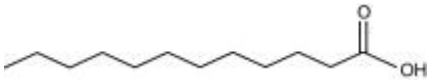
Myristic acid	Tetradecanoic acid	544-63-8	14:0	$C_{14}H_{28}O_2$	228.38	
Myristoleic acid	*cis*-9-Tetradecenoic acid	544-64-9	14:1	$C_{14}H_{26}O_2$	226.26	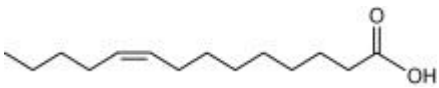
Palmitic acid	Hexadecanoic acid	57-10-3	16:0	$C_{16}H_{32}O_2$	256.43	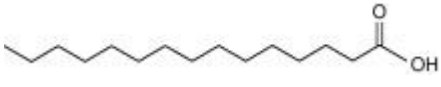

Common Name	Formal Name	CAS. No.	Abbreviation	Molecular Formula	Molecular Weight	Molecular Structure
Palmitoleic acid	*cis*-9-Hexadecanoic acid	373-49-9	16:1	$C_{16}H_{30}O_2$	254.42	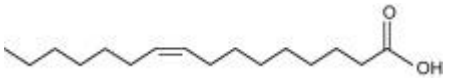
Stearic acid	Octadecanoic acid	57-11-4	18:0	$C_{18}H_{36}O_2$	284.48	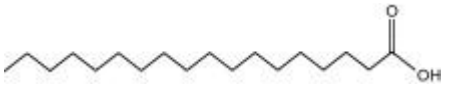
Oleic acid	*cis*-9-Octadecenoic acid	112-80-1	18:1	$C_{18}H_{34}O_2$	282.47	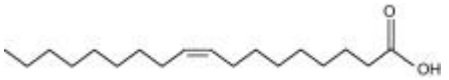
Linoleic acid	*cis*-9,12-Octadecadienoic acid	60-33-3	18:2	$C_{18}H_{32}O_2$	280.46	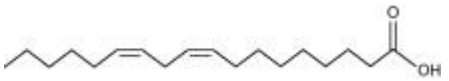
Linolenic acid	*cis*-9,12,15-Octadecatrienoic acid	463-40-1	18:3	$C_{18}H_{30}O_2$	278.44	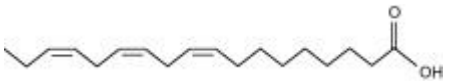
Arachidic acid	Eicosanoic acid	506-30-9	20:0	$C_{20}H_{40}O_2$	312.54	
Gondoic acid	*cis*-11-Eicosenoic acid	5561-99-9	20:1	$C_{20}H_{38}O_2$	310.53	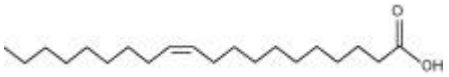
Behenic acid	Docosanoic acid	112-85-6	22:0	$C_{22}H_{44}O_2$	340.60	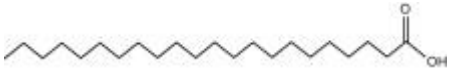
Erucic acid	*cis*-13-Docosenoic acid	112-86-7	22:1	$C_{22}H_{42}O_2$	338.58	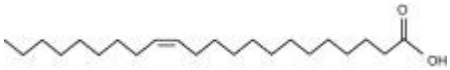

Hoekman et al.(Hoekman et al. 2012)have summarised the chemical compositions of 12 of the most common biodiesels derived from vegetable oil and animal fat in the market and these are listed in table 2.3. All the results are the mean values calculated based on the values in other literature. Most of the fuels are composed of C18 compounds, while coconut is dominated by C12 and palm is dominated by C14. For the fuels dominated by C18, the percentage of saturated (18:0), mono-unsaturated (18:1) and di-unsaturated (18:2) varies

considerably. The FA of rapeseed and canola is mostly C18:1; corn, safflower, soya bean and sunflower contain mostly C18:2; jatropha and yellow grease have nearly the same amount of C18:1 and C18:2.

The standard deviation of each feedstock between those obtained in different literatures is also calculated. It can be seen that the compositional profile of yellow grease is more variable than those of other feedstocks because the yellow grease, composed of used vegetable oil, might contain vegetable oils with any carbon percentage which significantly affects the compositions of FAs in yellow grease.

Table 2.3 The compositions of common used feedstocks et al. 2012)

Fatty Acid		Camelina		Canola		Coconut		Corn		Jatropha		Palm		Rapeseed		Safflower		Soy		Sunflower		Tallow		Yellow Grease	
Common Name	Abbrev.	mean	dev	mean	Dev	mean	Dev	mean	Dev	mean	Dev	mean	Dev	mean	Dev	mean	Dev	mean	Dev	mean	Dev	mean	Dev	mean	Dev
Capriotic	6:0					0.6	0.3															0.1			
Caprylic	8:0					6.8	1.9					0.8	1.3												
Capric	10:0			0.1		5.4	1.1					0.5	0.9	0.6								0.1			
Lauric	12:0	0.4				47.7	5.4			0.1	0.2	0.3	0.3	0.1	0.1			0.1	0.2	0.1	0.3	0.2	0.1	0.2	0.6
Tridecylic	13:0																								
Myristic	14:0	2.7	3.6			18.5	1.3			0.3	0.5	1.1	0.5	0.0	0.0	0.1	0.1	0.1	0.2	0.1	0.1	2.6	0.7	0.8	0.6
Myristoleic	14:1																					0.3	0.2		
Pentadanoic	15:0																					0.6	0.3	0.1	
Pentadecenoic	15:1																					0.1			
Palmitic	16:0	6.1	1.5	4.2	1.0	9.1	1.7	11.5	1.7	14.9	2.1	42.5	3.2	4.2	1.1	8.2	1.7	11.6	2.0	6.4	1.8	24.3	2.8	16.5	5.6
Palmitoleic	16:1			0.3	0.3	0.1	0.2	0.2	0.2	1.0	0.5	0.2	0.1	0.1	0.1	0.1		0.2	0.3	0.1	0.1	2.6	1.0	0.9	1.1
Hexadecadienoic	16:2																								
Hexadecatrienoic	16:3																								
Heptadecanoic	17:0			0.1						0.1		0.1		0.1				0.1	0.1	0.1		1.4	0.2	0.1	0.1
Heptadecenoic	17:1			0.1				0.1												0.1		0.6	0.3	0.1	
Stearic	18:0	2.8	0.4	2.0	0.4	2.7	0.7	1.9	0.3	6.1	1.7	4.2	1.1	1.6	0.7	2.5	1.0	3.9	0.8	3.6	1.1	18.2	4.5	7.1	3.9
Oleic	18:1	16.8	3.0	60.4	2.9	6.8	2.1	26.6	2.2	40.4	6.7	41.3	2.9	59.5	7.8	14.2	3.2	23.7	2.4	21.7	5.3	42.2	4.1	44.6	9.3
Linoleic	18:2	17.0	2.3	21.2	1.8	2.1	1.4	58.7	2.8	36.2	6.1	9.5	1.8	21.5	2.8	74.3	8.3	53.8	3.5	66.3	7.6	4.4	2.9	25.1	10.3
Linolenic	18:3	35.6	3.4	9.6	2.1	0.1	0.1	0.6	0.4	0.3	0.2	0.3	0.1	8.4	1.3	0.1	0.1	5.9	2.6	1.5	2.6	0.9	0.7	1.1	1.1
Stearidonic	18:4																					0.4		0.5	
Arachidic	20:0	1.4	1.3	0.7	0.3	0.1	0.1	0.3	0.2	0.2	0.1	0.3	0.1	0.4	0.5	0.1	0.1	0.3	0.3	0.3	0.2	0.2	0.1	0.3	0.1
Gondoic	20:1	14.4	2.8	1.5	0.2	0.0		0.1		0.1		0.1	0.1	2.1	3.0			0.3	0.1	0.2	0.2	0.6	0.2	0.5	0.1
Eicosadiensic	20:2	1.5	0.2	0.1										0.1											
Eicosatrienoic	20:3	0.8																							
Eicosatetraenoic	20:4																								
Eicosapentaenoic	20:5																								
Behenic	22:0	0.9	0.6	0.3	0.1			0.1	0.1	0.2	0.1	0.1		0.3	0.3			0.3	0.2	0.6	0.4	0.1	0.1	0.4	0.2
Erucic	22:1	3.1	0.8	0.5	0.2	0.0	0.0	0.1	0.1	0.1	0.1	0.0		0.5	0.5			0.1	0.1	0.1	0.1	0.1		0.1	0.1
Docosatetraenoic	22:4					0.0																			
Docosapentaenoic	22:5																								
Docosahexaenoic	22:6																								
Lignoceric	24:0	0.7	0.5	0.2	0.1	0.0		0.1	0.1	2.6	3.5	0.1		0.1				0.1	0.1	0.2	0.2			0.2	0.2
Nervonic	24:1	0.2		0.2		1.0				0.1				0.1	0.1			0.3	0.6					4.4	
Other/Unknown		1.0		2.2				0.3		1.2	1.1	0.9	0.9	4.3	4.4	0.8	0.8	4.1	4.7	0.1		2.0	1.2		
Total		104.1		101.2		101.1		100.2		102.7		101.2		99.9		99.5		100.8		101.2		100.0		103.1	
No. of References		6		14		14		12		20		27		20		9		39		18		16		19	

Dominant species in FAME Composition Other major species (>= 10%) in FAME composition

There is rarely literature which has studied the growth condition affects (such as water, humidity, sunshine period, nutrients, temperature, etc.) upon the FA profiles of vegetable oil or animal fat. Only one study in field experiments was conducted with Jatropha and this found that the growth conditions didnot result in a significant change in the profile of Jatropha FA,

even though the total amount of FA did(Kheira and Atta).Another study on sunflower showed that the iodine number of sunflower FA was affected(Gustavo et al. 2009).

Table 2.4Averaged fuel properties of methyl esters from different feedstocks(Hoekman et al. 2012)

Property	Camelina		Canola		Coconut		Corn		Jatropha		Palm		Rapeseed		Safflower		Soy		Sunflower		Tallow		Yellow Grease	
	mean	dev	mean	dev	mean	dev	mean	dev	mean	dev	mean	dev	mean	dev	mean	dev	mean	dev	mean	dev	mean	dev	mean	dev
Sulfur Content, ppm	2	2	2	0	3	1	4	1	5	6	2	2	4	3	ND		2	2	2	3	7	8	5	5
Kinematic Viscosity @ 40 °C, mm^2/s	3.80	0.55	4.38	0.27	2.75	0.24	4.19	0.33	4.75	0.58	4.61	0.56	4.50	0.35	4.14	0.13	4.26	0.39	4.42	0.26	4.69	0.44	4.80	0.48
Cloud Point, °C	3	1	-2	1	-3	3	-3		5	3	14	2	-3	2	-4	2	0	2	2	1	13	2	8	5
Pour Point, °C	-7	3	-6	3	-9	5	-2	2	0	5	13	2	-10	3	-7	1	-4	3	-2	2	10	3	3	7
CFPP, °C	-3	2	-9	4	-5	1	-8	6	ND		9	5	-12	6	-6		-4	2	-2	1	13	2	1	5
Flash Point, °C	136		153	29	113	6	171	16	152	20	163	17	169	16	174	7	159	18	175	9	124	35	161	22
Cetane No.	50.4	1.6	53.7	1.5	59.3	9.7	55.7	2.9	55.7	3.0	61.9	3.6	53.7	2.9	51.1	1.8	51.3	4.6	51.1	3.2	58.9	2.1	56.9	4.2
Cetane Index*	ND		61.5		ND		60.9		ND		50.5	4.4	54.7	5.0	ND		52.3	5.7	55.0	8.4	59.1		48.5	
Iodine Value	152.8	2.5	108.8	1.3	18.5	16.3	101.0		109.5		54.0	6.1	116.1	6.7	141.0		125.5	5.4	128.7	4.6	65.9	15.6	88.9	16.2
Specific Gravity	0.882	0.007	0.883	0.003	0.874	0.001	0.883	0.005	0.876	0.009	0.873	0.008	0.879	0.010	0.879	0.012	0.882	0.007	0.878	0.011	0.878	0.006	0.879	0.010
Lower Heating Value, MJ/Kg	ND		38.9	1.6	35.2		39.9		37.7		37.3	2.3	37.6	1.6	ND		37.0	1.9	35.3	2.1	37.2	0.2	37.6	1.6
Higher Heating Value, MJ/Kg	45.2		41.3	3.1	38.1		43.1	2.7	40.7	1.5	40.6	1.5	41.1	2.3	42.2	2.7	39.7	0.8	40.6	2.4	39.7	0.2	39.4	1.1
Avg. Chain Length	19.10		18.20		13.40		17.80		18.30		17.20		17.90		17.80		17.90		18.10		17.30		18.50	
Avg. Unsaturation	1.81		1.34		0.12		1.46		1.15		0.62		1.31		1.63		1.50		1.59		0.59		1.06	
No. of References	7		15		7		6		23		44		39		4		59		20		12		37	

ND = No Data found in literature
* = No accepted method for determining cetane index of biodiesel

Kent Hoekman et al.(Hoekman et al. 2012) also collected all the fuel properties of each biodiesel fuel from various literature and calculated the mean value of each property with the standard derivation. This is showed in table 2.4. Based on the average values of physical/chemical properties, they made a correlation matrix of the different biodiesel fuels (excluding the coconut-derived FAME since it differed from the other FAME in many ways.) The correlation matrix is shown in Table 2.5 and the correlation values which are more than 0.70, 0.80, and 0.90were highlighted by different shading colours. The minus shows the

correlation between the two properties is inverse proportional. The matrix clearly demonstrates the relationships between each fuel property and highlights some highly correlated fuel properties.

Table 2.5The correlations of each fuel properties(S.Kent Hoekman et al. 2012)

Properties	Sulfur	Vis.	CP	PP	CFPP	Flash Point	Cetane No.	Cetane Index	Iodine Value	Specific Gravity	LHV	HHV	Avg. Chain Length	Avg. Unsat.
Sulfur	1.00													
Viscosity	0.60	1.00												
Cloud Point	0.43	0.57	1.00											
Pour Point	0.42	0.59	0.93	1.00										
CFPP	0.46	0.48	0.96	0.93	1.00									
Flash Point	-0.45	-0.04	-0.51	-0.32	-0.52	1.00								
Cetane No.	0.49	0.69	0.77	0.87	0.69	-0.22	1.00							
Cetane Index	0.14	-0.51	-0.40	-0.29	-0.27	-0.28	-0.18	1.00						
Iodine Value	-0.50	-0.72	-0.75	-0.87	-0.70	0.21	-0.97	0.15	1.00					
Specific Gravity	-0.26	-0.62	-0.69	-0.68	-0.67	-0.08	-0.61	0.58	0.54	1.00				
Lower Heating Value	0.12	-0.29	-0.34	-0.19	-0.35	-0.05	0.20	0.52	-0.15	0.51	1.00			
Higher Heating Value	-0.41	-0.84	-0.41	-0.47	-0.38	-0.06	-0.42	0.63	0.56	0.44	0.66	1.00		
Avg. Chain Length	-0.32	-0.39	-0.34	-0.56	-0.44	-0.13	-0.59	-0.12	0.67	0.48	0.05	0.49	1.00	
Avg. Unsaturation	-0.59	-0.79	-0.82	-0.87	-0.76	0.35	-0.94	0.20	0.96	0.65	0.03	0.62	0.65	1.00

= Correlation factor ≥ .70
= Correlation factor ≥ .80
= Correlation factor ≥ .90

2.4. PERFORMANCES AND EMISSIONS FROM BIODIESEL COMBUSTION

2.4.1. Engine Power

Numerous amounts of engine tests have been conducted by researchers and engineers to study the engine performance, emissions and durability of the engine when fuelled with biodiesel or its blends. Current automotive engines are always designed and manufactured taking the usage requirements into account. Although biodiesel fuels have a lower gross heat value of combustion (GVH), the power generated by using biodiesel fuels is normally the same as using mineral diesel, since the fuelling is not 100% in most of the driving cases. However, at full load condition, when the fuelling rate is at its maximum, or at partial load with constant

fuel consumption or constant fuelling rate, the power generated using biodiesel is decreased as compared with that of using mineral diesel. This is caused by the lower GHV of combustion of biodiesel fuels(normally 8% lower in volume basis or 14% lower in mass basis). Many researchers have found that the loss of power output is lower than the loss of heating value. Kaplan et al. (Cafer Kaplan et al. 2006) tested an engine at full and partial loads (the latter was controlled by constant fuel injection) using sunflower oil methyl ester and mineral diesel and their results showed that the loss of power ranged between 5% and 10%. Cetinkaya et al. (Cetinkaya et al. 2005)compared waste oil biodiesel and mineral diesel at full load conditions and the torque reduction was only between 3% and 5% when using biodiesel. Similar results were found by Lin et al (Yuan-Chung Lin et al. 2006)when using mineral diesel, neat palm oil biodiesel and a 20% palm oil biodiesel/diesel blend. The reduction of power at full load was 3.5% when neat biodiesel was used and 1% when a biodiesel blend was used, respectively. Some researchers also found that the loss of power was very closely related to the reduction of heating value. Murillo et al.(Murillo et al. 2007)compared the power output with using mineral diesel and used cooking oil biodiesel in a marine outboard 3-cylinder engine at full load. The use of biodiesel reduced power by 7.14% compared to mineral diesel, which is almost the same as the loss of heating value. However, some researchers surprisingly found power or torque increases when using biodiesel. Altiparmak et al. (Altiparmak et al. 2007)observed that the maximum torque was increased by 6.1% when using a 70% blend of tall oil biodiesel, with respect to the maximum torque when mineral diesel was used.

2.4.2. Brake Specific Fuel Consumption

The brake specific fuel consumption (BSFC) is the specific value between the mass of fuel consumption and the brake effective power. Most of the researchers found that the BSFC was

increased when using biodiesel and the increasing rate was similar to the reduction of heating value. Turrio-Baldassarri et al.(Turrio-Baldassarri et al. 2004)found a 2.95% increase in the mean BSFC from the ECE R49 test cycle in a 6-cylinder 7.8litre engine fuelled with 20% blends of rapeseed oil biodiesel in mineral diesel. A similar sized engine was tested by Hansen and Jesen (Hansen and Jensen 1997)with neat rapeseed oil biodiesel and the results showed a 14% increase in BSFC with respect to the case of using mineral diesel. Lapuerta et al. (Lapuerta et al 2005) tested a 2.2litre engine with biodiesels derived from different waste oils and again found that the increase in BSFC was similar to the loss of heating value in all cases.

2.4.3. Thermal Efficiency

Thermal efficiency is the ratio between the engine power and the energy of fuel injection. According to the previous paragraph, it can be proposed that the thermal efficiency would not be changed significantly when using biodiesel. Tsolakis(Tsolakis 2006), Graboski et al. (Graboski et al. 1996),Senatore et al. (Senatore et al. 2000), Canakci(Canakci 2005), Monyem and Van Gerpen (Monyem and Gerpen 2001), Shaheed and Swain (A Shaheed and Swain 1999) and Lapuerta et al. (Lapuerta et al. 2008) showed that there was no significant variations in thermal efficiency when using different types of biodiesels. However, some researchers found the thermal efficiency varied with biodiesel blend ratios. Ramadhas et al. (Ramadhas et al. 2005) tested 10%, 20%, 50%, 75% blends and neat biodiesel derived from Indian rubber seed oil in a single-cylinder engine. They found that the maximum thermal efficiencies were achieved when the 10% and 20% blends were used. Labeckas and Slavinskas (Labeckas and Slavinskas 2006) used 5%, 10%, 20%, 35% blends and neat rapeseed oil biodiesel in a 4.75litre engine and the highest thermal efficiency was achieved with the 5% and 10% blends.

2.4.4. Effect on NOxEmissions

Most of the researchers reported that the NO_x emission was increased slightly when using biodiesel fuels (Choi and Reitz 1999; Schumacher et al. 1994;Yuan et al. 2005; Marshall et al. 1995). Only a few authors found that the NO_x emission obtained using biodiesel was almost the same (Nabi et al. 2006; Durbin et al. 2000) or slightly lower (Peterson and Reece 1996; Lapuerta et al. 2005) as compared to that obtained when using mineral diesel. Various reasons were proposed to explain the increasing NO_x emission obtained when using biodiesel fuels. The most common and solid argument was the advanced injection caused by the fuel properties, especially in the pump-line-nozzle system. When the biodiesel was injected, the rise rate of fuel pressure in the pump was higher due to the higher bulk modulus and the fuel propagation was quicker towards the injector due to its higher sound velocity. In addition, the higher viscosity resulted in less leakage in the pump as a consequence of higher pressure in the injection line. Therefore, an earlier and quicker needle lift was observed as compared to the case of mineral diesel. Many authors have used this reason to explain the observed higher peak temperature and NO_x emissions in their literature(Abdul Monyem & Jon H.Van Gerpen 2001;K Yamane et al. 2001;M.E.Tat and J.H.Van Gerpen 2003). Monyem and Van Gerpen (Monyem & Gerpen 2001) and Szybist(Szybist et al. 2005b)even found a good correlation between the start of injection and the NO_x emissions. However, some investigations were conducted using fixed injection timing but even these observed increases in NO_x emissions. The literature (Ban-Weiss et al. 2007; Lapuerta et al. 2002; Nabi et al. 2004)proposed that this was due to the slightly higher adiabatic flame temperature obtained when using biodiesel fuels. Cheng et al. (A S Cheng et al. 2005) maintained both the start of combustion and the rate of premixed combustion and they also observed NO_x increases. They attributed this to the decreased soot formation which lead to a reduction of soot radiative temperature transfer and

subsequently increased the adiabatic flame temperature. This reason might explain the NO_x emission increasing in a common rail engine, where the injection timing would not be affected by fuel properties. Another reason which may have caused the increased NO_x emission is the increased cetane number of biodiesel. As the cetane number increased, the ignition delay was shortened which resulted in advanced fuel combustion (Monyem & Gerpen 2001).

Some researchers tested different types of biodiesel fuels and found the correlations between the NO_x emissions and fuel properties, such as the mean carbon chain length and iodine number. Graboski et al. (Graboski et al. 2003) tested different biodiesel fuels derived from different oils in a 11.1litre engine. Their results showed that the NO_x emissions increased as mean carbon chain length decreased, and the NO_x emissions even had a significant linear relationship with the iodine number. However, when the iodine number was lower than 38, the NO_x emissions did not change significantly. Petersonet al. (Peterson et al. 2002) and Tat(Tat 2003) also found that the NO_x emissions increased with higher iodine number and more saturated biodiesel. With engines equipped with common rail injection systems, the effect of biodiesel saturation on NO_x increases was less significant as compared to the older engines (Knothe et al. 2005).

Some methods were developed to compensate for the effect of biodiesel on NO_x emissions. Since the advanced start of injection/combustion caused the increase of NO_x emissions, delaying injection/combustion was proposed in order to reduce the NO_x emissions back to those obtained when using mineral diesel. Leung et al. (Leung et al. 2006)proposed to increase the injection pressure or change the size of some injection pump components, in order to prevent the increases in NO_x emissions without any penalty in particulate matter (PM). Last et al (Last et al. 1995) proposed to delay the start of injection and increase the

EGR rate. Their results showed increases in the NO_x emissions without penalties in both PM and fuel consumption when using biodiesel fuels. Another method proposed by many researchers was to reduce the fuels components with certain undesirable properties, for example, reducing the mean carbon chain length of biodiesel (Chapman et al. 2003), increasing the saturation of biodiesel fuels (Chapman and Boehman 2006;Szybist et al. 2005a; McCormick et al. 2003), using low aromatic content mineral diesel when blending with biodiesel fuels (McCormick et al. 2003), blending anti-oxidation additives in fuels (Melissa A.Hess et al. 2005; McCormick et al. 2003) and using water-biodiesel emulsions (Lin and Shiou-An Lin 2007).

2.4.5. PM Emissions

It is reported by most researchers that PM emissions were reduced significantly when using biodiesel fuels or blend biodiesel in mineral diesel (Monyem & Gerpen 2001; Cardone et al. 2002; Staat and Gateau 1995; Graboski & McCormick 1998; Lapuerta et al. 2002; Wang et al. 2000). Krahl et al. (Krahl et al. 1996)recognized that the reduction in PM emissions when using biodiesel fuels was lower in heavy duty engines than that in light duty engines. This conclusion was also confirmed by (Hansen & Jensen 1997; Lapuerta et al 2002; Bagley et al. 1998). A few researchers found almost the same level (Turrio-Baldassarri et al. 2004) or even a reduced level (Munack et al. 2001; Peterson & Reece 1996; Hansen & Jensen 1997) of PM emissions when using biodiesel fuels as compared to those obtained when using mineral diesel. They attribute this trend to the significant increases in the soluble organic fraction (SOF), which compensates for the reduction in the insoluble fraction or soot. Such an increase in SOF is probably due to the unburned hydrocarbon produced when using biodiesel fuels which have a lower volatility, making it is easier to be condensed and adsorbed on the particle surface. Yamane et al. (Yamane et al. 2001; Haas et al. 2001) optically visualized the fuel

injection from the combustion chamber and observed that the evaporation and fuel/air mixing were slower when using biodiesel compared with that observed when using mineral diesel. They used this to explain the increase in SOF in their tests. Many literatures summarized the relative reduction in different biodiesel blend ratios and found that, in most occasions, the reductions in PM emissions were more effective when using lower biodiesel blend ratios. Haas et al. (Haas et al. 2001) observed a 20% reduction when using 20% biodiesel blends, but only 50% decreasing with neat biodiesel. Both Armas et al. (Armas et al. 2006) and Last et al. (Last et al. 1995) observed that the maximum relative reduction in PM emissions was obtained when a 30% biodiesel blend was used.

Some researchers studied the effect of engine load on PM emissions when using biodiesel fuels and most of them found larger reductions at high loads when using biodiesel fuels (Leung et al 2006; Durbin and Norbeck 2002; Last et al 1995). Leung et al. (Leung et al. 2006) explained that since the particles are mainly formed during the diffusion combustion period and the diffusion combustion period increases at the high load, the oxygen content of biodiesel may be more effective to reduce the PM emissions. Durbin and Norbeck (Durbin & Norbeck, 2002) gave another explanation that the SOF was sharply increased at low load when using biodiesel fuels which compensated for the reductions in PM emissions at low load.

The chemical and physical properties of different types of biodiesel fuels may also affect the reductions in PM emissions. Kado and Kuzmicky (Kado and Kuzmicky 2003) observed lower PM emissions when using biodiesel derived from animal fats than when biodiesel derived from vegetable oil was used. Knothe et al.(Knothe et al. 2005) tested lauric (C12:0), palmitic (C16:0) and oleic (C18:0) methyl esters and found the highest PM emissions when using oleic methyl ester.

The reasons for reduction of PM emissions when using biodiesel fuels are discussed by many researchers:

- The oxygen content of the biodiesel fuels helped to convert carbon to CO/CO_2 in the combustion process, rather than to soot precursors (Dec 1997). Frijters and Baert (Frijters and Baert 2004) tested various biodiesel fuels and found a good correlation between oxygen content and PM emissions. Another issue about the efficiencies of different oxygenated fuel in the reduction of PM emissions was investigated by Mueller et al. (Mueller et al. 2003). They used tri-propylene glycol methyl ester and di-butyl maleate (an ester) and found that the decarboxylation of the ester group directly formed CO_2 and only reduced one carbon atom from the formation of soot precursors, while the oxidation through the C-O bond reduced two carbon atoms in the methyl ester group.
- The air needed for the complete combustion of biodiesel is reduced (Lapuerta et al. 2002), which probably reduced the fuel rich zone in the fuel/air mixture.
- Biodiesel fuels do not contain any aromatics, which are considered as soot precursors (Chang and Gerpen 1997;Heywood 1998; Lapuerta et al. 2002;Schmidt & Gerpen 1996; Wang et al. 2000). Schmidt and Van Gerpen (Schmidt & Van Gerpen 1996) blended Octadecane ($C_{18}H_{38}$) and soybean oil biodiesel (mainly contained C18:1 and C18:2) with mineral diesel respectively for the engine tests. Both of the blends showed significant reductions in PM emissions and the decrease observed when using soybean oil biodiesel blends was more significant than the case of octadecane blends.
- The advanced combustion due to the high cetane number or advanced injection. This effect would prolong the period of soot in the high temperature atmosphere and promote soot oxidation (Cardone et al. 2002;Chang & Van Gerpen 1997). Choiet al.

(Choi and Bower 1997) observed that this effect was more obvious if the start of injection was more advanced.

- The structures of particles are different between biodiesel fuels and mineral diesel. Boehman et al. (Boehman et al. 2005) observed the transmission electron microscopy (TEM) images of soot from 20% soybean oil biodiesel blend and mineral diesel and found that the grapheme segments were more amorphous and disordered arranged in the case of the biodiesel blend, which meant higher reactivity of soot from the biodiesel blend. Their results analysed by thermogravimetric analysis showed that the soot from the biodiesel blend had a lower oxidation temperature. Song et al. (Song et al. 2006) also confirmed the faster oxidation velocity in the case of biodiesel soot from TEM images. The oxidation velocity of biodiesel soot was up to six times faster than the case of mineral diesel soot (Jung et al. 2006).
- The Sulphur free nature of biodiesel fuels reduced the sulphate formation, which was one of the major types of PM (Choi & Bower 1997; Lapuerta et al. 2002;W.G.Wang, Lyons et al. 2000). In addition, sulphur was commonly an active centre for unburned hydrocarbon adsorption which resulted in soot formation (Durán et al. 2006). However, as sulphur content reduced dramatically in diesel fuels in the market, the importance of this reason became less.
- The lower final boiling point of biodiesel fuels resulted in the biodiesel becoming more easily vaporized which provided less possibility of forming soot or tar (Lapuerta et al. 2002).

Particle size distributions have also been investigated by many researchers because the small particles are more harmful to the environment and respiratory system of human beings and they are more difficult to be filtered or trapped by aftertreatment systems. The majority of

researchers reported that the number of nucleation mode particles increased and the number of accumulation mode particles decreased when using biodiesel fuels. Chuepeng et al.(Chuepeng et al. 2011) testeda modern V6 turbocharged engine using 30% rapeseed oil biodiesel blends and found that the number and mass of nucleation mode particles were higher in most of the engine conditions while the size of nucleation mode particles was reduced in all the engine conditions. For the accumulation mode particles in their tests, the B30 aerosol showed smaller particle size and number in most of the engine conditions and the total particle mas was always higher. Krahl et al. (Krahl et al. 2004.) tested biodiesel fuels derived from soybean oil, rapeseed oil and palm oil and observed increasing particle number in the sizes below 30nm or 40nm. Some researchers observed a global reduction in particle number and size, but did not find significant increases in the small particle concentration (M. Lapuerta, J.Rodríguez-Fernández& John R.Agudelo 2008;Susan T.Bagley, Linda D.Gratz, John H.Johnson, & Joseph F.McDonald 1998). A few studies even showed decreases in the concentration of small particles.

2.4.6. Total Hydrocarbons

Almost all the researchers found sharp decreases in THC emissions when using biodiesel fuels or their blends. The highest reduction in all the literature reviewed of THC emissions was up to 75% when neat soybean oil biodiesel was used by Last et al.. According to the report by EPA, biodiesel blends with lower blend ratios were more effective than those with higher blend ratios. Last et al. (Last et al. 1995) tested 10%, 20% and 100% soybean oil biodiesel in a heavy duty engine and their results showed that the THC emissions reduced by 28%, 32% and 75%, respectively, thus higher relative reductions occurred with lower biodiesel blend ratio. Meanwhile, the THC reduction with biodiesel fuels were also confirmed to be affected by many other parameters, such as the injection pressure (Leung, Luo, & Chan

2006), the presence of an oxidative catalytic convertor (Munack et al. 2001;Aakko et al. 2002) and the quality of reference diesel fuel (Assessment and Standards Division (Office of Transportation and Air Quality of the US Environmental Protection Agency) 2002;Krahl et al.. 2003). The effect of injection pressure combined with using biodiesel fuels was studied by Leung et al. (Leung et al. 2006) and they observed increasing THC with both diesel and biodiesel fuels when injection pressure was increased. Krah et al. (Krahl et al 2005)observed reductions of up to 40% when comparing biodiesel fuels with conventional diesel, and reductions of around 20% if the reference fuel was changed to a high cetane, ultra-low sulphur and low aromatic diesel.

The correlation between fuel properties and THC emissions was also investigated by many researchers. Groboski et al. (Graboski et al. 2003) tested different methyl esters and observed higher reductions in THC emissions as the carbon chain length or the saturation of the fuels was increased. Knothe et al. (Knothe et al. 2005) showed the same trend as the carbon chain length increased, but did not find any trend about the saturation of the fuel.

The reasons for the reductions in THC emissions when using biodiesel fuels were discussed by many researchers, and are as follows:

- The oxygen content in the biodiesel fuels promoted more complete combustion (Pinto et al. 2005).
- The higher final distillation points of biodiesel fuels lead to better vaporization and combustion for the final fraction of biodiesel fuels, thereby decreasing the THC emissions (Turrio-Baldassarri et al. 2004; Murillo et al. 2007).

- The start of injection and combustion was advanced when using biodiesel fuels. Storey et al. (Storey et al. 2005) confirmed that the more advanced the fuel injection, the lower the THC emissions.
- The THC emissions were normally analysed by the flame ionization detector (FID). This technique may have lower sensitivity when measuring oxygenated compounds produced by oxygenated biodiesel fuels (Rakopoulos et al. 2007;Hansen & Jensen 1997).
- The sample line for the detector is normally heated up to 191°C to prevent hydrocarbon condensation. However, the higher molecule weights and less volatile components of biodiesel fuels normally produced hydrocarbons with higher molecule weights and boiling points compared with the cases of mineral diesel. Therefore, 191°C may not be high enough to prevent the hydrocarbon condensation in the sample line (Hansen & Jensen 1997;Schmidt & Van Gerpen 1996;Scholl and Sonrenson 1993).
- More hydrocarbons produced using biodiesel fuels were adsorbed onto the particles. Chang and Van Gerpen (Chang and Van Gerpen 1998) investigated the hydrocarbon adsorption on the particles by modelling and predicted that 13%-29% of the hydrocarbons produced by using biodiesel fuels were absorbed onto the particles while only 1% were absorbed in the case of mineral diesel. Since the total reduction of THC emissions when using biodiesel fuels was 50% in their experimental work, the adsorption of THC only partly explains the total reduction when using biodiesel fuels.

2.4.7. Carbon Monoxide

The CO emissions were found to reduce when using biodiesel fuels according to most researchers (Pinto et al 2005; Ramadhas 2011;Assessment and Standards Division (Office of Transportation and Air Quality of the US Environmental Protection Agency) 2002;Hansen et al. 2005). In some research studies, the trend of CO reduction was found to be linear with oxygen content (Ullman et al. 1994) or biodiesel blend ratio (Graboski & McCormick 1998). In the results from Knotheet al. (Knothe et al. 2005), the CO emissions were reduced as the carbon chain length increased. Hamasaki et al. (Hamasaki et al. 2001) tested various biodiesel fuels with different acid values and reported lower CO emissions as the acid value was increased. They attributed this trend to the higher hydroperoxide concentration due to its higher acid value. Again, the engine load conditions would affect the CO reduction when using biodiesel fuels. It has been confirmed by many researchers that the CO reductions were significant at high load but no remarkable decreases and even some increases were observed at low load (Choi & Bower 1997; Silva et al. 2003).

The common reasons used to explain the CO reductions when using biodiesel fuels are given as follows:

- Biodiesel contains oxygen in its molecules promoting the combustion (Pinto et al 2005; Wedel 1999;Ullman et al. 1994). Ullman et al. (Ullman et al. 1994) designed some tests to assess the effects of aromatic content, oxygen content and cetane number of fuel, respectively, on CO emissions. They found a good linear relationship between CO emissions and oxygen content/cetane number.
- Biodiesel fuels always have higher cetane numbers, which were confirmed to reduce the CO emissions in (Ullman et al. 1994). Sharp (Sharp 1994) also confirmed this

trend by adding a cetane enhancer to 20% biodiesel blends which resulted in the lowest CO emissions compared with the cases of mineral diesel and 20% biodiesel blends without additives.

- The advanced start of injection and combustion, which has been mentioned in previous sections. The results form Storey et al. (Storey et al. 2005) showed that the CO emissions were reduced when the start of injection was advanced.

2.4.8. Non-Regulated Emissions

2.4.8.1.Aromatics and Polyaromatics

Aromatic and polyaromatic compounds are toxic and confirmed to lead to genetic mutation and cancer. It is very difficult to predict their mutagenic and carcinogenic effects since they are formed by various types of polyaromatic hydrocarbons (PAHs) with different mixing methods. Most researchers reported that the PAH emissions reduced when using biodiesel fuels (Pinto et al 2005;Cardone et al. 2002;Graboski & McCormick 1998) due to the absence of PAH in biodiesel fuels or the enhanced adsorption of PAH on the particles when using biodiesel fuels (Kado et al. 1996; Turrio-Baldassarri eta l. 2004). Hasen and Jensen (Hansen & Jensen 1997) compared 15 PAHs from the emissions when mineral diesel and rapeseed oil biodiesel were used. They only found phenanthrene when using biodiesel and it was 8 times lower that of using mineral diesel.

2.4.8.2.Oxygenated Compounds

There are also some oxygenated compounds in the engine emissions and they are thought to be precursors of ozone formation in the troposphere. Some researchers believe that the oxygenated compounds would be increased when using biodiesel fuels due to the oxygen content in the biodiesel fuels (Pinto et al 2005; Staat & Gateau 1995;Tritthart and Zelenka

1990). However, many other researchers observed that the oxygenated compounds decreased or they observed no significant differences (Munack, et al. 2001;Assessment and Standards Division (Office of Transportation and Air Quality of the US Environmental Protection Agency) 2002;Sharp et al. 2000). They argued that the decomposition of esters through decarboxylation reduced the possibility to form oxygenated combustion intermediates as compared to that of using mineral diesel. Some researchers found correlation between glycerine content in biodiesel fuels and acrolein concentration in the emissions (Staat & Gateau 1995;Graboski & McCormick 1998).

2.5. USING BIODIESELS IN COLD START

2.5.1. Cold Start Phenomena and Cold Start Issues

The instantaneous engine emissions during cold start can be divided into two different periods: a first period with increasing then decreasing emissions because of the progressive change of the engine speed or catalyst temperature, followed by a period when the engine is running at a stable idling (Jean-Marc Andréand Robert JOUMARD 2005). The excess emissions during cold start can be measured from either a chassis dynamometer or engine dynamometer and subsequently be collected in exhaust samples bags. Misfire is a significant problem at cold start. It can be identified when the instantaneous engine speed at the end of the exhaust stroke is lower than that at the start of the intake stroke. Another easy way to identify the misfiring of the engine is to check the in-cylinder pressure and ROHR. When the engine is cranked to a certain speed, a large quantity of fuel is injected to ensure successful firing and that enough energy is present in the system so that a high in-cylinder pressure can be achieved enabling the cold start frictions during the first several cycles to be overcome. Figure 2.4shows the engine speed and in-cylinder pressure during cold start at 20°C.

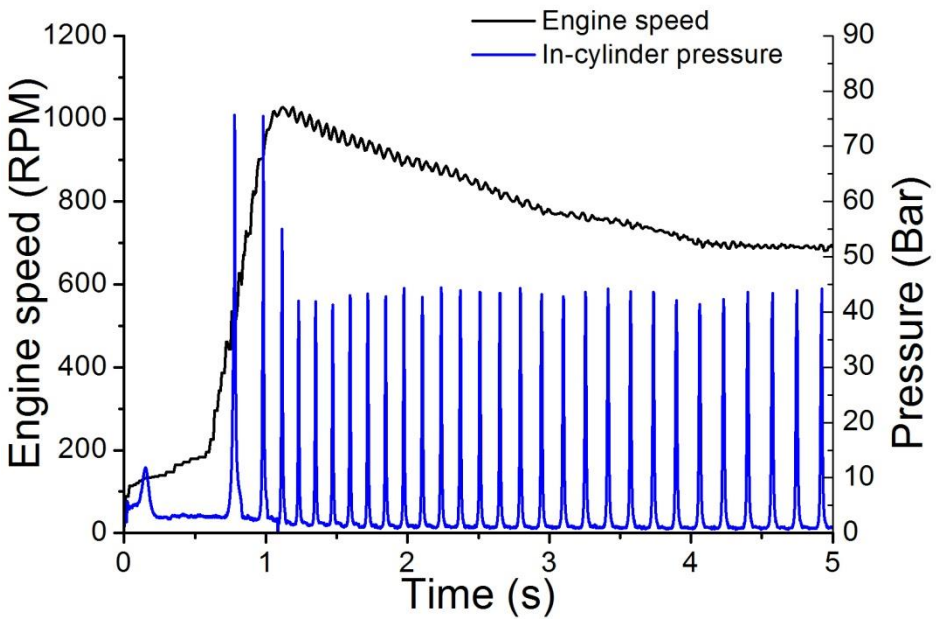

Figure 2.4Typical engine speed and in-cylinder pressure during cold start

When a vehicle is kept outside overnight in cold ambient temperatures, the temperature drop of the engine will cause a lot of problems. The low temperature of the engine oil results in the viscosity increasing and less efficiency of the lubrication which leads to a friction increase and a reduction in the cranking speed. When the engine is started, the air temperature in the cylinder and intake manifold is much lower than that during any other engine operation mode. The low temperature of cylinder wall and pistons also causes excessive heat losses and blow-by losses. All the above effects reduce the compression temperatures and pressures which results in poor fuel evaporation and mixing with air. Moreover, battery performance also decreases at low temperatures. Smaller cars with downsized engines have smaller displacement volumes and lead to lower compression ratios therefore resulting in an incomplete combustion. The combustion instability causes rough operation and high noise during engine start. Figure 2.5 shows the relationship between the parameters influencing the cold starting of the engine(Last et al. 2008).

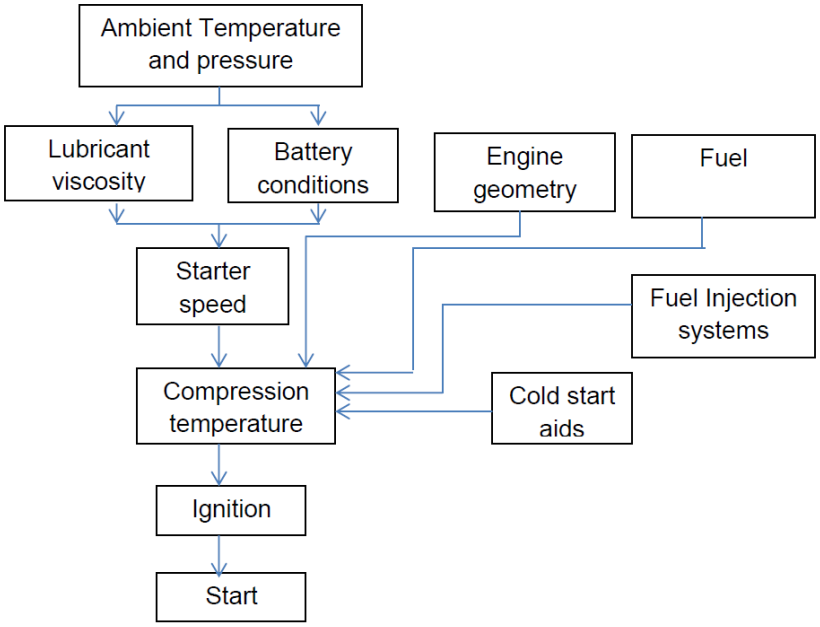

Figure 2.5Relationship between the parameters for engine cold start (Last, 2008)

The desirable characteristics of cold start are for the engine to be fired at the first cycle with minimum noise, avoid misfire/poor combustion cycles and reach a stable idle speed within the minimum number of cycles. Han et al. analysed the combustion instability of a diesel engine during cold start at various ambient temperatures and observed that combustion instability increased when the ambient temperature were reduced(Han et al. 2001). Cycle-by-cycle analysis of in-cylinder pressure (Figure 2.6) showed that the number of misfiring cycles was increased with the reduction in ambient temperature. They attributed the instability to the early fuel injection at very low temperatures which may result in the liquid fuel droplet adsorbing on the cold walls and hinder fuel vapour formation and mixing with the air. They also observed a sharper rate of pressure rise as the engine fired after many misfiring cycles, due to the accumulated residual fuel in the cylinder. Alt et al.(Alt et al. 2005) found a good correlation between cold start noise and the start of fuel injection. They proposed to optimize the cold start noise by recalibrating the start of fuel injection.

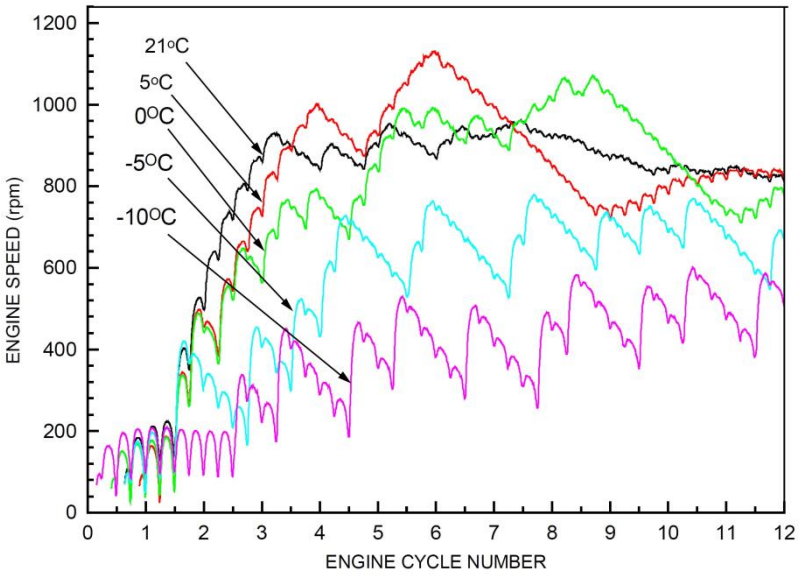

Figure 2.6Combustion stability of diesel engines during cold start at varying ambient conditions(Han, 2001)

Engine emissions during cold start generally increase as ambient temperatures decrease. Weilenmann et al. conducted the engine tests of urban driving cycles at different ambient temperatures of -7, 10 and 23ºC. They reported that CO and HC emissions were increased when the ambient temperature was decreased. They also found a significant linear relationship between the ambient temperature and cold start emissions. Armas et al. evaluated the pollutants emissions in the cold/warm start tests when using diesel, biodiesel and GTL (Armas et al. 2013). They reported that all the emissions were higher during cold start than during warm start in all the cases.

The efficiency of the catalyst during cold start was also investigated by some researchers. Blackwood et al. studied the efficiency of the diesel oxidation catalyst (DOC) during cold start and reported that the DOC could not oxidize CO and THC emissions during engine start and idle conditions due to the low exhaust temperature. However, the particulates in the exhaust were deposited on the surface of catalyst during cold start. Blackwood et al. (Blackwood 1998) conducted some tests on a modern light-duty diesel engine. The tests were

designed from a stepped cold start to three steady state conditions of idle, 10 and 15kW, respectively. They found that the oxidation catalytic converter acted as a particulate trap during the cold start. The ratio of deposition was higher at the idle condition and low speed conditions as compared to the cases at the high speed conditions(Andrews et al. 2000).

2.5.2. Effects of Fuel Properties on Cold Start

The composition of mineral diesel was determined by the origin of the crude oil and the formulation which varies with different refineries. The fuels also contain mandatory additives to meet the required government regulated fuel specifications. In addition, some additives are used to improve the quality of fuels for brand marketing. Meanwhile, part of the mineral diesel in fuel stations is allowed to be substituted for biodiesel. As reviewed in the previous section, biodiesel fuels show various properties depending on the feedstock. The different fuel properties will lead to different performance and emissions in engine start and warm up. Important fuel properties such as density, viscosity, volatility, cloud point cold filter plugging point and cetane number have effects on fuel injection and on the preparation of an air-fuel mixture suitable for auto-ignition (Owen 1995). The heavy fraction in the fuel influences the fuel atomization while the light fraction improves cold temperature performance. Low volatility compositions in the fuel improve fuel vaporization and make the engine easier to be started at cold ambient conditions.

Starck et al. (Starck 2010)studied the effect of fuel volatility and cetane number at -25°C cold start with various compression ratios (16 to 14) and reported that the increases in cetane number and volatility would improve the cold start performance. In addition, the viscosity of the fuel was increased at cold ambient conditions and resulted in pumping losses in the fuel injector.

Fuel with a low cetane number can increase the ignition delay and cause a higher pressure rise rate at engine start. Hara et al. conducted several tests on a single cylinder, direct-injection diesel engine in a cold cell at ambient temperatures varying from -5ºC to 25ºC to investigate the effects of a cetane improver and iso-octyl nitrate (ION) on cold start performances. They reported that the fuels with higher cetane number improved the engine cold start performance. For the fuels with added ION additives, they did not find significant differences in the engine cold start with the cases of using regular fuels at ambient temperature above 5ºC(Figure 2.7) (Hara et al. 1999). Wong et al.(Wong and D.E.Steere 1982) studied the effect of a cetane improver named 2-ethyl hexyl nitrate on ignition delay in an engine partially warmed up. They found that the ignition delay was not changed significantly with the cetane improver blended into the fuel. This was also confirmed by Sutton and Mitchell in a warmed up engine(Sutton 1986;Mitchell 1993) .

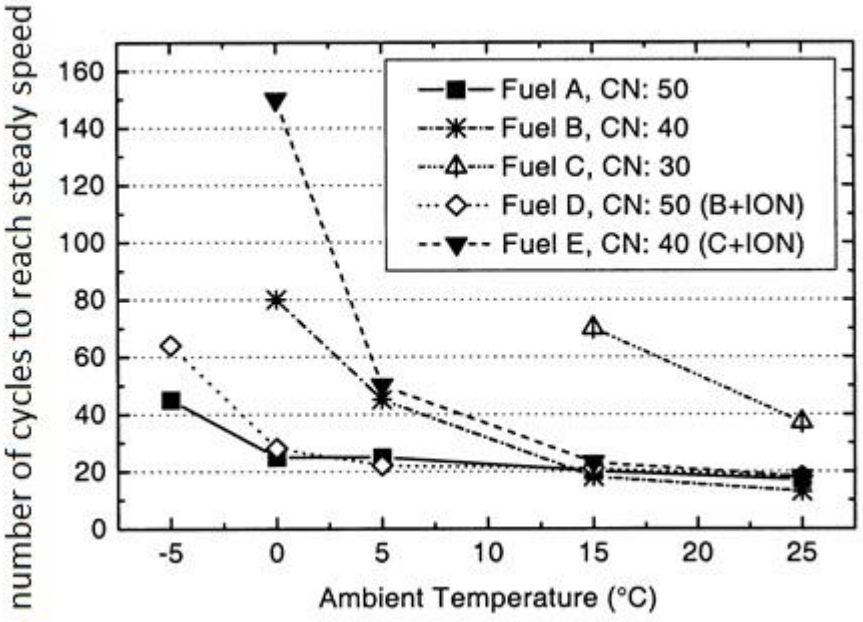

Figure 2.7Engine startability with respect to fuel(Hara 1999)

Mann et al. (Mann, 1999) conducted cold start tests in two heavy duty engines; one was a Euro II engine and the other one was an engine controlled by an ECU without any cold start

aid, in order to study effects of the fuel properties. They reported that the ECU controlled engine was improved in all aspects regarding engine performance and emissions during low temperature cold start. They found that the cetane number was the dominant fuel parameter which affected the cold start performance at low ambient temperatures, and the use of a cetane improver could reduce the THC emissions.

Liu et al. (Liu et al. 2003) reported that the reduction in the cetane number from 50 could result in a significant increase in ignition delay and this effect would be less when the cetane number ranged between 50 to 60. Clerc et al. (Clerc 1986) investigated the effect of cetane number (ranging from 26-61) during cold start in light duty vehicles and reported that the vehicles were relatively insensitive to the changes in cetane number when it was above 40.

Kitanon et al.(Kitanon et al. 2006)conducted experiments in a low compression ratio diesel engine to investigate the effects of fuel properties on the cold start performance and emissions. They blended high cetane number fuels with Gas-to-Liquid (GTL) fuel in order to auto-ignite the air-fuel mixture more easily at low compression pressures and temperatures. They found that the fuels with higher cetane number could reduce the start time and improve the engine stability during start. However, at very low temperature, fuel volatility became the dominant factor affecting the performance during cold start, even when the high cetane number fuels were used.

The chemical compositions of fuel also have an influence on their cold flow characteristics. Paraffinic content in the fuel causes it to readily form a wax in low temperatures which blocks the fuel line(Owen et al. 1995). Aromatic and naphthenic contents have a better cold flow characteristic but with the penalty of a low cetane number. If the fuel cooling is continuous, crystals begin to be separated and a cloud/haze appears; the temperature at which

this happens is known as the cloud point. If the fuel is further cooled beyond the cloud point, waxes begin to form and agglomerate. The temperature at which waxes begin to cover the filter and block the fuel delivery line is called the Cold Filter Plugging Point (CFPP). The CFPP is limited to fuels sold in cold climates and arctic zones(ATC(the Technical Committee of Petroleum Additive Manufacturers in Europe) 2013).

Cold flow characteristics of fuel can be improved, i.e. by reducing the CFPP and by adding cold flow improvers. The most common flow improvers are copolymers based on ethylene-vinyl acetate monomers ($C_{18}H_{30}O_6X_2$)(BP 2002), and amines and amides(Chevron 2012). Winter diesel is also designed and manufactured for severe winter or arctic regions. The specification of winter diesel meeting EN 590 is given in Table 2.6.

Table 2.6 Arctic and severe winter climate fuel requirements(BSI 2013)

Property	Units	Limits					Test method
		Class 0	Class 1	Class 2	Class 3	Class 4	
CFPP	ºC, max	-20	-26	-32	-38	-44	EN 116
Cloud point	ºC, max	-10	-16	-22	-28	-34	EN 23015
Density	kg/m^3, min-max	800 -845	800-845	800-840	800-840	800-840	EN ISO 3675
Viscosity	cSt, min-max	1.5-4.0	1.5- 4.0	1.5- 4.0	1.4-4.0	1.2-4.0	EN ISO 3104
Cetane number	min	49	49	48	47	47	EN ISO 5165
Cetane index	min	46	46	46	43	43	EN ISO 4264
Distillation % recovered at 180°C	% (v/v) max	10	10	10	10	10	EN ISO 3465
% v/v recovered at 340°C	% (v/v) min	95	95	95	95	95	

2.5.3. Biodiesel in Cold Start

Biodiesel is a renewable alternative fuel which can be fully or partially substituted for mineral diesel. The biodiesel properties and their effects on engine performance and emissions were

reviewed in the previous sections. Since different feedstocks are used to produce biodiesel fuels, they have different cold flow properties and consequently they have different impacts on the cold flow properties of the final diesel blend(UNECE 2009). The different effects on the cold flow properties of biodiesel fuels have been studied by (Ma 1999, 2001, NREL 2004, Cetinkaya 2005, Joshi 2007, Tang 2008, Sarin 2010).

Table 2.7 Typical cold flow properties of biodiesel from different feed stocks(UNECE 2009)

Feedstock	Cloud point (°C)	CFPP (°C)	Viscosity (cSt)
Rapeseed	-5	-18 to -12	5.0
Sunflower	-1 to +3	-7 to -3	4.4
Soybean	-7 to +3	-6 to -2	4.0
Coconut	9 to 12	8	4.8
Palm	13 to 16	5 to 11	4.3 to 5.0
Tallow	10 to 20	9 to 14	4.8

Tang et al. studied the fuel properties and precipitate formation of different biodiesels at low temperatures (Tang 2008). They reported that store temperature and duration, biodiesel blend ratio and feedstock affected the mass of precipitate. They found that the precipitate formation was increased when the store temperature decreased. Starck et al. developed a methodology to evaluate the performance of diesel engine coldstart and then they used this methodology to assess the impact of different fuels. Their engine tests were conducted at -25ºC on a common rail, four-cylinder Euro 4 diesel engine. They reported that the use of biodiesel increased the start delay and opacity number of emissions. However after injection strategies optimization,

the performance of using biodiesel fuel became much closer to that obtained when using diesel fuel.(Starck 2011)

Armas et al. tested vegetable oil methyl ester during cold and warm start and reported that biodiesel content reduced the smoke opacity due to the oxygen molecule content and the absence of aromatics (Armas et al. 2006). The regulated and unregulated gaseous emissions of biodiesel fuels during cold start were also investigated by Lea-Langton (Lea-Langton et al. 2009). They started the engine from cold and reached the required load without an idling period. Their results showed that the THC and CO emissions obtained when using biodiesel were reduced at the low target power and they were almost identical with those of mineral diesel at the high target power. On the contrary, formaldehyde emission, the predominant aldehyde obtained using biodiesel, showed similar trends as that of mineral diesel at the low target power.

2.6. CONCLUSIONS

Fuel properties have significant influences on fuel storage, the fuel supply system, the injection system and the engine combustion and thus they affect the performance and emissions of the engine both at the start and steady state conditions. Biodiesel fuels can be produced from various feedstocks and show different properties. Investigating the correlation between fuel properties and engine emissions is helpful to reduce engine calibration work and choose suitable streams of refinery components and performance enhancement additives. However, there is not any model to predict the relationship in the literatures. Proposing a validated model is necessary. Meanwhile using biodiesels may cause some problems due to the high viscosity and CFPP, especially ambient temperature at minus degree. The physical

and chemical analysis of particles at start conditions can reveal the particle sources and formation preferences during start which cannot be found in the literatures.

Chaper 3. EXPERIMENTAL SETUP AND FACILITY

This chapter introduces the experimental facilities which were used in this study. A modern V6 3.0-litre CRDI twin turbocharged and intercooled diesel engine was used. The engine was tested withtwo different operating systems, shown in figures3.1 and 3.2. One is the Cadet V14 operating system from CP engineering with an eddy-current water-cooled dynamometer provided by the Dynamometer Services Group Limited (DSG Ltd); which can be called the steady test cell. The other one is the Puma operating system with an AVL AC machine capable dynamometer provided by AVL, which is called the cold test cell. The steady test cell was initially designed for steady state engine testing. The room temperature could be maintained at 25˚C even when the engine was fully warmed up and running at full load. The cold start tests at 25˚C were also conducted in this test cell. The cold test cell was more functional than the steady test cell. A more powerful dynamometer provided the ability to run transient tests. The cooling system in the cold test cell could keep the engine running at -20˚C conditions for 3minutes idling and -7˚C conditions for a whole NEDC. Details are described in this chapter. The emission measurement equipment is also introduced in this chapter. For example, the Horiba MEXA7100DEGRand AVL smoke meter for steady state measurement, and the AVL i60, Cambustion fast FID/NOx and DMS500 for transient measurement.

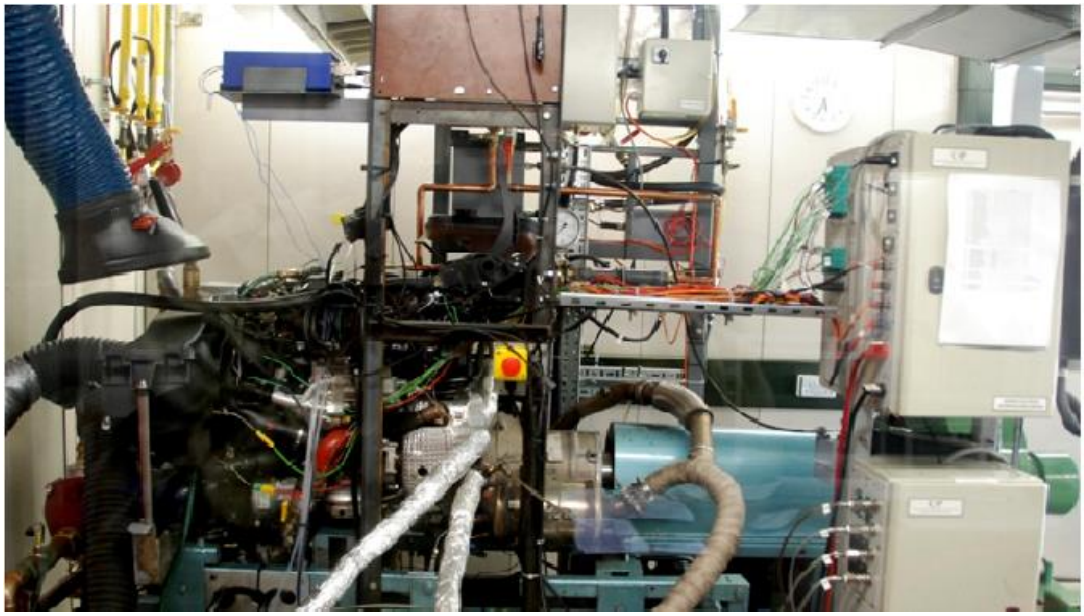

Figure 3.1Picture of steady test cell

Figure 3.2Picture of cold test cell

3.1. ENGINE SPECIFICATION

All the experiments were conducted in a modern V6 3.0litre diesel engine, with twin-turbocharger, water cooling system and common rail direct injection system. The engine was equipped with a cooled EGR system, and a variable geometry turbocharger for better performance and emissions. A split injection strategy consisting of two pilot injections, a main injection and a post injection was employed at medium loads to attain better engine performance. Table 3.1, and Figure 3.3 and 3.4 show the engine specifications, engine layout and the power curve of the engine, respectively.

To maintain stability, air inlet temperature, engine coolant temperature and fuel temperature were maintained at constant values. Ambient relative humidity was monitored and kept approximately between 35 and 40%. An AVL optical encoder with 720-degree resolution was fixed on the crankshaft to trigger the in-cylinder pressure measurements.

Table 3.1 Experimental engine specifications

Bore	84.0 mm
Stroke	90.0 mm
Displacement	2993 cm^3
Maximum torque	600 Nm @ 2000 rpm
Maximum power	199.1 kW @ 4000 rpm
Compression ratio	16.1:1
Connecting rod length	160.0 mm

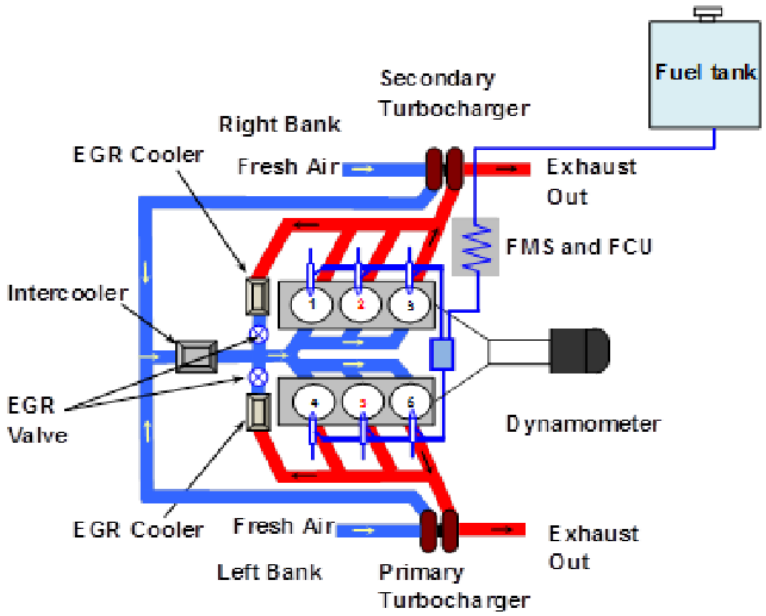

Figure 3.3The layout of the engine test setup

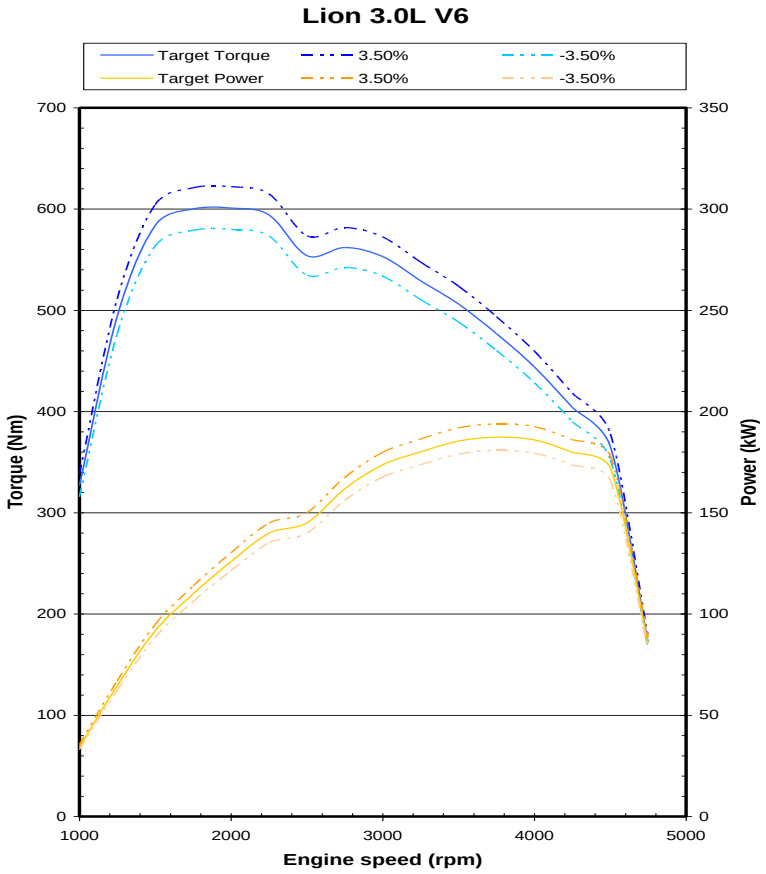

Figure 3.4The engine power curve

3.2. OPERATING AND CONTROL SYSTEMS IN STEADY TEST CELL

3.2.1. Dynamometer

The engine was loaded by an eddy-current type water-cooled Schenck dynamometer model W230 from Dynamometer Services Group Limited (DSG Ltd). Some specifications and (absorbed) performance curve for the dynamometer are listed and indicated in Table 3.2 and Figure 3.5 respectively. The dynamometer was chosen to cover the full engine speed and torque range (see Figure 3.4 and 3.5).

Table 3.2 Dynamometer specification in the steady test cell

Model	W230
Rated torque	750 Nm
Maximum speed	7500 rpm
Power	230 kW
Moment of inertia	0.53 kgm^2
Torsional stiffness	0.593×10^6 Nm/rad
Weight	480 kg

.

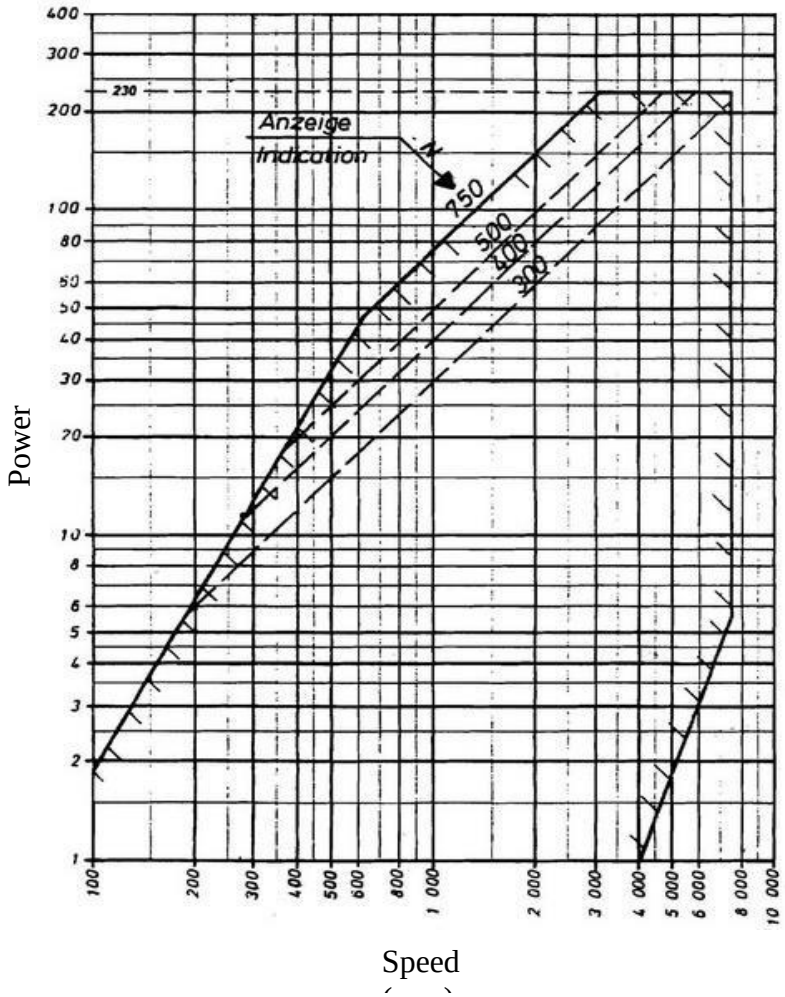

Figure 3.5 Engine dynamometer performance curve from DSG Ltd

3.2.2. The Engine Operating System

The dynamometer speed and torque could be automatically or manually controlled by the Cadet software from CP engineering. An actuator was also connected to the Cadet electric box to control the engine speed. A PID control for the actuator was set in the Cadet system to control the throttle position to obtain the target engine speed and torque. The temperatures of the engine coolant and air inlet after the turbocharger were also maintained at the target temperatures. A FMS1000 fuel measuring system combined with a FCU1000 fuel cooling unit from CP Engineering were applied to measure the fuel consumption and maintain the fuel

temperature at 25°C. The ventilation system in the test cell could maintain the room temperature at 25°C, even if the engine was running at full load.

The engine operating behaviours, such as injection strategies, EGR rate and boost pressures were controlled by the settings in an Electrical Control Unit (ECU). The ECU was connected to a computer through a CAN card and could be read and controlled through INCA software provided by ETAS. The INCA software was able to communicate with Cadet System through an Ethernet cable.

In-cylinder pressure was measured by a piezo-electric pressure transducer and the cycle-by-cycle data was recorded and processed by the AVL indicom software and hardware. The Exhaust gas smoke average number was measured by an AVL smoke meter. The Cadet system was connected to the indicom system and smoke meter through a series cable and it was used to control their measuring and recording. A Horiba MEXA7100DEGR was used to measure the other compositions of the exhaust gas such as NO_x, THC, CO and CO_2, and it sent the measurements to the Cadet System through an Ethernet cable. There were also some thermocouples and pressure transducers connected to the Cadet electric box which provided temperatures and pressures in some important parts of the engine. With all the control and measurement systems and equipment connected with the Cadet System, shown in figure 3.6, the engine tests and data recording could be automatically operated by the Cadet System; something which reduced the impact of human mistakes on the results.

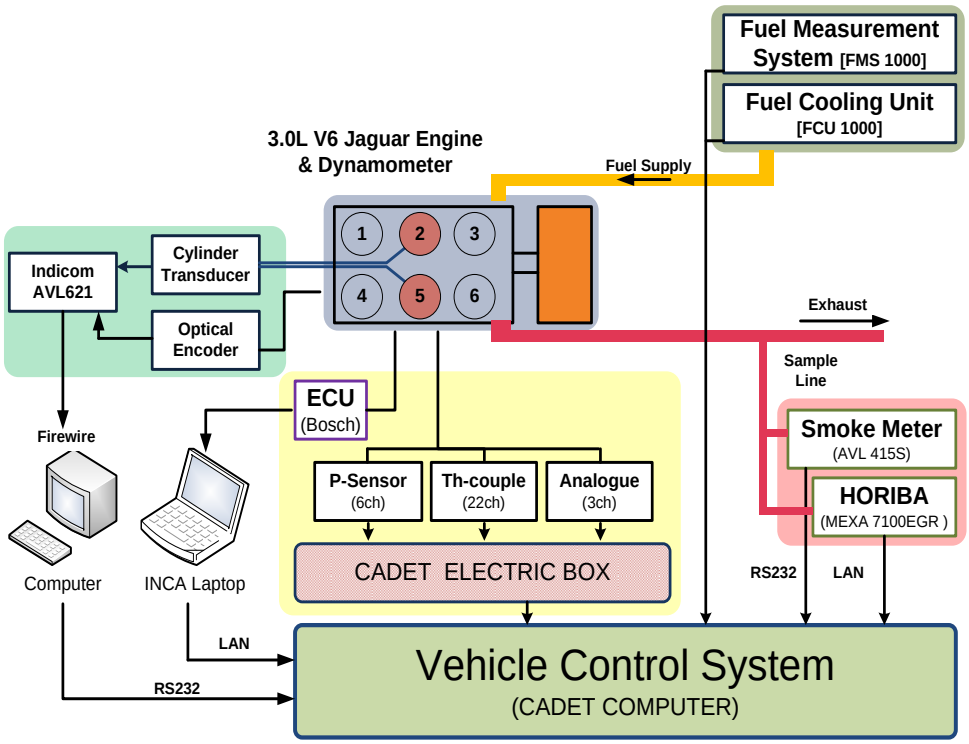

Figure 3.6Diagnostics arrangement of the test engine

3.2.3. Engine Cooling Systems

There were two individual cooling systems for engine coolant and air after the turbocharger. Figure 3.7 shows the schematic diagram of engine coolant cooling systems. The heat exchanger was from Bowman Ltd, model GL 320. Plant water was supplied as a heat absorber. In the Bowman heat exchanger, the plant water flow was opposite to the engine coolant flow due to the high efficiency of heat exchange within the counter-flow regime. The water flow in the pipe was controlled by a 3-way valve from the Honeywell Company. The actuator on the 3-way valve was adjusted by a digital controller using compressed air. Therefore, the valve open rate was controlled based on the signal provided by the measurement of engine coolant-out temperature.

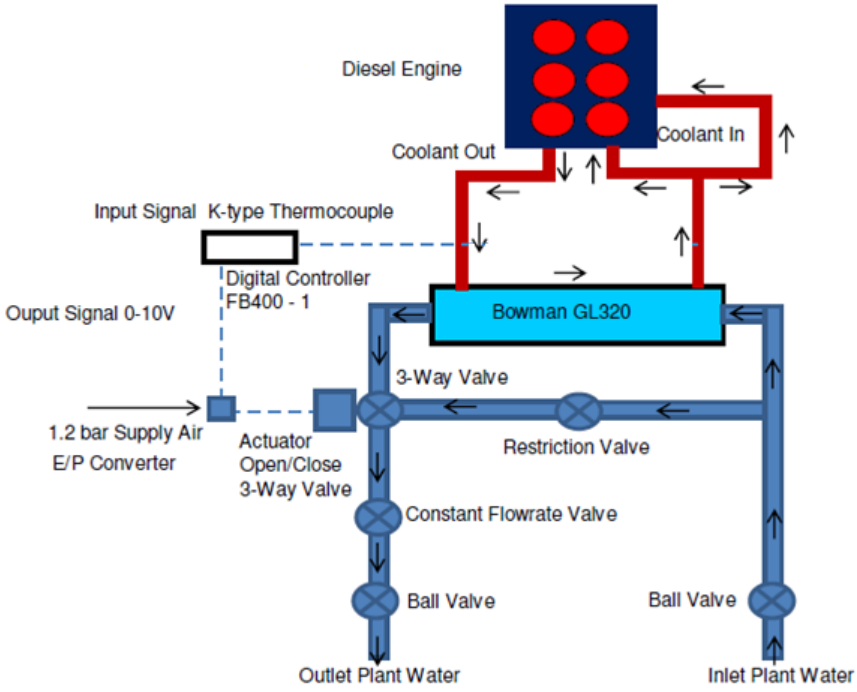

Figure 3.7Schematic of cooling control system for engine coolant in the steady test cell

The intercooler system for air after the turbochargers is almost the same as the engine coolant cooling system. The charged air is cooled by the same plant water with counter-flow using the 3-way valve to control the water flow rate. The only difference is that the heat exchanger in the intercooler system allows higher maximum flow rate.

3.2.4. Fuel Measuring System (FMS) and Fuel Cooling System (FCU)

Figure 3.8 shows the schematic diagram of the FMS1000 and FCU1000. The FMS1000 system was controlled and monitored by CADETV12. The software could also record and display the data obtained on the computer. The system used a 20N load cell to measure the consumed fuel. The 20N load cell could neutralize any vibration, as the construction was stiff and had no moving parts. A small fuel cell with a volume of 1 litre was mounted at the top of the 20N load cell. During the measuring process, CADETV12 closed the solenoid valve so that fuel was taken only from the small fuel cell. After a short settling period, the net mass of fuel taken from the fuel cell was measured. The sample data and the averaged value were sent

to the Cadet system at a rate of up to 10 Hz. During the steady state tests, the Cadet System calculated the brake specific fuel consumption (BSFC). The FMS-1000 was also capable of monitoring fuel during the transient conditions, for a specific time as short as 100 ms.

The fuel cooling unit (FCU) was used to control the temperature of fuel supplied to the engine. The temperature of the returned fuel was normally between the temperatures of 35 and80°C depending on the engine load. As the return fuel was piped back to the fuel measurement unit, the fresh and return fuel mixed together. The mixed fuel was then pumped through one or more heat exchangers before it was injected into the engine cylinder. In this test cell, two Bowman heat exchangers using plant water were used. When heating was required, a 3kW heater fitted in the header tank was activated by the control system. When cooling was required, two solenoid valves operating in tandem were operated to allow the plant water through the heat exchanger. The plant water temperature in the header tank was monitored by a PRT.

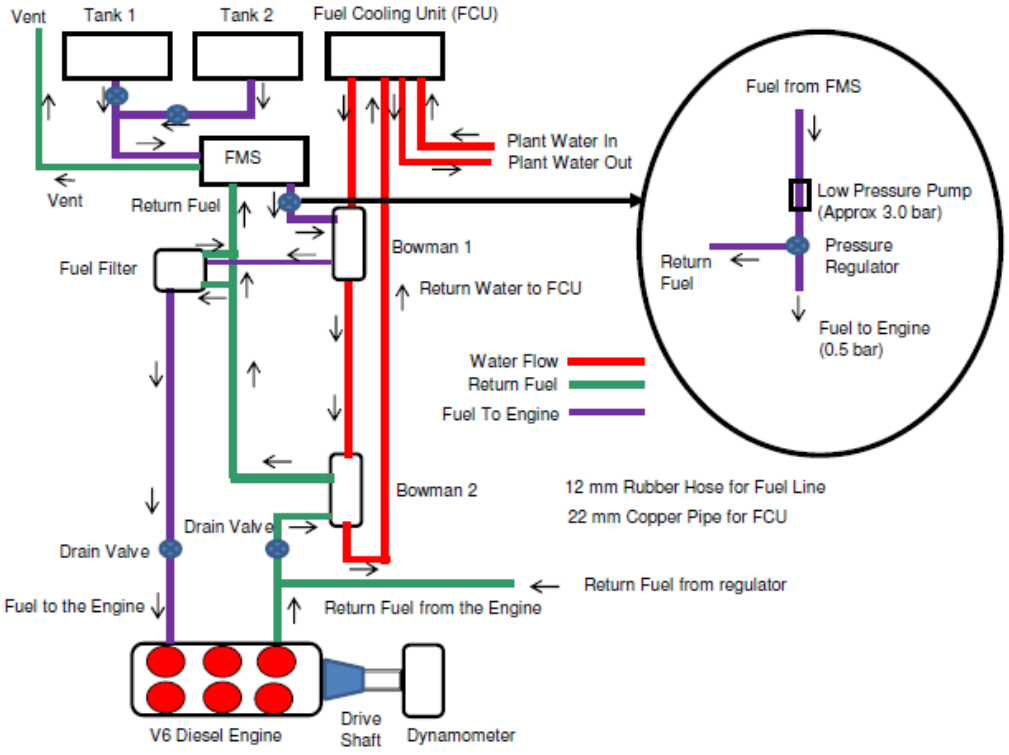

Figure 3.8The schematic of the FMS and FCU system arrangement in the steady test cell

3.3. OPERATING AND CONTROL SYSTEM IN COLD TEST CELL

The cold test cell was designed for cold start study with the following capacities:

1. To maintain the fuel temperature at -7 and -20°C for a whole New European Driving Cycle (NEDC) and 3 minutes idling, respectively.
2. To cool down the temperatures of the engine coolant, oil and the environment of the surrounding engine to -7 or -20°C through a whole night of soaking.
3. Engine and Dynamometer Control system capable of full simulation of the downstream transient duty as seen by the engine, including driving cycles, for example, NEDC and FTP75.

3.3.1. Dynamometer

The cold chamber transient test facility at the University of Birmingham is a unique testing facility in the United Kingdom, and it was used for this study. The dynamometer used in this test cell was an AVL foot mounted AC machine with squirrel cage rotor. For the supply and control of the AC drive and auxiliary devices, a control cabinet was connected directly to the main supply to allow the execution of torque and speed control loops. Table 3.3 and figure 3.9 show some of the specifications and the (absorbed) performance curve for the dynamometer.

Table 3.3 Dynamometer specification in cold test cell

Model	Dynodur 270
Nominal torque	485 Nm
Maximum speed	10,000 rpm
Nominal power	270 kW
Moment of inertia	0.31 kgm^2
Coolant	Forced air cooling, air quantity approx. 2,200m^3/h
Weight	700 kg

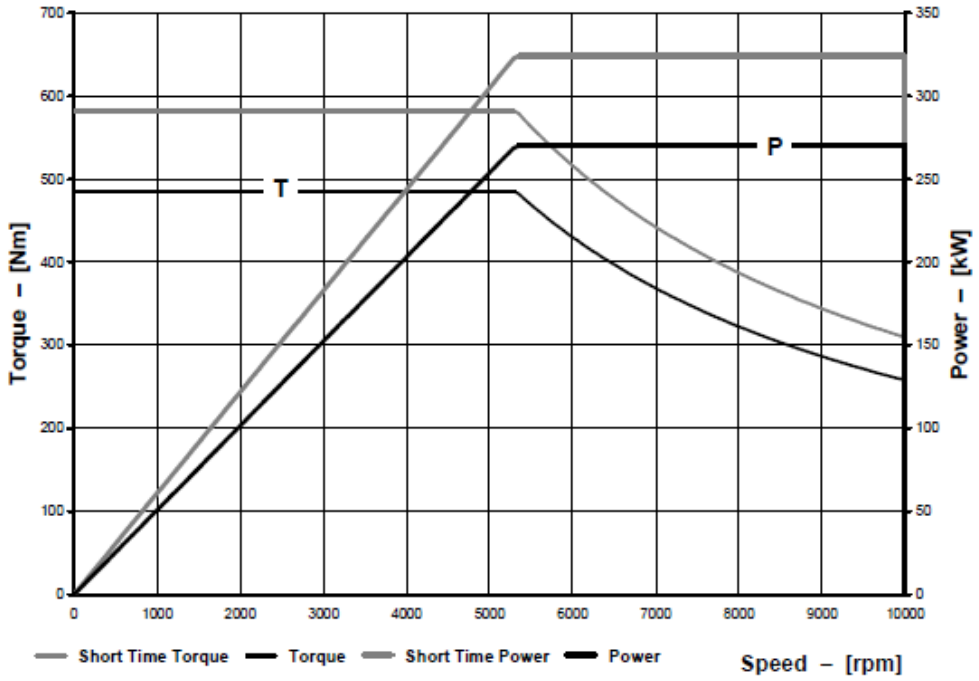

Figure 3.9Engine dynamometer performance curve from AVL Dynodur 270

3.3.2. Operating System

The AVL puma system was utilized to control the dynamometer and engine. The control functions for all parts of the conditioning systems were created in the puma system. The temperatures of fuel, the air inlet, and the engine coolant and oil could be controlled to meet the needs of the operator down to -20°C by individual control units. The INCA system was installed to provide a connection between the puma system and the ECU. Therefore, engine control parameters, such as injection strategies, boost pressure and so on, could be controlled through commands from the puma system. The AVL indicom system provides in-cylinder pressure measurements cycle-by-cycle and this could also controlled by the puma system. AVL Cameo will be installed and connected to the puma system in the future, in order to investigate the techniques of self-calibration at transient conditions. AVL i60 was also controlled by the puma system to obtain the gaseous emissions such as NO_x, THC, CO and CO_2. All the experimental setup used for this study is shown in Figure 3.10.

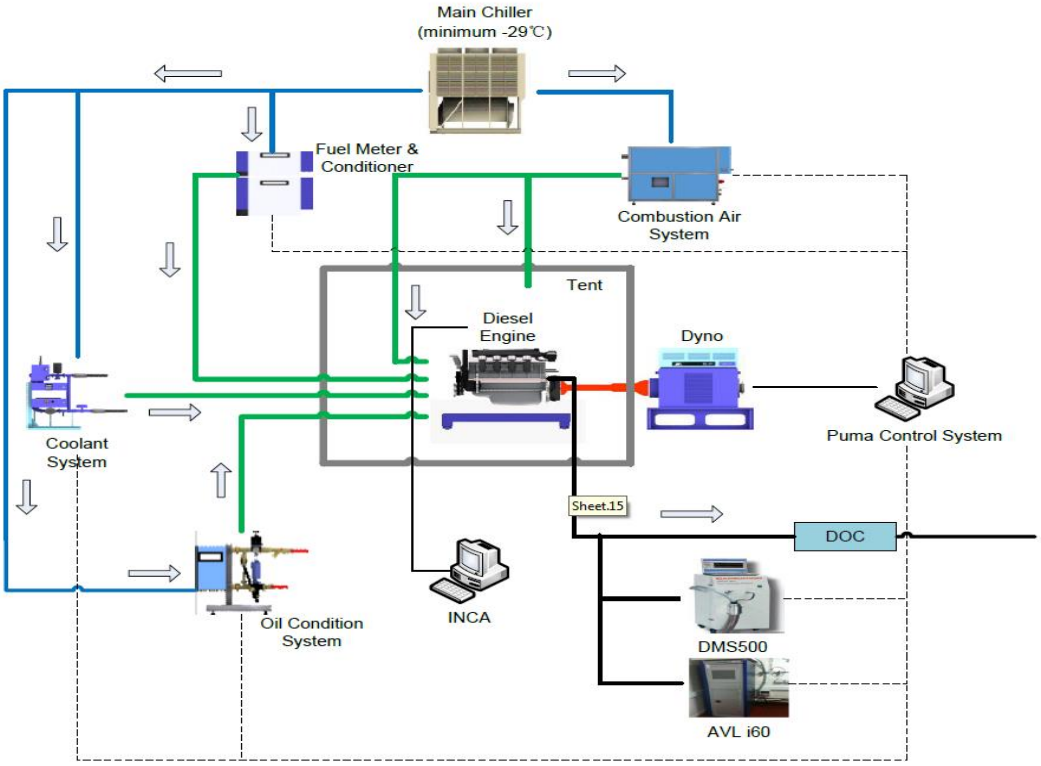

Figure 3.10Schematic of cold cell transient test facility

3.3.3. Engine Insulation Enclosure

The engine was mounted inside the insulated enclosure, where the temperature could be varied from ambient to -20ºC. The climatic enclosure was constructed with a rigid insulated floor plate, which supported an extruded aluminium frame shown in figure 3.11. The frames were designed as curtain hangers, so that the modular insulated panels, made from silicone glass cloth with a sandwich of elastomeric foam, could be hung on the frame and secured together with Velcro strips. The fully sealed test cell is shown in figure 3.2. Fluid service pipes and instrumentation cabling was brought in and out of the enclosure between the panels. Thus, the environment around the engine could be "soaked" to low temperature (down to -20°C) using the recalculating cold fluids and air for several hours before engine start. The

enclosure was utilized for performing specific tests at low temperature where the engine had to be allowed to soak at a specified temperature for several hours before testing.

Figure 3.11The sealed climatic enclosure

For conventional testing under ambient conditions, the insulated panels were removed from the frame to allow test cell ventilation air to pass around the engine.

3.3.4. Conditioning System

The whole low temperature circuit was supplied with chilled water (58% Glycol) at approximately -30ºC which was stored in a 1500 litre tank on the roof. The chilled water was then distributed to the engine coolant, oil, and fuel, as well as the combustion air conditioning system to reduce its temperature. The ambient circuit was supplied with conventional cooling water from another supply tank.

3.3.5. Coolant and Lubricant Oil Conditioner

This unit contained two cooling circuits and was used to condition the engine coolant and oil. The two systems were designed in the same way. At normal ambient temperatures during

conventional testing, the two circuits maintained engine coolant and oil at 90°C and 95°C respectively. For low ambient temperature tests, it was possible to maintain the temperatures of circulating coolant and oil down to -20ºC while the engine was stationary in order to perform a low temperature soak before an emissions test or a cold start. The flow schematic of engine coolant/oil circulation is shown in figure 3.12. A 3-way valve was used to control the amount of fluid going through the heat exchangers either using conventional water or chilled water.

The red lines show the fluid direction in the normal engine tests in which the coolant/oil temperatures did not exceed 90/95°C. A flow control valve in the coolant/oil pipeline controlled the flow rate to make sure the temperatures were maintained at the target values. The blue lines show the circuit for the cooling before engine start. The fluid was pumped by an extra pump since the engine was not running when this circuit was operating. The flow rate of chilled water was adjusted by a flow control valve to control the temperature of engine coolant/oil.

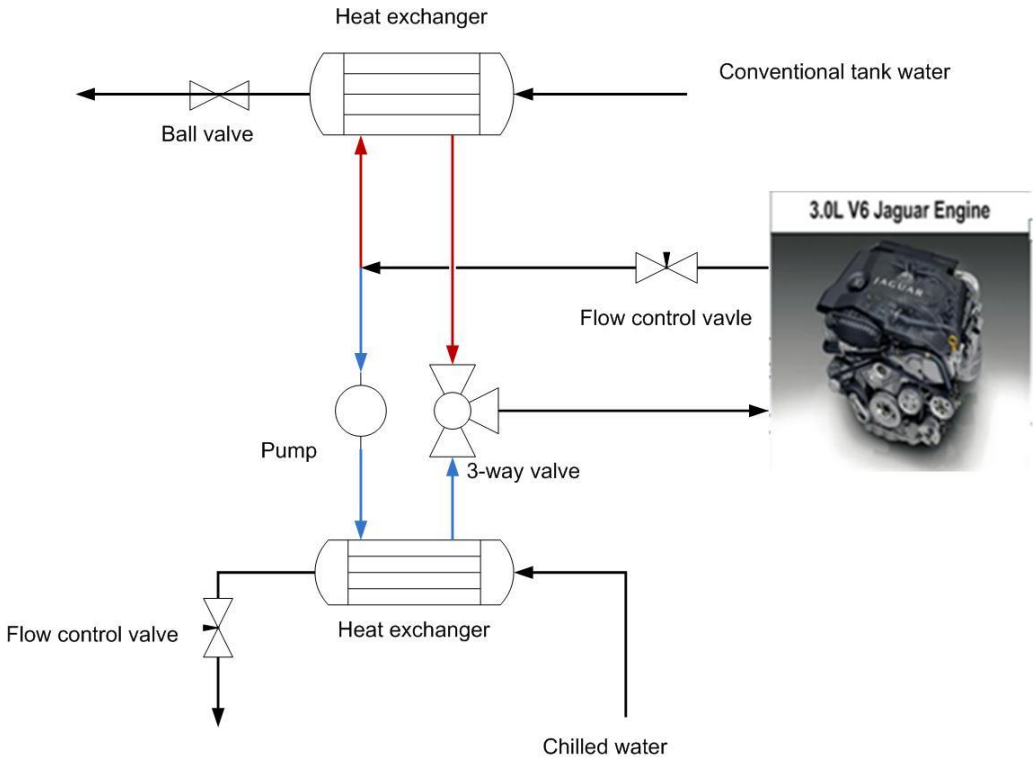

Figure 3.12Schematic of the cooling system for engine coolant in the cold test cell

3.3.6. Fuel Conditioner

An AVL735S Fuel meter and a 753C fuel conditioner were connected with an extra cold start unit. The fuel meter provided the instantaneous fuel consumption measurement with a high accuracy flow sensor (an accuracy of 0.12% for the whole system under real test bed conditions). An additional measurement of fuel density could be used for quality control. The volumetric consumption information was also available. The AVL fuel conditioner with integrated heating provided highly accurate and stable temperature regulation; this was connected with the fuel meter (figure 3.13). The fuel temperature could be pre-selected within the range of -10 to 80°C. The highly precise temperature control provided a constant pre-set fuel temperature for the engine and guaranteed high measurement accuracy for the whole test system. Continuous gas bubble separation ensured that the fuel supply to the engine was free

of bubbles. The integrated monitor also outputted a warning when gas bubbles occurred in the measurement system.

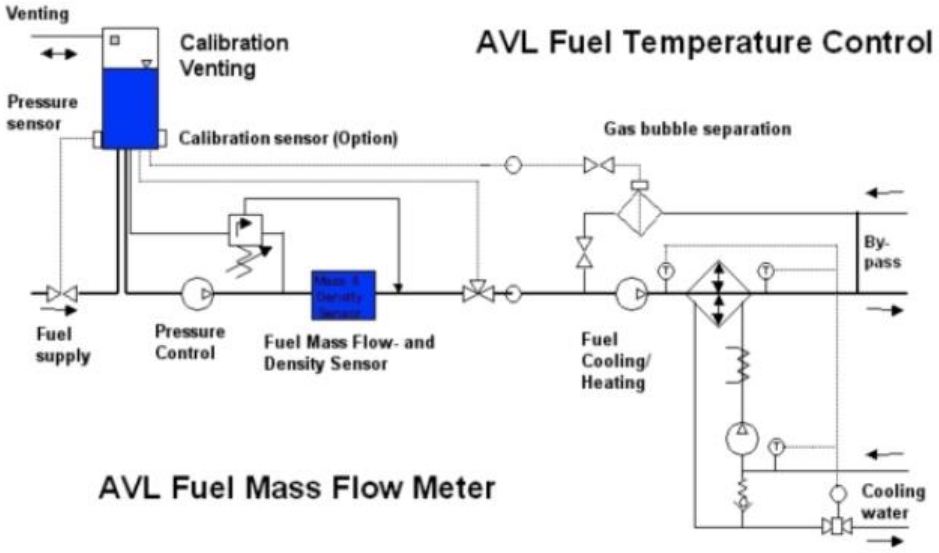

Figure 3.13The schematic of AVL fuel meter and conditioner system

An additional cold start unit was mounted in a covered frame to supply further cooling for the fuel circuit, down to -20°C. All electrical components (pump, valve) were controlled by the electrical control box via the Puma operating system. Figure 3.14 shows the system scheme of the cold start unit.

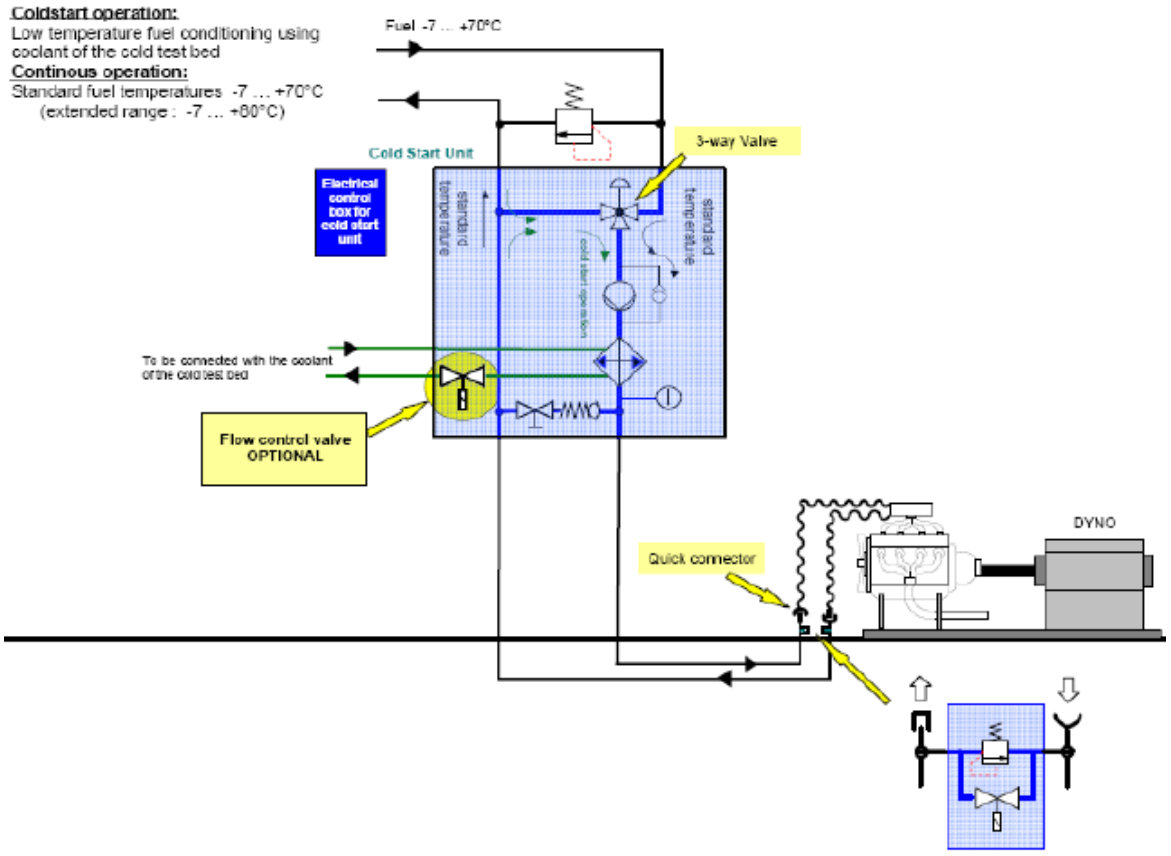

Figure 3.14Schematic of the cold start unit

3.3.7. Air Conditioner

The combustion air system was located in the plant room adjacent to the test cell and consisted of an AVL ACS1600 unit with an air dehumidifier in order to supply the cold air without water vapour to the insulated enclosure when conducting cold tests. The system therefore provided a simulation of standard conditions of the intake air and s simulation of extreme conditions of the intake air for checking the calibration and the engine performance. For normal ambient tests, the combustion air system supplied air at constant speed/pressure and temperature, normally at 25°C. The system supplied chilled air up to 500m^3/h for testing below 0°C and up to 1600 m^3/h for ambient testing.

3.4. MEASUREMENT EQUIPMENTS

3.4.1. In-cylinder Pressure Measurement and Analysis

In-cylinder pressure was measured by a piezo-electric pressure transducer and the cycle-by-cycle data was recorded and processed by an AVL Indimodule 621. The encoder provided a pulse signal every 0.5 CAD to trigger the recording, so that the in-cylinder pressure could be reviewed and analysed based on crank angle. The software Concerto provided calculation of the RoHR and MFB from the in-cylinder pressure using the first law of thermodynamics

$$Q_i = \frac{K}{\kappa - 1}\left[\kappa \cdot p_i \cdot (V_{i+n} - V_{i-n}) + V_i \cdot (p_{i+n} - p_{i-n})\right] \quad . \qquad (3.1)$$

Where, n is the interval (1CAD),κ is the polytropic coefficient, P is in-cylinder pressure, V is volume and K is constant.

Since the polytropic coefficient depends on temperature, indicom uses a second coefficient to calculate the range after TDC. By setting the second coefficient to a value slightly smaller than the coefficient used before TDC (which is determined by engine design), the calculated RoHR would not increase further at the end of combustion. This provides a more accurate calculation for the RoHR curve. The polytropic coefficient is 1.40 for air at 20°C. For the diesel engine at compression stroke, most of the gas in cylinders is air with higher temperature, so 1.37 was chosen for this period. At expansion stroke, the gas in cylinder is composed with large portion of combustion products, thus 1.30 was used during this period.
Exhaust Gas Measurement Instruments

3.4.1.1.Horiba MEXA 7100DEGR/ AVL AMA i60

Two different types of emission measurement equipment, Horiba MEXA7100DEGR for the STEADY test cell and AVL i60 for cold test cell, were used to measure the gaseous emissions,

such as NO/NO_x, THC, CO, CO_2 and O_2. The sample lines and the pre-filter were heated up to 191°C and maintained at this temperature during the tests in order to avoid emission condensation. The system was calibrated by suitable span and zero calibration gases before measuring. All the filters were changed regularly to protect the system and to maintain the best performances. The measuring principle of each analyser and its specifications are shown in table 3.4. Most of the analysers in AVL AMA i60 have a faster response time than those of Horiba MEXA7100DEGR. Thus, the AVL AMA i60 is more suitable for cold start and transient condition measurements.

Table 3.4 Specifications of the Horiba MEXA7100DEGR and AVL i60

Emission compositions	Measurement principle	Response time T10-90
CO	non-dispersive Infrared method (NDIR)	≤3.0s for Horiba MEXA ≤1.2s for AVL i60
CO_2	non-dispersive Infrared method (NDIR)	≤1.5s for Horiba MEXA ≤1.0s for AVL i60
THC	flame ionization detection (FID), heated	≤2.5s for Horiba MEXA ≤0.5s for AVL i60
NO/NO_x	chemi-luminescence detection (CLD), heated, dry	≤2.5/3.0s¬ for Horiba MEXA ≤2.0/2.5* for Horiba MEXA ≤1.0/1.0s¬ for AVL i60 ≤0.5/0.6s* for AVL i60
O_2	magneto-pneumatic detection (MPD) Paramagnetic Detector	≤2.0s for Horiba MEXA ≤3.5s for AVL i60

¬: NO/NO_x in low concentration (less than 50ppm)
*: NO/NO_x in high concentration (more than 50ppm)
Cambustion Fast FID

3.4.1.2.Cambustion Fast FID and Fast CLD

The Cambustion Fast FID provided continuous THC measurement with a response time of less than 0.9ms. The principle of Fast FID to measure the THC is the same as that used in the Horiba MEXA7100DEGR and AVL i60. Figure 3.15 and 3.16 shows the differences between conventional FID in the Horiba MEXA7100DEGRand the AVL i60, and the fast response FID.

The sample gas is introduced into a hydrogen flame inside the FID. The burning of hydrocarbons in the sample gas produces ions. The ions can be detected using a metal collector which is differentially charged with a high DC voltage. The current across this collector is thus proportional to the rate of ionisation which in turn depends upon the concentration of HC in the sample gas.

The ionisation process is very fast, so the slow time response time of conventional FIDs is mainly due to the sample gas processing. The Cambustion fast response FID analysers use conventional detection principles and they simplify the sampling system to give millisecond response times.

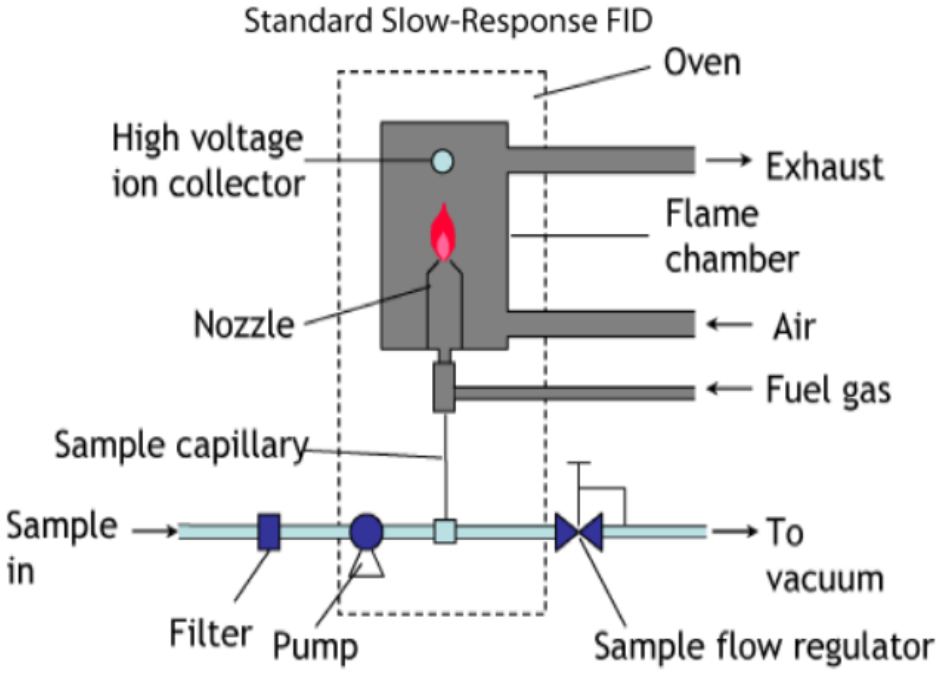

Figure 3.15 Principal of the standard FID analyzer

Source: http://www.cambustion.com/products/hfr500/fast-fid-principles

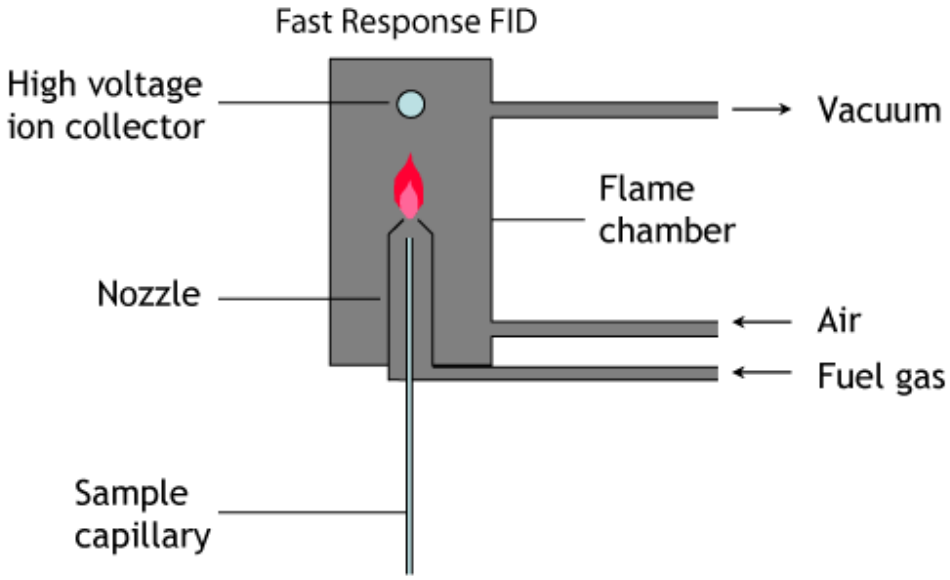

Figure 3.16Principal of the Cambustion Fast FID analyser

Source: http://www.cambustion.com/products/hfr500/fast-fid-principles

Instantaneous NO/NO_x (with NO_2 converter) measurement could be provided by the Cambustion Fast CLD. Its basic principle is conventional CLD which is also used in the Horiba MEXA7100DEGR and AVLi60, shown in figure 3.17. However, the fast sample gas handling system provided the good response time of 2ms. There action which is the basic principle for the CLD is the reaction between NO and O_3 (ozone). The reaction emits the photons which can be detected by a photo multiplier tube (PMT). The CLD output voltage is proportional to NO concentration.

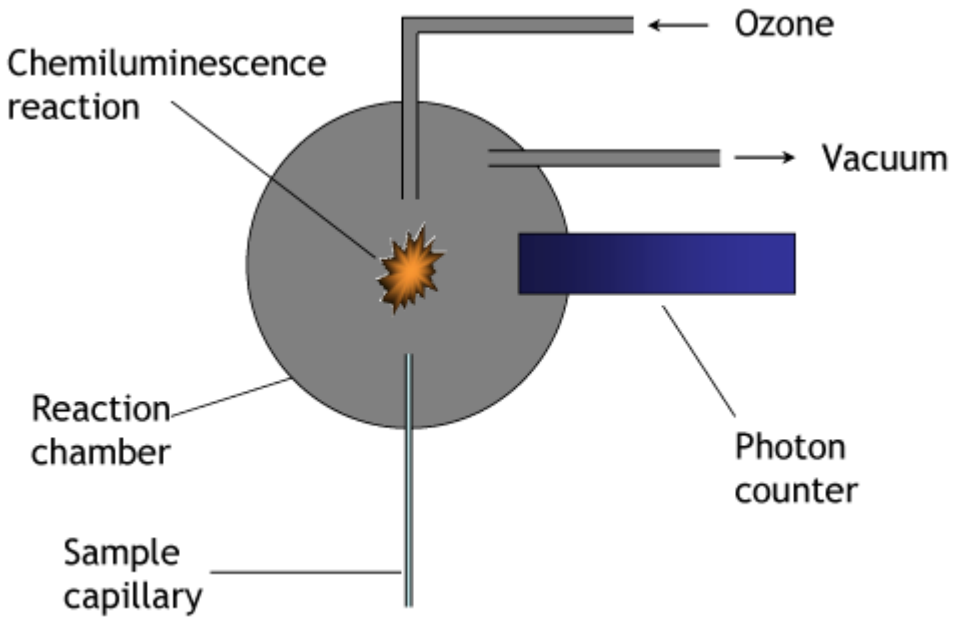

Figure 3.17Principal of the Cambustion Fast CLD analyzer

Source: http://www.cambustion.com/products/cld500/cld-principles

3.4.2. PM Emission Measurement

3.4.2.1.Smoke Meter AVL415s

The AVL 415S was used to measure smoke levels in terms of the Filter Smoke Number (FSN) at steady state conditions. It operates through the intake of a known and variable volume of exhaust gas through a paper filter. The opacity of the paper provides the emission soot

concentration. The number 0 is assigned to a clean filter and the number 10 is assigned to a completely black filter. The sampling time is approximately 30 seconds and each sample is averaged using up to 5 measurements.

3.4.2.2.Cambustion DMS500

The instantaneous particulate emission was measured in the study by the Differential Mobility Spectrometer (DMS500) from Cambustion Ltd. The results from the DMS500 can be represented by number, mass and the size distributions. The software is designed to separate the nucleation and accumulation mode particles automatically in the results sheets. The measurement particle sizes range between 10nm to 1000nm with a $T_{10\text{-}90\%}$ response time of 200ms and a recording rate of up to 10Hz.

The particles are classified according to their different electrical mobility in parallel (rather than in series as in a scanning instrument), as shown in figure 3.18. The diluted gas passes through a unipolar corona charger first. The particles are then charged with positive electric charge and the relative amounts of charge are approximately proportional to the particle surface areas. The filtered sheath flow then takes charged particles into the classifier. The positive high voltage electrode forces the positively charged particles towards the electrometer detector. Particles with different mass and charge quantity are located at different parts along the classifier. Since the classifier consists of 22 electrometer detectors, the charge quantity and travelling length of the particles are then measured and used to calculate particle size/number spectrums.

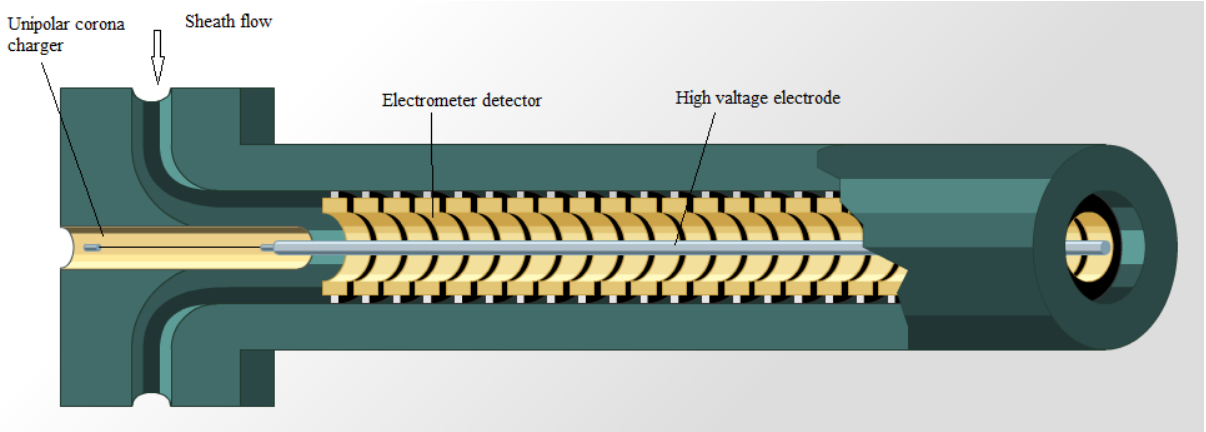

Figure 3.18 The principal of Cambustion DMS500analyser

http://www.cambustion.com/products/dms500/aerosol

DMS500 provides a built-in 2 stage dilution system; therefore no external system is required for raw exhaust measurements. The sample line is heated up to 150°C to avoid condensation. For the primary dilution, the mass flow is controlled by HEPA filtered compressed air and normally fixed at a dilution ratio of 5:1 for diesel engine measurement. The secondary high ratio diluter is controlled by a rotating disc with maximum dilution ratio of 500:1. The secondary dilution ratio can be controlled from the DMS500 interface and is automatically accounted for in DMS500 output.

The Cambustion software can record the measurement results and separate the particles according to whether they are nucleation or accumulation mode particles automatically. The separation is conducted based on the normal distribution of the two mode particles along with the particle size.

3.4.2.3.Smart Sampler

An AVL Smart sampler SPC 472 was used to collect the particulates from the exhaust. Their parts are shown in figure 3.20. The SPC is a partial flow dilution system for the gravimetric measurement of particulates incorporated with Windows-based control software, Laminar

flow Element (LFE), thermal mass flow controllers (MFCs) and a mobile filter panel. The total flow rate and sample ratio were kept constant, so that the particulates on the filters represented the real PM emissions, especially when the engine was running at transient conditions. The temperature at the sample head was maintained at 171°C when it was sampling the exhaust gases in order to avoid condensation. A dilution air conditioner was attached for cooling/heating the dilution air to the regulatory temperature ranged between 20°C and 30°C at the tunnel inlet. The control software was able to automatically start and end the sampling process. By precisely controlling the temperatures and times of the sampling process, good repeatability was achieved in the tests.

(a) (b) (c)

Figure 3.19 The smart smapler (a) thermal mass flow controllers (MFCs); (b) Operating system; (c) Filter panel and dilutor.

3.4.2.4.2D GC/MS

Gas Chromatograph (GC) coupled with a Mass Spectrometer (MS) is widely used to identify the chemical compositions, especially the organic compounds, of the emissions in engine research. The GC separates different molecules in a mixture based on the differences in their properties; normally volatility. The mass spectrometer then breaks each molecule into ionized fragments which could be detected with their mass-to-charge ratio and identified using a NIST library. However, due to the variety of compounds in the PM emissions, conventional GC often failed to separate many compounds.

Recently, advances in two-dimensional gas chromatograph ($GC \times GC$) have resulted in successful measuring of a wide range of volatile and semi-volatile organic compounds of PM emissions. Figure 3.21 shows a comparison of the results from 1D GC and 2D GC analysis of the same urban aerosol sample. The white line is the result from 1D GC and the surface plot is the result from 2D GC. It can be seen that the peaks in the 1Dchromatogram are well separated along the second dimension of the 2D plane. The invisible peaks in the 1D plot are turned to visible in the surface plot.

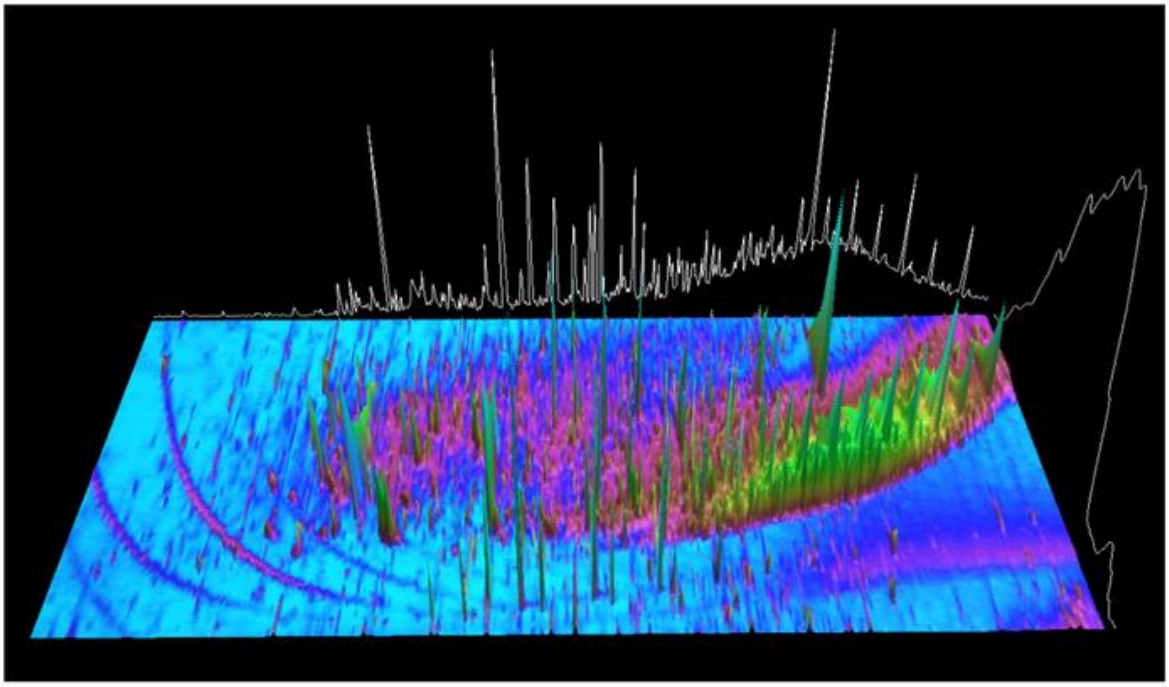

Figure 3.20 The chromatogram examined by 2D-GC-TOFMS compared with GC/MS.(Alam, 2013)

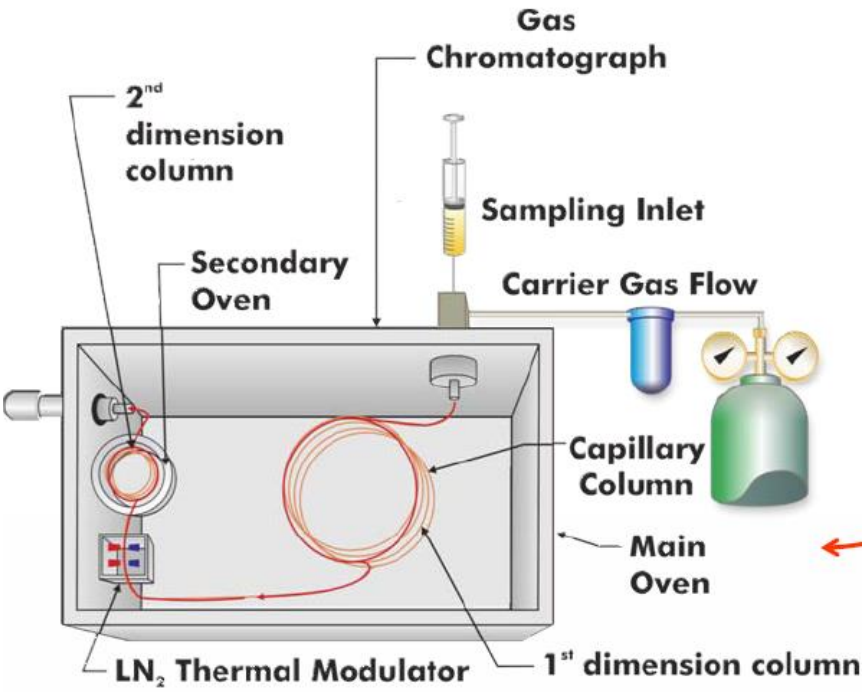

Figure 3.21 The schematic of 2D-GC

The schematic of 2D GC is shown in figure 3.22. When the sample passes through the 1st column, the modulator traps and releases sequential portions of the 1st column effluent and injects it into the 2nd column of different selectivity where it is separated and detected.

The 1st column has the length, inner diameter and film thicknesses of 15–30m, 0.25–0.32mm and 0.1–1μm, respectively. The 2ndcolumn is shorter, narrower and thinner, with dimensions of 0.5–2 m for length, 0.1mm for inner diameter and 0.1μm for film thickness. The stationary phases of the columns can be non-polar or polar, depending on the material of the column. Typically, 2D-GChas a non-polar stationary phase in the 1st column and a polar stationary phase in the 2nd column.

Different molecules in the mixture have different chemical properties and relative affinity for the stationary phases of the columns. Those differences allow the molecules to be separated as the sample travels through the column. The molecules are retained by the column and then come off from the column at different times (called the retention time) which allows the mass spectrometer downstream to detect the molecules separately.

In2D-GC, the sample will pass through both of the columns and it will be trapped by two different aspects of selectivity. This is controlled by the modulator, which is placed between the two columns. The effluent in the 1st column is periodically sampled and injected into the 2ndcolumn by the modulator. After the separation in the 2nd column is completed, the next sampling and injection start. This period is so short that each peak from the 1st column is divided to several slices for the separation in the 2nd column. In this way, all compounds are subjected by and resolved by the two different separation mechanisms. Therefore, the peaks from2D-GC become narrower compared with the peaks from traditional 1D-GC.The design

of the two columns (the 1st column is longer and wider than the 2nd column) ensures that the total separation in the 2nd column is completed in the run time of the 1st column analysis.

The separation period of the 2nd column is so short (10-100ms) that a good detector with a fast response time is needed. Fast time-of-flight mass spectrometers (TOFMS), which operate with spectral acquisition rates of 100-200 Hz, are well-suited for 2D-GC and have been utilized for numerous studies.

The results of 2D-GC can be shown in the traditional 1D version, contour plot and surface plot (in figure 3.21). The contour plot of mineral diesel analysis by 2D-GC is shown in figure 3.23. Each dot presents a peak in the surface plot. The colours indicate the intensities of the response (pink<yellow<green). The contour plot clearly shows the different groups of the compounds in a particular patch of the 2D plane which provides a great advantage in group-type analysis. The pattern of peak position may also make it possible in many mixtures to identify or recognize the mixture with good reliability.

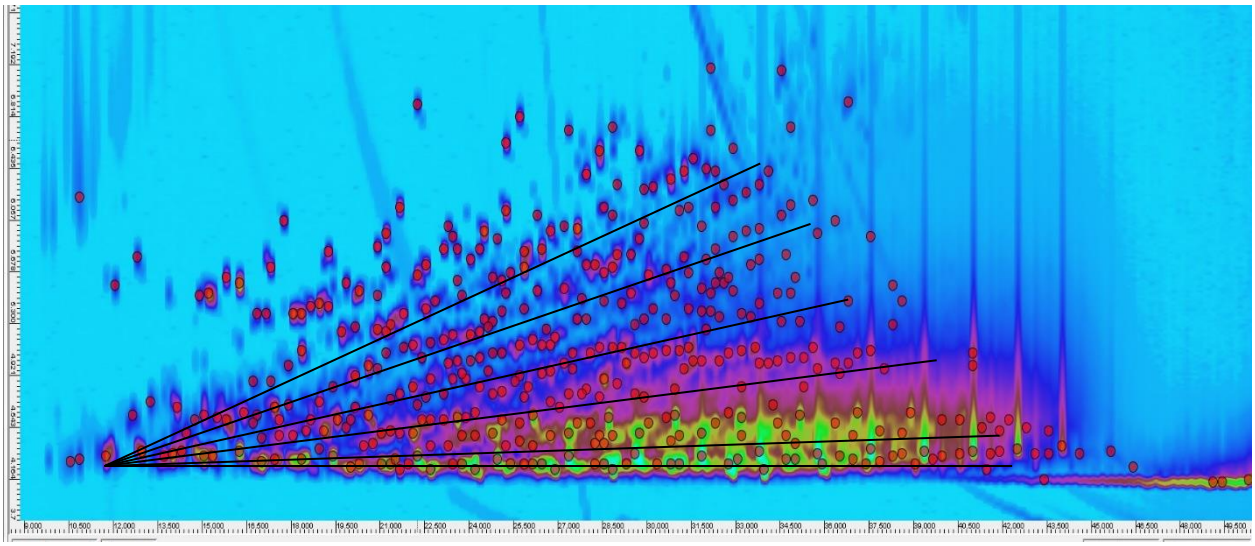

Figure 3.22 The contour plot of ion current chromatogram of diesel fuel

enlarged capacity and high sensitivity. The characteristics and advantages of 2D-GC make it a

useful technique for analysing complex mixtures, for example, the particulates emissions from a diesel engine.

3.5. FUEL LISTS

The biodiesel fuels which were used in this study are listed in table 3.4. All the biodiesels were blended with mineral diesel (zero sulphur) in order to avoid the sulphur effects on engine emissions. For the cold start at minus temperatures, winter diesel, which has lower CFPP, was used and blended with biodiesels to prevent fuel circuit blockage (discussed in section 2.5.2).The properties of all the fuels are listed in the appendix A1.

Table 3.5 List of tested fuels

B10s	TME10	XXX	JME10	RME1-10	RME2-10	SME10	HVO10	6
B30s	TME30	UVOME30	JME30	RME1-30	RME2-30	SME30	HVO30	7
B60s	TME60	UVOME60	XXX	XXX	XXX	SME60	HVO60	4
								17

Chaper 4. COMBUSTION AND EMISSIONS OF BIODIESEL FROM VARIOUS FEEDSTOCKS AT STEADY CONDITIONS

In this chapter, the combustion characteristics and emissions of using different biodiesel blends were compared with those of mineral diesel. The selected biodiesel-diesel blends for this study are Used Vegetable Oil Methyl Ester (UVOME), Rapeseed Methyl Ester (RME), Tallow Methyl Ester (TME), Jatropha Methyl Ester (JME), Soybean Methyl Ester (SME) and Hydrogenated Vegetable Oil (HVO). They were blended with mineral diesel in 10%, 30% and 60% by volume. The objective was to understand the effect of using different biodiesel to the combustion and emissions characteristics in an unmodified commercial engine. This is called sensitivity tests. Meanwhile, different amount of EGR addition has pronounced effect on atomization, vaporization, mixing, combustion and consequently on the in-cylinder pressure and emission variations. When EGR combined with the effects of different fuel properties, the overall interaction determines the final engine performance and emission quality.

4.1. TEST CONDITIONS AND PROCEDURE

The pressure transducers (AVL GU13G piezo transducer) are located in cylinder 2 and cylinder 5. The pressure history is recorded by using AVL Indicom combustion analyser. The average of pressure history comes from 100 engine cycles is presented. The fuel properties, engine test conditions and fuel injection events and EGR rate are shown in appendix table A2 and A3respectively. The selected speed and load conditions were derived from New European Drive Cycle(NEDC). The ECU signals for engine operating parameters such as air mass flow-rate, fuel mass flow-rate, start of pilot and main injection, temperature of coolant and lubrication, intake manifold pressure, injection pressure, etc. can be monitored,

calibrated, and recorded using INCA V5.3 software from ETAS. Two series of engine tests were conducted, one is sensitivity tests and the other is EGR swept tests.

For the sensitivity tests, each of the engine test conditions was completed at least three times to ensure results were repeatable. Besides that, the engine was run at a certain time period for the temperatures stabilization and measurements. A reference mineral diesel was conducted at set reference points before and after of each biodiesel-diesel blend. Comparison of these results (before and after) is used to ensure the complete engine test system was always generating results which remained accurate and repeatable.

For the EGR swept tests, the EGR was varied from 0% to ECU reference value (RV)with increments of 5% for different biodiesels and their blends. When EGR percentage was close to the RV value, more refined increments of EGR were used, namely at RV-5%, RV-2%, RV, RV+2% and RV+5%. Measurements were taken one minute after EGR was set to its new value to assure steady conditions. Results with three different engine loads are presented, namely low load (1500 RPM, 32 Nm), medium load (2250 RPM, 95 Nm) and high load (2500 RPM, 196 Nm).

All the test environments were precisely controlled during the experiments. An operating environment temperature of 25 ± 1°C, fuel temperature of 25±2 °C, air intake temperature of25±1 °C, engine coolant temperature of 90 ± 1°C and relative humidity is approximately 35-40 percent were kept constant and monitored .

In this chapter, results with two different engine loads are presented, namely low load (1500 RPM, 72 Nm), high load (1500 RPM, 143 Nm) with using HVO blends and UVOME blends. The fuel properties and injection strategies are listed in the appendix table A1-A3.All HVO blends have higher cetane number than diesel. But cetane numbers of UVOME blends are lower than mineral diesel. The viscosity of mineral diesel is slightly higher than HVO. HVO

heat of combustion is higher than mineral diesel and UVOME. Pflaum et al. have shown that the boiling point of mineral diesel is slightly higher than HVO but much lower than methyl ester biodiesel(Pflaum, 2010). The fuel chemical compositions are also presented in appendix table A4. The composition of HVO and UVOME are very simple, only paraffin and methyl ester respectively. The carbon chain length of paraffins in HVO is mainly from C15 to C18. Methyl ester, as converted from vegetable oil or fat, only contains long chain alkyl. Mineral diesel contains more than 60% naphthenic and aromatics.

4.2. COMBUSTION CHARACTERISTICS OF USING DIESEL AND BIODIESEL BLENDS

The in-cylinder pressure and Rate of Heat Release (ROHR) for different fuels at 1500 RPM, 72 Nm are compared in Figure 4.1. At this condition, the post injection was disabled. Only results for 4 different EGR rate are presented. The three humps of the ROHR curve indicate the two pilot injections combustion and the main fuel injected. The peak in-cylinder pressure appears around the second pilot fuel injection. For the main injection combustion only one hump was observed indicating that most of the fuel was combusted in premixed combustion mode.

As the EGR rate was increased, the combustion pressure for all fuels was decreased dramatically. The pilot combustions were also weakened especially the first pilot combustion which disappeared when EGR rate reached 46% except for HVO blends. Meanwhile, combustion of HVO blends always led to higher in-cylinder pressure and shorter ignition delay of first pilot injection than other fuels. And these effects became more significant as the blending ratio and EGR rate increased.

Two reasons might increase the combustion pressure of HVO blends. The first one is the high cetane number which advanced the start of combustion and results higher combustion

pressure. The second one is the long chain paraffin in HVO which is easy to be broken down than naphthenic and aromatics of mineral diesel.

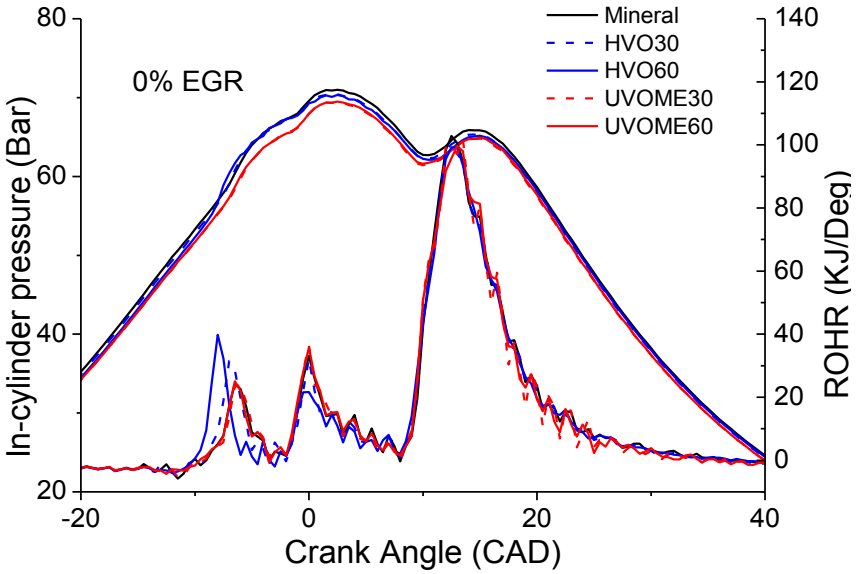

(a) 0% EGR rate

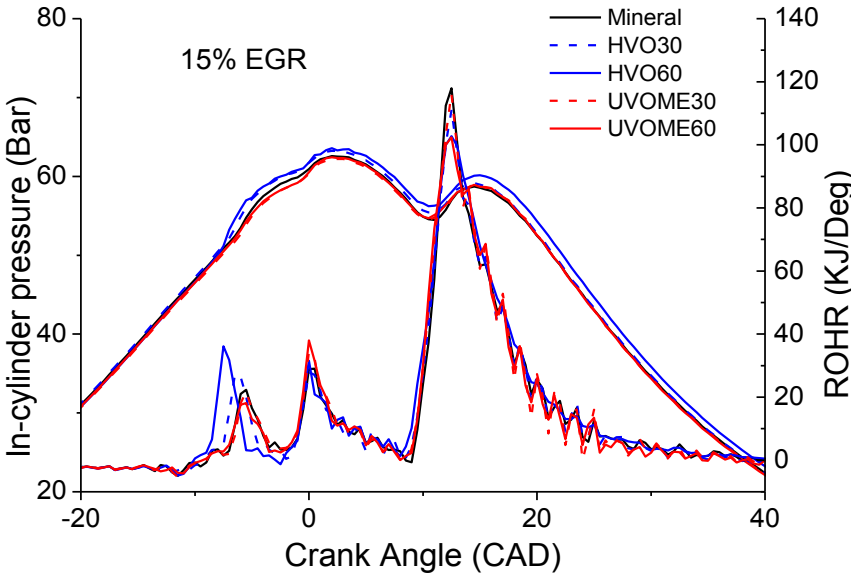

(b) 15% EGR rate

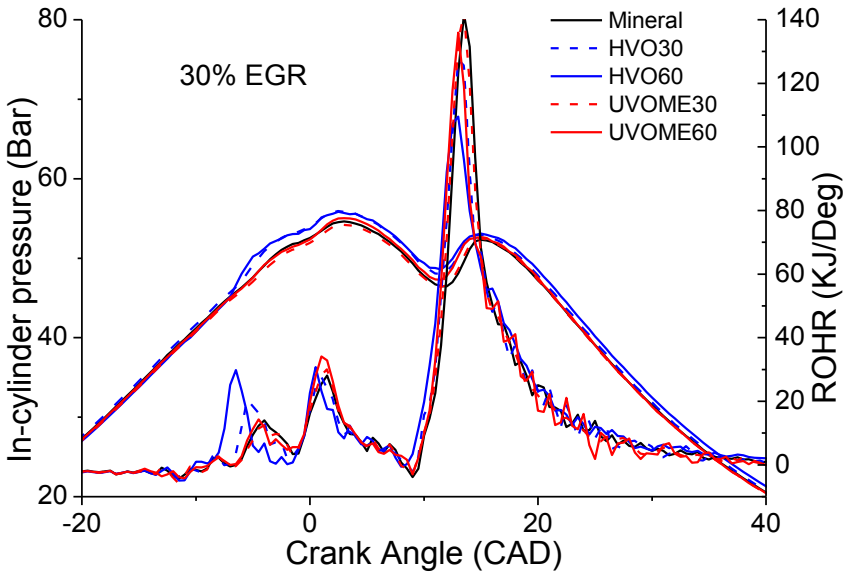

(c) 30% EGR rate

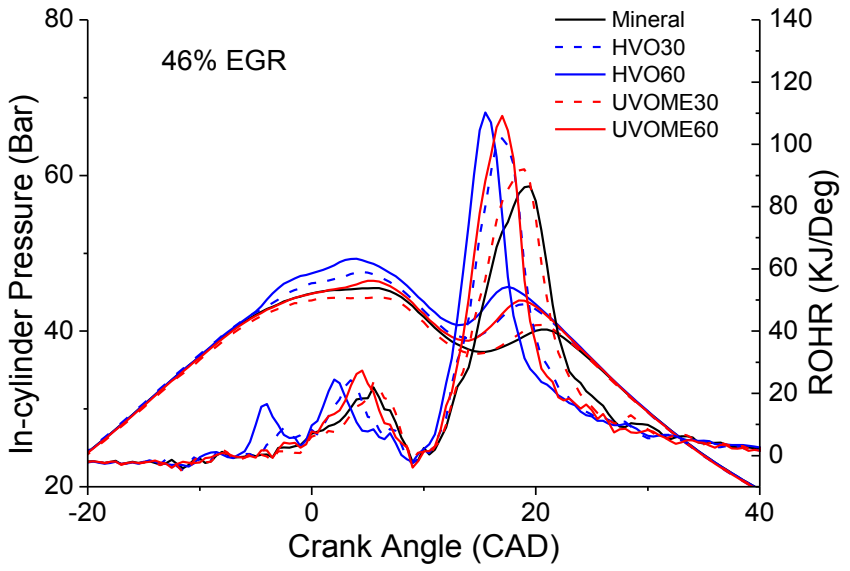

(d) 46% EGR rate

Figure 4.1 The in-cylinder pressure and Rate of Heat Release for different fuels with various EGR rate at 1500RPM, 72Nm with different EGR rates

Combustion of UVOME blends led to lower or similar combustion pressure level compared with the case of mineral diesel. This is mainly due to UVOME's high viscosity and boiling point which can cause poor premixing and incomplete combustion. As premixed combustion dominant at this condition, this disadvantage became more serious.

With the EGR rate increased from 0 to 30%, the peak heat release rate of main combustion was increased. The combustion of mineral diesel tended to have the highest heat release rate in the main combustion because the two pilot combustion of mineral diesel was not as significant as the cases of the other fuels due to its low cetane number. Hence, the pilot combustion of mineral diesel had more residual fuel for main combustion than the cases of the other fuels. The residual fuel was well premixed and improved the following main combustion of mineral diesel.

However, with 46% EGR, the combustion temperature was decreased obviously so that the ROHR of all the fuels showed significant differences compared with the cases of the low EGR rate. The combustion of HVO60 had the shortest ignition delay and the highest heat release rate due to its highest cetane number and the improved fuel/air premixing due to the effects of its pilot combustion.

With engine load increased from 72 Nm to 143 Nm, the EGR effect on combustion pressure and heat release become insignificant according to figure 4.2. A forth hump of ROHR curve can be observed representing the diffusion combustion of fuel. At high torque mode, the combustion pressure of mineral diesel was lower than all biodiesel blends. For HVO blends, its higher combustion pressure is because of the higher cetane number and paraffin content which were discussed before. The reason for higher combustion pressure of UVOME blends is UVOME's higher combustion efficiency in diffusion combustion mode since its long chain alkyl is easier to be pyrolysed and combusted than the naphthenics and aromatics of mineral diesel. Meanwhile, the C-O and C=O radicals also contributed to better diffusion combustion.

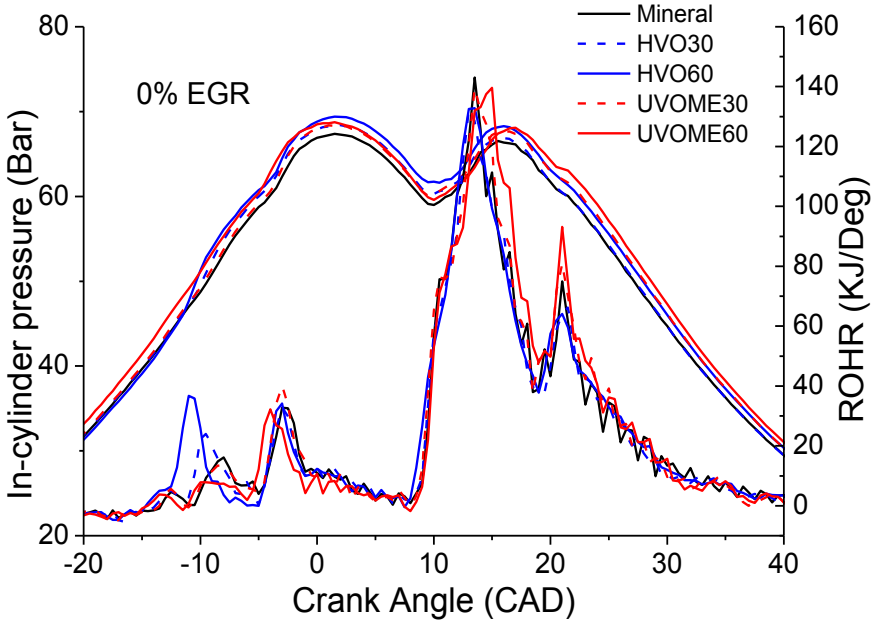

(a) 0% EGR rate

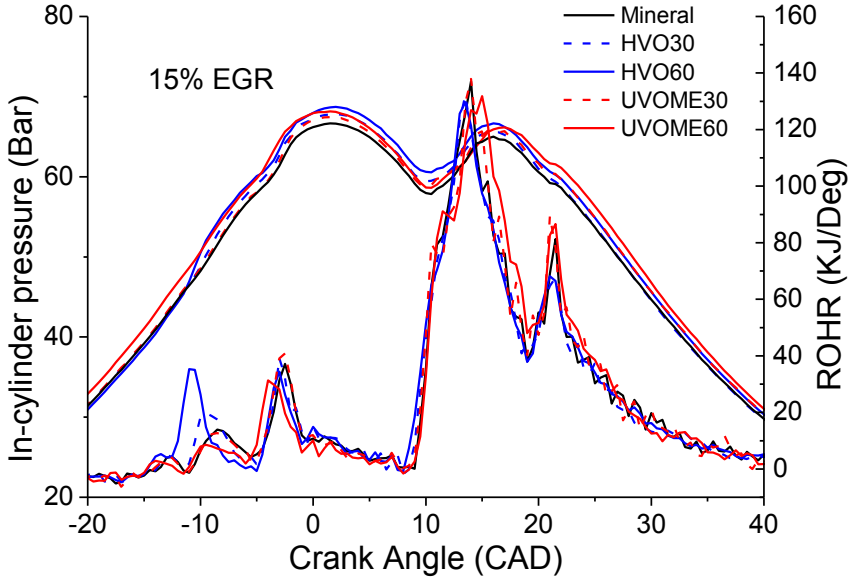

(b) 15% EGR rate

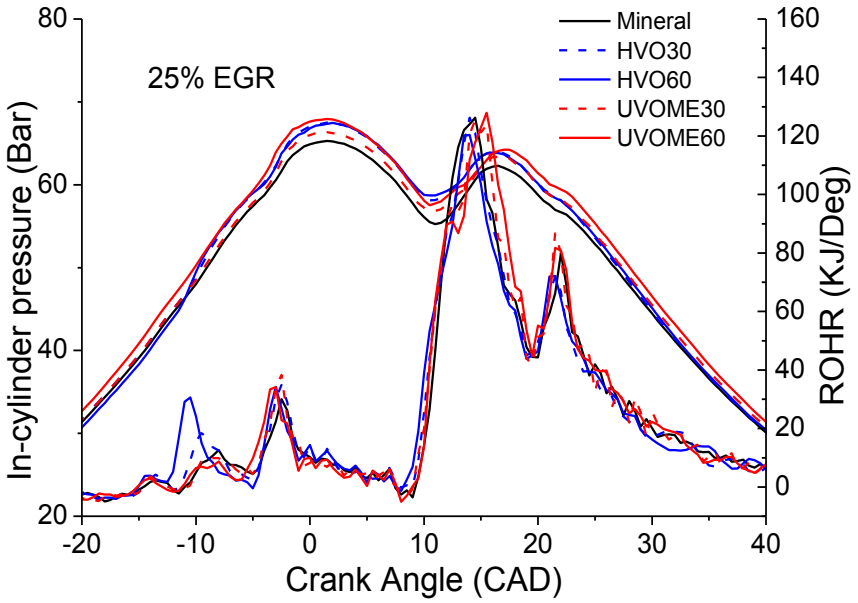

(c) 25% EGR rate

Figure 4.2 In-cylinder pressure and Rate of Heat Release for different fuels with various EGR at 1500RPM, 143Nm with different EGR rates

The peak in-cylinder pressure of various EGR rate is presented in Figure 4.3 which shows the overall trend of each EGR rate as discussed before. As the EGR rate was increased, the peak in-cylinder pressure was decreased slightly at high load while the decreasing of in-cylinder pressure at low load was quite significant. It is caused by the different VGT adjusting strategies used at the two engine loads. At low load, the turbine opening rate was kept constant. As the EGR rate was increased, the exhaust pressure before turbine was decreased and resulted in a reduced boost pressure of inlet air. Combined the effects of the reduced boost pressure and the increased EGR rate, the in-cylinder pressure of low load was decreased obviously. However, at high load, the turbine opening rate was increased as the EGR rate increased in order to supply sufficient inlet air mass. The improved boost pressure of inlet air compensated the effect of the EGR and caused the slight decreasing of the in-cylinder pressure.

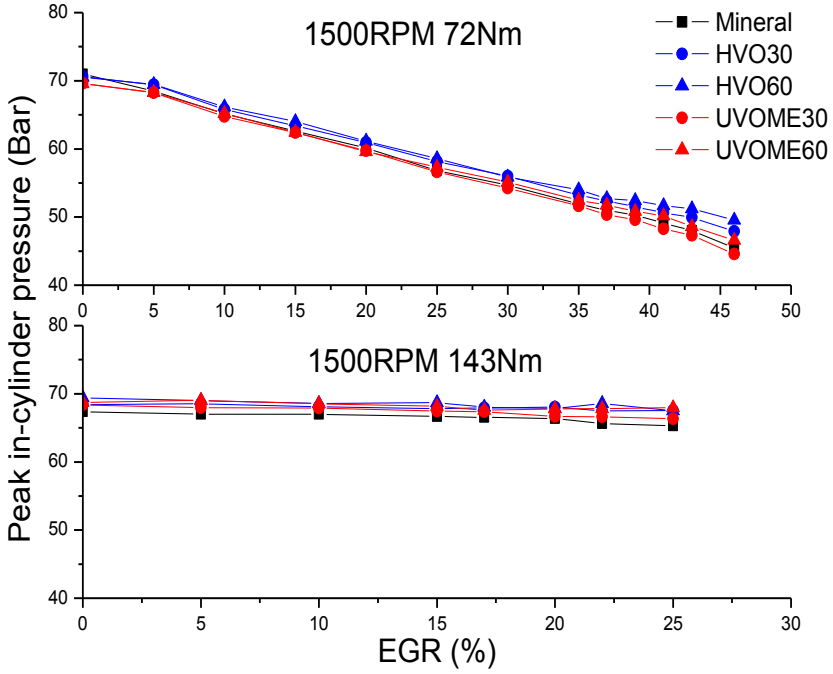

Figure 4.3 Peak in-cylinder pressure for various EGR rate

The 50% Mass Fraction Burned (MFB50) and the durations from MFB50 to MFB90 for all EGR rate are presented in Figure 4.4. Since multi-injection was employed, the main injection ignition delay for each fuel was almost identical. Hence, MFB50 and the time from MFB50 to MFB90 are presented to indicate the early and late stages of combustion respectively.

Compared with mineral diesel, the HVO blends combustion characteristics were almost the same initially. As EGR rate increased, its MFB50 appeared earlier than the case of mineral diesel due to high cetane number of HVO. With the increased EGR rate, the late stage combustion durations of HVO blends were longer than the cases of mineral diesel at low load but lower or similar at high load. At low load, the heat release rate of HVO blend was lower than that of mineral diesel except the case of 46% EGR. This caused higher late stage combustion duration. At high load, the combustion characteristics of HVO blends were similar with the cases of using mineral diesel. Thus, the late stage combustion duration of HVO was also similar with that of mineral diesel and sometimes even a little lower.

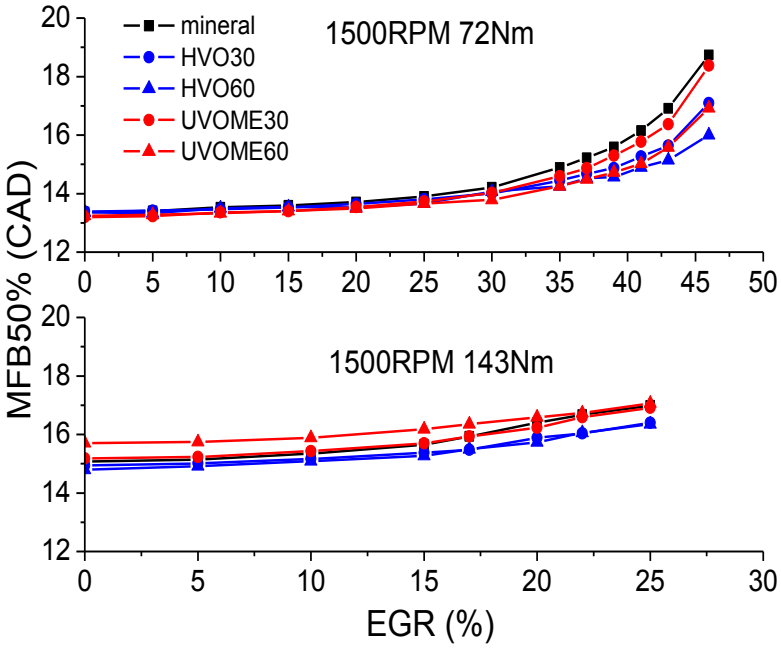

Figure 4.4 The MFB50 of each fuel for various EGR rates

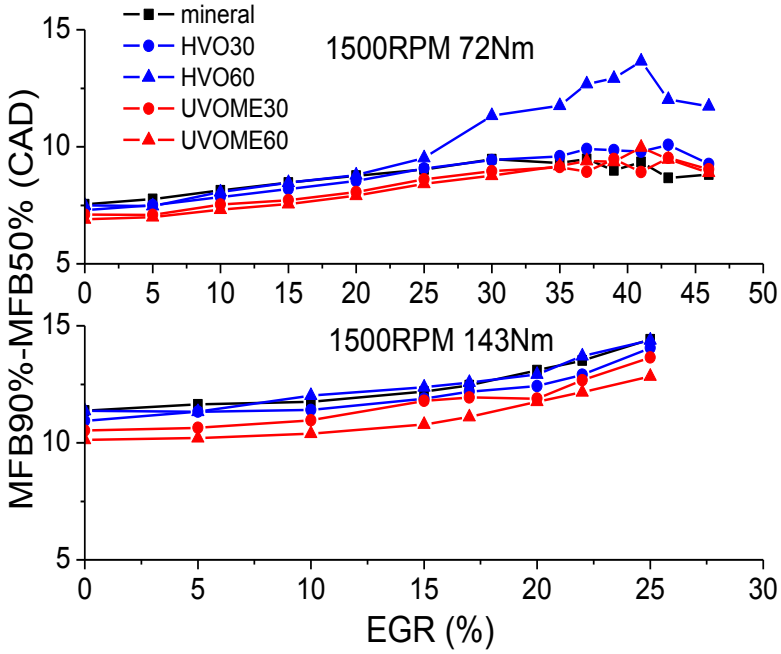

Figure 4.5 MFB90-MFB50 of each fuel for various EGR rates

The late stage combustion duration of UVOME blends was shorter than other fuels except the EGR rate is higher than 39%. This is due to the effects of oxygen and long chain alkyl content which was discussed before. The high combustion duration at high EGR rate might be caused

by the low temperature which had deeper effects on the vaporization and atomization of UVOME blends than those of mineral diesel.

Another phenomenon observed is the decrease of duration between MFB50 and MFB90 for EGR rate bigger than 40% at low load. This is because fuels were better premixed due to long ignition delay as high EGR rate lowered the combustion temperature and pressure.

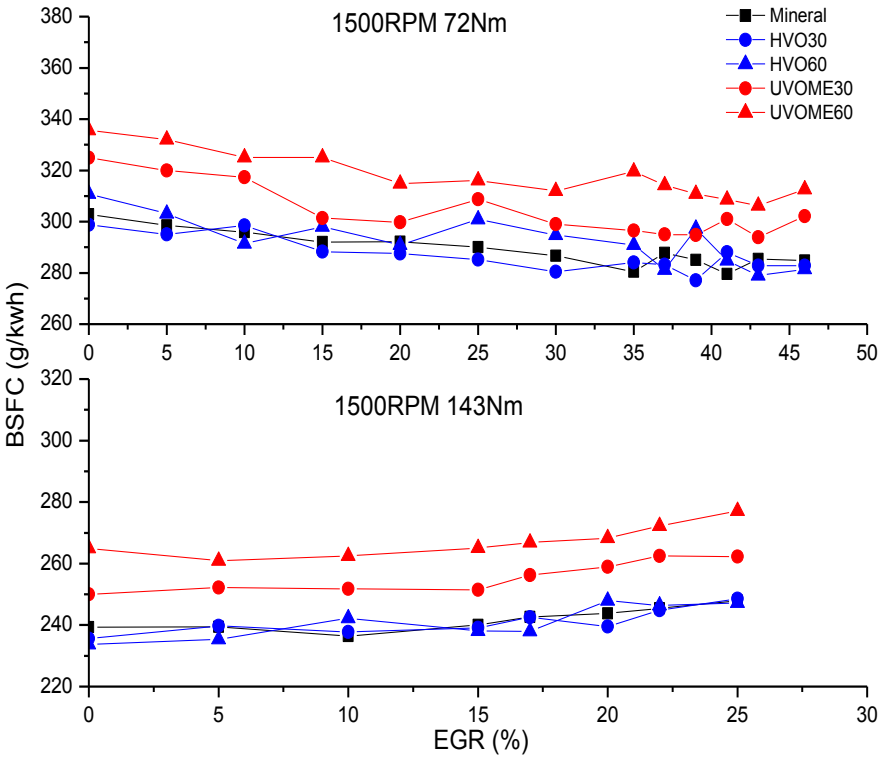

Figure 4.6 Brake specific fuel consumption for various EGR rate

BSFC at different loads were measured and they are presented in Figure 4.6. As EGR rate increased, the BSFC was decreased as EGR rate increasing at low load but increased at high load because the premixed combustion dominated the whole combustion process at low load. The longer ignition delay caused by high EGR rate resulted in an improved air/fuel premixing and combustion. At high engine load, the diffusion combustion rate was reduced due to the combustion temperature decreasing caused by EGR addition. The BSFC of UVOME blends were always higher than other fuels caused by its low energy density.

4.3. ENGINE EMISSIONS OF USING DIESEL AND BIODIESEL BLENDS

4.3.1. Gaseous Emissions

Figure 4.7 presents the NOx, THC and CO emissions for each fuel as the EGR rate was increased. Based on the results, the NOx emission was decreased almost linearly as EGR rate increased. The levels of NOx emission for different fuels were almost the same except for HVO60 which was lower when EGR rate was less than 20%, due to the high saturated and long chain fuel form lower NOx (McCormick, 2001). As high EGR rate was employed to reduce the NOx emission, this chemical effect was not significant any more.

The THC and CO emissions are originated by incomplete combustion which is directly related to the local air fuel ratios and temperatures. Both the THC and CO emissions showed clear increasing trends with EGR rate increases, due to the reduced air percentage causing less complete combustion. Meanwhile, the THC and CO emissions increasing rates were lower at low EGR rate when the engine was running at the low load, especially after 35% EGR. This is because of the low combustion rate caused by the low air/fuel ratio due to high EGR rate.

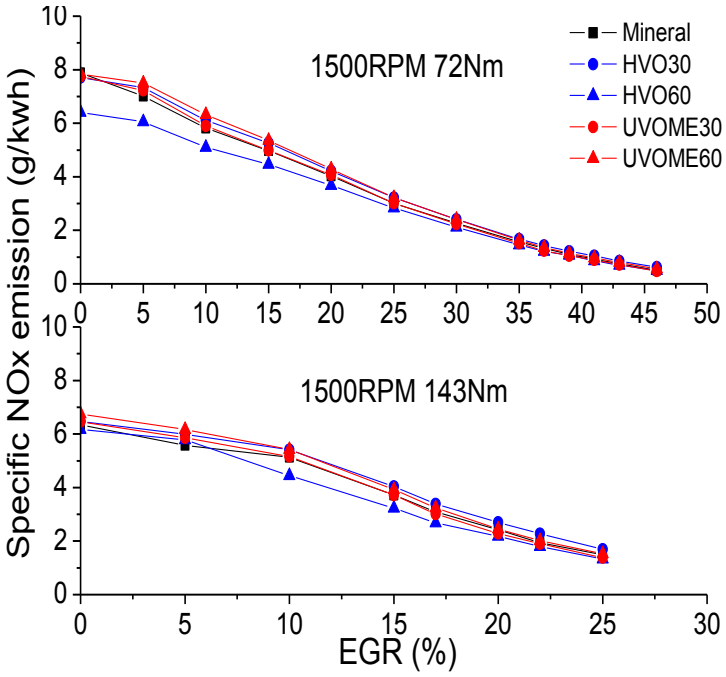

Figure 4.7Specific NOx emissions of each fuel for various EGR rate.

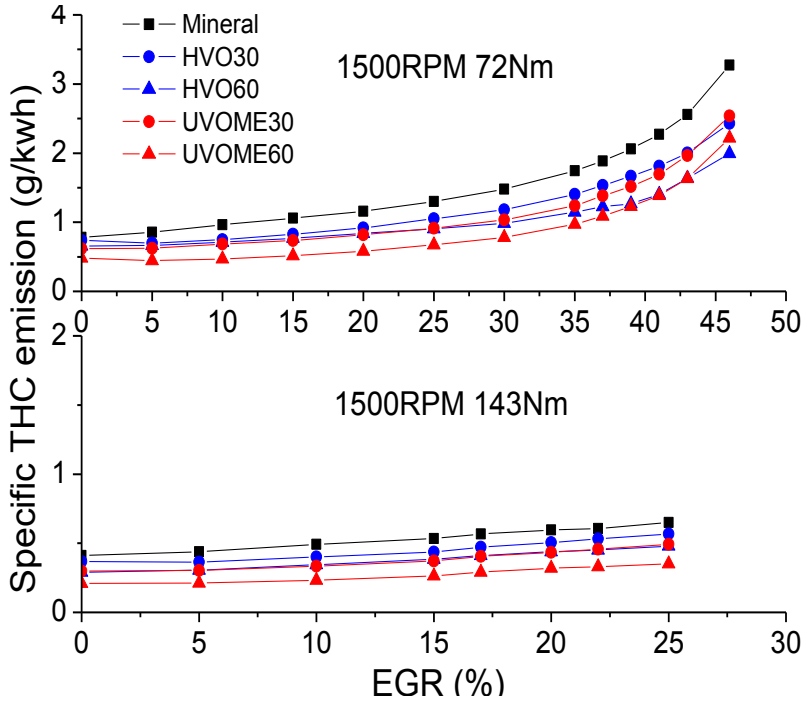

Figure 4.8Specific THC emissions of each fuel for various EGR rate

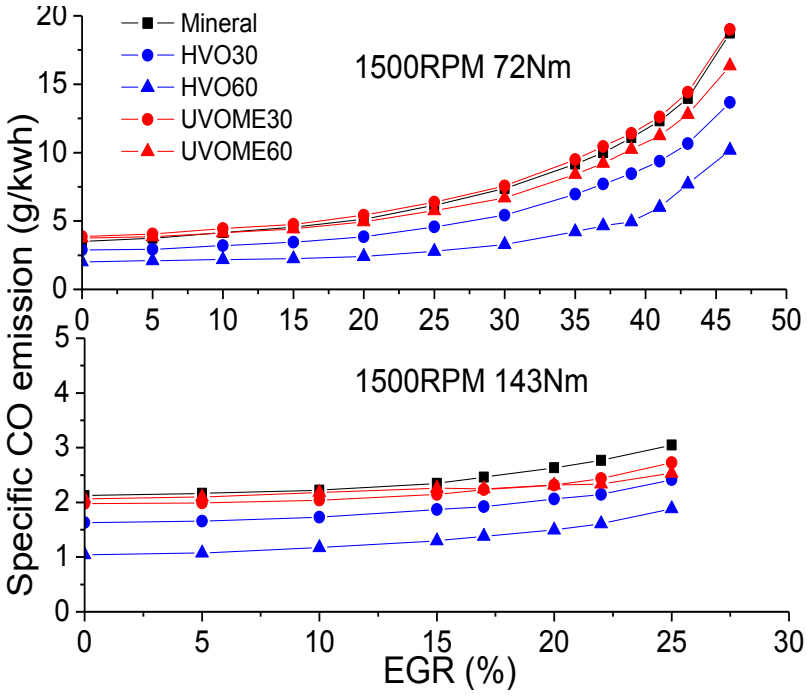

Figure 4.9Specific CO emissions of each fuel for various EGR rate

Combustion of biodiesel blends all led to lower THC and CO emissions than the case of mineral diesel. But THC of UVOME was lower while its CO was higher than HVO, due to the oxygen contained in UVOME blends.

4.3.2. Smoke Emission

The smoke number of each fuel for Various EGR rate is presented in Figure 4.10. The EGR effect was investigated in three ranges: low EGR (0-15%), medium EGR (20-35%) and high EGR (>35%).

Low EGR Effect

When EGR rate is less than 15%, the smoke emission of each fuel remained constant or even slightly decreased even though the increasing of EGR rate reduced the combustion temperature and oxygen intake, due to better air/fuel premixing caused by EGR addition.

The smoke levels of using biodiesel blends were less than that of using mineral diesel, because the aromatic and naphthenic in mineral diesel is easier to form unsaturated hydrocarbon and PAH, the precursors of soot. Comparing the same blend ratio of HVO and UVOME, combustion of HVO blends always led to higher smoke emissions than that of UVOME blends. HVO only contains long chain paraffin which produce less PAH and subsequently less smoke emission. On the other hand, UVOME has no aromatic content and the existing C-O and C=O do not easily form hydrocarbon and then soot. Thus, UVOME produces less smoke than other fuels.

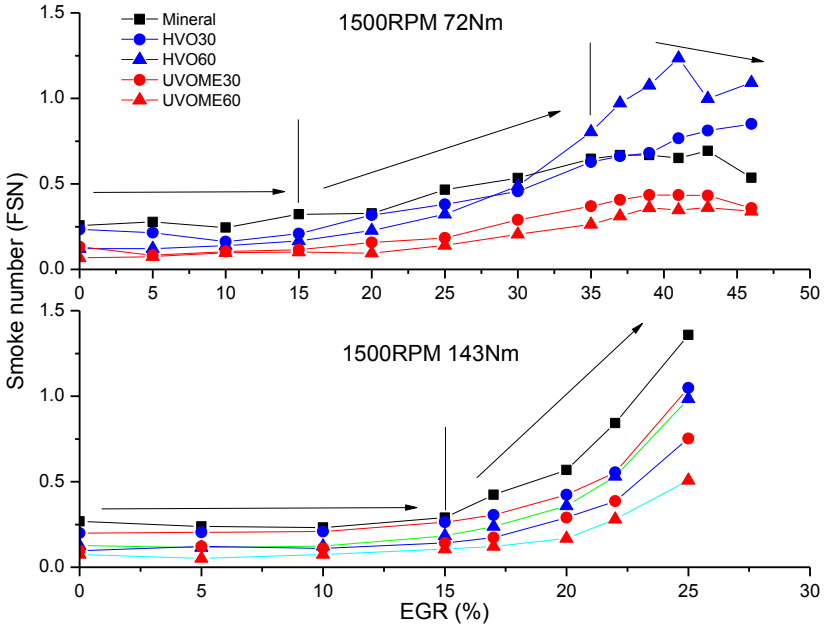

Figure 4.10 Smoke emission for various EGR rate

Medium EGR Effect

At medium EGR rate, the smoke emission of each fuel increased dramatically as EGR rate increased. Although the premixing was improved, the decease of combustion temperature and air/fuel ratio were more pronounced at medium EGR rate. Higher smoke increasing rates were observed at medium EGR rate.

High EGR Effect

High EGR rate was only applied at low engine load. The smoke levels of mineral diesel and UVOME blends were increased slowly and then decreased as EGR rate was increased. This is due to their low temperatures which do not lead to the unsaturated hydrocarbon and PAH coagulation and consequently transformation into soot. However, HVO blends had increasing rates even in the high EGR rate. HVO has higher cetane number, energy density, and the long chain paraffin is easier to be broken up than aromatic and naphthenic in mineral diesel. Thus, the temperatures of HVO blends combustion are always higher than other fuels and this can be confirmed by the combustion pressure and heat release rate discussed before. The high

combustion temperatures of HVO blends helped the unsaturated hydrocarbon and PAH coagulation and consequently increased the soot formation compared with other fuels.

4.4. CONCLUSIONS

Engine performance and emissions of two biodiesels namely HVO and UVOME and their blends were compared with diesel. EGR effects on both biodiesel and diesel were analysed as well. Following conclusions have been drawn:

1. EGR improved the initial fuel atomization/vaporization and fuel/air mixing prior to ignition. These improvements were obvious at low EGR% which results in BSFC and the smoke emission decrease at low EGR%. This effect was also observed at high EGR% with the low engine load.
2. High EGR% diluted the charged air and decreased NOx emission significantly, but deteriorated the combustion and resulted peak in-cylinder pressure drop and other emissions increase.
3. Shorter ignition delay, longer combustion duration and higher in-cylinder pressure of biodiesels showed the potential of engine performance improvement. The only drawback of biodiesel was the high fuel consumption. But for HVO, the fuel consumption was lower than diesel especially with high EGR%.
4. Emissions were improved using biodiesel. Almost all emissions (smoke, THC and CO) were reduced except NOx which didn't change significantly.

Chaper 5. CORRELATION OF ENGINE SMOKE EMISSIONS WITH ENGINE LOADS, EGR RATES AND FUEL PROPERTIES

This chapter describes the effects of engine loads, EGR rates and fuel properties on engine smoke emissions. The effects of cetane number, viscosity, GHV of combustion and oxygen content were studied with the six most common feedstocks selected. The correlation between the fuel properties and the engine smoke emissions was evaluated by regression analysis. A smoke index, which contains fuel properties, was created to predict the smoke number. The relationship between the smoke index and smoke number was also affected by the engine loads and EGR rates. The verification of the index in different engine conditions shows that the indices represented the smoke number emissions well.

5.1. ENIGNE LOAD EFFECTS ON SMOKE REDUCTION WITH USING BIODIESEL BLENS

Figure 5.1 to 5.3 shows the smoke number change rates of three biodiesels (UVOME, RME and HVO, respectively) compared with the cases of using mineral diesel in different blend ratios and engine loads. The EGR rates for all the tests were set to 0% in order to compare the engine load effect only. The colour represents the change rates of the smoke number when using biodiesel blends. The change rate was calculated as follows:

$$\text{Change rate} = \frac{\text{Smoke}_{\text{biodiesel}} - \text{Smoke}_{\text{diesel}}}{\text{Smoke}_{\text{diesel}}} \times 100\% \qquad (5.1)$$

For the UVOME blends, the highest reduction rate obtained when biodiesels were used occurred at high load (more than 6 Bar BMEP) and high biodiesel blend ratio. However, at low load and low blend ratio, the reduction of smoke emission was not as significant as the cases at high load. There was even a small increase around 3 Bar BMEP when only 10%

UVOME was blended. When the engine load was lower than 3 Bar BMEP, the main injection timing was set around -5.7˚BTDC and when the engine load was higher than 3 Bar BMEP (including 3 Bar), the main injection timing was set around -4˚BTDC. In addition, there was no post injection at 3 Bar BMEP. These data sets can be found in appendix table A3. The injection strategies at 3 Bar BMEP resulted in shorter ignition delay and less combustion in the late combustion phase. When using 10% UVOME-diesel blend, the increased viscosity of fuels counteracted the effects of the shorter ignition delay and earlier combustion as a result of the benefits provided by the oxygen content and reduced aromatics, which resulted in the smoke number increasing in this case. With the increasing of the UVOME blend ratio, the smoke number change rate also reduced. This reduction was fastest around 6 Bar BMEP. This meant that the smoke would reduce more with less UVOME blended in the mineral diesel around 6 Bar BMEP. In addition, the reduction of smoke change rate with blend ratio increase was quite slow between 2 and 3 Bar BMEP which meant that more UVOME was required to be blended in the mineral diesel to achieve the equivalent smoke change rate.

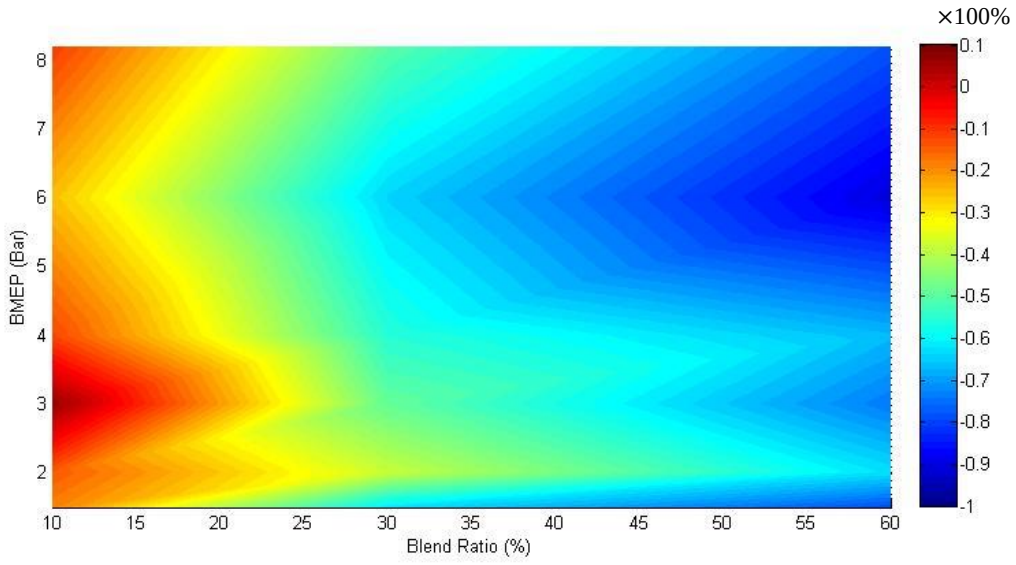

Figure 5.1 Contour plot of smoke reduction at various engine loads with different UVOMEblend ratio

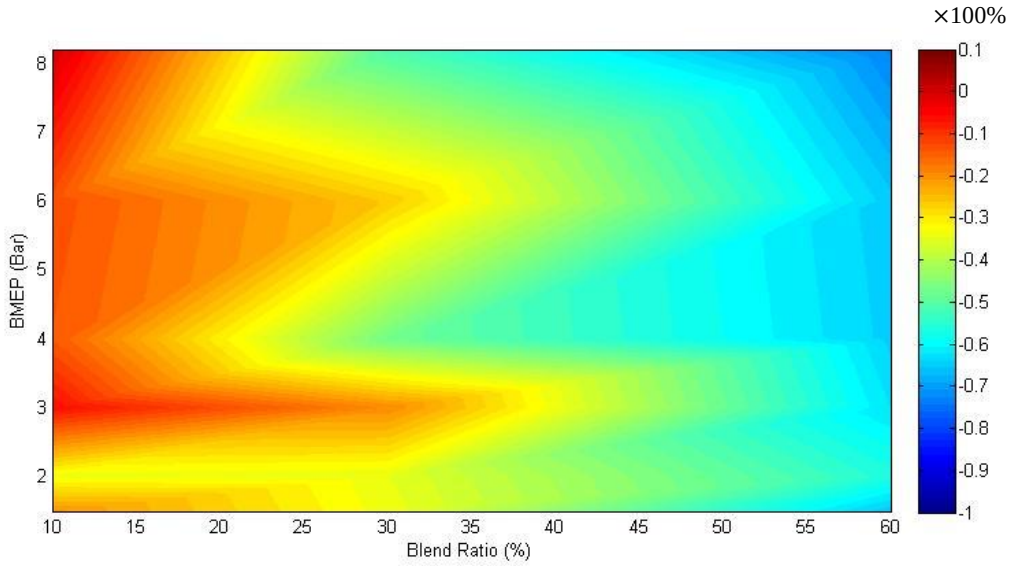

Figure 5.2 Contour plot of smoke reduction at various engine loads with different RME blend ratio

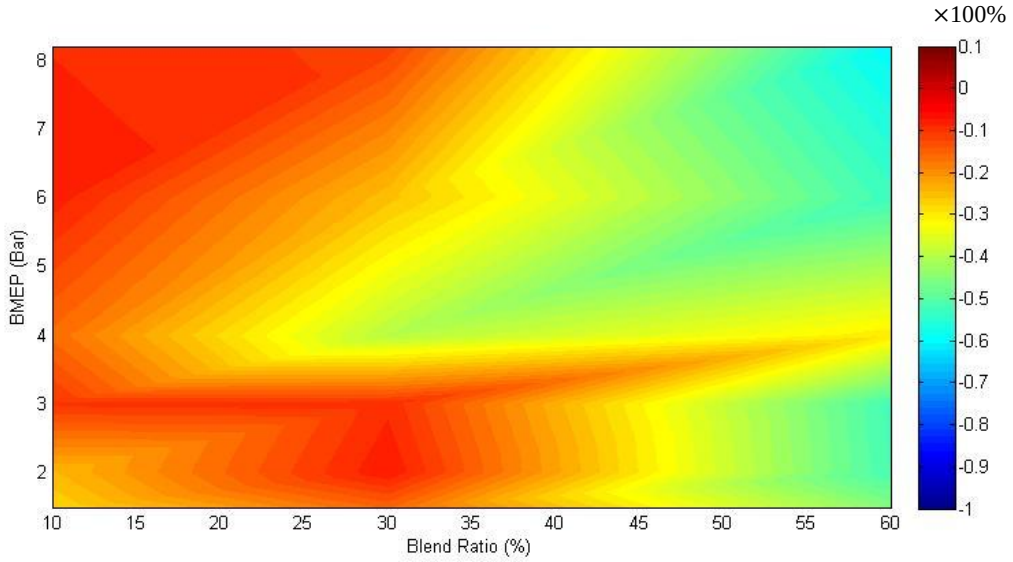

Figure 5.3 Contour plot of smoke reduction at various engine loads with different HVO blend ratio

When the fuel was changed to RME-diesel blends, the smoke reduction was less significant than that obtained when UVOME-diesel blends were used in most of the cases. The highest smoke change rate obtained when using RME-diesel blends also occurred at high load with high blend ratio. At 3 Bar BMEP, the smoke reduction obtained using RME was also not significant when the blend ratio was low. This was caused by similar reasons to when UVOME at low load with low blend ratio was used. As the RME blend ratio increased, the

smoke change rate also decreased and the most significant decrease occurred around 4 Bar and 7 Bar BMEP which means the effect of RME blend ratio was the most obvious around 4 Bar and 7 Bar BMEP.

The smoke reduction of using HVO-diesel blends was not as significant as with the cases of using methyl ester biodiesel because HVO does not contain oxygen. Meanwhile, the high cetane number of HVO might shorten the ignition delay and cause less vaporization and atomization which reduced the effect of smoke reduction. The highest reduction rate also occurred at high load with high HVO blend ratio. The smoke number of 3 Bar BMEP still showed a lower reduction rate when using HVO blends, and the smoke reduction was more significant when the HVO blend ratio at 4 Bar BMEP was increased.

5.2. EGR EFFECTS ON SMOKE REDUCTION WITH USING BIODIESEL BLENDS

5.2.1. EGR Effects at Low Load

Figure 5.4 to 5.6 show the EGR effects on smoke number when using biodiesel blends at 3 Bar BMEP. The results of 3 different biodiesels, UVOME, RME and HVO, are presented here. The colour shows the smoke number change rate which was calculated in the same way as in the previous section.

For each biodiesel, the highest smoke reduction usually occurred at a high blend ratio and low EGR rate. The area of the highest smoke reduction was different for each biodiesel. The use of UVOME always had a more significant smoke reduction than the cases of using the other two biodiesels. Meanwhile, the smoke reduction of using HVO was not significant compared with those of using two methyl ester biodiesels because there is no oxygen content in HVO

fuel. Meanwhile, the smoke number with a low biodiesel blend ratio was not reduced significantly and for some cases, it even increased slightly. This was explained in the previous section; it was due to the combined effects of a special injection strategy and the high viscosity of biodiesels. Since the viscosity of UVOME is the highest and HVO has the lowest viscosity, the smoke number increase was more significant when UVOME was used and less significant when HVO with low blend ratio was used.

When the EGR rate was increased, the smoke reduction obtained when using biodiesel tended to be less significant; for HVO, the smoke number even increased about two times. According to figure 2.2, the high EGR rate reduced the in-cylinder temperature and resulted in low temperature combustion, which reduced the soot formation. However, the HVO has higher heat value than other fuels, which increased the in-cylinder temperature. Thus, higher EGR rates were needed to reach low temperature combustion than the cases of other fuels.

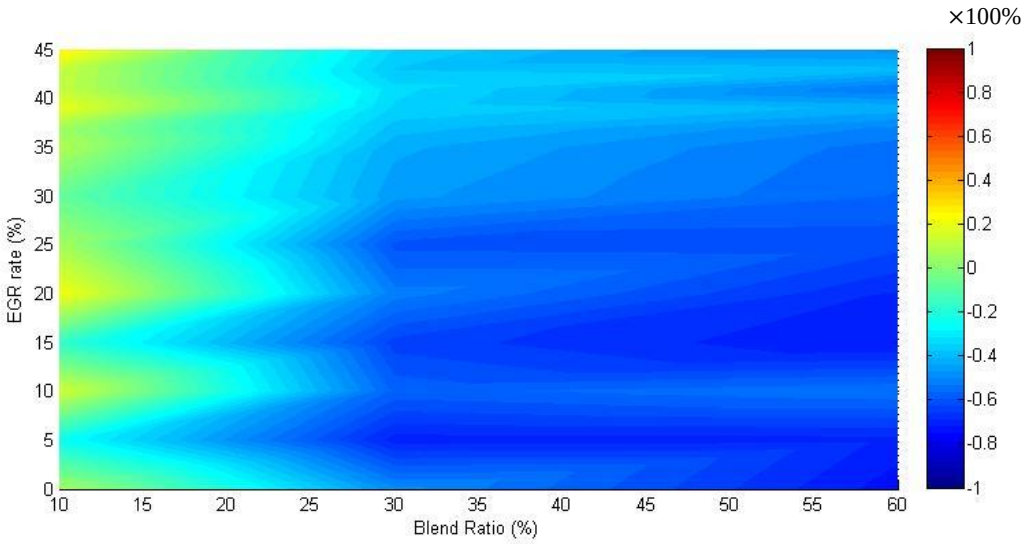

Figure 5.4 Contour plot of smoke reduction at various EGR rates with different UVOME blend ratio at 3 Bar BMEP

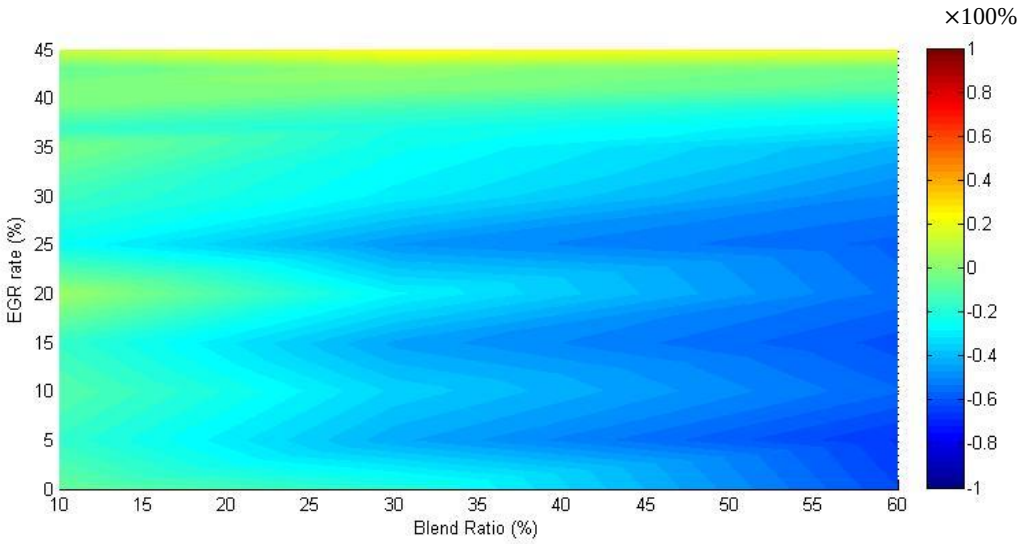

Figure 5.5 Contour plot of smoke reduction at various EGR rates with different RME blend ratio at 3 Bar BMEP

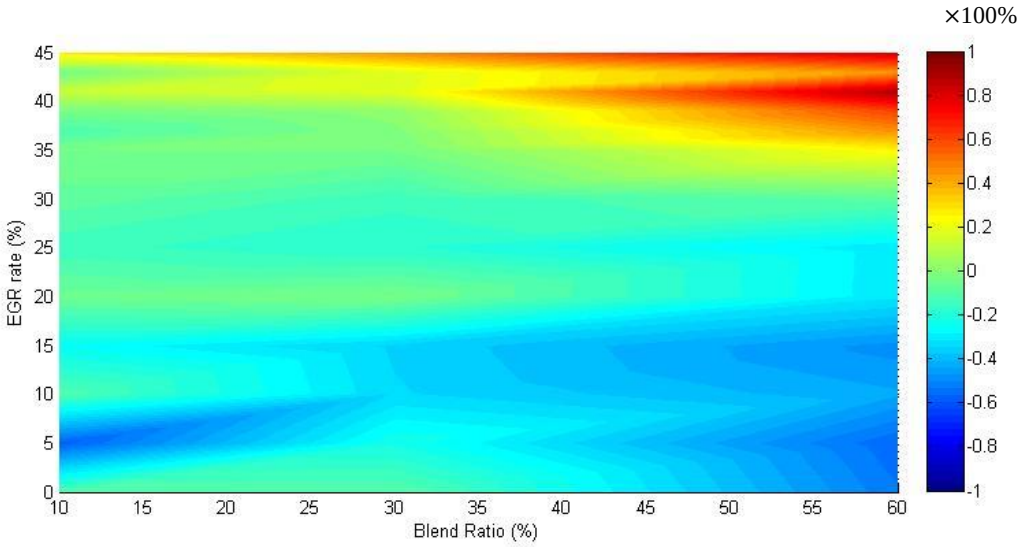

Figure 5.6 Contour plot of smoke reduction at various EGR rates with different HVO blend ratio at 3 Bar BMEP

5.2.2. EGR Effects at High Load

At 6 Bar BMEP, the EGR effects on the smoke number are shown in figure 5.7-5.9, representing three biodiesels with different blend ratios. Like the EGR effects at 3 Bar BMEP, the useof UVOME always had a more significant smoke reduction effect than other two fuels at 6 Bar BMEP. Since the highest EGR rate at 6 Bar BMEP was just 25%, the smoke number

reduction was not changed too much when theEGR rate was increased. However, at a 15% EGR rate, there was a small increase of smoke number with low blend ratio for each biodiesel, and at a 15% EGR rate, the smoke number change was reduced less as the blend ratio was increased as compared to the cases at the other EGR rates. However, at 3 Bar BMEP with 15% EGR rate, the smoke change rate was reduced more when the blend ratio was increased. In the previous chapter, the results showed that when the EGR rate was lower than 15%, the smoke number obtained when using mineral diesel was slightly decreased or it at least remained constant as the EGR rate was increased. When the EGR rate was increased to more than 15%, the smoke number was increased significantly. This means that 15% wasa critical EGR rate for engine combustion and it caused the unusual smoke reduction when biodiesels were used in this study. In the previous chapter, the smoke number decrease was due to the EGR rate which prolonged the ignition delay to improved fuel atomization and vaporization which counteracted the dilution effects of EGR at low EGR rate. After the EGR percentage was increased to more than 15%, the dilution effects dominated. Hence, the 15% EGR rate might be the point at which the two effects were compensated by each other when mineral diesel was used. When B10 was used with a 15% EGR rate at low load, the ignition delay was increased more significantly since the in-cylinder temperature was lower. This caused the smoke reduction obtained when using biodiesel to be more significant. However, at high load, the increase of ignition delay might be too small to improve the poor atomization and vaporization caused by the high cetane number and high viscosity of biodiesels. Therefore, the smoke number change was not significant at high load with a 15% EGR rate.

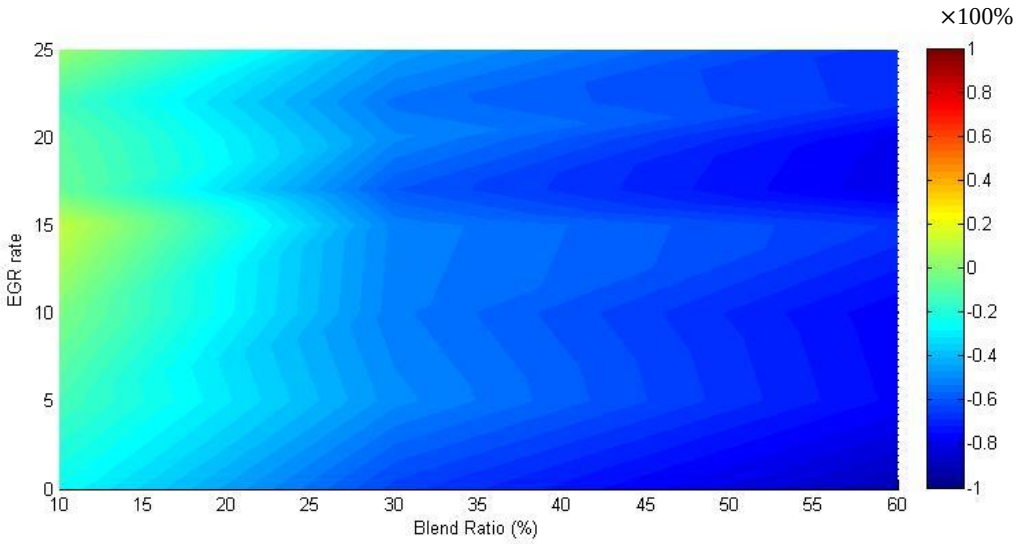

Figure 5.7 Contour plot of smoke reduction at various EGR rates with different UVOME blend ratio at 6 Bar BMEP

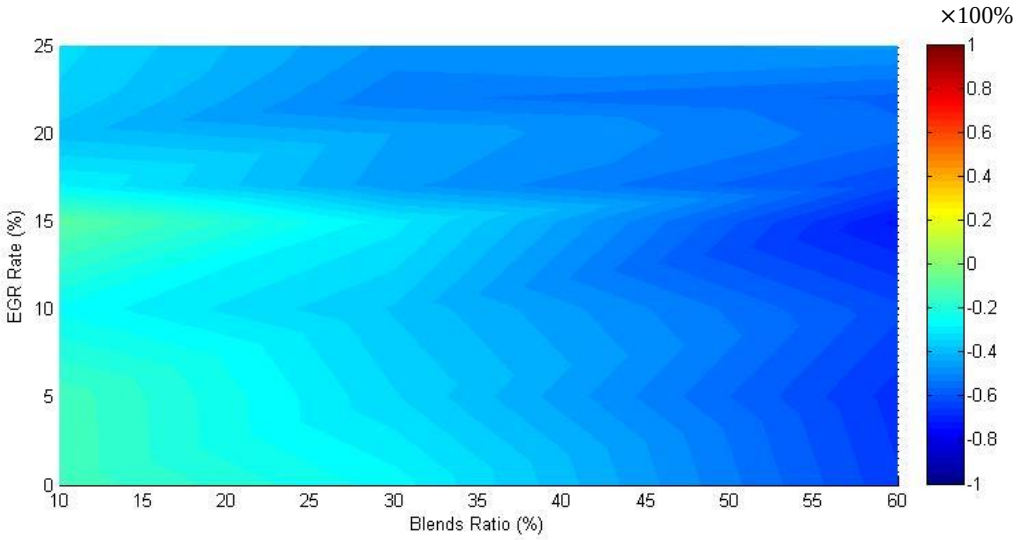

Figure 5.8 Contour plot of smoke reduction at various EGR rates with different RME blend ratio at 6 Bar BMEP

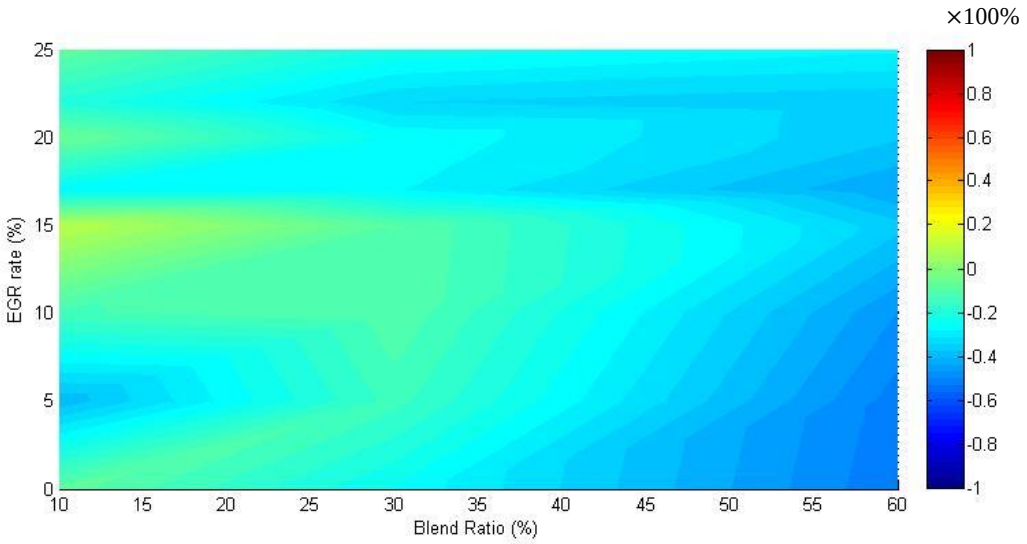

Figure 5.9 Contour plot of smoke reduction at various EGR rates with different HVO blend ratio at 6 Bar BMEP

5.3. REGRESSION ANALYSIS BETWEEN FUEL PROPERTIES AND SMOKE NUMBER

In the previous section, the effects of engine loads and EGR rates when using biodiesels were studied. For different types of fuel, the smoke number change was different due to their differing properties. The FSN (Filtered Smoke Number) is measured by smoke meter, which reveals the opacity of smoke, or how black the smoke is. To analyse how the fuel properties affected the smoke emission, regression analysis was suggested in order to quantify the correlations between fuel properties and the FSN.

5.3.1. Sample of Experimental Results

The emissions for all biodiesels under 2 Bar BMEP (1250RPM and 48Nm) with 0% EGR ratewere chosen for the regression analysis. All of them are represented in figure 5.10 below. Only methyl ester biodiesels were compared in this stage since the properties of HVO and its

relationship with smoke emissions was totally different. The properties of HVO will be considered in the next section.

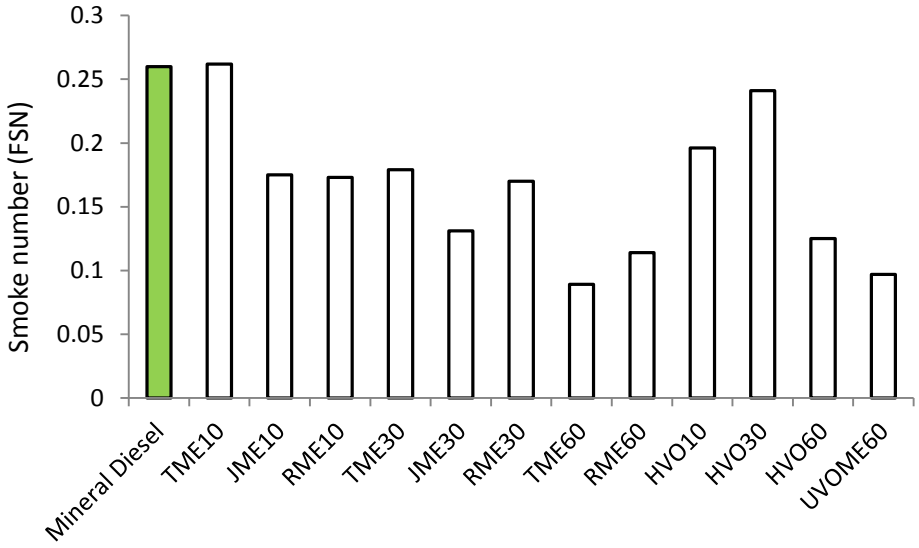

Figure 5.10Smoke number of all tested fuels

For fuels produced from different feedstocks, most of the biodiesels had a lower smoke number than that of mineral diesel. Only TME10 had a slightly higher smoke than the cases of mineral diesel. The variations of all the fuels were caused by different feedstocks and blend ratios. Some authors compared the emissions of using different biodiesel based on whether the biodiesels were derived from plants or animals. But here, no such relationship could be found. Whether the fuel was produced from agricultural, waste or animal feedstock, it was not the key factor in evaluating their smoke levels.

5.3.2. Linear Regression Analysis

The main aim of this section is to indicate the effects of the fuel properties of biodiesel on smoke number. The empirical correlations of fuel properties and emissions are quantified in this part. The correlation between each property was estimated and listed in Table 5.1. The

value used to evaluate the relationships was between -1 and 1. If the absolute value is more close to 1, it means the correlation was more significant. If the absolute value is more close to 0, the relationship was considered as not significant. The negative value means the relationship is inverse proportional.

According to table 5.1,the density, Gross Heat Value (GHV) of Combustion and oxygen content are highly interrelated to each other because the high oxygen content increases the density and decreases the GHV. The Cetane number of the biodiesel is weakly related to the other properties. The viscosity of the biodiesel also shows correlations with density, GHV and oxygen content, but it is not as significant as the relationships between these three fuel properties. Density and GHV are easily and cheaply measured, thus these are good parameters for the correlation analysis.

It should be noted that all the results presented in this section are engine specific with certain loads and 0% EGR rate. The effects of engine load and EGR rate on fuel properties will be discussed in the next section. All the tested fuels are blended fuels and mineral diesel is also included in the analysis.

Table 5.1Correlation of each fuel property

	Cetane	density	viscosity	Gross heat of combustion	oxygen content	surface tension
Cetane	1					
density	0.149682	1				
viscosity	0.507446	0.812126	1			
Gross heat of combustion	-0.20954	-0.98151	-0.78967	1		
oxygen contain	0.342641	0.944942	0.824874	-0.96042	1	
surface tension	0.588286	0.693182	0.932279	-0.67479	0.807922	1

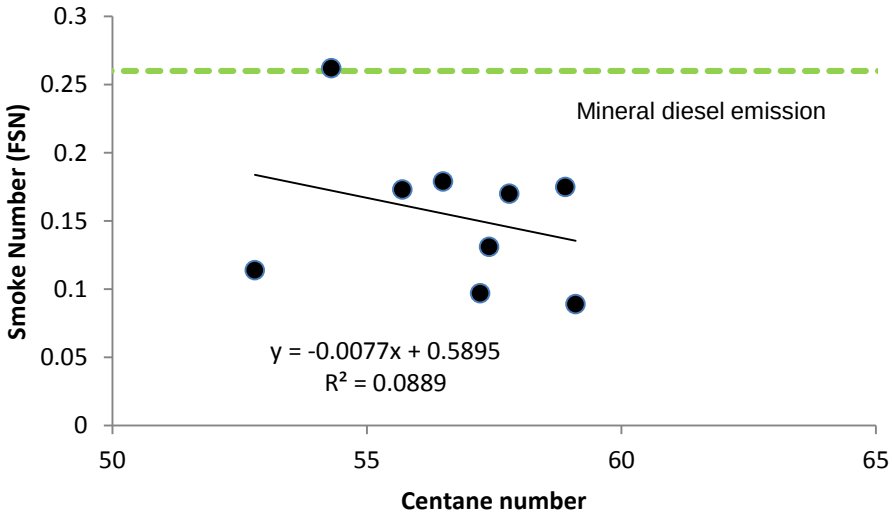

Figure 5.11Effects of cetane number on the smoke number

Figure 5.11shows the correlations between smoke number and cetane number. The regression analysis results indicated that the relationships between smoke number and cetane number was not significant. Figure 5.12 below shows the relationships between smoke number and fuel viscosity. The linear regression did not show a significant relationship between smoke number and viscosity. However, the correlation might still exist if more data could be added.

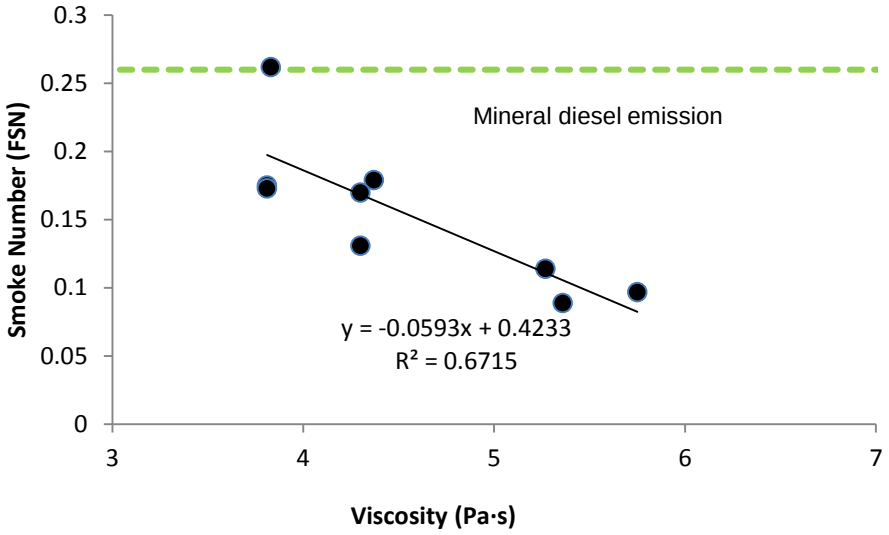

Figure 5.12Effects of viscosity on emissions of smoke number

Figure 5.13represents the regression analysis of smoke number with GHV. The regression showed a reliable relationship between smoke number and GHV of combustion and the prediction explains more than 70% of the variance.

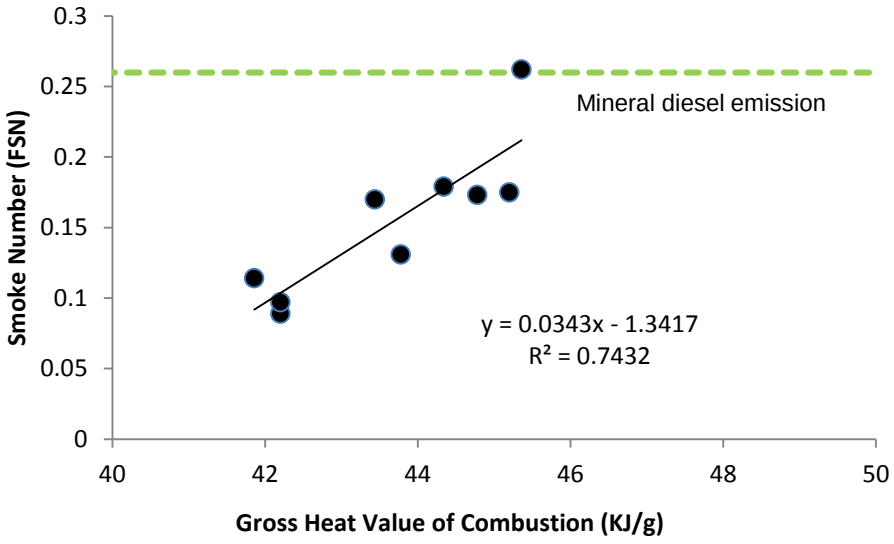

Figure 5.13Effects of GHV on emissions of smoke number.

For the biodiesels used in the tests, their GHVs were highly correlated to the oxygen content. Fuels with lower GHV always had higher oxygen content which resulted in lower smoke

emissions. In addition, GHV also affected the fuel injection system. With a certain engine load with the same engine, the use of fuels with low GHV always resulted in high fuel quantity demand. In order to increase the fuel injection quantity in the cycle, the injection pressure or injection duration or sometimes both are increased by the ECU. In the tests, the increase of the fuel injection pressure was much more obvious than the cases of increased injection duration. By increasing the injection pressure, the fuel penetration and atomization improved which resulted in a high percentage of premixed combustion and thus reduced the smoke emissions.

Figure 5.14shows the linear regression between smoke number and oxygen content; there is a significant relationship between smoke and oxygen content. The estimated equations match the actual value in 84%of the cases which indicates that the regression equations did not occur by chance. The oxygen effect is clear, significant and also easy to explain. The oxygen atom in the molecule combined with carbon atom and formed a C-O or a C=O bond which were not easy to be broken down. Thus the soot and hydrocarbon formation was reduced in the combustion.

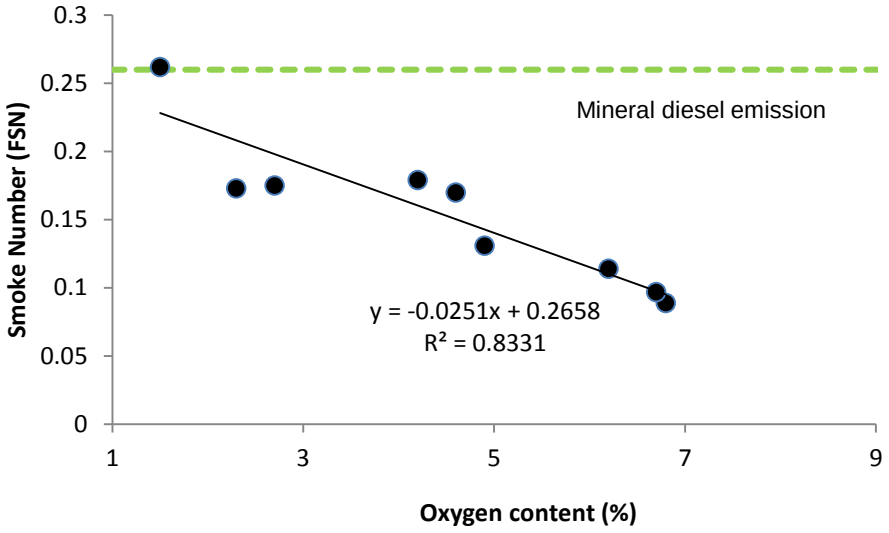

Figure 5.14Effects of oxygen content on emissions of smoke number.

It should be noted that oxygen content, fuel density and GHV were highly interrelated with each other. Even though the regression model of fuel density was not presented, the significant regression between smoke and fuel density could still be predicted. In addition, oxygen content was highly reverse correlated to GHV. The higher the oxygen content, the less energy the fuel contained. However, the energy of fuel wasnot only decided by the oxygen content; there are some other properties which affected the GHV of fuel, such as carbon chain length and degree of unsaturation of fuel molecules.

5.4. SMOKE NUMBER INDEX OF BIODIESEL BLENDS

5.4.1. Smoke Index Suggestion

The analysis in the previous section has shown some linear relationships between fuel properties and smoke numbers. The smoke number decreased significantly when the fuel contained oxygen. However, this correlation was only valid when the fuel contained oxygen. When the mineral diesel and HVO blends were added to the regression analysis, the coefficient of determination R2 of smoke-viscosity, smoke-GHV and smoke-oxygen in the

previous section were reduced to 0.566, 0.462 and 0.589 respectively which cannot indicate a clear and significant relationship. To correlate the fuel properties and smoke emissions, all the fuel properties were considered again to create a smoke index to quantify the relationships. GHV was highly correlated to fuel density and oxygen content, and it was also very easily measured. Hence, GHV was chosen to be the key factor to indicate the relationship. To include oxygen free biodiesel fuels, other correction factors were added to make the index fit the regression.

Firstly, the Reynolds number and Weber number were considered. Reynolds number is the ratio between inertial force and viscosity force which mainly affects the fuel spray propagation speed and penetration. While Weber number is the ration of inertial force and surface tension force, which mainly affects the fuel break-up. They are related to the fuel spray characteristics which have effects on the combustion and emissions. They were calculated by equations 5.2 and 5.3. Re is the Reynolds Number, We is the Weber number, ρ_{fuel} is the density of the fuel, V is the velocity of fuel injection, D represents the diameter of the nozzle hole,μ is the viscosity of the fuel and σ is the surface tension of the fuel. Since all the regressions presented here are linear and the Weber number contains a quadratic item, the Reynolds number was chosen to be one of the correction factors.

$$Re = \frac{\rho_{fuel} VD}{\mu} \tag{5.2}$$

$$We = \frac{\rho_{fuel} V^2 D}{\sigma} \tag{5.3}$$

All of these parameters are easily obtained, except the velocity of fuel injection. Since it is not easy to measure the velocity of fuel injection from tests one by one, a simple calculation for the global velocity was proposed as follows:

$$V = \frac{\dot{m}_{fuel}}{\rho_{fuel} nA} \tag{5.3}$$

$$A = \pi \frac{D^2}{4} \tag{5.4}$$

Here, $\dot{m}_{fuel}$ is the fuel mass flow rate, n is the number of nozzle holes and A is the area of a nozzle hole.

Cetane number was also added into the index, even though no relationship was found between Cetane number and smoke emissions. Without Cetane number in the equation, the determination coefficient R^2 would be reduced dramatically. For example, figure 5.15 and 5.16 represent the relationships between the calculated smoke index and the measured smoke number in two engine conditions. The determination coefficient R^2 for each condition was larger than 0.9. This meant that the smoke number could be explained by the smoke index I very well. Additionally, if the cetane number was removed from the equation, the determination coefficient R^2 ofthe two conditions would be reduced to 0.75 and 0.85, respectively. This reduction also occurred in other engine conditions because the cetane number affects the relationship between GHV and smoke number. Thus cetane number can be a correction factor when oxygen-free fuels was included.

Combining all the parameters (cetane number, gross heat value and Reynolds number) discussed in previous paragraph, considering the regression analysis in the previous section, it can be found that the FSN is inversely proportional to cetane number and gross heat value while direct proportional to Reynolds number, the following smoke index (inversely proportional to FSN) can be created:

$$I = CN \times \frac{GHV}{Re} \tag{5.5}$$

Here, I is the smoke index, and CN is the cetane number. The index shows a significant linear relationship with the smoke emissions in most of the engine conditions.

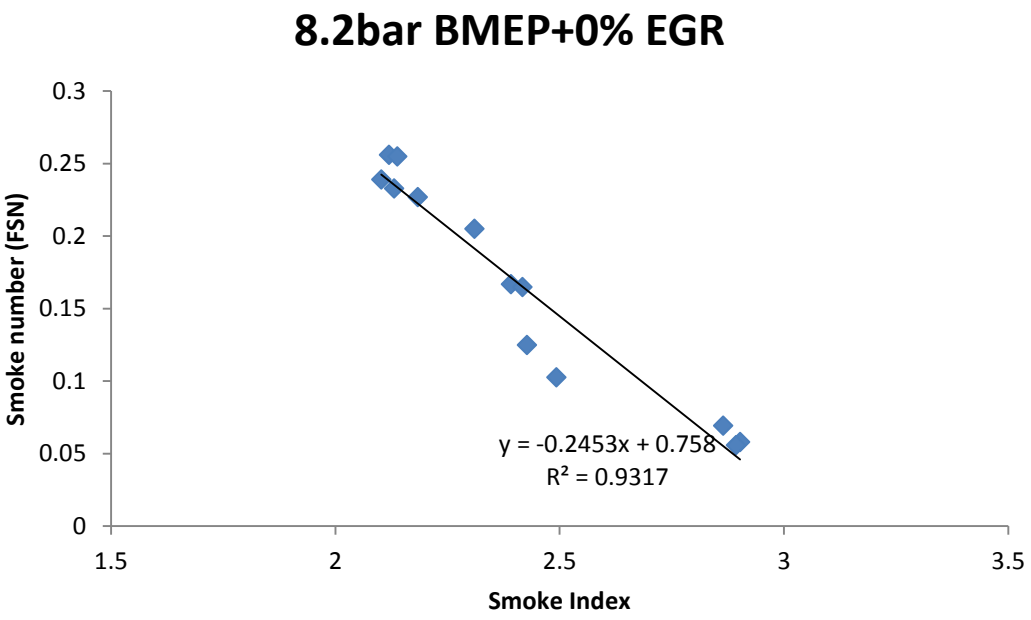

Figure 5.15 The linear regression between smoke index and smoke number at 8.2 Bar BMEP and 0% EGR rate.

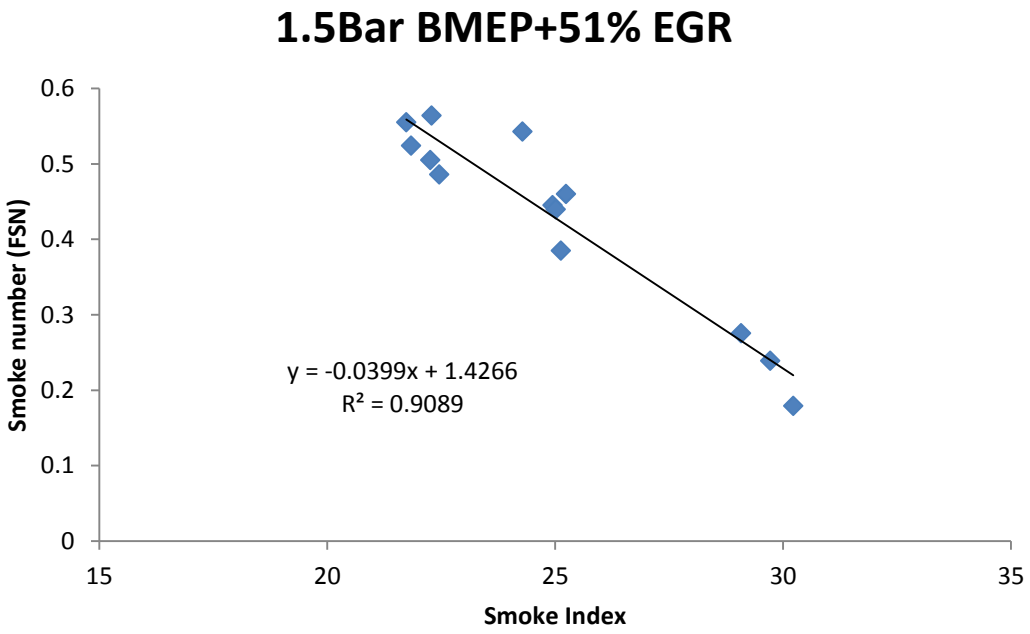

Figure 5.16 The linear regression between smoke index and smoke number at 1.5 Bar BMEP and 51% EGR rate.

5.4.2. Regression of the Smoke Index in Different Engine Conditions

If the smoke index created in the previous section is truly a good indicator of the smoke number, it should also be applicable for all the engine loads and EGR rates. Figure 5.17 shows the determination coefficient R^2 at different engine loads and EGR rates. It can be observed that the values of R^2 are larger than 0.7 in most of the cases except at 3 bar BMEP with an EGR rate higher than 37%. Therefore, the linear relationships between smoke index and smoke number were significant at various engine loads and EGR rates. The smoke index could be used to predict the smoke emissions at most of the engine conditions.

When the EGR rate was increased higher than 35% at 3 Bar BMEP, the prolonged ignition delay would cause an increase of premixed combustion and lead to the decrease of smoke number. This was discussed in the previous chapter. As the premixed combustion dominated the combustion process, the smoke emissions would mainly be determined by the percentage of premixed combustion. Hence, the smoke index was not applicable at the engine conditions when the combustion was dominated by the premixed combustion.

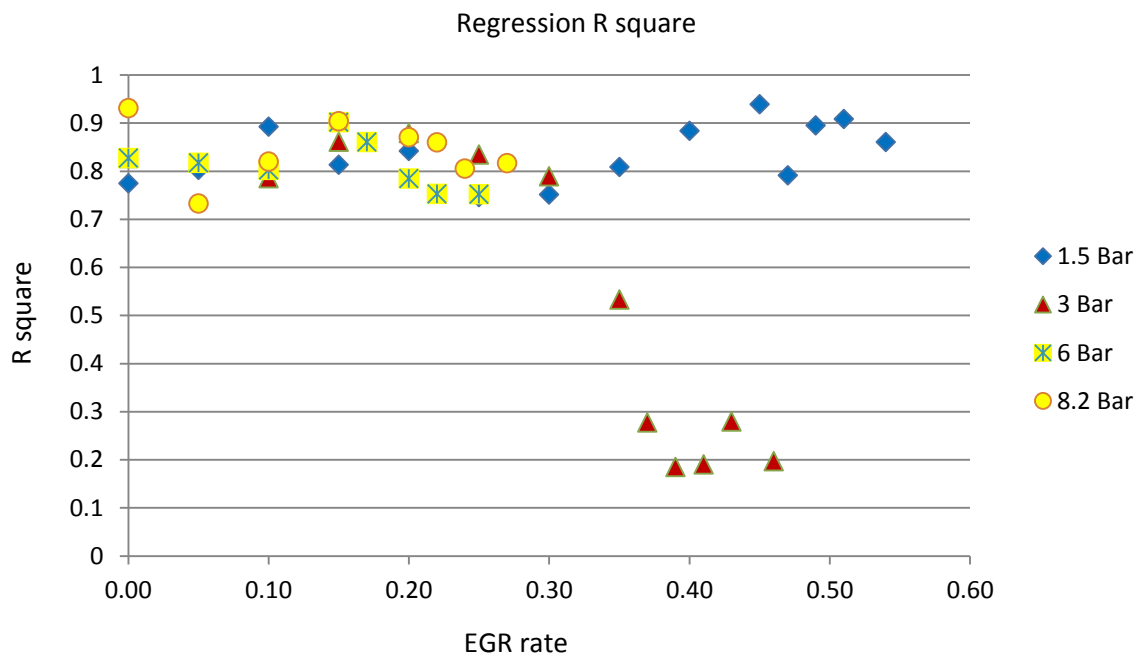

Figure 5.17 The R2 of linear regression between smoke index and smoke number at different engine conditions.

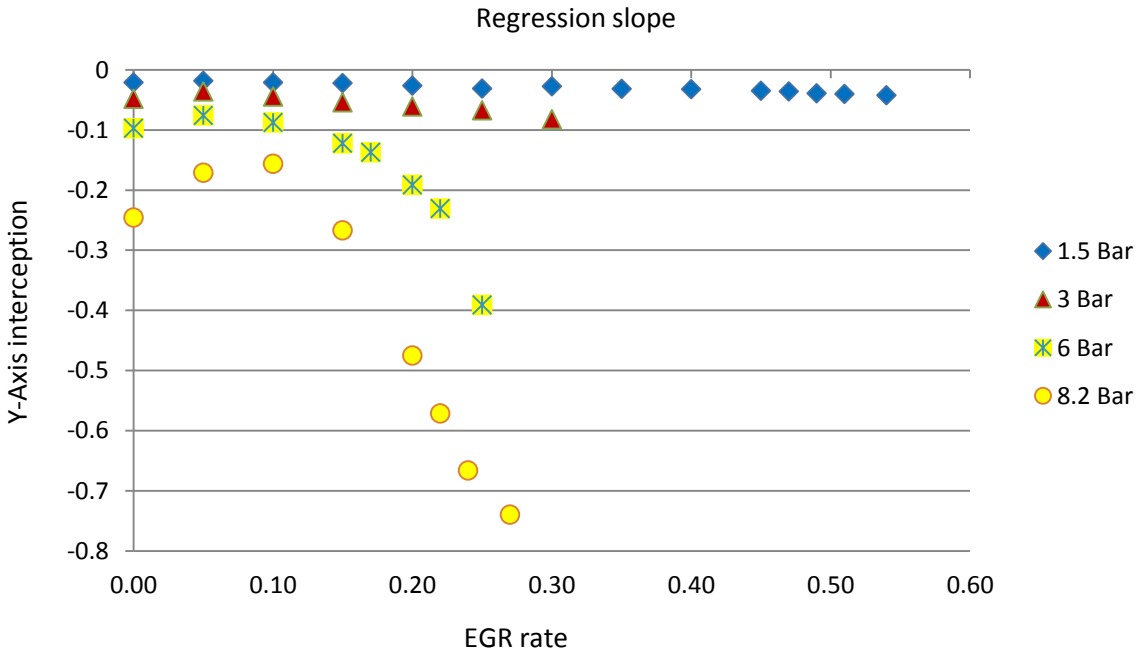

Figure 5.18 The slope of linear regression between smoke index and smoke number at different engine conditions.

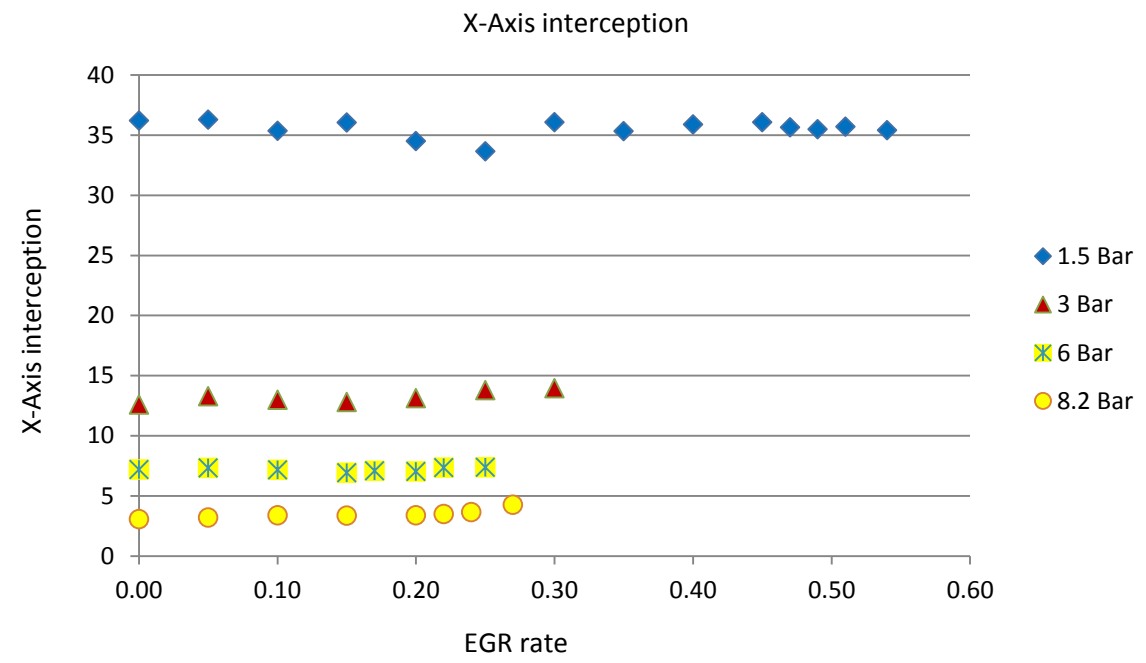

Figure 5.19 The X-Axis interception of linear regression between smoke index and smoke number at different engine conditions.

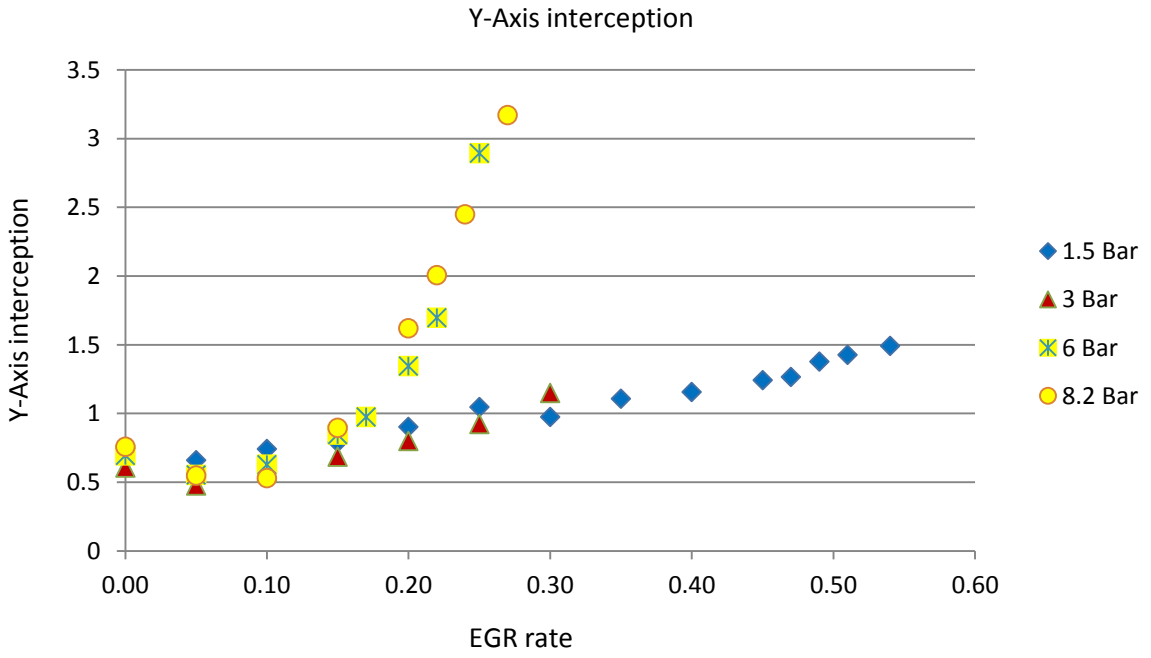

Figure 5.20 The Y-Axis of linear regression between smoke index and smoke number at different engine conditions.

The points at which the determination coefficient R2 was lower than 0.7 were deleted and the subsequent values of slope for the regression equations are presented in figure 5.18. The slope indicated the proportional relationships between the smoke number and smoke index. It can be seen that the value of the slope changed with EGR rate via a quadratic relationship, and it can be seen they decreased as BMEP increased. The X-Axis and Y-Axis interception of the regression equations in different engine conditions are also shown in figure 5.19 and 5.20. The X-Axis interception only changed with engine load and the EGR rates did not affect the interception point too much. The X-Axis interception is the boundary condition of each engine condition which means that the smoke number is 0. For the real life situation, this means that the EGR effects on smoke number would be reduced when the use of one fuel reduced the smoke number. Y-Axis interception is the product of the slope and X-Axis interception. Since the X-Axis interception changed within the BMEP, the regression equation can be expressed as the following format:

$$\text{Smoke number} = \mathrm{F_1(BMEP, EGR\%)} \times \mathrm{I} + \mathrm{F_2(BMEP)} \times \mathrm{F_1(BMEP, EGR\%)} \quad (5.6)$$

Here, I is the smoke index, $\mathrm{F_1(BMEP, EGR\%)}$ is a function of BMEP and EGR rate, and $\mathrm{F_2(BMEP)}$ is a function of BMEP. The two functions were fitted by the fitting toolbox in MatLab. For the first function, the data used to make the surface fitting were the values of the slope at 1.5, 3, 6 and 8.2 Bar BMEP with EGR rates of 0%, 5%, 10%, 15%, 20% and 25%. The data of 1.5 Bar and 2 Bar BMEP with EGR rate from 30% to 51% and all the data of 4 Bar BMEP were used to validate the final model. For the second function, the averaged value was calculated and a curve fitting was made. The fitting method for the two functions was polynomial.

Figure5.21 shows the surface fitting of the first function. Where x is BMEP and y is EGR rate. The coefficients of the regression model and the quality of the fitting are also shown below. The polynomial order for the EGR rate was 2 which can be seen in figure 5.18. 3 polynomial orders (1, 2 and 3) were tried, and the determination coefficients were 0.8917, 0.92 and 0.9897, respectively. Further increasing of the polynomial order did not improve the quality of the fitting significantly. To achieve the best fitting, the polynomial order of BMEP was chosen as 3. This also agreed with the trends in figure 5.1to 5.3 in the previous section.

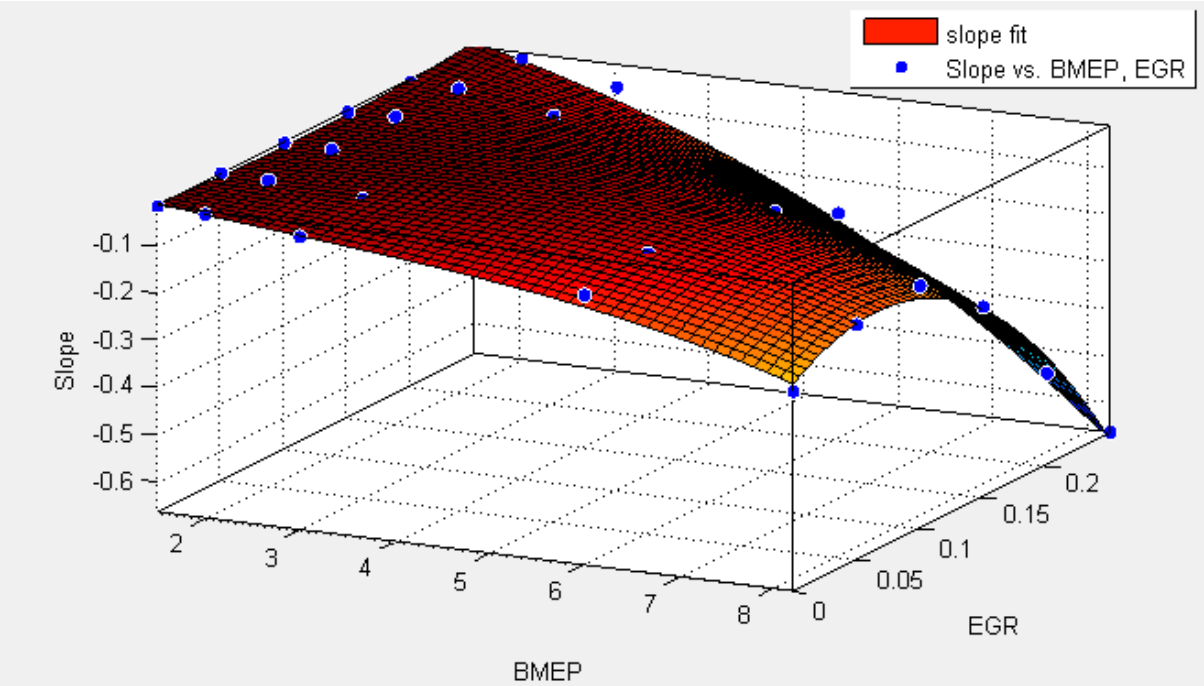

Figure 5.21 The surface fitting model to predict regression slope based on BMEP and EGR rate

Fitting model for $F_1(BMEP, EGR\%)$*:*

$F_1(x,y) = p00 + p10*x + p01*y + p20*x^2 + p11*x*y + p02*y^2 + p30*x^3 + p21*x^2*y + p12*x*y^2$

Coefficients (with 95% confidence bounds):

p00 =0.02583 (-0.06225, 0.1139)

p10 =-0.03246 (-0.09787, 0.03295)

p01 =-1.044 (-1.686, -0.4023)

p20 =0.004463 (-0.009472, 0.0184)

p11 =0.568 (0.3429, 0.7931)

p02 =4.73 (2.604, 6.855)

p30 =-0.0005243 (-0.001445, 0.0003968)

p21 =-0.0242 (-0.04441, -0.003998)

p12 =-2.433 (-2.869, -1.996)

Quality of fit:

SSE: 0.007084

R-square: 0.9897

Adjusted R-square: 0.9858

RMSE: 0.01837

SSE is the sum of squares due to the error of the fit. A value closer to zero indicates a fit that is more useful for prediction. R-square is the determination coefficient. Adjusted R-square is the degrees of freedom adjusted R-square. A value closer to 1 indicates a better fit. RMSE is the root mean squared error or standard error. A value closer to 0 indicates a fit that is more useful for prediction. All the values of this fitting indicated that the fitting can reliably predict the true value.

The second function was obtained by using the curve fitting toolbox in MatLab, and is shown in figure 5.22. Since the variable is the BMEP, the polynomial order of 3 was chosen and the fitting also showed a high significance level. The fitting model was also resolved where x in is the value of BMEP.

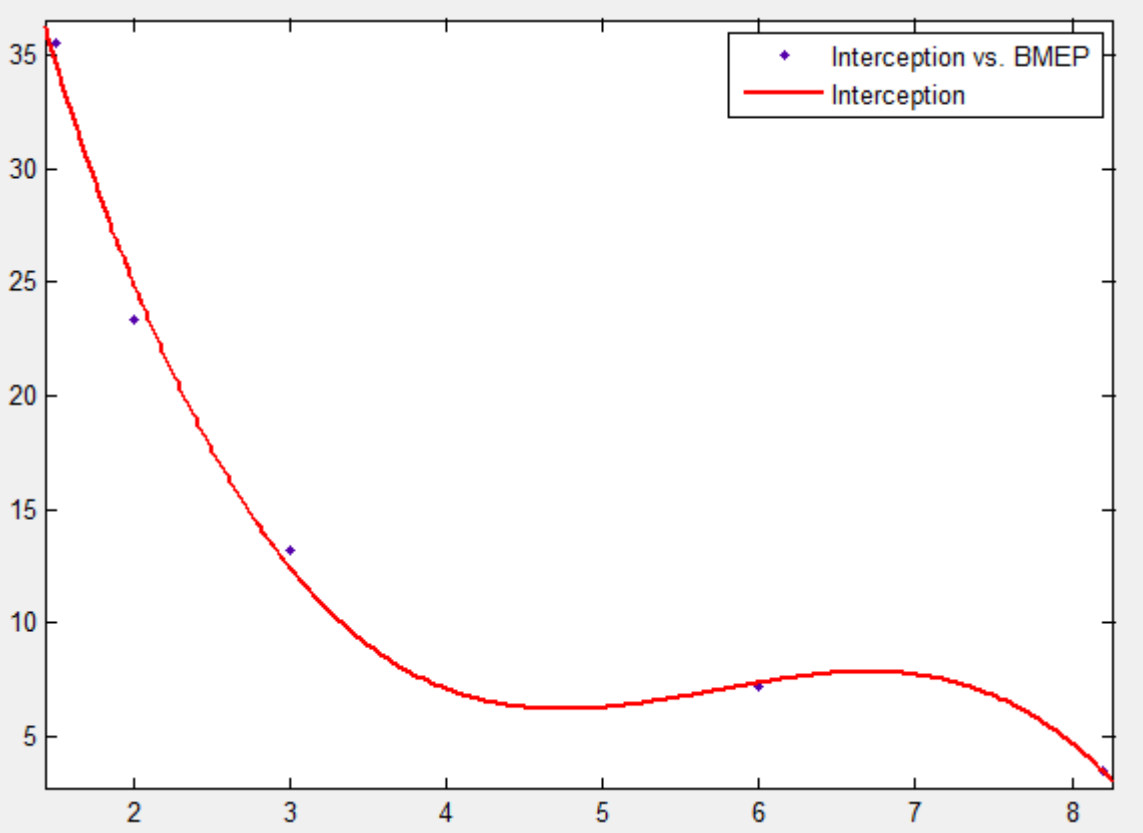

Figure 5.22 The curve fitting model to predict X-Axis interception of regression based on BMEP and EGR rate

Fitting model for $F_2(BMEP)$

$F_2(x) = p1*x^3 + p2*x^2 + p3*x + p4$

Coefficients (with 95% confidence bounds):

p1 = -0.4393 (-1.902, 1.024)

p2 = 7.54 (-14.23, 29.31)

p3 = -41.87 (-138, 54.22)

p4 = 82.04 (-34.83, 198.9)

Quality of fit:

SSE: 3.799

R-square: 0.9944

Adjusted R-square: 0.9776

RMSE: 1.949

With equation summarized above, the smoke number of biodiesel could be predicted. The validation is shown in figure 5.23 which compared the measured smoke number and predicted smoke number. It can be seen that some of the predicted results agreed with the measured results very well. But some of the predicted results did not agree well with the measured results because the multiplication of the predicted models amplifies the errors and leads to the mismatch.

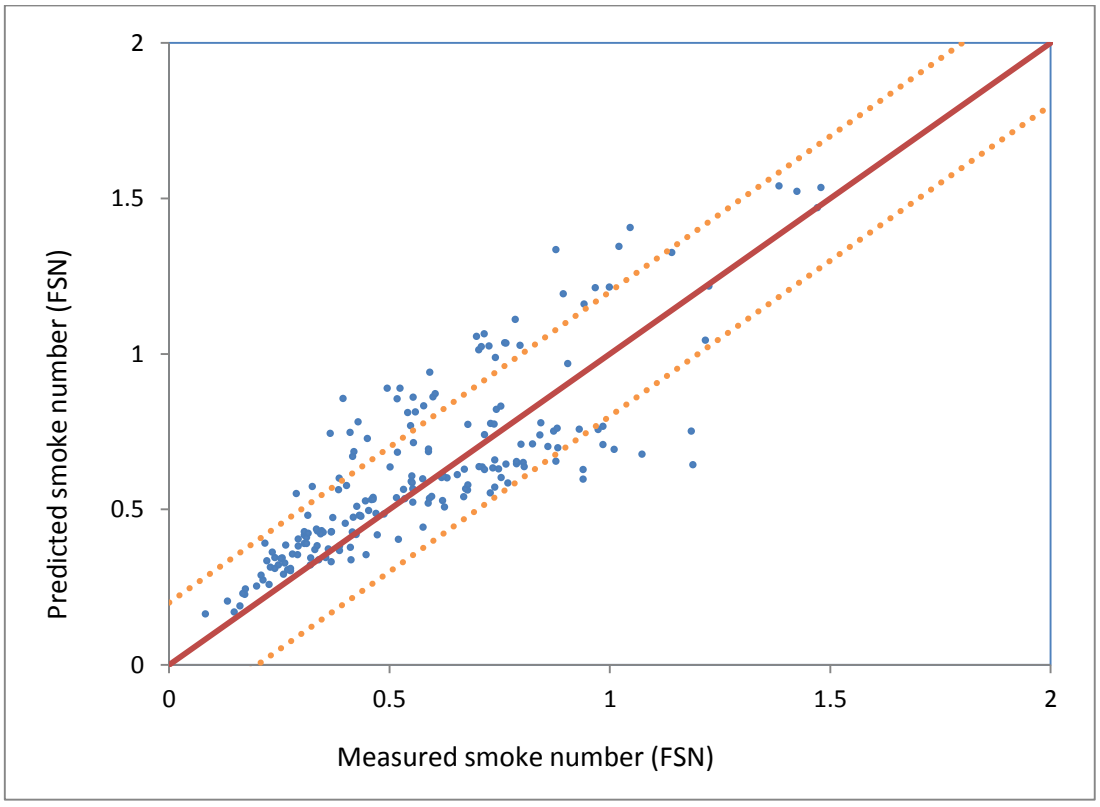

Figure 5.23 The comparison between prediction and actual smoke number with ±20% error band.

5.5. *CONCLUSIONS*

The engine tests were carried out with the blends of biodiesel produced from several different feedstocks. The effects of fuel properties, engine loads and EGR rates on smoke emissions were analysed. For the biodiesel fuels, the oxygen content of the fuel reduced the smoke number. This property was observed in significant linear relationships between the fuel

oxygen content and the smoke emissions. The GHV of combustion also showed highly significant linear relationships with smoke emissions. The NOx emission was not correlated to the two properties according to the regression analysis. An equation which contained the three parameters was proposed to predict the smoke emissions by statistical analysis. In the equation, a smoke index, which included the GHV of combustion, cetane number and Reynolds number, was proposed and showed a significant linear relationship with the smoke number in most of the engine conditions. The slope and interception of their linear regression were also fitted in functions related to the engine loads and EGR rates. Parts of the experimental data were used to validate the regression model and the prediction agreed with experimental data well.

Chaper 6. COLD AND WARM START WITH USING DIFFERENT BIODIESEL FUELS

6.1. TEST CONDITIONS AND PROCEDURES

In this chapter, engine performances and emissions during cold start at 20°C and warm start with coolant temperature at 90°C were studied. At 20°C cold start, the room temperature was maintained at 20°C by a ventilation system. The engine was kept power-off in room temperature at least 9 hours before start to ensure the engine is fully cooled down to the 20°C.With battery fully charged and measurement equipment fully warmed up, the engine was started and maintained at idle for 3 minutes. After engine stopped, the starter motor was switched on without fuel injection for several seconds so that the engine eliminated the residual gas in all cylinders. In addition, the crank shaft was adjusted to make sure engine started with the same piston and valve positions every time. Each test was repeated for three times check the repeatability.

In warm start test, the procedures were almost the same with cold start. The only difference was to heat up engine coolant to 90°C before the tests. An external engine coolant circulation with 3KW heat capacity was built for engine coolant warming up before engine start. The aim is to set the engine condition close to hybrid electric vehicle (HEV). In the HEV system, the engine coolant might be warm due to heat exchange of battery or other facilities when the vehicle is powered by the motor. Therefore, the engine is possible to start at the conditions with warm coolant but cool engine oil and other parts. In addition, researchers also developed thermal energy storage device (TESD) which is able to charge the coolant temperature before engine start (Gumus 2009). By heating up the coolant only, the effect of engine coolant temperature is able to be investigated.

The Cambustion Fast FID/CLD and DMS500 were connected before catalyst to measure the emissions of THC, NO and particle matter. The NOx detector of fast CLD was disabled in order to reduce the measurement delay. The THC and NO signals were recorded by an in-house labview data acquisition program through an NI card. To synchronize all the control and measurements variables from different system, the starter motor voltage and in-cylinder pressure signal were recorded together with emissions signals in real time. Figure 6.1 shows the data acquisition system and external coolant heating system.

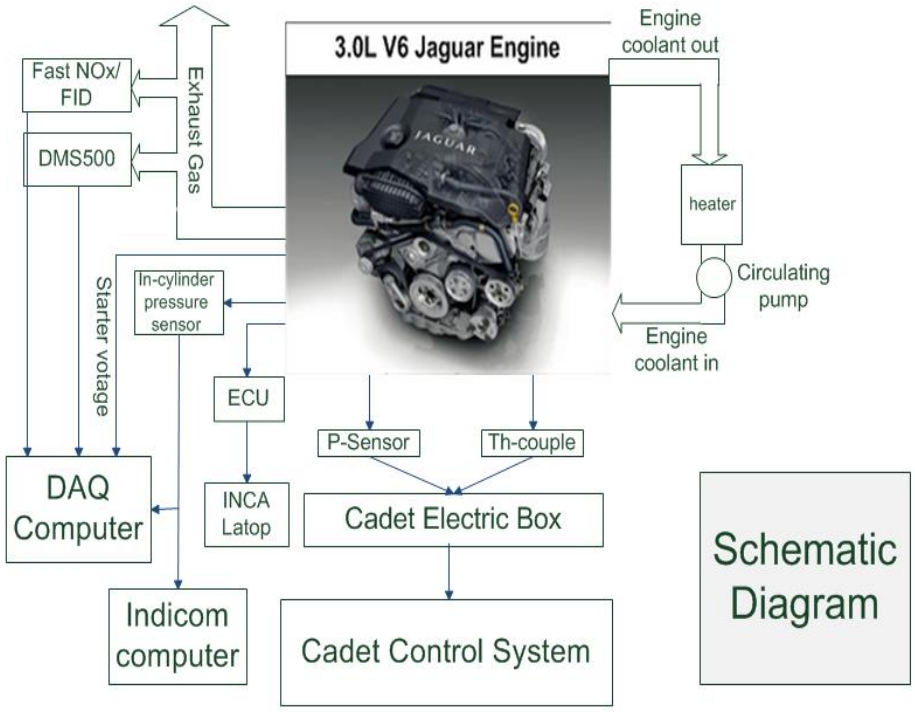

Figure 6.1The schematic of engine control and data acquisitions systems

6.2. THE ENGINE PERFORMANCES AND COMBUTION CHARACTERISTICS OF COLD START

6.2.1. Engine Performances During Cold Start

Figure 6.2shows the cold start characteristics fuelled with mineral diesel. The engine was cranked by a starter initially. Once 200RPM was achieved, fuel was injected with a large quantity to ensure the first cycle firing. The high power of the first 2 fired cycles increased the back pressure which is capable to increase the output of turbocharger. Hence, an increased air mass flow was observed and followed the changes of engine speed.

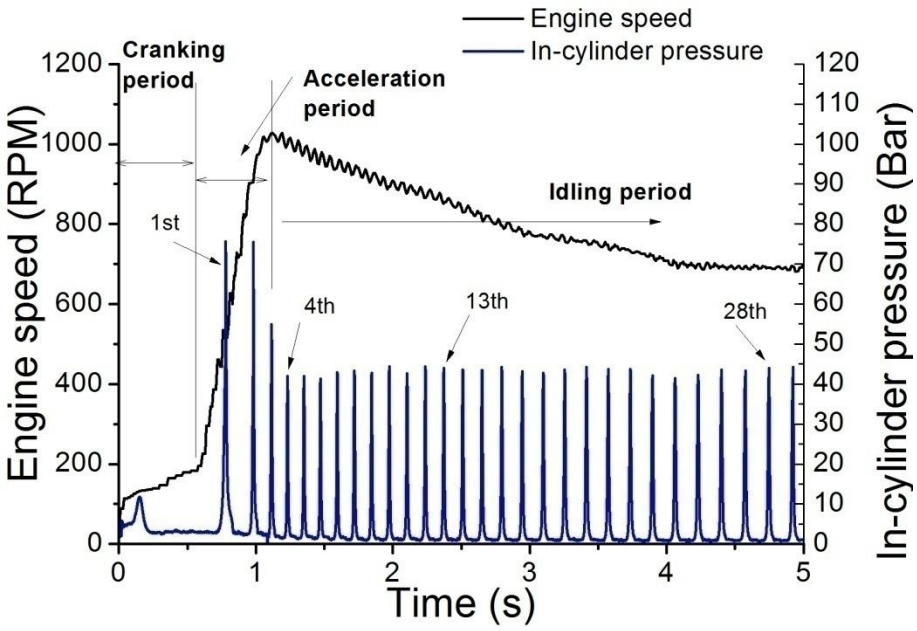

Figure 6.2 Engine speed and in-cylinder pressure of cold start with using mineral diesel.

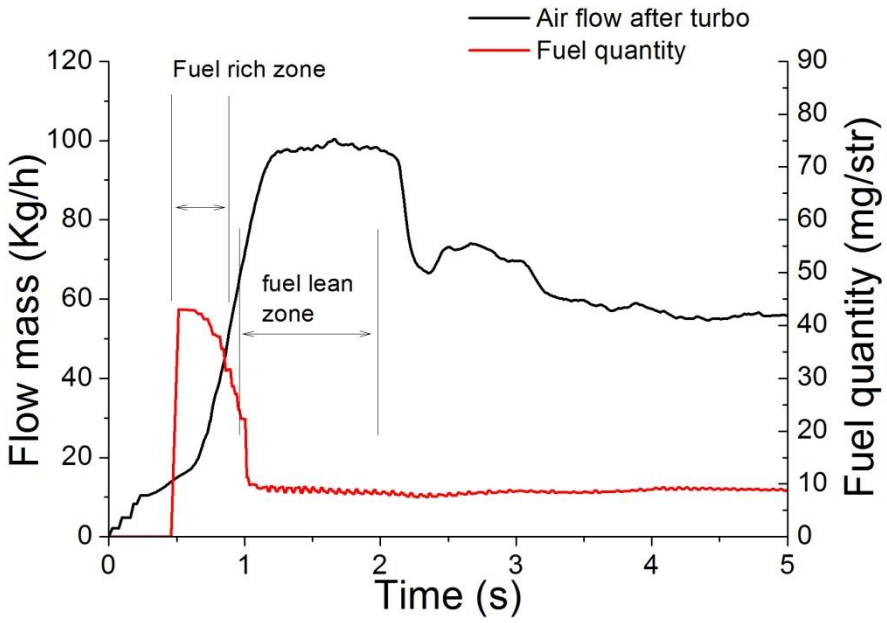

Figure 6.3 Fuel injection quantity and air flow mass after turbocharger of cold start with using mineral diesel.

The engine speed would reach the peak in several cycles. This period can be called acceleration period. After the acceleration period, fuel injection quantity was decreased to a low level and kept steady to maintain the idle speed. Engine control parameters, such as the open rates of VGT and EGR valves, were adjusted to ECU setting values, which caused the air flow fluctuation.

Figure 6.4 gives the air/fuel ratio (AFR) calculation varies with time for different fuels. During the acceleration period, AFR of using each fuel was almost identical. The low AFR was also observed at the beginning because the air inlet flow is low due to turbocharger lag while large quantity of fuel was injected to avoid the misfire. After the acceleration, AFR was increased rapidly due to the reduction of fuel injection quantity and increase of air inlet mass. The AFR of using mineral diesel was almost 25% higher than that of using RME60 at the peak. As engine get steady, the AFR of HVO60 was approximately 18% higher than the cases

of using mineral diesel and RME60because HVO60 has the highest energy density which resulted in less fuel injection to maintain the idle condition.

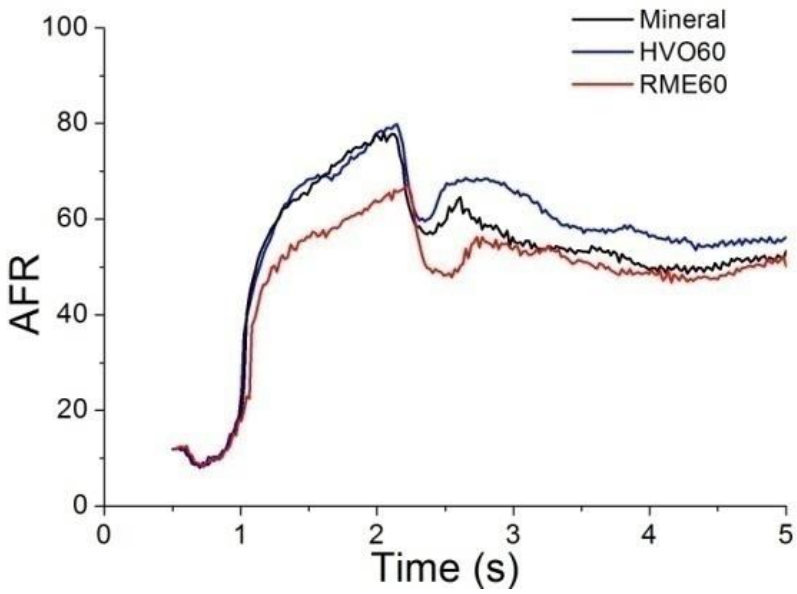

Figure 6.4AFR of cold start with using different fuels

Figure 6.5 shows the in-cylinder pressure and ROHR of the 1st, 4th, 13th and 28th fired cycles. The four cycles were pointed out in figure 6.2 which was four different situations as engine start. 1st cycle was the first fired cycle. The fuel was injected steadily from 4th cycle while max EGR rate was observed at 13th cycle. At last, 28th cycle was picked out to present the combustion after a period of steady idle.

In the 1st fired cycle, combustion of RME60 has the shortest ignition delay (1 CAD advanced than the SOC of other fuels) with the highest combustion pressure and ROHR value in all the fuels (approximately 26% and 50% higher than the cases of using mineral diesel respectively)due to the low stoichiometric ratio of RME60. For the same AFR at engine started, air/fuel mixture of RME60 had higher lambda value than those of other fuels, subsequently improved combustion with using RME60.

6.2.2. Engine Combustion During Cold Start

In the 4th cycle, split fuel injection was employed (two pilot injection and one main injection). Only the second pilot combustion is observed clearly on the ROHR curve. The first pilot injected fuel was misfired due to low temperature and low AFR. The combustion ofHVO60 and mineral diesel were almost the same. However, poor performances of using RME60 can be observed and may cause by two reasons. One is that the high initial boiling point and surface tension of RME60 led to bigger droplet diameter (Pflaum et al. 2010) which affected the air/fuel premixing. The other one is that it's too lean (AFR is around 50 at this time) for RME60 combustion.

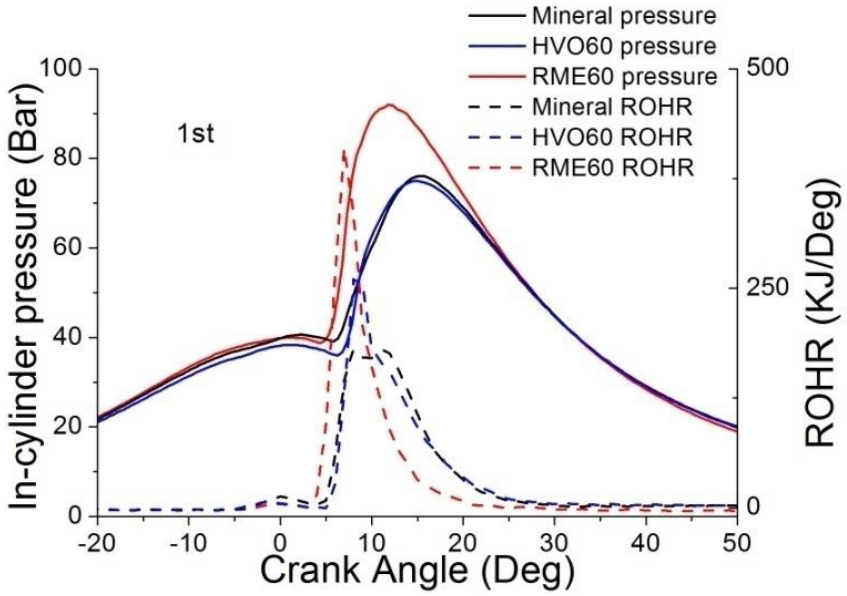

(a) The 1st cycle

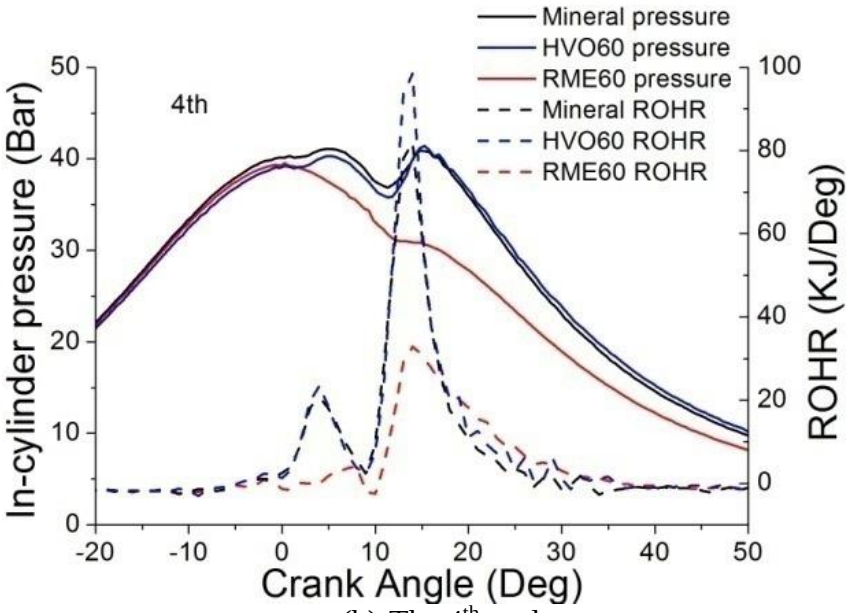

(b) The 4th cycle

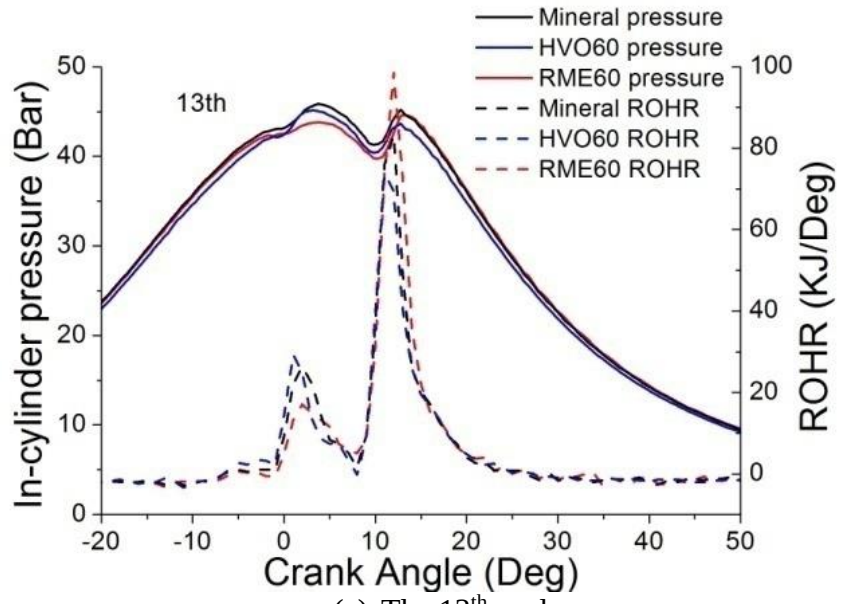

(c) The 13th cycle

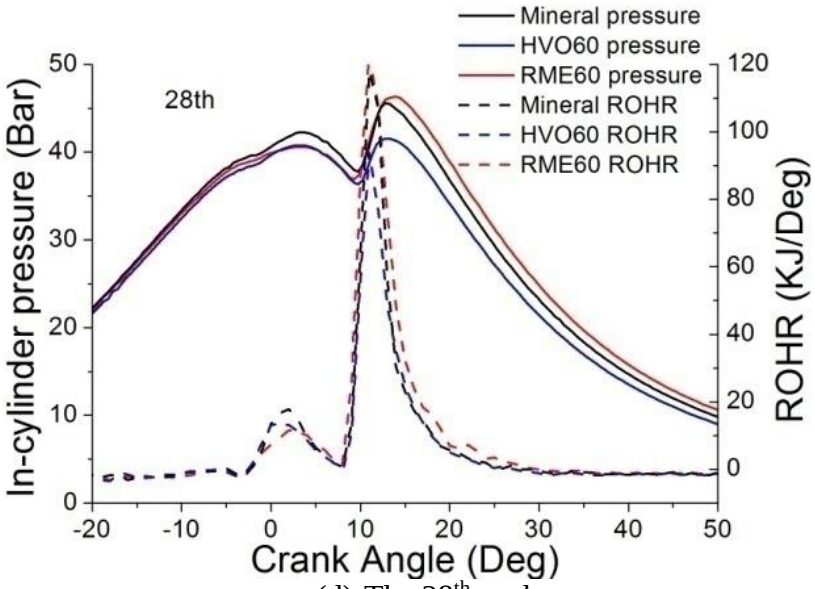

(d) The 28th cycle

Figure 6.5. In-cylinder pressure and ROHR with using different fuels at different time during cold start

As air inlet mass reduced after 4th cycle, the combustion of all fuels became similar. This can be observed on cycle 13th. After several cycles at idle period, the peak of the in-cylinder pressure and ROHR was increased (this can be observed by comparing the in-cylinder pressure and RoHR at 13th and 28th cycle) because the premixed combustion was improved as engine temperature increased.

The HVO60 from pilot injection was ignited earlier than those of other fuels due to its high cetane number. Meanwhile, combustion of RME60 from pilot injection always had lower heat release rate than the cases of other fuels. This might be caused by its high initial boiling point and surface tension which was discussed before.

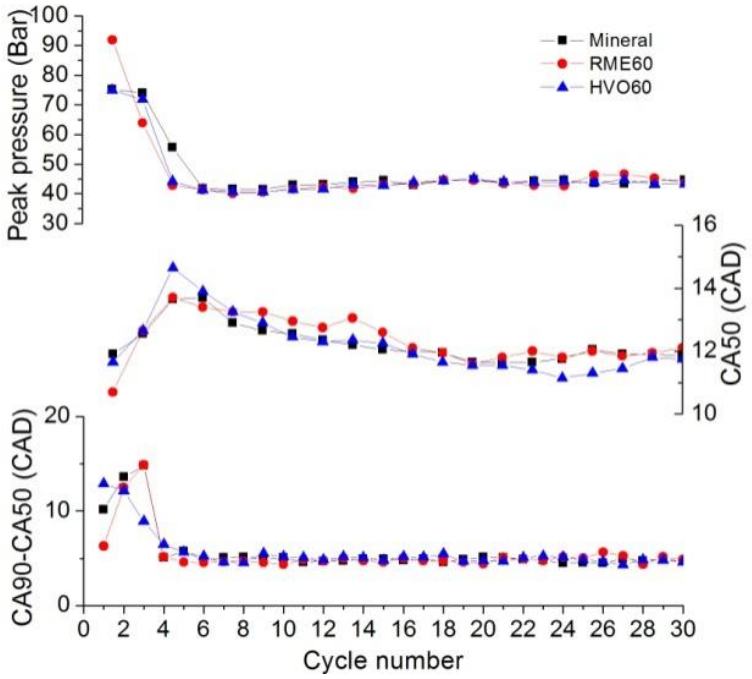

Figure 6.5Combustion characteristics with using different fuels.

Figure 6.6 presents the combustion characteristics of each fuel including peak in-cylinder pressure, CA50 (crank angle at 50% of Mass Fraction Burned) and time between CA90 and CA50. As pilot injection was employed in the combustion, the combustion of main injection fuel started almost at the same time for each fuel. In this paper, 50% MFB and the time between 50% MFB and 90% MFB were used to present the combustion rate of early combustion stage and late combustion stage respectively. In the first two acceleration cycles, combustion of RME60 led to higher peak in-cylinder pressure and combustion rate than those of other fuels due to the higher lambda value when engine started. As fuel injection quantity was getting steady after the 3rd cycle, combustion of all fuels indicated similar peak pressure and combustion duration.

6.3. ENGINE EMISSIONSDURING COLD START

6.3.1. Gaseous Emissions

Figure 6.6 and 6.7 indicate the NO and THC emissions with using different fuels in real time. The peak at 1s is the NO and THC emissions of the acceleration period. The whole process can be roughly divides into 2 parts: acceleration period, the time from engine start cranking to engine speed reached the peak (around 0.8-1.2s in figure 6.6 and 6.7), and idle period, the later time with steady emissions (from 1.2s to the end in figure 6.6 and 6.7)

6.3.1.1. Acceleration period

Comparing the area underneath the peak of each fuel, the combustion of RME60 produced the highest NO but the lowest THC, which corresponds with its higher combustion pressure and ROHR of the 1st cycle shown in figure 6.4. In addition, the oxygen content of RME60 is another reason for low THC emission. The combustion of HVO60 and mineral diesel produced almost the same level of NO emission due to their similar combustion characteristics of first 2 cycles which discussed previously. Meanwhile, the THC of using HVO60 was slightly lower than that of using mineral diesel because using of HVO60 always has better pilot combustion than the cases of using other fuels and leads to improved combustion when main injection occurred.

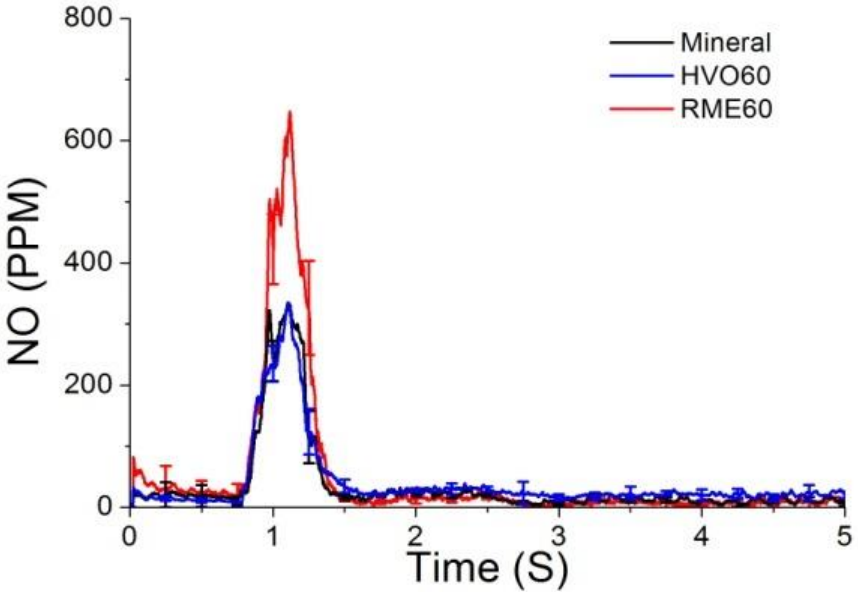

Figure 6.6 NO emission levels of cold start with using different fuels

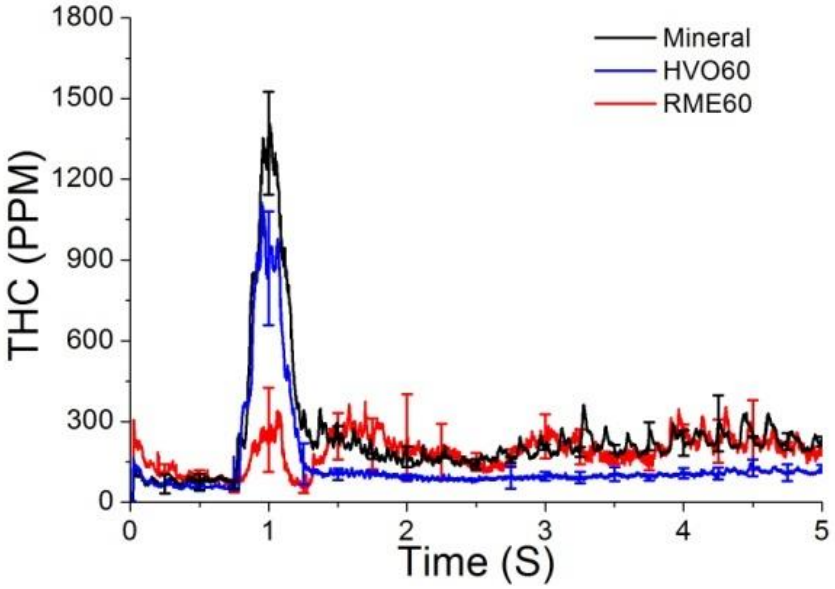

Figure 6.7 THC emission levels of cold start with using different fuels

6.3.1.2.Idle period

The NO emission was reduced to a low level at idle period because only small quantity of fuel was injected for maintaining idle. The THC emission of using RME60 was reduced first due

to high air mass inlet and then increased to the similar level of using mineral diesel. This is due to the low combustion pressure and heat release of pilot injected fuel which resulted in poor premixing of main injected fuel. The penalty of poor premixing with using RME60counteracted the benefit of its oxygen content and led to a similar THC level with that of mineral diesel.

Meanwhile, THC emission of using HVO60 was decreased to the lowest level, which was almost half of the cases of using RME60 and mineral diesel. This is due to the aromatic reduction and improved combustion of using HVO60.

6.3.2. Particle Matter

Figure 6.8 and 6.9 show the PM emissions of using the three fuels in both nucleation mode and accumulation mode presented in concentration. As measurement of DMS500 is slower than that of Fast FID/CLD, the PM results were indicated approximately0.2sdelay compared with THC and NO on the scale which matched the T_{10}-T_{90} time of DMS500.. The results are also divided to acceleration period (around 1.0-1.4s in figure 6.8 and 6.9) and idle period (from 1.5s to the end in figure 6.8 and 6.9) as the gaseous emissions section.

6.3.2.1.Acceleration period

The nucleation particle number was 3-10 times lower than the accumulation particle number(depending on different fuels) at this period because the low AFR resulted in high soot formation rate but less soot oxidation. The accumulation particle with using RME60 was the lowest at this period due to its improved combustion and oxygen contain.

6.3.2.2.Idle period

During idle period, the nucleation particles increased 3-8 times over that of acceleration period because the fuel was better premixed and resulted in slower coagulation and aggregation of small nuclei particles to larger accumulation particles. This resulted in reduced accumulation particles while increased the nucleation particles.

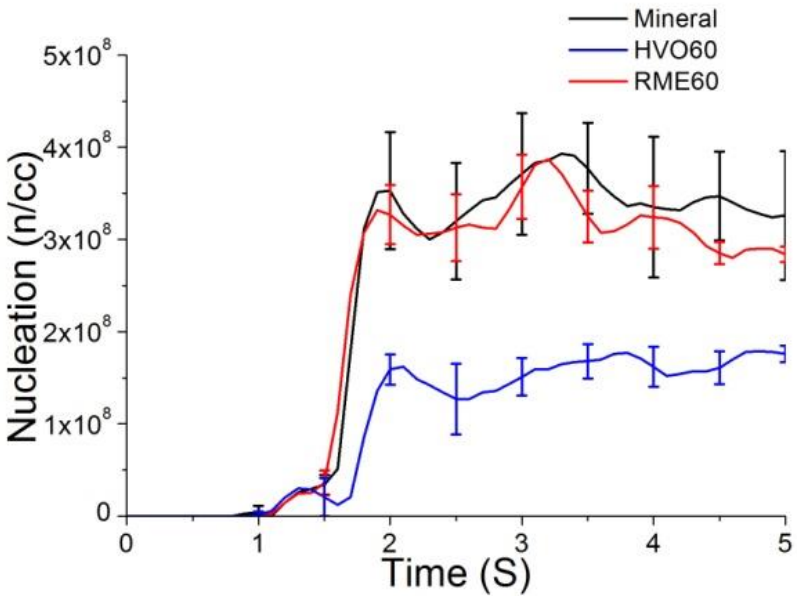

Figure 6.8Nucleation particle emissions of cold start with using different fuels

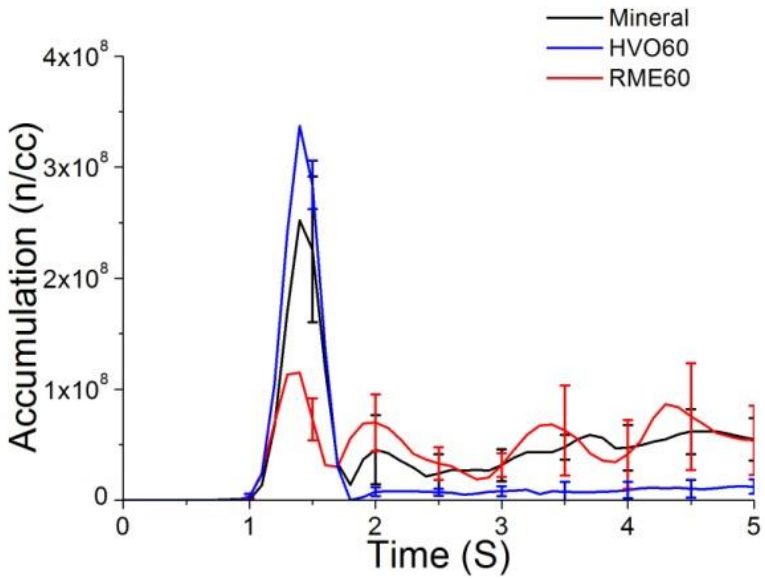

Figure 6.9Accumulation particle emission of cold start with using different fuels number

Combustion of RME60 had similar levels of nucleation and accumulation particles with those of mineral diesel at this period. This trend is the same with the trend of their THC emissions. Meanwhile, particles of the two modes with using HVO60 were almost 3 times lower than the cases of using other fuels. This is due to the combined effects of reduced aromatic of HVO and improved combustion which were discussed before.

6.3.2.3.Particle Spectrum Distribution in the First Second of Start

Figure 6.10 shows the particle distributions of every 0.1 second during the first second of engine start. With high injected fuel quantity and low air flow inlet initially (1.0s-1.3s), the large size particulates dominated the PM emissions due to the high fuel/air ratio during engine start. During this period, the combustion of RME60 always produced particles with lower concentration in all particle sizes. The peak concentration when using RME60 was shifted towards a smaller diameter. After 1.3s, the engine speed decreased to idle speed gradually and subsequently the fuel injection quantity was decreased to maintain the idle speed. Therefore, the global particle size was decreased to less than 100nm. When the engine conditions became

steady, the combustion of HVO60 produced the lowest particle emission with the smallest mean diameter while the combustion of RME60 produced the highest particle emission. This is because the particle emissions are mainly composed of small nucleation particles and methyl ester biodiesels always produce higher nucleation mode particle sat idle conditions with high AFR.

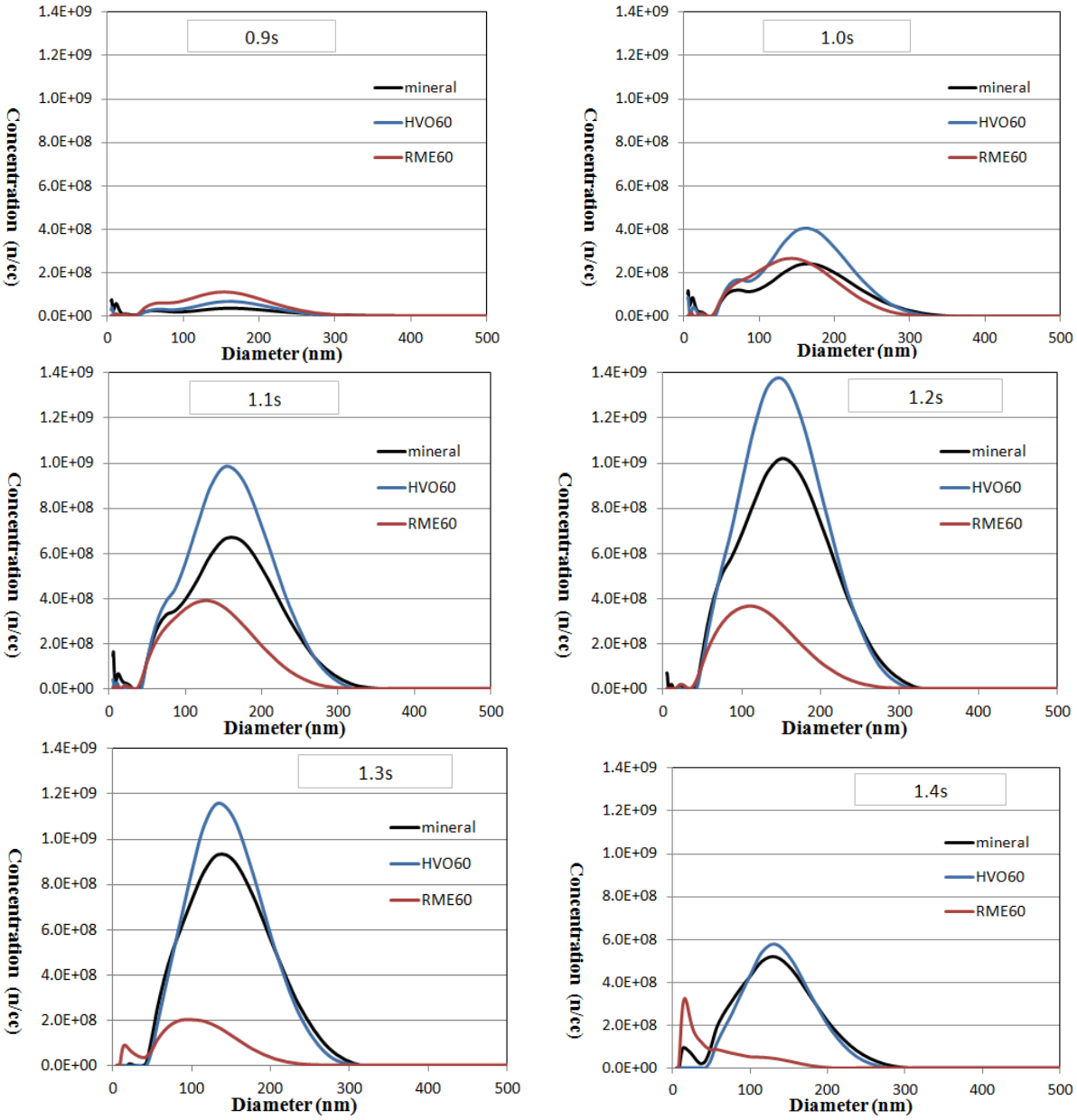

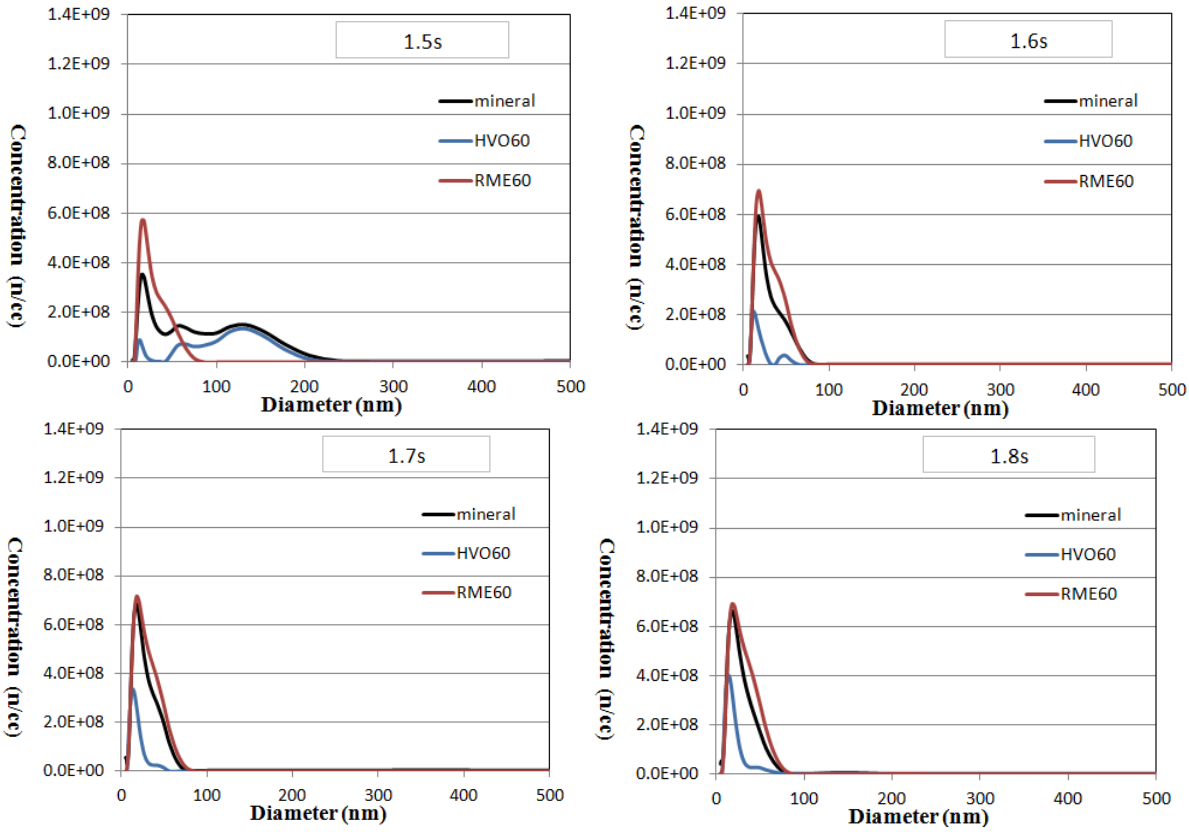

Figure 6.10 Particle distributions from 0.9s to 1.8s of engine cold start forevery 0.1s

6.4. CONCLUSIONS

The V6 engine cold start characteristics were studied. The cold start engine performance and emissions of two biodiesel blends, RME60 and HVO60, were investigated and compared with mineral diesel. Warm start cumulative emissions of each fuel during the first 10 seconds were also calculated to investigate the engine coolant temperature effects.

Based on the cold start test, the combustion of RME60 had the highest combustion pressure and ROHR in the first fired cycle due to its low stoichiometric ratio. Influenced by the good combustion and oxygen content, high NO emission, low THC and low particles were observed when using RME60 at cold start. However, as the engine was in its idle period, the combustion pressure and ROHR of pilot injected fuel reduced because of the high initial

boiling point, surface tension and AFR. This led to THC and particle emissions increases in the idle period.

The combustion and emissions of HVO60 and mineral diesel were similar in the acceleration period. However, its high cetane number resulted in a high combustion pressure and ROHR of pilot injected fuel during the idle period. Combined with the effect of reduced aromatic content of HVO60, emissions obtained when using HVO60 were significantly improved, except for NO.

As engine coolant temperature was increased, the emissions of THC and PM decreased while NO increased except for the NO and THC emissions obtained when using HVO60. During warm start, the combustion of biodiesel led to higher THC/PM and lower NO than in the cases of using mineral diesel, due to the fuel impinging effect. However, the accumulation particles obtained when using RME60 during warm start were lower than that of mineral diesel, due to oxygen content in the fuel.

However, the smoke index in chapter 5 cannot be used in cold start conditions because there are time delays between the sprayed fuel/engine loads/EGR rates and the combustion products in the exhaust pipe. Meanwhile, the combustion of previous cycles might have effects on the current combustion cycle. Hence, the smoke index created at the steady conditions was not able to predict the smoke emissions in the cold start conditions.

Chaper 7. PERFORMANCES AND EMISSIONS OF USING WINTER DIESEL AND BIODIESEL BLENDS DURINGAT SUBZERO DEGREE CONDITIONS

In this chapter, the cold start tests were conducted at ambient temperatures of 20°C, -7°C and -20°C for winter diesel and one commonly used biodiesel blend. The winter diesel was used in this study since the conventional diesel would block the fuel line and cause the start failure.

Every test was repeated at least three times and the results were averaged and the outliers were removed. The methods used to reduce test variation were the same as the tests in the last chapter. Only RME (rapeseed methyl ester) was blended with winter diesel in 10% by volume. The engine performance and emissions obtained when using RME10 and winter diesel were studied. The aim of this study was to investigate the engine performance and emissions at very low temperature when using winter diesel and compare this with the case of using RME10. The engine was equipped with a glow-plug in each cylinder to improve startability at low temperatures. The AVL AMA i60 was used to detect the gaseous emissions, such as NO_x, THC, CO and CO_2. The particle number and mass in both nucleation mode and accumulation mode was measured by the Cambustion DMS500. The particle size distribution was also obtained from the DMS500.

7.1. ENGINE PERFORMANCESOF USING WINTER DIESEL DURING COLD START

The engine speed and fuel injection quantity during cold start and idling period is analysed in this section. Idle speed stability is also calculated here.

7.1.1. Engine Speed

Figure 7.1 shows the variation of engine speed during cold start at different ambient temperatures. The cranking period is the time from the start of motor cranking to the start of the engine combustion. This is followed by the acceleration period in which the engine speed increased rapidly and then decreased to the idle speed.

It is observed that the variation of ambient temperature affects the start characteristics and idle speed stability. The time taken to reach the peak speed was increased with the reduced ambient temperature due to the higher peak speeds caused by high injection quantity and longer cranking periods required at cold ambient conditions. The cranking speed was also observed to decrease as the ambient temperature reduced due to higher frictional losses at cold ambient conditions. The observed peak speed at -20 ºC and -7°C was 4% and 12% higher than that at 20 ºC cold start operations, respectively. The peak engine speed at -20°C was lower than that at -7°C which might be the reasons of higher frictional losses and incomplete combustion of fuel at the -20°C conditions.

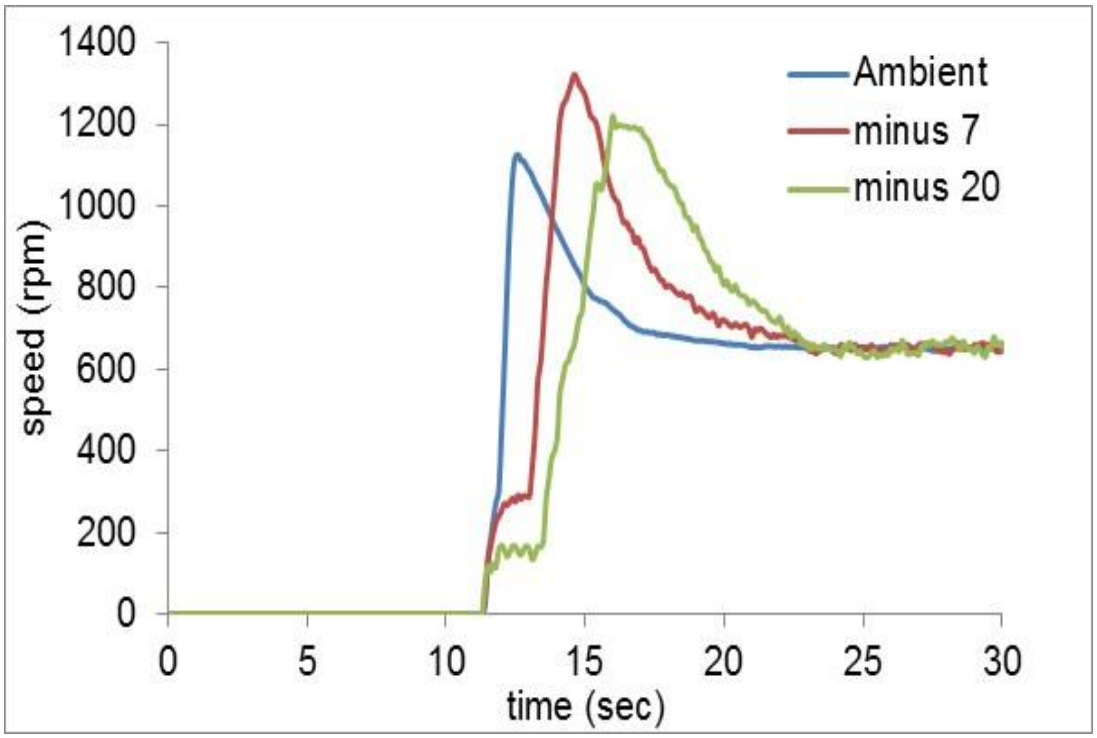

Figure 7.1Engine speed at different ambient temperatures

7.1.2. Fuel Consumption

Figure 7.2 shows the quantity of the fuel injected during the cold start calculated from the ECU signals. It was observed that the fuel injection quantity increased as the ambient temperatures were reduced. More quantity of fuel was injected during the start of the engine in order to ensure the firing and to increase the temperature in the cylinder. Then the fuel injection quantity was reduced once the engine reached peak speed and it attempted to maintain idle speed. The fuel vapours and pyrolysis products which were not completely burned were condensed and released to the atmosphere as unburned hydrocarbons or particulates.

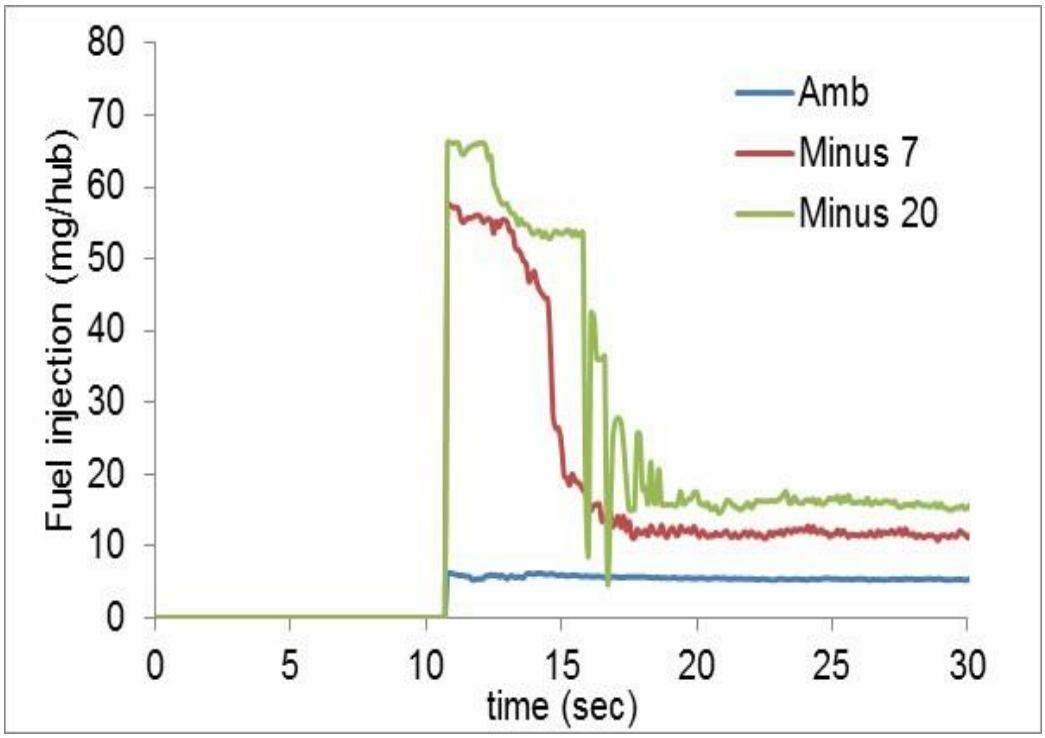

Figure 7.2Fuel consumption of the engine at different ambient temperatures

7.1.3. Idle Speed Stability

Figure 7.3 shows the coefficient of variance (COV) of the idle speed at different ambient conditions. The COV was calculated from 30 sec of the engine start to 180 sec of the engine start when the engine was maintained at the idle speed. It is only calculated at sub-zero degree cold start because the stability of cold start is quite poor at sub-zero degree. The COV for the idle speed was higher for the cold conditions as compared to that of the normal temperature conditions.

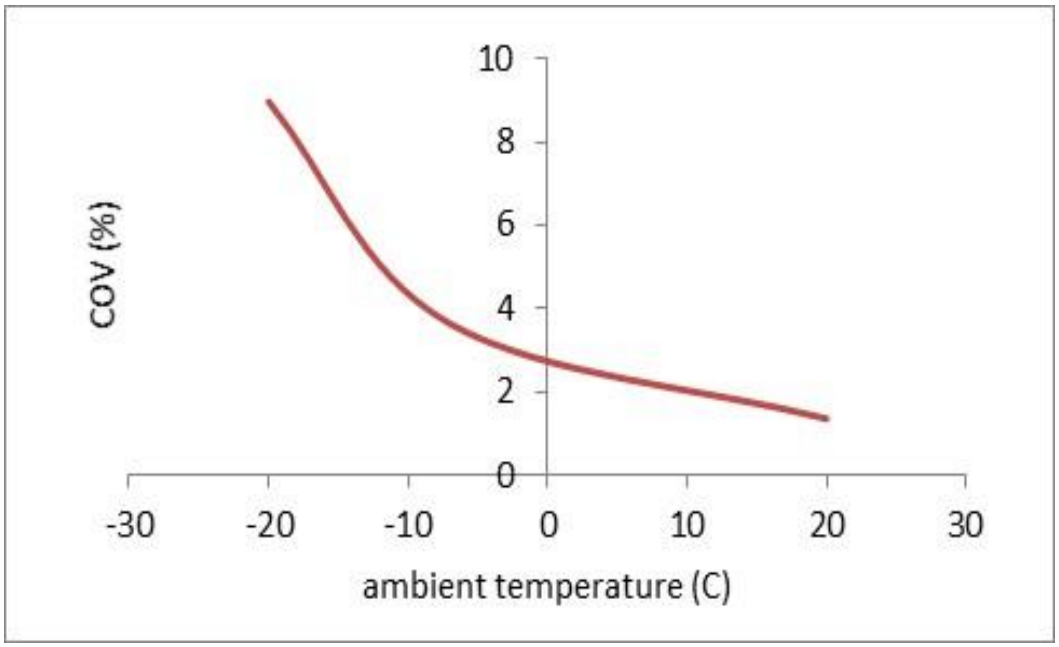

Figure 7.3Coefficient of Variation for idle speed at different ambient temperatures

7.2. ENGINE EMISSIONS OF USING WINTER DIESEL DURING COLD START

The gaseous emissions (NO_x, THC, CO and CO_2) from the engine exhaust pipe were measured before the diesel oxidation catalyst using the AVL AMA i60 emission analyser.

7.2.1. Gaseous Emissions

7.2.1.1.NOx Emissions

Figure 7.4 shows the NO_x emissions from the engine start to idle period at different ambient temperatures. It was observed that NO_x emission was relatively high at very low cold ambient conditions compared to the normal ambient conditions. The engine was calibrated in such a way that the EGR valve was opened when the temperature equalled or was higher than normal ambient temperatures in order to avoid formation of condensates in the EGR lines. The disabled EGR operation at minus degree ambient conditions contributed to the increase in NO_x emissions. Meanwhile, the increased fuel injection quantity at minus degree ambient

conditions also led to increases in the combustion temperature and consequently increases in the NO_x emission. Two peaks of the NO_x emissions were observed in the first 60 seconds. The first peak appeared around 15s which was the time when engine reached the highest speed and injection quantity. This peak was caused by the high combustion temperature of the large fuel injection during the acceleration period of cold start. The first peak at -20°C condition was lower than that at -7°C condition. Even though the fuel injection quantity was higher than that at the -7°C condition, more incomplete combustion occurred at -20°C condition due to the low temperature and air/fuel ratio. This resulted in a lower combustion temperature and a lower NO_x emission at the -20°C condition when compared to that at the -7°C condition. The second peak of the NO_x emissions measured at -20°C and -7°C ambient conditions were approximately 150% and 50% higher respectively in comparison to that observed at the normal ambient condition. During cold start, high fuel injection pressure and quantity during the acceleration period resulted in fuel adsorbed or condensed onto the surface of piston crown or cylinder wall. The lower the ambient and fuel temperature, the higher the quantity of fuel adsorption due to the increased fuel injection quantity, viscosity and surface tension. The adsorbed fuel was vaporized and participated in the combustion after several cycles when engine became slightly warmer which led to an increase of in-cylinder temperature. The increases of in-cylinder pressure were reduced when the ambient temperature increased, thus these caused the highest second peak of the NO_x emissions at -20°C and the lowest at 20°C.

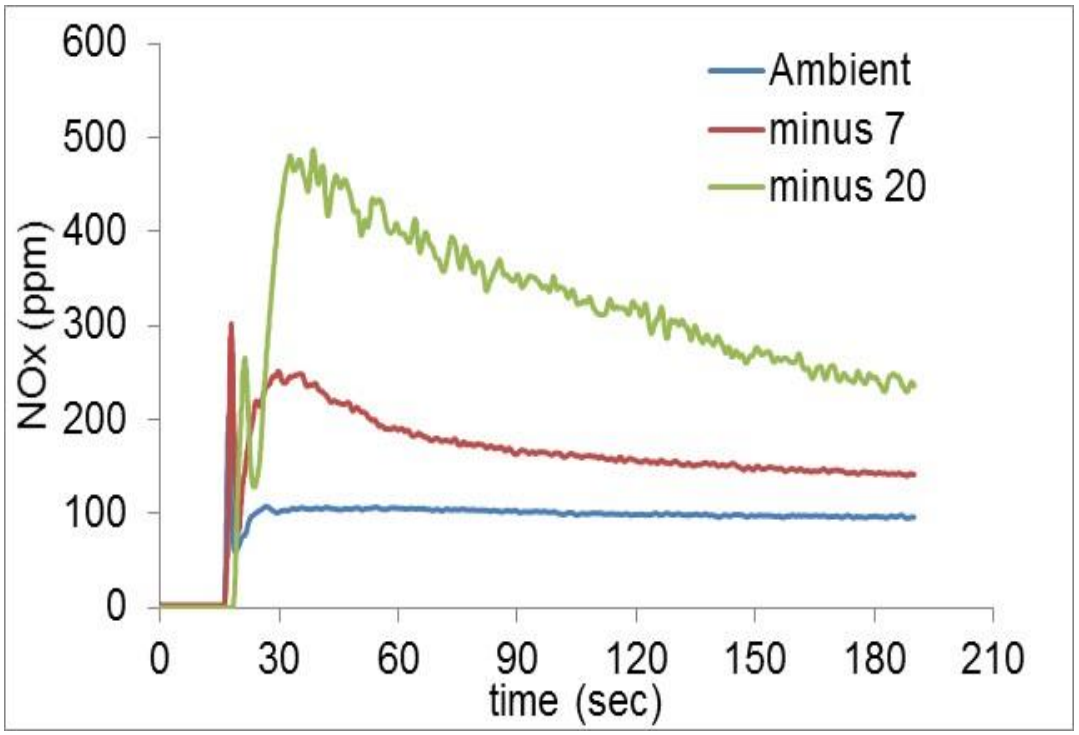

Figure 7.4NOx emissions at different ambient

7.2.1.2.THC Emissions

Figure 7.5representsthe THC emissions at different ambient temperatures. The THC emissions at minus degree ambient temperatures were several times higher than thoseat20°C conditions. The peak THC emissions observed at minus degree ambient temperatures were about 15 times higher than those observed at20°C conditions. After the acceleration period, the THC concentrations were reduced and maintained during the idle period. The higher THC emissions at lower temperature conditions were caused by the lower surface temperatures of the cylinder which increased the heat losses and blow-by effects during compression and resulted in the reduction of the air/fuel mixture temperature at TDC and increased the ignition delay and fuel condensation. Meanwhile, fuel injection quantity was increased at lower temperature conditions and caused an excess amount of accumulated fuel in the combustion chamber which was released as unburned hydrocarbons. Moreover, the cold temperature of

the fuel injector tip and piston also increased the THC emissions when the fuel came into contact with them due to absorption-desorption of fuel vapour.

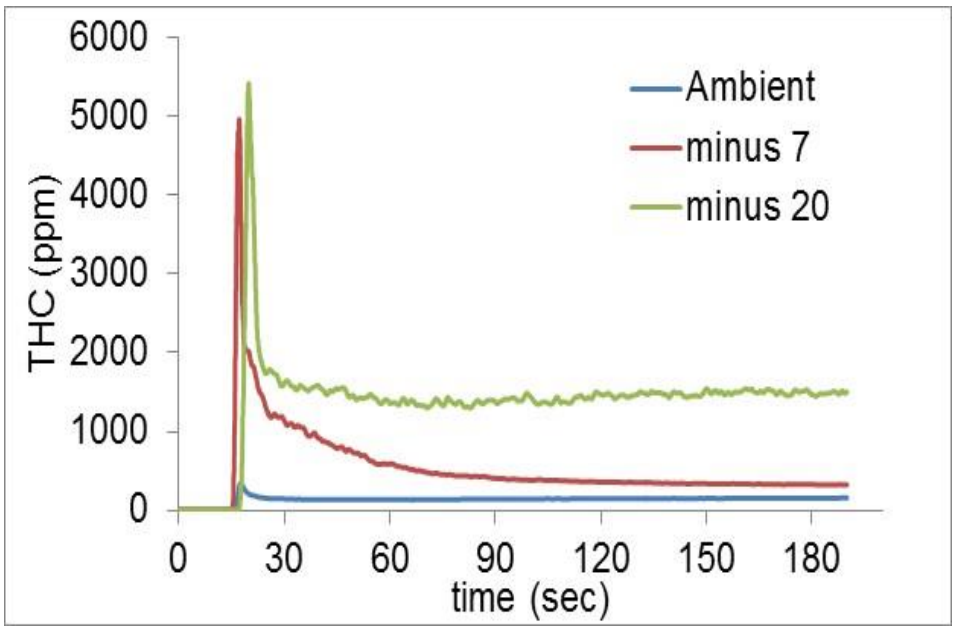

Figure 7.5THC emissions at different ambient temperatures

7.2.2. Characterization of Particle Emissions

The exhaust particle emission was measured using the Cambustion DMS500 analyser for characterizing the particle emissions in terms of its number concentration, size, distribution and surface area. The nucleation and accumulation mode particles were separated based on calculation from the size distribution.

7.2.2.1.Particle Number Concentration

Figure 7.6 shows the particle number concentration both in nucleation and accumulation mode during cold start at different ambient temperatures. Both the nucleation and accumulation mode particles reached their peak during the acceleration and then decreased while engine was steadily reaching the idle condition. The peak concentrations of the

nucleation mode particle number during the acceleration period at -7°C and -20°C conditions were approximately 50% higher and 10% lower than the case at the 20°C condition. This was due to the synergy of two effects: one is the increased viscosity of fuel and cold cylinder wall, piston and injector tips at lower ambient temperature which led to an increased number of nucleation mode particles; the other one is the increased nuclei condensation and adsorption onto the surfaces of soot when the ambient temperature was reduced. At -7°C conditions, the first factor dominated and resulted in the highest particle emissions in number during the acceleration period. At -20°C conditions, the second factor was dominant and the particle number was even lower than that at 20°C conditions. Considering the particle size distribution in figure 7.7 and 7.8, the peak concentration of small size particles was shifted towards smaller diameters when the ambient temperature decreased. This meant that the particles at the -7°C condition had a higher number but lower mass as compared to those at the 20°C condition.

For the accumulation mode particles, the peak concentrations by number at -7°C and -20°C conditions were approximately 35% and 55% higher respectively than those observed at normal ambient temperatures. The time covered by the peak was increased when the ambient temperature decreased. The higher fuel injection quantity and very low ambient temperatures caused the increase in incomplete combustion of the fuel which led to the formation of more particles.

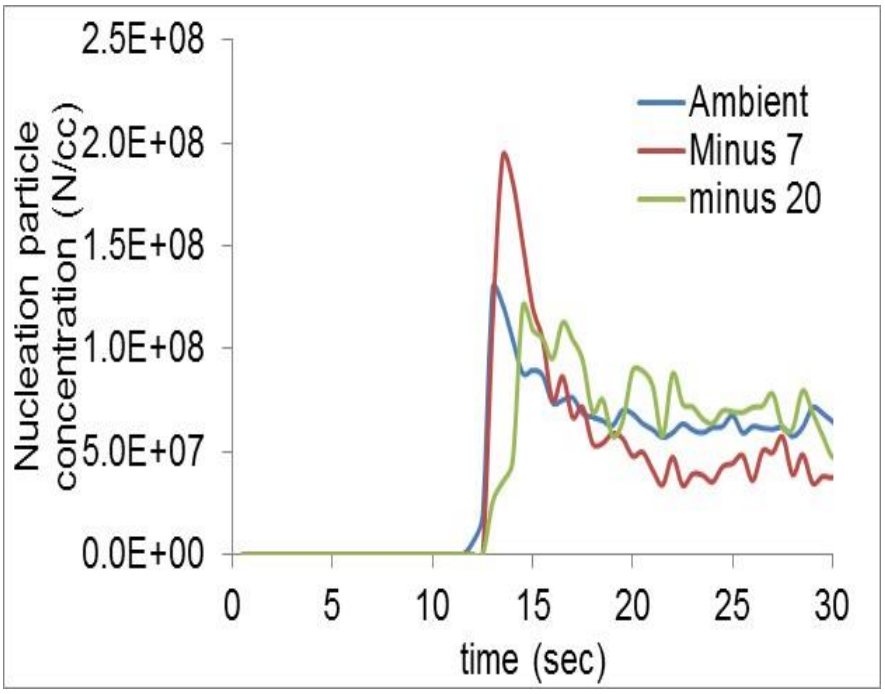

(a) Nucleation mode particle concentration

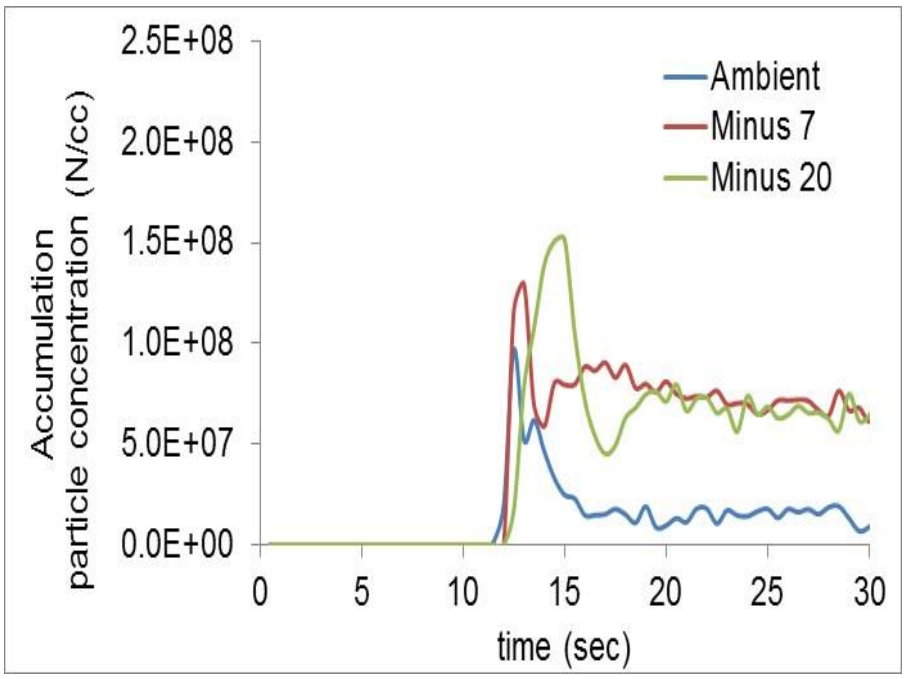

(b) Accumulation mode particle concentration

Figure 7.6 The Particle number concentration nucleation mode particles and accumulation mode particles during the cold start

7.2.2.2.Particle Size Spectral Density

The average size distribution during the acceleration period is shown in figure 7.7. The particle numbers in the size between 10nm to 100 nm were higher at 20°C and -7°C conditions whereas at -20°C conditions the peak of particle concentration was shifted towards the larger size. This result was also supported by comparatively higher number of larger size particles due to the accumulation of smaller size particles at very cold ambient conditions.

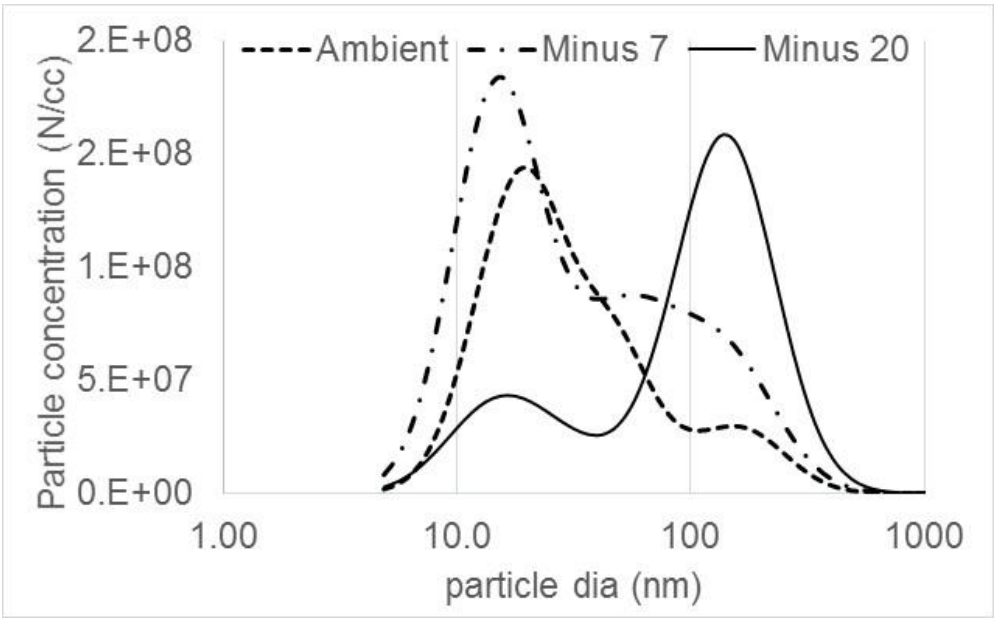

Figure 7.7Particle size distribution during cold start at different ambient temperatures

The particle size distribution observed during the idle period at different ambient temperatures is shown in Figure 7.8. During the idle period, the exhaust PM was dominated by particles with a size range of 10-100 nm for the all ambient temperature conditions. The peak value of particles was increased with reducing temperature and shifted towards the smaller particle size. As the engine was continuing its warm-up during the idle period, the EGR, boost pressure and fuel/air ratio were controlled and the oxidation of the fuel-air mixture was improved, hence the global size of the particle was decreased. It can be observed that around

10% of particles were in the size of less than 10 nm and 50-80% of the particles were in the size range between 10nm and30 nm. The total number of the small size particles (10nm-30nm) was reduced with the decreases in the ambient temperature and the large sized particles were formed more at very cold temperature conditions.

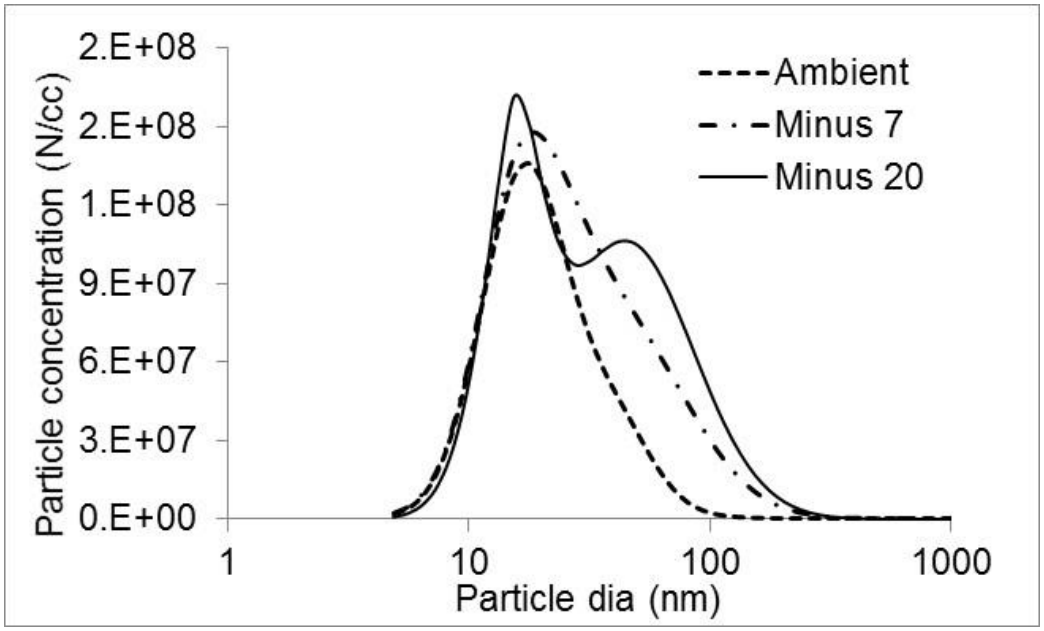

Figure 7.8Particle size distribution during idle at different ambient temperatures

7.2.2.3.Particle Surface Area

Particle surface area is a measure of active sites available for adsorption of volatile hydrocarbon fractions and PAHs which are largely toxic species and determined by particle diameter and number distributions. The particle surface area is also an indicator showing the effectiveness of particles which interact with the respiratory system of human beings, which consequently determines their effect on the health(Agarwal, 2013).

Figure 7.9 shows the averaged surface area (calculated by equation 7.1) of nucleation and accumulation mode particles during cold start at different ambient temperatures. As the ambient temperature decreased, the surface area of accumulation mode particles increased

while that of nucleation mode particles decreased. The smaller size particles always have significantly higher surface area per unit particle mass compared to that of larger particles, thus this improved the condensation/adsorption of toxic compounds such as VOC's and PAH's. Therefore, smaller particles tend to become more hazardous for human health compared to larger particles.

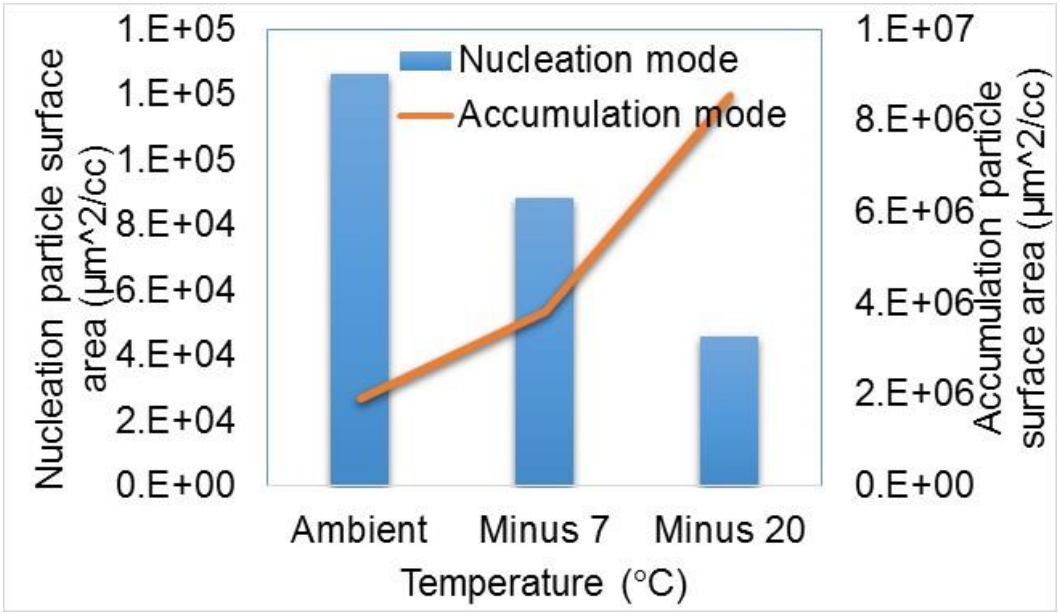

Figure 7.9Surface area of particles during cold start at different ambient temperatures

Assuming the particles are spherical in shape, the surface area is thus calculated as follows:

$$dS = dN.4\pi r_p^2 \quad (7.1)$$

Where, dS is the surface area concentration of size range with mean radius r_p and dN is the number concentration of particles. The sum of dS of particles in all sizes is then the total surface area.

Figure 7.10represents the total surface areas of particles with different sizes. The total particle surface area was observed to be higher at low temperature conditions compared to normal ambient temperatures. The smaller size particles were larger in number at normal ambient

temperatures compared to cold ambient conditions. However, the number count of accumulated particles (100-500 nm) at cold ambient conditions almost equalled that of the smaller size particles at ambient and hence the total surface area of particles at the cold ambient conditions were higher than those observed at the normal ambient conditions.

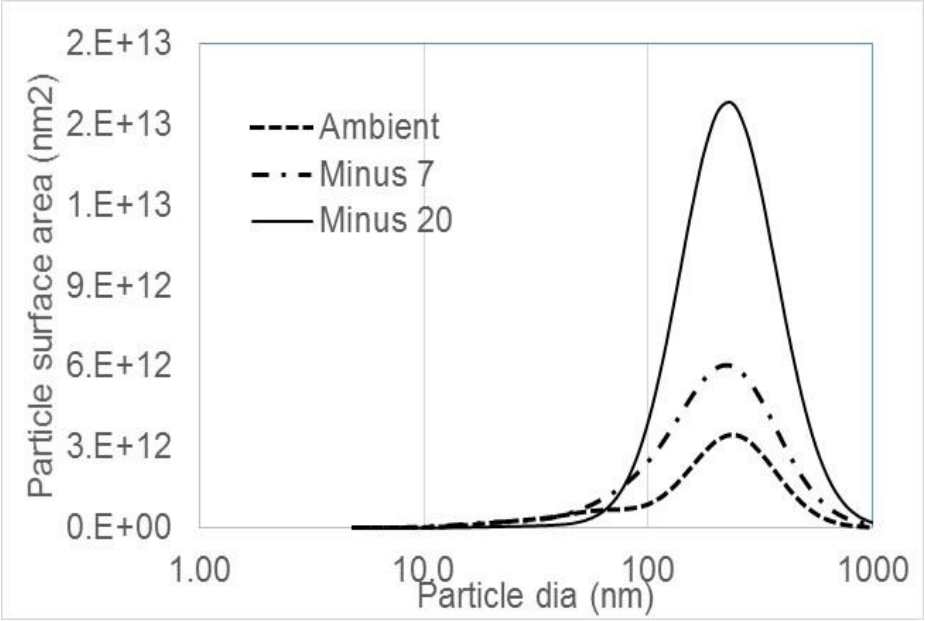

Figure 7.10Surface area distribution of particles during the cold start at different ambient temperatures

Figure 7.11 shows the surface area of particle emissions observed at idle conditions at different ambient conditions. It was observed that the total particle surface area was higher at cold ambient conditions compared to those observed at normal ambient. The surface area of particles was shifted towards the larger diameter particles at cold ambient, because the accumulation particles were higher in numbers at cold ambient. Hence the surface area of the particles was also higher with respect to the larger diameter particles at very cold ambient temperatures.

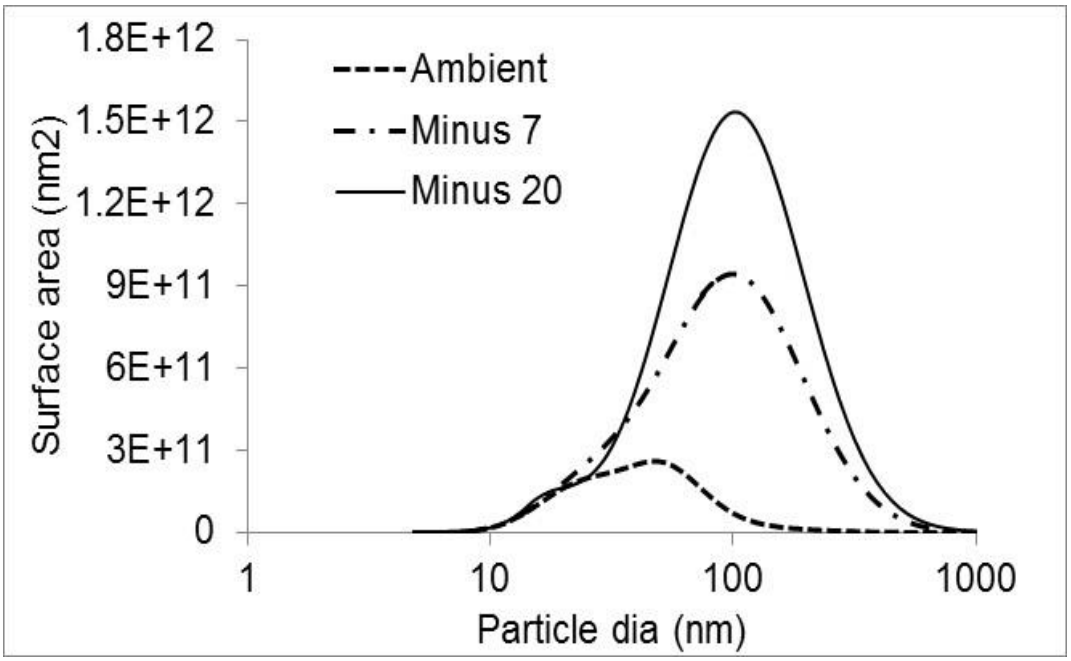

Figure 7.11Surface area distribution of particles at idle conditions at different ambient temperatures

7.3. CUMULATIVE EMISSIONS OF USING BIODIESEL IN COLD START

RME was blended into the winter fuel by volume 10% for the tests. The cumulative emissions of RME10 and winter diesel were compared in this section. Figure 7.12 shows the air/fuel ratio of each fuel at different ambient temperatures. It can be observed that the AFRs achieved when using RME10 were always lower than those of using winter diesel at each ambient temperature. This was caused by the higher fuel injection quantity and lower mass of inlet air flow due to the lower heating value of RME fuel.

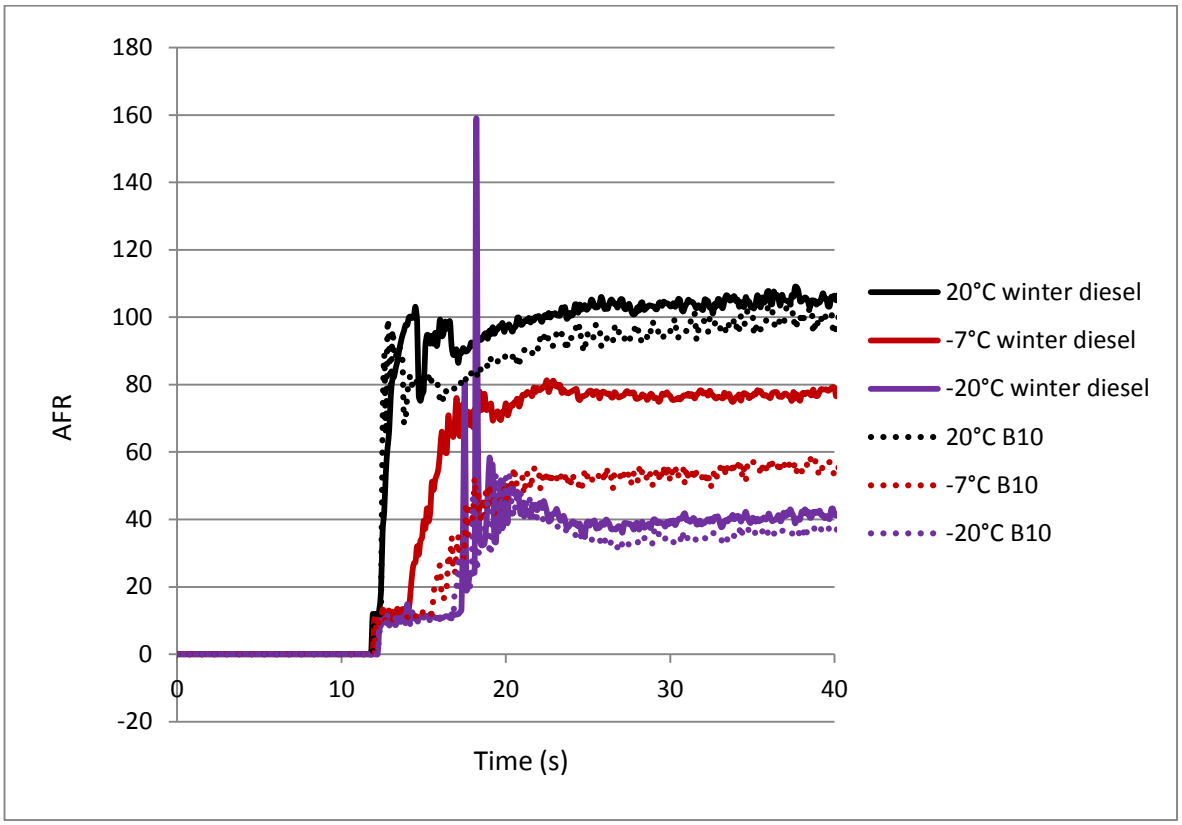

Figure 7.12The air/fuel ratio during engine start at different ambient temperature for both of the fuels.

7.3.1. Cumulative Emissions During Acceleration Period

7.3.1.1.Gaseous Emissions

Figure 7.13 and 7.14 show the cumulative NO_x and THC emissions at cold start during the acceleration period. The acceleration period for each cold start was defined as the time when the fuel injection started to the time when the engine speed reached its peak value. It was observed that the NO_x emissions obtained when using RME10 and winter diesel increased as the ambient temperature decreased. This was because of the high quantity of fuel injection which was discussed in the previous section. The combustion of RME10 always produced lower NO_x emissions at all ambient temperature conditions due to the lower heating value of RME which reduced the combustion temperature. This effect could be more significant during

the acceleration period since large amounts of fuel were injected during this period. Another reason might be the higher viscosity of RME10 resulted in less fuel atomization and vaporization which caused worse fuel/air mixing and combustion.

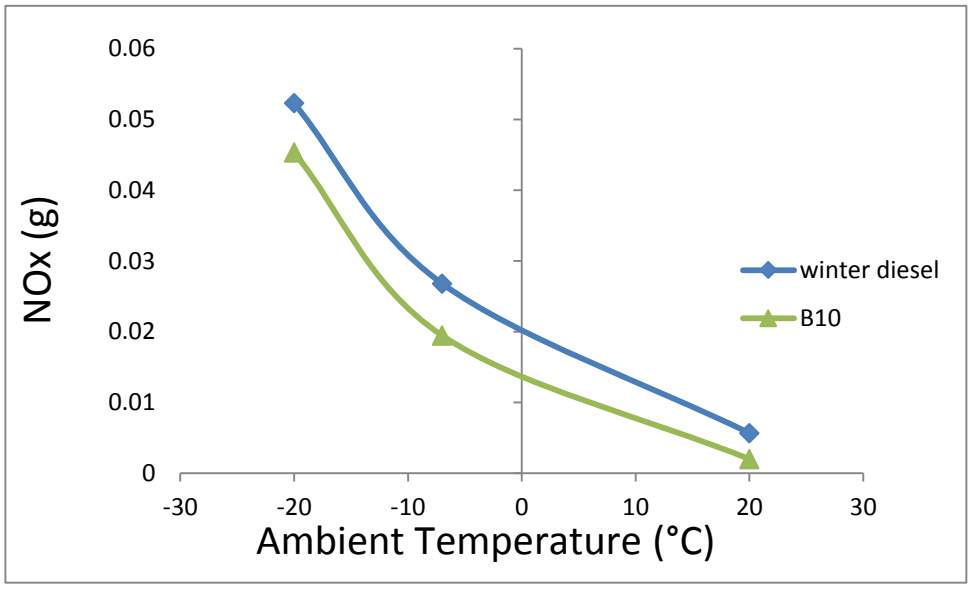

Figure 7.13Cumulative mass of NOx emissions during acceleration period of cold start

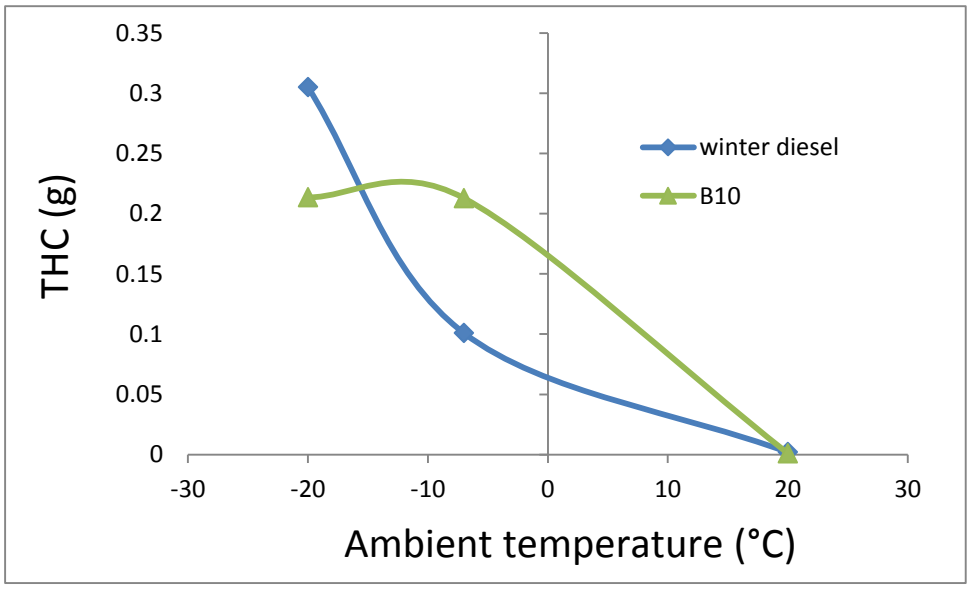

Figure 7.14Cumulative mass of THC emissions during the acceleration period of cold start

At 20°C conditions, the THC emission was slightly lower when using RME10 compared to that observed when using winter diesel. When the ambient temperature dropped from 20°C to -7°C, the THC emissions increased sharply for both of the fuels. This increase was more significant when using RME10 as compared to the case of winter diesel. However, as the ambient temperature reduced further to -20°C, the THC increase observed when using winter diesel was even sharper than that observed when the temperature reduced from20°C to -7°C, whereas the THC emissions of RME10 did not change significantly. This might have been caused by two opposite effects due to the properties of RME. One is the high viscosity of RME10 which was discussed in the previous paragraph. Meanwhile, the high cetane number of RME10 may have decreased the ignition delay and also caused the THC emissions to increase. Another effect which may account for the THC emissions decrease is the oxygen content in RME10. An additional reason for the decrease of THC emissions when using biodiesel at -20°C may be that hydrocarbons produced by the combustion of biodiesel were of high molecular weight and boiling point which increased the condensation of THC emissions. When the ambient temperature was at 20°C or -20°C, the fuel atomization and vaporization was determined mainly by the ambient temperature, thus RME10 with oxygen content resulted in lower THC emissions than when winter diesel was used. Meanwhile, the hydrocarbon condensation of heavy HC's produced using biodiesel may be relatively more significant compared to those produced using winter diesel at -20°C conditions. At -7°C conditions, with an intermediate temperature, the viscosity dominated the fuel atomization and vaporization process and caused higher THC emissions when RME10 was used.

7.3.1.2.Particles Emissions

Figures 7.15, 7.16, 7.17 and 7.18 show the total particle number and mass during the acceleration period at different ambient temperatures for each fuel. The particles, either

nucleation or accumulation mode, counted by number or mass, increased as ambient temperature decreased for each fuel. For nucleation mode particles, the number and mass of the particles were slightly higher when RME10 was used at 20°C conditions. However, when the ambient temperature dropped to minus degrees, the number of nucleation mode particles was lower when using RME10 whereas the mass was higher. For the accumulation particles, the particle numbers when RME10 was used were 30%-40% higher than those obtained when winter diesel was used at all temperature conditions. In addition, the particle mass obtained when RME10 was used was approximately 50% higher than that obtained when winter diesel was used, only at minus degree conditions. The possible reason might be the low ambient temperature which resulted in a higher viscosity of the biodiesel. The higher viscosity of the biodiesel then caused less atomization and vaporization which led to more particles being produced with a larger size. Meanwhile, the high cetane number of RME10 reduced the ignition delay and cause higher particle emissions.

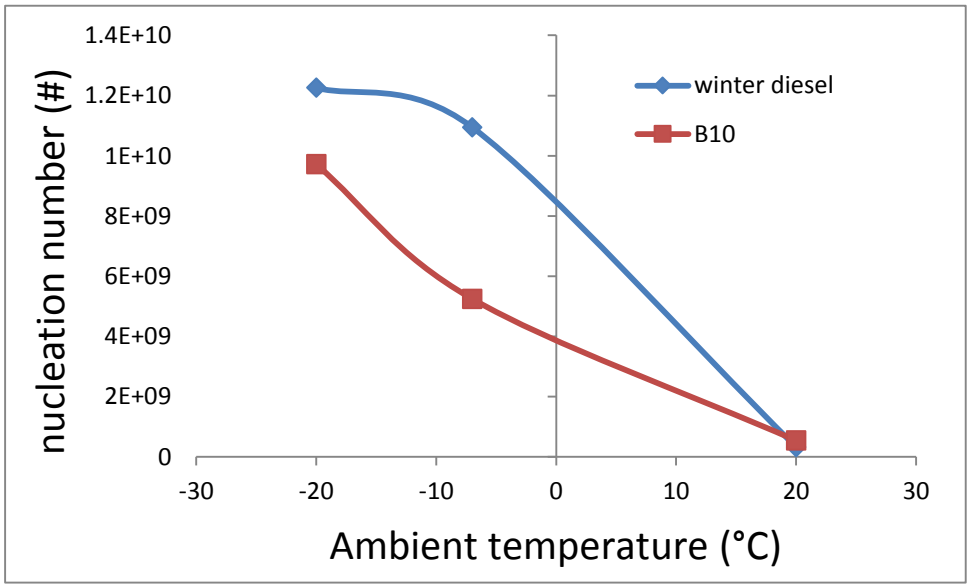

Figure 7.15Cumulative number of nucleation particles during the acceleration period of cold start

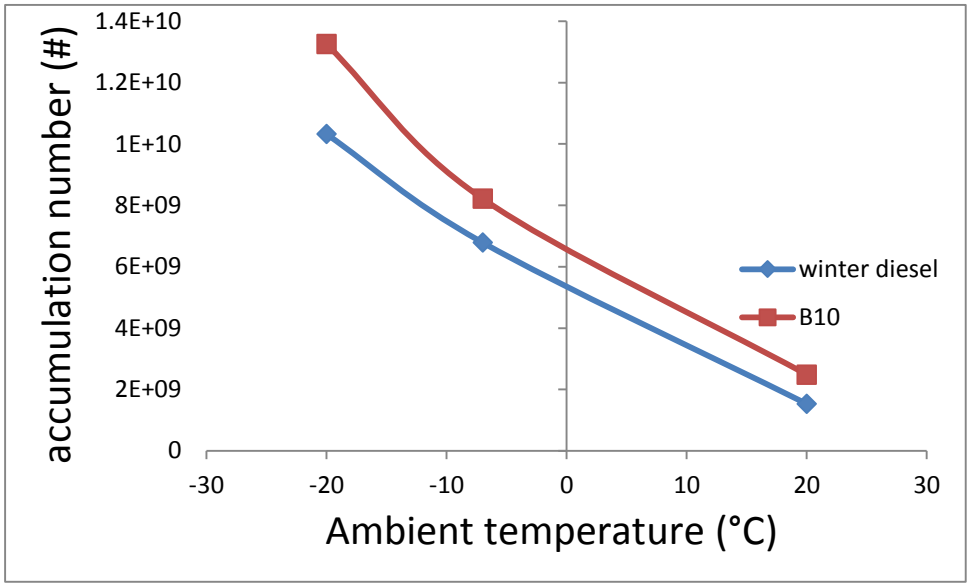

Figure 7.16Cumulative number of accumulation particles during the acceleration period of cold start

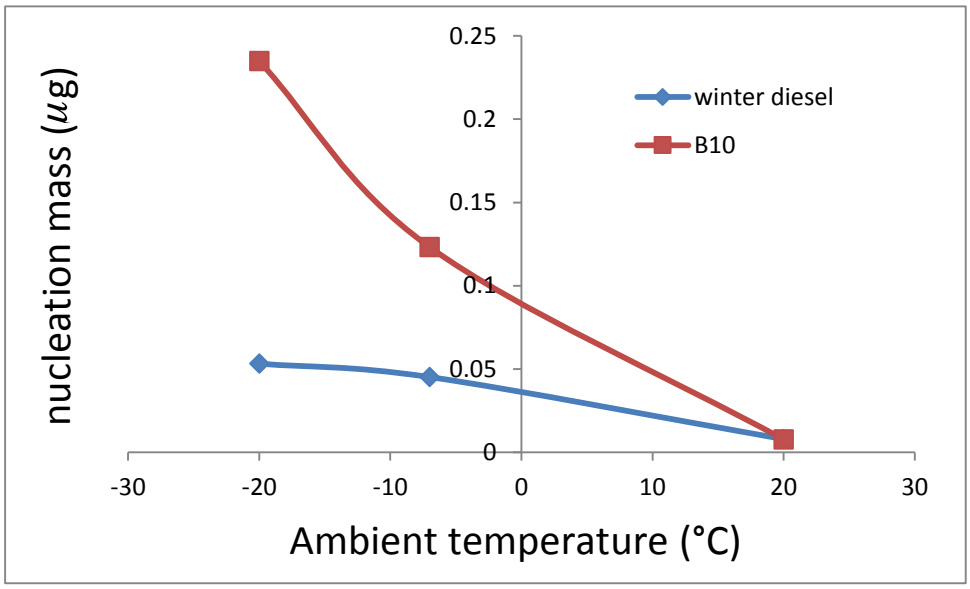

Figure 7.17Cumulative mass of nucleation particles during the acceleration period of cold start

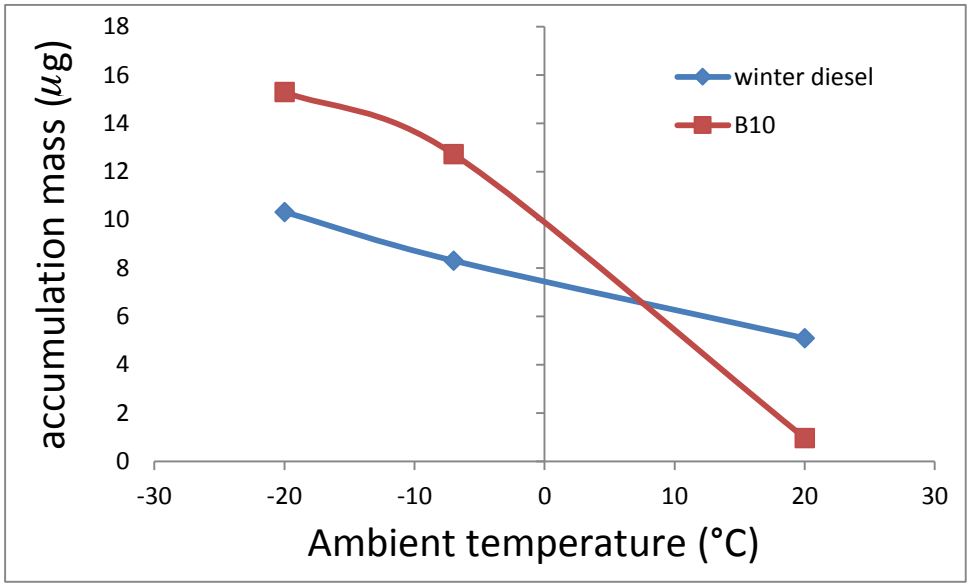

Figure 7.18Cumulative mass of accumulation particles during the acceleration period of cold start

7.3.2. Cumulative Emissions during Idle Period

7.3.2.1.Gaseous Emissions

Figure 7.19 and 7.20 show the cumulative NO_x and THC emissions during idle conditions in the first 30 seconds (exclude the acceleration emissions). The NO_x emissions obtained when using RME10 were still lower than those obtained when using winter diesel, only at 20°C and -20°C conditions. At -7°C condition, the NO_x emissions increased when using RME10 due to the 60% higher AFR compared to when winter diesel was used. Although the heating value of RME10 was less than that of winter diesel, the low inlet air flow when using RME10 resulted in the increases of in-cylinder temperature; hence this increased the NO_x emissions. Meanwhile, the THC emissions obtained when using the two fuels were almost the same at 20°C and -20°C conditions whereas the combustion of RME10 produced more than 2 times the THC emissions as compared with the case of winter diesel, due to the high cetane number

of the biodiesel which advanced the combustion and led to high THC emissions.

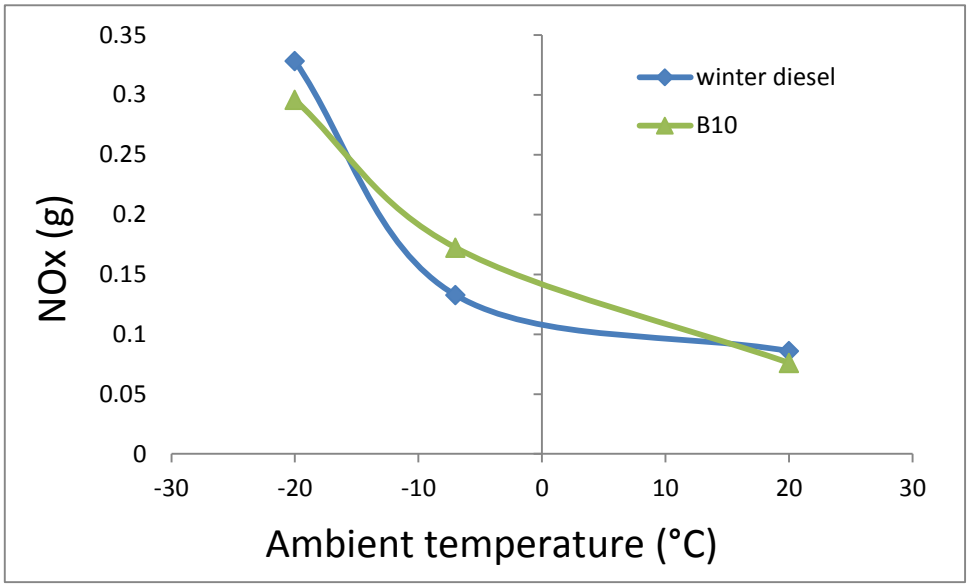

Figure 7.19Cumulative mass of NOx during idle period in the first 30s of cold start

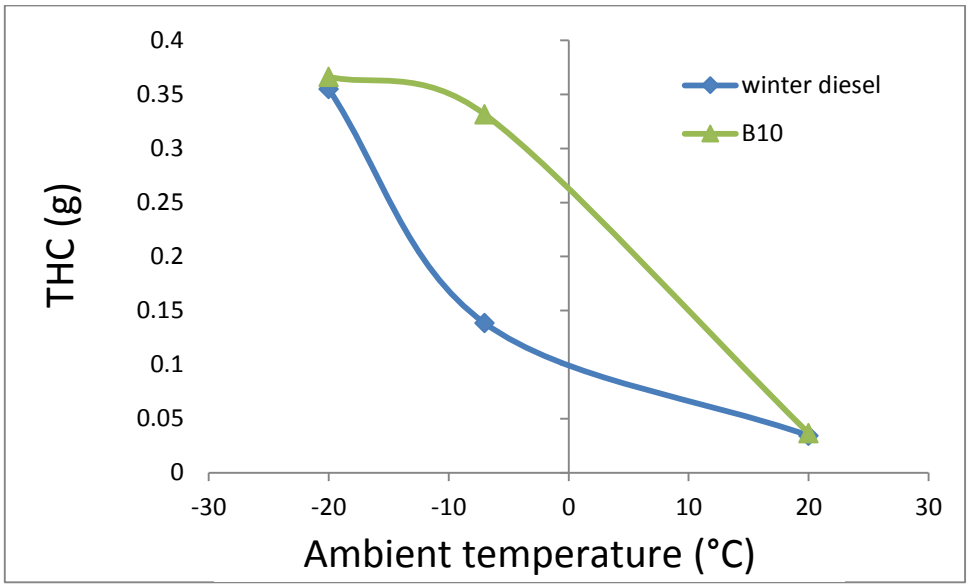

Figure 7.20Cumulative mass of THC during idle period in the first 30s of cold start

7.3.2.2.Particle Emissions

Figures7.21, 7.22, 7.23 and 7.24 show the total particle number and mass during the idle period at different ambient temperatures for each fuel. For the nucleation mode particles, the

use of RME10 always produced lower particle number and mass, except for the 20°C condition in which the mass of nucleation mode particles was higher when RME10 was used. Considering the high accumulation particles produced when using RME10, the increased adsorption of nuclei may occur and resulted in lower nucleation mode particles.

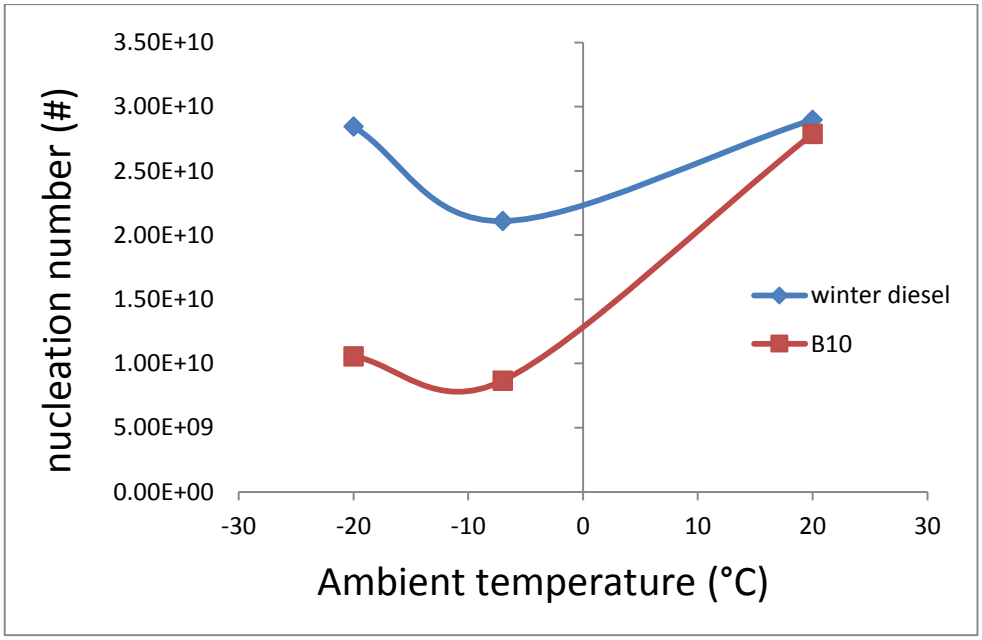

Figure 7.21Cumulative number of nucleation particles during idle period in the first 30s of cold start

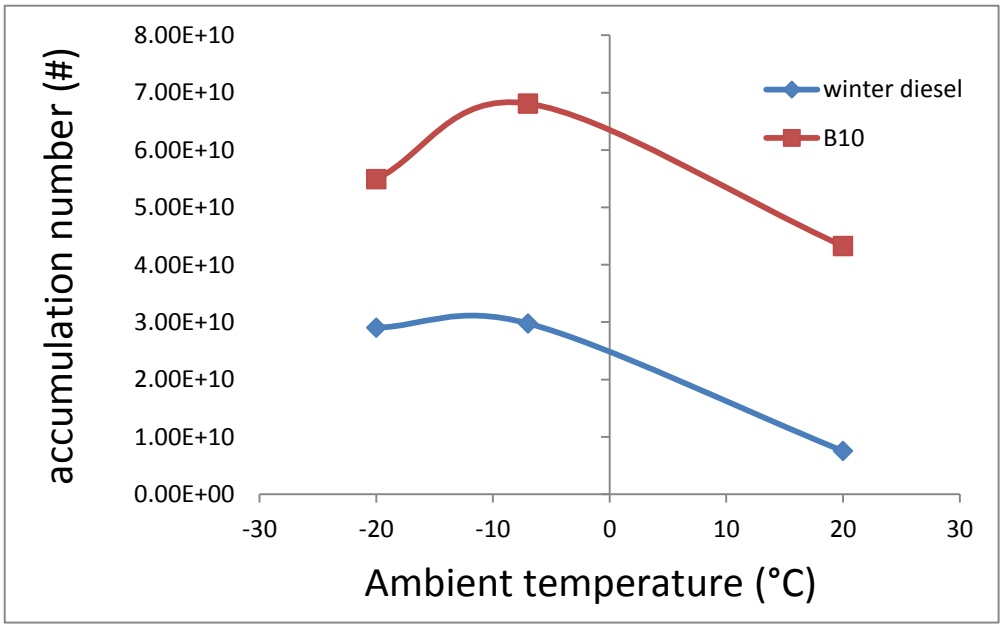

Figure 7.22Cumulative number of accumulation particles during idle period in the first 30s of cold start

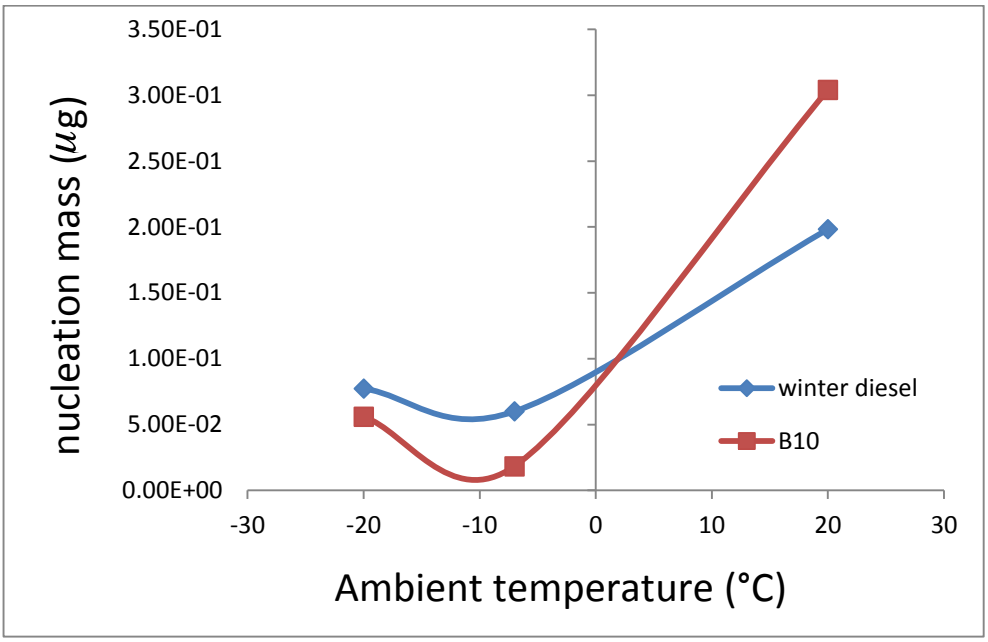

Figure 7.23Cumulative mass of nucleation particles during idle period in the first 30s of cold start

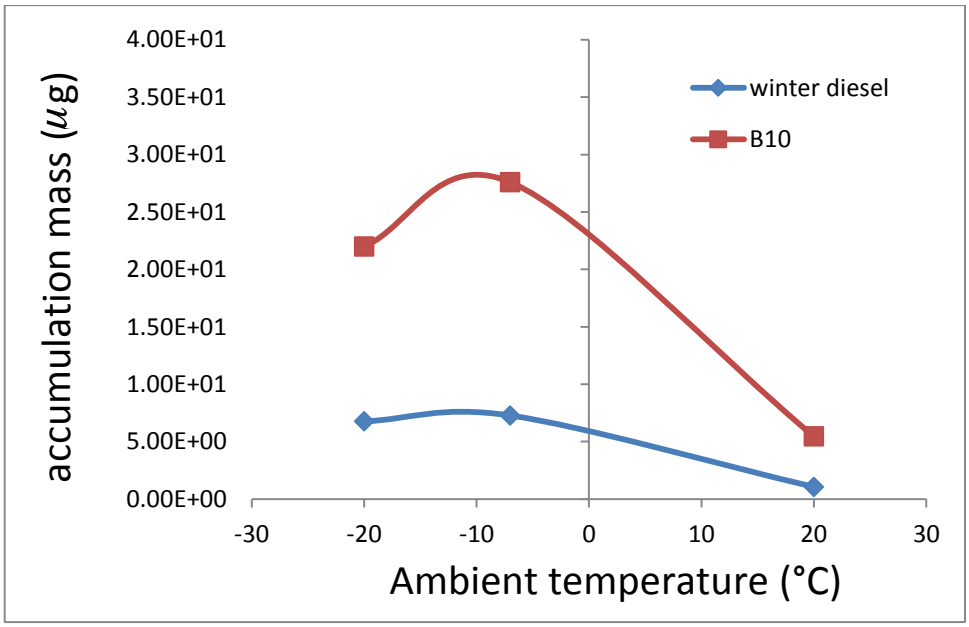

Figure 7.24Cumulative mass of accumulation particles during idle period in the first 30s of cold start

For the accumulation mode particles, it was surprising that increased accumulation mode particles were observed when using RME10 at all the conditions in both of number and mass. Several reasons may have led to this result. The first one is the high cetane number of RME10

which shortened the ignition delay and increased the particle emissions. The second one may be the high viscosity of RME10 which resulted in less atomization and vaporization. The last but not the least was the decreased AFR of RME10 which reduced the particle oxidation. In addition, the total accumulation mode particles were always the highest at -7°C conditions for both of the fuels. The reason is that the volume of the air inlet reduced while the number/mass concentration of accumulation mode particles increased as the ambient temperature reduced.

7.4. CONCLUSIONS

The cold start and idle behaviour of a diesel engine in terms of engine performance, gaseous emissions, particle number, size, surface area and mass resolved characteristics of the exhaust emissions from the latest generation common rail direct injection fuel injection system at very cold ambient conditions was investigated. Based on the analysis of the test result, the following can be concluded:

1. The engine needed more time to reach to a stable idle speed with the drop in ambient temperature and it consumed more fuel at very cold ambient temperatures compared to normal ambient conditions.
2. The cold start hydrocarbon and nitrogen oxide emissions at sub-zero temperatures were several times higher compared to those observed at normal ambient temperatures.
3. During the cold start, the nucleation mode particle concentration was higher at normal ambient temperatures whereas the accumulation mode particle concentration was higher at cold ambient temperatures. The particles in the size range of 10-100 nm were higher for the cold start at ambient and -7°C whereas at very cold ambient (at -20°C) the particle concentration shifted towards the larger size of particles. This wasdue to the incomplete combustion of fuel and the consequent formation of larger sized particles during the cold start.

4. The surface area of the accumulation mode particles was higher than that of the nucleation mode and the total surface area of the particles increased with the decreases in ambient temperature. Particles in the size range of 100-500 nm were observed in large numbers at very cold ambient temperatures and thus increased the particle surface area at cold start and idle.
5. The mass of accumulation mode particles was higher than the nucleation mode particles and the particle mass increased during cold start and idle as the ambient temperature decreased. The particles mass at idle conditions was about $1/10^{th}$ of that of cold start for all the temperature conditions. The engine had been warmed up during the idle period which reduced the exhaust emissions and hence reduced the particle mass during idle as compared to cold start.
6. Since the heating value of biodiesel was lower than that of mineral diesel fuel, the biodiesel blend in winter diesel did not improve the engine combustion. In most of the cases, the emissions of NO_x decreased and the emissions of THC and particles (both in nucleation and accumulation) increased when B10 fuels were used.

Chaper 8. THE CHEMICAL CHARACTERISTICS OF PARTICULATES EMISSION USING BIODIESEL BLEND DURING COLD START

In this chapter, a 2D-GC/MS was used and attention was focused on the SVOC in particulate emissions. Special solvent was used to extract all the SVOC of the filtered particulates. By the separation of 2D-GC and analysis of MS, many of the chemical compositions were identified and their quantities were provided. The mass spectrums of SVOC were used to compare the differences between using winter diesel and biodiesel blends during cold start at 20˚C and -7˚C conditions. Four major organic species, PAHs, alkyl-cyclohexanes, alkanes and oxygenated compounds, were quantified and these indicated that biodiesel reduced most of the organic carbon at 20˚C cold start but increased the alkanes dramatically at -7˚C cold start.

8.1. TEST CONDITION AND PROCEDURE

The cold start procedure was the same as the tests in previous sections. For collecting the particulates on a glass fiber filter, a smart sampler with Constant Volume System was used. The operation system of the smart sampler was integrated with the puma operating system, so that the sampling could be triggered in the automatic test sequences. The sampling started 10 seconds before engine start and finished 10 seconds after the engine was stopped, and a sample ratio of 0.1% was used. The filtered particles were then extracted using nonane and sent into the 2D-GC by carrier gas helium. The flow rate was set to a constant flow of 1ml/min. The 1st column was a SGE BPX5 with 30m length, 0.25mm ID and a film thickness of 0.25μm. For the 1st column, the initial temperature was set at 120˚C for 2 min then it was raised at a rate of 2 degrees/min to 210˚C, followed by a rise rate of 1.5 degrees/min until

325˚C was reached. The 2nd column was a SGE BPX50 with 2m length, 0.1mm ID and a film thickness of 0.1µm. The initial temperature of the secondary oven was set at 120˚C for 2 min then raised at a rate of 3 degrees/min to 200˚C, followed by a rise rate of 2 degrees/min until 300˚C was reached, then finally its temperature was raised at a rate of 1 degrees/min until 330˚C was reached. The modulator had an initial temperature of 220˚C for 2 min then its temperature was raised by 2 degrees/min until it reached 310˚C, which was followed by a temperature rate rise of 1.5 degrees/min until 400˚C was reached. The TOF MS program scanned the molecules from 35m/z to 520m/z

8.2. THE SPECTRUM OF SVOC IN PM EMISSIONS ANALYSED BY 2D-GCMS

The particulates collected by filter papers at 20°C and -7°C cold start using winter diesel and B30 were analysed by 2D-GC/MS to investigate the SVOC in the PM emissions. The result of each case is shown in figure 8.1 to 8.4 respectively. The X-axis is the retention time of the first column and Y-axis is the retention time of the second column. Each dot in the plot is considered to be one chemical component. The alkane species and alkyl-cyclohexane species are clearly indicated along the dotted line as the retention time increased. The colour of the dots along the alkyl-cyclohexane obtained when using B10 are much lighter than those obtained using winter diesel which means that the use of B10 probably resulted in less alkyl-cyclohexanes than when winter diesel was used.

PAHs are normally detected around the circled areas in the plot but they not limited to these areas. It can be seen that the emissions of B10 cold start at 20°C and -7°C conditions are “cleaner” than other cases in the same ambient temperature conditions. Less components were

found around the PAH formation area and the other parts with using biodiesel blend according to the plot due to the aromatic-free nature of biodiesels which reduce the PAHs emitted.

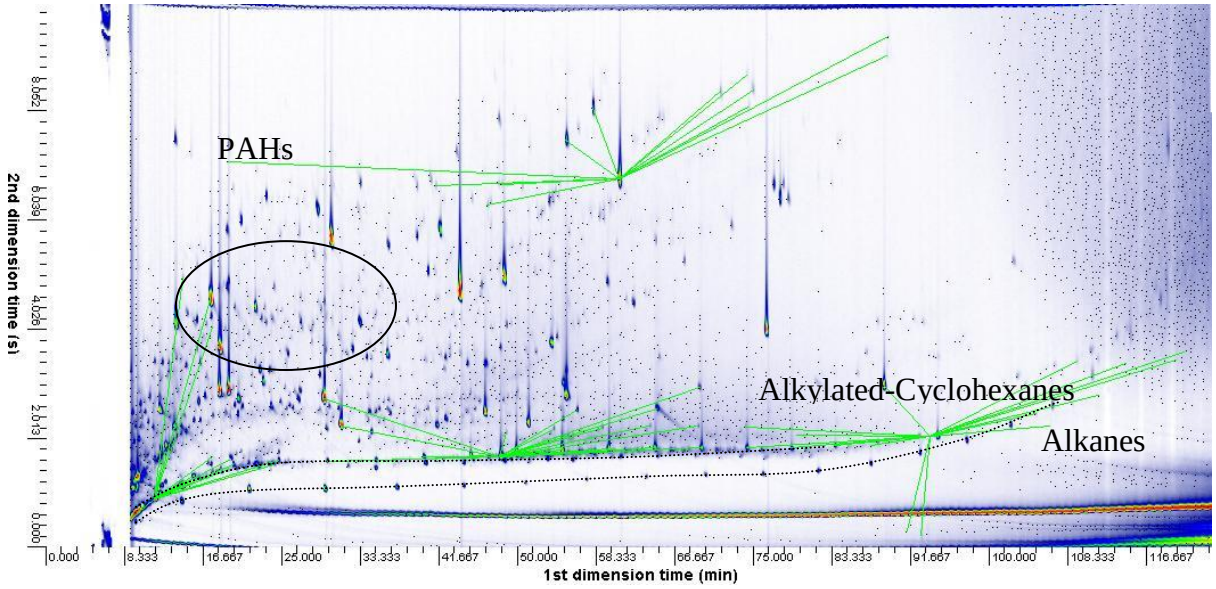

Figure 8.1Contour plot of total ion current chromatogram of the PM sampled in the 3 minutes cold start using winter diesel at 20°C.

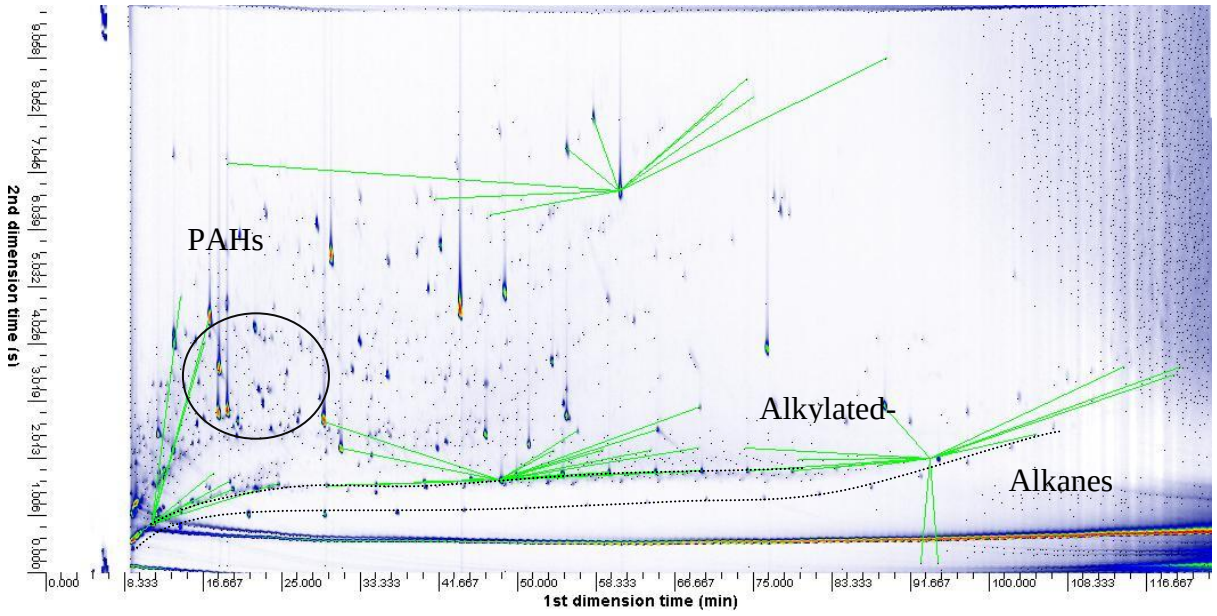

Figure 8.2Contour plot of total ion current chromatogram of the PM sampled in the 3 minutes cold start using winter diesel at -7°C.

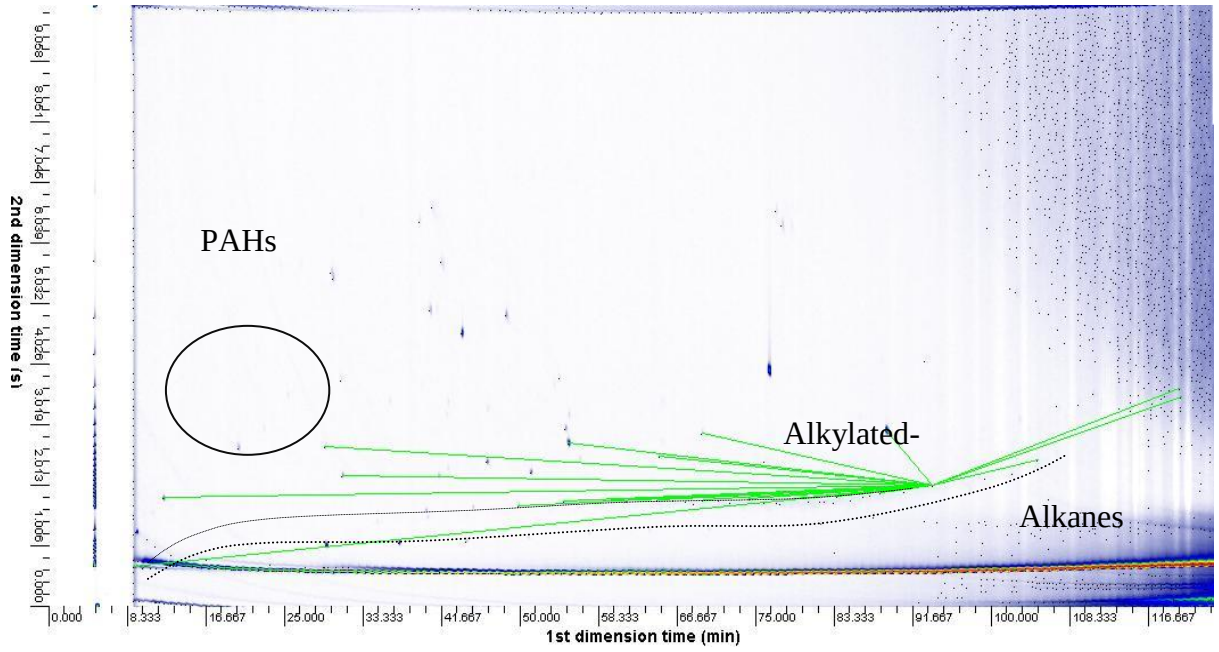

Figure 8.3Contour plot of total ion current chromatogram of the PM sampled in the 3 minutes cold start using B10 at 20°C.

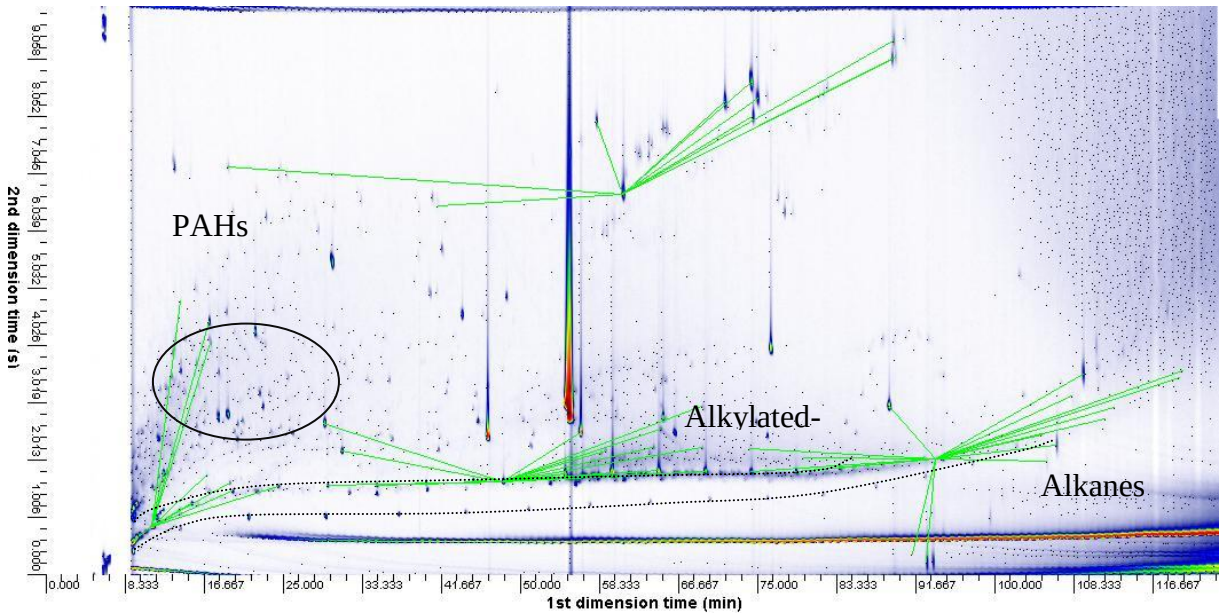

Figure 8.4 Contour plot of total ion current chromatogram of the PM sampled in the 3 minutes cold start using B10 at -7°C.

8.3. CHEMICAL COMPOSITIONS OF SVOC IN PARTICULATES EMISSION AT COLD START

By comparing the mass spectrum of each dot with the database from the NIST library, the molecules in the compounds could be identified with more than 90% confidence. The volume underneath each peak in the surface plot indicated the intensity of the response and related it to the amount of the composition, which was also calculated. A calibrated standard provides the relationship between the amount and the volume (intensity of the response) of the composition. In such a way, the quantity of each composition of SVOC in PM detected by the 2D-GC was obtained and listed in table 7.1. The “nd” in the table means the molecules were not detected or the amount of this molecule was too small to be detected.

Four different types of SVOC are summarized: PAH, Alkylated-cyclohexanes, Alkanes and oxygenated compounds. The total amounts of each species are also calculated. No matter what fuel was used and no matter the ambient temperature, the main species in SVOC of particulate emissions at cold start are alkanes and oxygenated compounds while alkylated-cyclohexanes were always the species detected in the lowest numbers.

From a chemical-reaction point of view, the organic carbon is formed from two routes: direct route (compounds native to the fuel which is emitted directly) and indirect route (intermediates and/or partial combustion products from fuel molecules pyrolysis and rebuilding). In diesel fuels, more than 40% of the compounds are alkanes and around 20% of the compounds are aromatics. Meanwhile, the methyl ester biodiesel contains alkyl/alkenyl. Hence, the SVOCs emitted through the direct route are possibly more dominated by alkane species. The alkanes and methyl ester would firstly be cracked into smaller molecules due to the high combustion temperature and in-cylinder pressure. The pyrolysis of aromatics and cycloalkanes may also produce simpler molecules. The smaller and simpler molecules cracked from the fuel molecules contain a large amount of alkanes and alkyls. These smaller and simpler molecules are then reunited into new structures, such as heavier alkanes, aromatics and cycloalkanes, which act as soot precursors. Since the structure of alkanes is much simpler than those of aromatics and cycloalkanes, the polymerization of heavier alkanes might occur in more than one way. Both the direct and indirect route can possibly produce more alkanes, therefore more alkane species can be found in the particulate emissions. The high emission of oxygenated compounds is mainly due to the triacetins, which is a fuel additive that can improve the engine efficiency in cold start, especially for biodiesel.

Table 8.1 The chemical compositions and their quantity in particle emissions identified by 2D-GC

Compound Name		winter diesel, 20°C cold start	winter diesel, -7°C cold start	B10, 20°C cold start	B10, -7°C cold start
PAHs	**Formular**	**ng/m^3**	**ng/m^3**	**ng/m^3**	**ng/m^3**
benzothiazole	C_7H_5NS	121.6154	119.8533	nd	65.6476
phenanthrene	$C_{14}H_{10}$	622.8884	737.2824	nd	nd
phenanthrene, 3-methyl-	$C_{15}H_{12}$	596.7879	709.755	nd	nd
fluoranthene	$C_{16}H_{10}$	628.4127	745.8907	nd	nd
pyrene	$C_{16}H_{10}$	634.1772	755.8233	nd	602.7519
cyclopenta[cd]pyrene	$C_{18}H_{10}$	399.3531	477.8052	nd	1777.282
Benzo[ghi]fluoranthene	$C_{18}H_{10}$	420.4897	500.6975	nd	1121.149
chrysene	$C_{18}H_{12}$	444.9889	516.2112	nd	409.8429
benz[a]anthracene	$C_{18}H_{12}$	450.5933	nd	nd	994.2391
benzo[b]fluoranthene	$C_{20}H_{12}$	740.0683	506.657	nd	498.5243
benzo[k]fluoranthene	$C_{20}H_{12}$	nd	nd	830.8054	nd
Benzo[j]fluoranthene	$C_{20}H_{12}$	367.2479	nd	nd	622.967
benzo[a]pyrene	$C_{20}H_{12}$	573.0133	772.283	nd	1115.148
benzo[e]pyrene	$C_{20}H_{12}$	537.2733	689.4414	nd	453.6071
sum		6536.909	6531.7	830.8054	7661.159
Alkyl-Cyclohexane					
cyclohexane, heptyl-	$C_{13}H_{26}$	99.75822	99.04218	nd	58.1783
cyclohexanes, methyl-hexyl-	$C_{13}H_{26}$ (branched)	9.847721	31.40592	nd	101.2124
cyclohexane, tridecyl-	$C_{19}H_{38}$	332.1004	nd	nd	nd
cyclohexane, tetradecyl-	$C_{20}H_{40}$	337.0643	388.128	nd	nd
cyclohexane, n-pentadecyl-	$C_{21}H_{42}$	326.1757	374.6008	nd	437.468
cyclohexane, hexadecyl-	$C_{22}H_{44}$	286.5447	332.7893	nd	477.9666
cyclohexane, n-heptadecyl-	$C_{23}H_{46}$	281.821	320.208	nd	347.0141
cyclohexane, octadecyl-	$C_{24}H_{48}$	646.2267	639.9884	nd	509.9099

sum		2319.539	2186.163	0	1931.749
Alkanes					
undecane	$C_{11}H_{24}$	752.1097	4545.062	591.2876	2704.298
dodecane	$C_{12}H_{26}$	64.05022	782.3102	nd	292.901
tetradecane	$C_{14}H_{30}$	33.5463	74.63637	nd	28.57521
hexadecane	$C_{16}H_{34}$	551.7126	657.1595	nd	601.9296
heptadecane	$C_{17}H_{36}$	480.777	671.1597	nd	640.5096
octadecane	$C_{18}H_{38}$	544.5069	676.8355	nd	653.598
nonadecane	$C_{19}H_{40}$	870.3624	1102.329	nd	800.9282
eicosane	$C_{20}H_{42}$	1609.502	1902.045	489.0931	1083.871
heneicosane	$C_{21}H_{44}$	1885.158	1977.06	nd	4735.536
docosane	$C_{22}H_{46}$	1736.642	1733.853	205.577	12241.09
tricosane	$C_{23}H_{48}$	1513.507	1197.966	342.6284	7920.267
tetracosane	$C_{24}H_{50}$	1484.124	1421.402	205.577	5797.958
pentacosane	$C_{25}H_{52}$	3487.988	1743.886	673.099	2801.041
hexacosane	$C_{26}H_{54}$	2180.867	1124.258	535.6844	1765.201
heptacosane	$C_{27}H_{56}$	1618.038	980.2489	527.227	1409.473
octacosane	$C_{28}H_{58}$	529.1573	726.6025	398.1794	868.8741
triacontane	$C_{30}H_{62}$	784.0291	546.6504	nd	601.4403
hexatriacontane	$C_{36}H_{74}$	479.7682	382.3766	233	244.3927
sum		20605.84	22245.84	4201.353	45191.88
Oxygenated Compounds					
triacetin	$C_9H_{14}O_6$	14940.59	16004.82	nd	1372.227
methyl 8-oxooctanoate	$C_9H_{16}O_3$	40.27158	180.8679	nd	280.4071
1(3H)-Isobenzofuranone	$C_8H_6O_2$	592.0642	706.6333	nd	347.5623
decanal	$C_{10}H_{20}O$	674.9292	2625.138	156.8978	1744.184
Dodecyl acrylate	$C_{15}H_{28}O_2$	819.0422	904.0555	302.5861	932.9772
isopropyl laurate	$C_{15}H_{30}O_2$	1776.113	2509.825	566.3747	902.0036
Pentanoic acid, 2,2,4-trimethyl-3-carboxyisopropyl, isobutyl ester	$C_{16}H_{30}O_4$	2991.546	5330.02	1008.912	1407.038
methyl stearate	$C_{19}H_{38}O_2$	571.0878	559.8201	407.2947	1371.532
Hexanedioic acid, dioctyl ester	$C_{22}H_{42}O_4$	531.6969	540.5224	238.7133	451.9954
sum		22937.34	29361.7	2680.778	8809.926

8.4. THE PROFILES OF SVOC EMISSIONS FROMUSING WINTER DIESEL AND BIODIESEL BLEND

8.4.1. PAH Series

At 20˚C conditions, the PAH emission in cold start are mainly found when using winter diesel due to the aromatic free nature and oxygen content of the biodiesel. In figure 8.5, the carbon number of the PAHs increased going from left to right on the X-axis. The combustion of winter diesel at cold start produced wider ranges of PAHs. Meanwhile, using B10 in cold start only produced heavier PAHs. The reduction of PAHs with using oxygenated fuel was also found in the research conducted by (Kitamura et al. 2001) and (Lea-Langton et al. 2012)They proposed three reasons for the PAHs suppression observed when using oxygenated fuels. Firstly, the aromatic precursors, such as acetylene and the propargyl radical from fuel molecules pyrolysis, are significantly reduced in the combustion of oxygenated fuel in comparison to the cases of hydrocarbon fuel, including diesel fuels. The reduction of aromatic precursors leads to the drastic suppression of PAH/soot formation. Secondly, the differences in molecular structures of the fuels result in a remarkable difference in the major reaction products. (BEATRICE et al. 1997)experimentally proved that glycolethers have a lower soot formation tendency than ether–alcohol, even if both of them were blended to form a fuel with the same fuel oxygen content. Therefore, for the correct selection of a specific oxygenated fuel to drastically improve the diesel combustion process, the molecular structure must be taken into account, as well as the fuel oxygen content. Thirdly, the oxygen bonds in the fuel play an important role in PAH growth. Two reactions were suggested by(Kitamura et al.

2001)according to the sensitivity analysis for the formation and the consumption of benzene in the normal heptanes oxidation process.

$$C_2H_4+OH=CH_3+HCHO \quad (8.1)$$

and

$$HCO+M=H+CO+M \quad (8.2)$$

In the combustion of hydrocarbons, the dehydrogenation of ethylene may form acetylene, which is thought to polymerise to benzene. As Eq. (8.1) showed, the OH radical, which is directly formed by decomposition of oxygenated fuel, reduces the ethylene and consequently reduces the acetylene and benzene. In addition, Marinov et al. (Marinov 1997)also pointed out that the hydrogen-atom pool is established by Eq. (8.2), which consumes the propargyl radical and benzene by hydrogen-atom abstraction reactions thereby limiting the growth of benzene.

More PAH species were formed as the ambient temperature dropped to -7˚C. For the B10, some of the PAH emissions at -7˚C condition are even more than that of using winter diesel. This is because of the increased fuel injection quantity and decreased viscosity by using biodiesel at -7˚C condition. The lower viscosity of large quantity of biodiesel resulted in more liquid fuel to form PAH emissions.

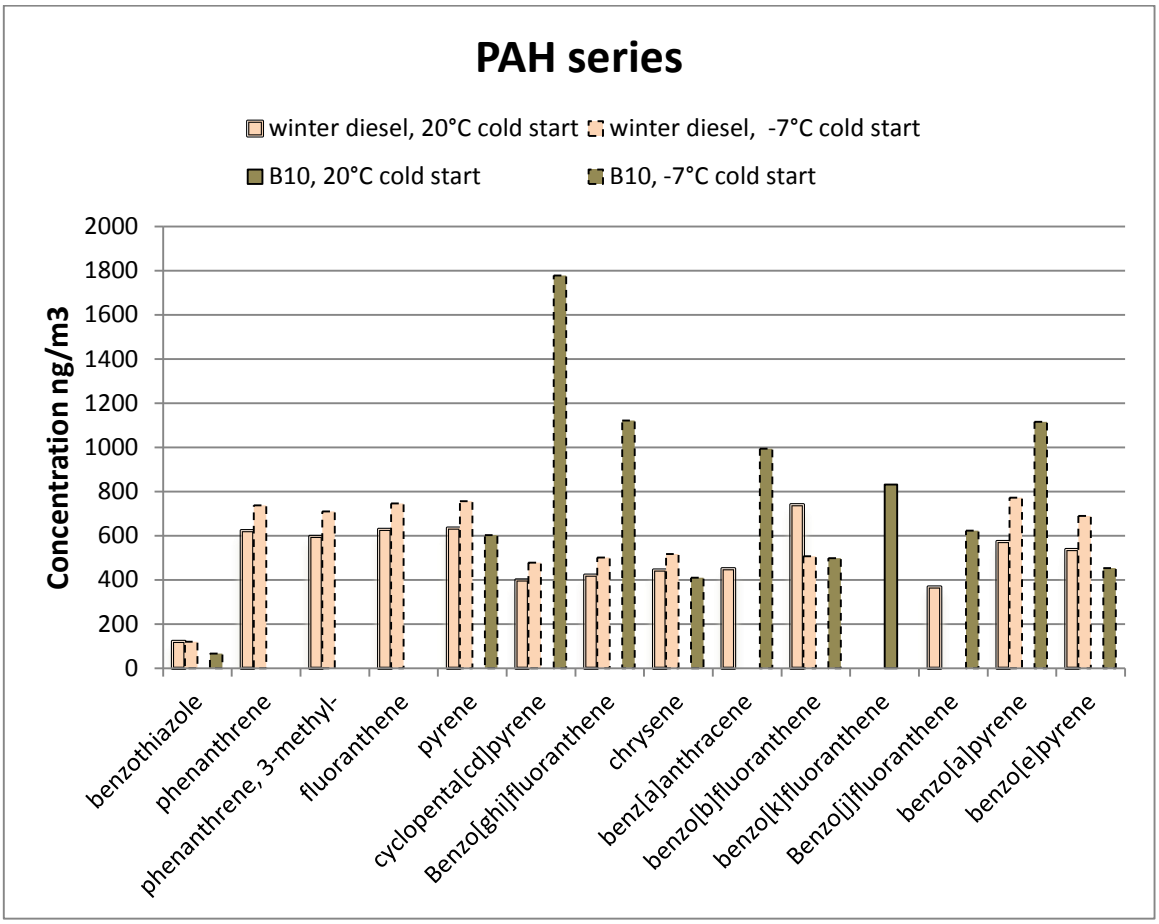

Figure 8.5 The quantity of PAHs emissions of using winter diesel and biodiesel blend during cold start at 20°C and -7°C conditions.

8.4.2. Alkyl-cyclohexane Series

Cycloalkanes may widely exist in diesel fuels, depending on the crude source and degree of hydroprocessing. The dehydrogenation of cyclohexane results in the formation of the initial benzene, which is followed by the addition reactions with other small radicals. A wider range of alkyl-cyclohexanes was found by using winter diesel either at the 20˚C condition or the -7˚C condition due to the cyclohexane free nature of biodiesel. The amount of octadecylcyclohexane was always the highest for all the cases. As the ambient temperature decreased from 20˚C to -7˚C, all the alkyl-cyclohexane species increased, or went from

undetectable to detectable, by using B10, except forheptylcyclohexane. For the winter diesel, the octadecylcyclohexane were found to slightly reduce when the temperature decreased, and the tridecylcyclohexane even disappeared at -7˚C.

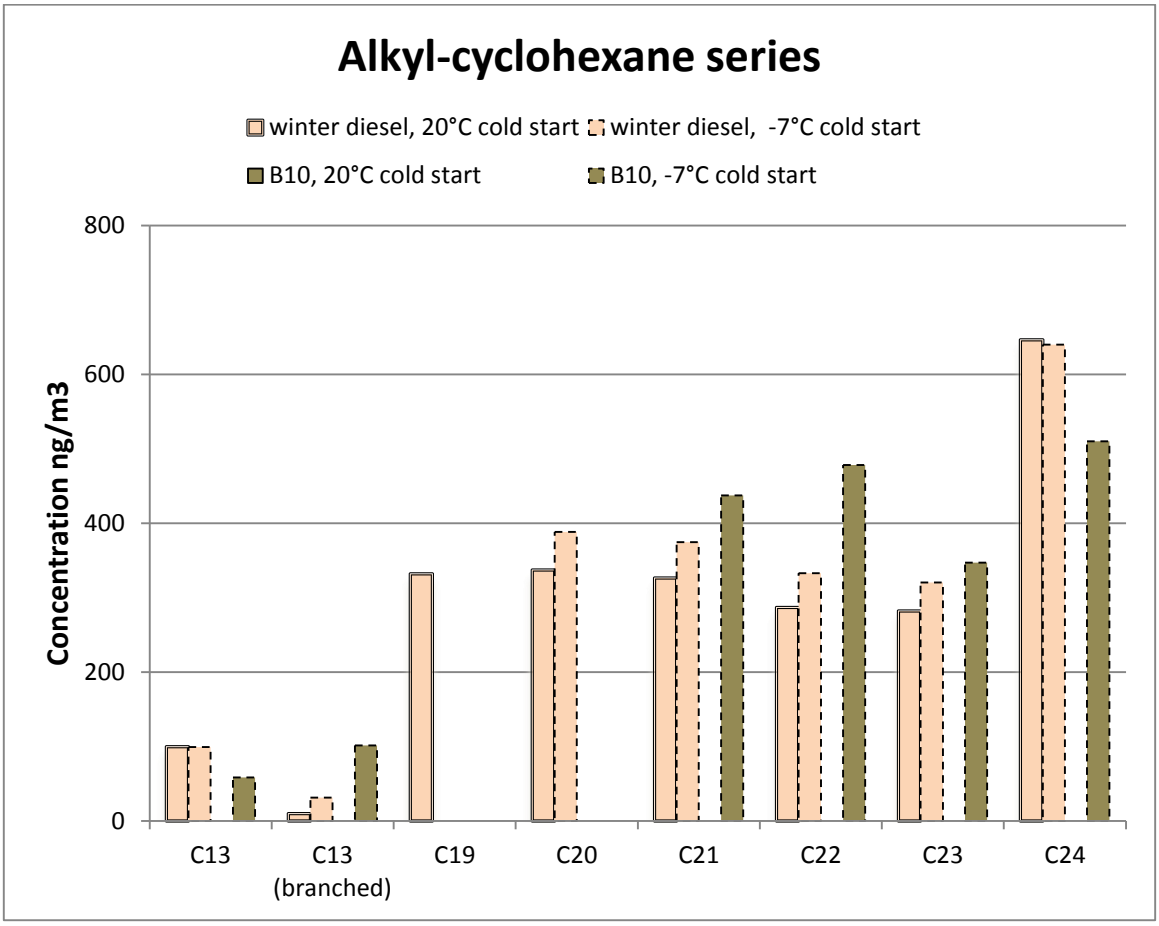

Figure 8.6 The quantity of alkyl-cyclohexane emissions of using winter diesel and biodiesel blend during cold start at 20°C and -7°C conditions.

8.4.3. n-Alkanes Series

Alkane species are another compound which is commonly found in diesel fuels and lubricant oil. The small radicals pyrolysed from alkanes play an important role in forming PAHs. The

alkanes in particulate emissions were either produced from the pyrolysis of longer alkanes or from the unconsumed fuel and lubricant oil.

When the engine was fuelled with winter diesel, the lighter alkane species (from C11-C20) at the -7˚C condition was higher than those at the 20˚C condition. Meanwhile, as the length of carbon chain increased from C14 to C21, the n-alkane emissions also increased to a peak at C21, heneicosane. As the length of the carbon chain increased further, the n-alkane emission at the -7˚C condition became lower than the cases at 20˚C, except C28. In addition a second peak appeared at C25 for both of the two conditions. This agreed with the results of (Black and High 1979). They suggested that the first hump was mainly formed by the unburned or partially burned fuel while the majority of the second hump was comprised of the unburned or partially burned lubricant oil. This can also explain the trends in figure 8.7. At the 20˚C condition, alkanes derived from fuel were lower due to the lower fuel injection quantity. More alkanes derived from lubricant oil were found at 20˚C caused by the higher viscosity of the lubricant oil which led to more lubricant oil remaining in the cylinder and being emitted in the exhaust gas.

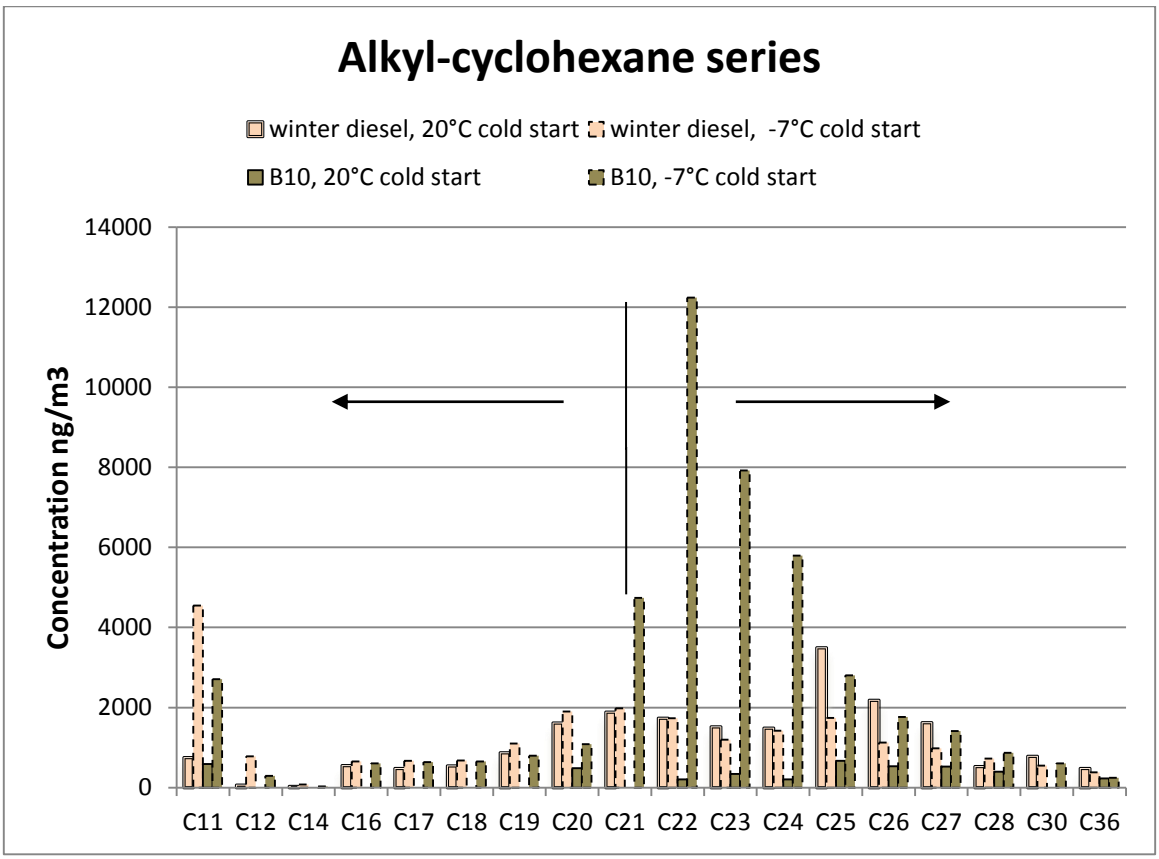

Figure 8.7 The quantity of n-Alkanes emissions of using winter diesel and biodiesel blend during cold start at 20°C and -7°C conditions.

When the fuel was changed to B10, the trend became different. The n-alkanes produced at the -7˚C condition were always higher than those produced at the 20˚C condition. Compared with the cases of winter diesel, using biodiesel reduced the alkane species within the carbon length range of C14 to C36 only at the 20˚C condition. Two peaks were observed at C20 and C25 which was suggested to be the peak of the fuel and lubricant oil derived alkanes respectively. According to the discussions in previous chapter, using biodiesel suppressed the PM emissions at the 20˚C condition due to the oxygen content. However, the lower temperature increased the viscosity of biodiesel and lead to higher PM emissions due to poor atomization

and vaporization. In the results of this test, when the ambient temperature decreased to -7˚C, the larger n-alkanes (C21-C30) were dramatically increased when using biodiesel, especially C21-C25. This might have been caused by the dramatic increase of unburned or partially burned fuel which increased the alkane emissions and shifted the peak towards the larger alkanes. Therefore, the two humps of fuel-derived alkanes and oil-derived alkane got closer and resulted in a large peak between C21 and C25.

8.4.4. Oxygenated Compounds

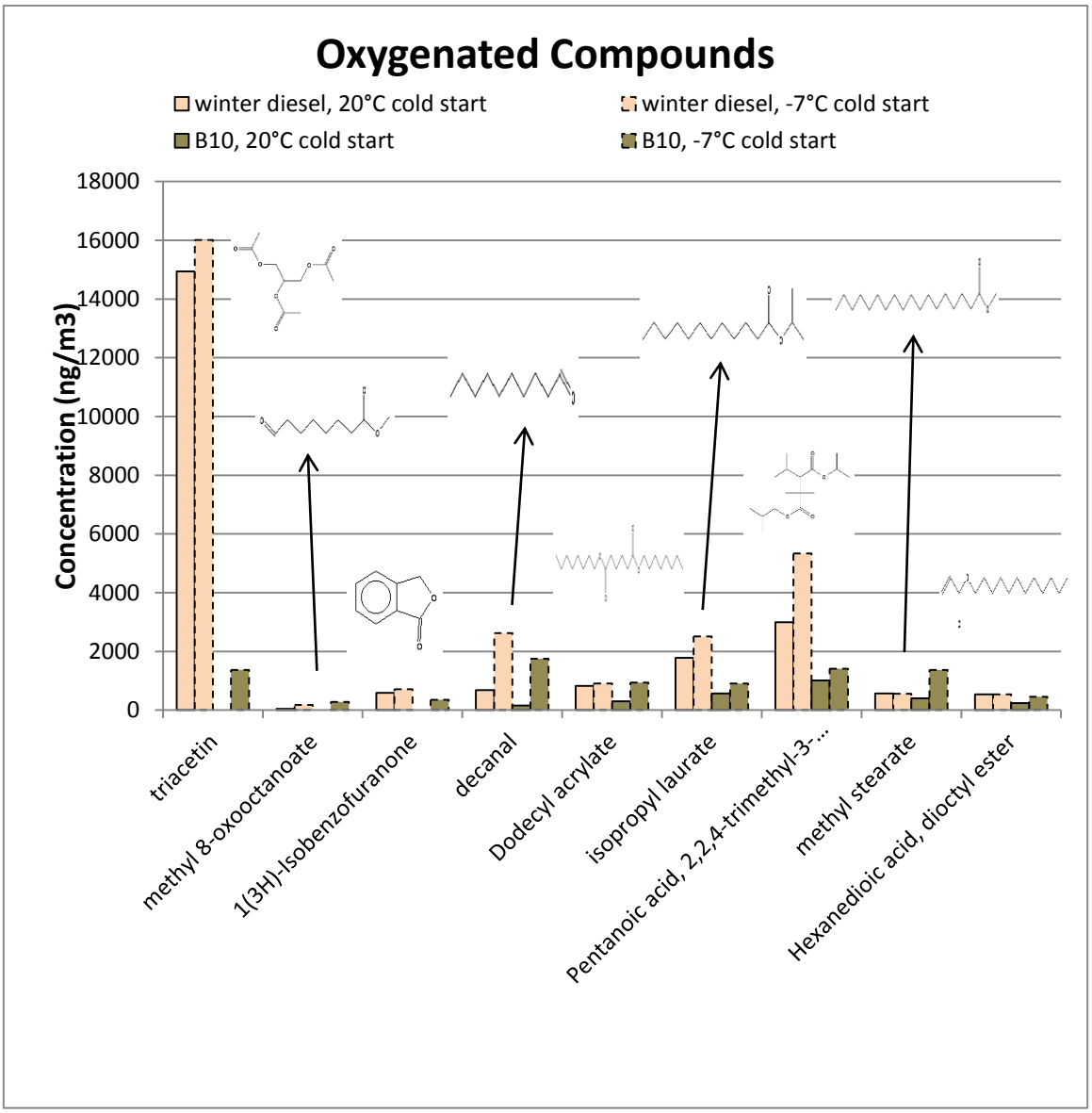

Figure 8.8 The quantity of Oxygenated Compounds emissions of using winter diesel and biodiesel blend during cold start at 20°C and -7°C conditions.

Several oxygenated compounds were also found in the exhaust particulates and their amounts are shown in figure 8.8. The dominant oxygenated compound obtained using winter diesel is triacetin. This is a fuel additive which improves the cold startability, especially for biodiesel

fuel. The triacetin was observed to reduce dramatically when B10 was used at 20˚C and -7˚C conditions, respectively. Biodiesel also reduced most of the other oxygenated compounds at 20˚C cold start. However, as the ambient temperature decreased, the methyl stearate was higher than those observed in other cases.

8.5. CONCLUSIONS

The characteristics of SVOC were analysed by 2D-GC/MS. Many chemical compounds were identified in the SVOC in PM. Four different organic species, PAHs, alkyl-cyclohexanes, alkanes and oxygenated compounds, from engine emissions were compared using winter diesel and biodiesel blends in cold start at 20˚C and -7˚C conditions. Alkanes and oxygenated compounds comprised the majority of the SVOC in particulates for all the cases. Two humps of alkane emissions were discovered along the length of carbon chain when using winter diesel and they are probably derived from fuel and lubricant oil, respectively. Following on from this suggestion, it can be concluded that the fuel-derived alkanes dominated at the -7˚C condition while the oil-derived alkanes dominated at the 20˚C condition. Biodiesel have a significant effect on the reduction of alkanes at 20˚C cold start, but they dramatically increase the alkanes at -7˚C cold start due to the large portion of unburned or partially burned fuel. The reduction of PAHs and alkyl-cyclohexanes were also significant when blending biodiesel fuels, even at -7˚C conditions. Some PAHs and alkyl-cyclohexanes were not found in the sample obtained when using biodiesel due to the special functional group in biodiesel molecules. Triacetin largely existed in the PM emissions when using winter diesel. The use of biodiesel blends reduced the oxygenated compounds at the 20˚C condition except methyl stearate.

Chaper 9. ONCLUSIONS AND FUTURE WORK

The research work in this thesis focused on the combustion and emissions of alternative fuels both during steady state and cold start. Three phases of experimental works were conducted in two engine test cells. In the first phase, biodiesel fuels derived from various feedstocks were blended with a zero sulphur diesel in different blend ratios and were tested at steady test conditions. The combustion characteristics and emissions of each fuel were compared and the correlations between fuel properties and emissions were analysed statistically. A smoke index was created to predict the smoke number in different engine conditions. In the second phase, two different types of biodiesel, RME (rapeseed methyl ester) and HVO (hydrogenated vegetable oil), were blended with zero sulphur diesel in 60% by volume. The combustion and emissions of each fuel were compared during cold start at 25°C and warm start with the engine coolant at 90°C. In the third phase, winter diesel was used to evaluate the performance and emissions during cold start at 20°C, -7°C and -20°C. RME was added into winter diesel in 10% by volume in order to study the biodiesel effects on cold start at very low temperature conditions. This chapter summarized the conclusions from the previous chapter and recommended some future work in this research area.

9.1. CONCLUSIONS

9.1.1. Combustion and Emissions of Biodiesel Blends

The combustion and emissions of mineral diesel and different biodiesel from various feedstocks were studied in a common rail direct injection 3.0 litre V6 diesel engine. EGR effects were investigated with both biodiesel and diesel. EGR application increased the ignition delay which improved the fuel atomization/vaporization and fuel/air mixing during the ignition delay. However, the combustion pressure and temperature were also reduced

when using EGR and this led to an increase of smoke level and THC emissions and a reduction of NO_x emissions. When the engine was running with low EGR rate (less than 15%), the first effect dominated and reduced the smoke and NO_x emissions slightly. In some specific engine loads and at a high EGR rate, the smoke and NO_x were reduced significantly due to the low combustion temperature.

9.1.2. Correlations of Fuel Properties and Emissions of Biodiesel Fuels

Biodiesels produced from 6 different feedstocks were blended with mineral diesel in 3 blend ratios. The relationship between fuel properties and engine emissions were investigated by statistical analysis. The Cetane number of the biodiesel was confirmed to have a good correlation with the NO_x emission. GHV of combustion and the oxygen content showed a highly significant linear relationship with the smoke and THC emissions. Based on the relationship between fuel properties and emissions, an index, which contained some of the fuel properties, was created to predict the smoke number. The smoke emissions at different engine conditions could also be predicted using the smoke index.

9.1.3. Cold Start and Warm Start with Using Biodiesel

The engine performance and emissions of two biodiesel blends, RME60 and HVO60, were investigated and compared with the cases of using mineral diesel at cold start. Warm start cumulative emissions of each fuel in the first 10 seconds were also calculated to investigate the engine coolant temperature effects.

The combustion of RME60 showed the highest in-cylinder pressure and ROHR in the first fired cycle due to its low stoichiometric ratio. Meanwhile, the use of RME60 increased the NO emission and reduced the THC and particles at cold start during the acceleration period

compared with those observed when using mineral diesel. During the idle period, the in-cylinder pressure and ROHR of the pilot injected fuel when using RME60reducedto the lowest observed across all the fuels due to the high viscosity and AFR of RME60. Hence, the THC and particle emissions were higher when using RME60 during the idle period. The combustion characteristics and emissions of HVO60 and mineral diesel were similar during the acceleration period. A higher in-cylinder pressure and ROHR of pilot injected fuel were observed when using HVO60during the idle period due to the high cetane number. Emissions obtained when using HVO60 were significantly improved except for NO due to the absence of aromatics in HVO. As the engine coolant temperature increased to 90°C before engine start, the emissions were improved in most cases. At warm start, combustion of biodiesel-diesel blends led to lower NO and higher THC/PM than those observed when using mineral diesel, due to the fuel impinging effect. However, the accumulation mode particles obtained when using RME60 at warm start were lower than those obtained when using mineral diesel, due to oxygen content of the fuel.

9.1.4. Cold Start at Subzero Degree Conditions

The cold start and idle behaviour of the diesel engine fuelled with winter diesel and a biodiesel-winter diesel blend at very cold ambient conditions was investigated. The results showed that a longer time was required for the engine to reach the stable idle speed when the ambient temperatures decreased. The THC and NO_x emissions during cold start at sub-zero temperatures were several times higher compared with the cases of 20°C ambient temperatures. The accumulation mode particles increased as the ambient temperature decreased. The nucleation particles were higher at 20°C and -7°C conditions whereas at the -20°C condition, more nuclei were adsorbed on the surface of large particles which resulted in nucleation mode particles that could not be specified properly. Due to the lower heating value

of biodiesel, the biodiesel blend in winter diesel could not improve the engine combustion. In most of the cases, the emissions of NO_x decreased and the emissions of THC and particles (both in nucleation and accumulation) increased when using B10 fuels.

9.1.5. Chemical compositions at cold start

The SVOCs were analysed in species and quantities with using winter diesel and biodiesel blend. Alkanes and oxygenated compounds were found to comprise the majority of the SVOC in particulates for all the cases. Two humps of alkane emissions were discovered along the length of carbon chain when using winter diesel and they are probably caused by the unburned or partial burned fuel and lubricant oil, respectively. Following on this suggestion, it can be concluded that the fuel-derived alkanes was higher at the -7˚C condition while the oil-derived alkanes emitted more at the 20˚C condition. Biodiesel have a significant effect on the reduction of alkanes at 20˚C cold start, but they dramatically increase the alkanes at -7˚C cold start due to the large portion of unburned or partially burned fuel. The reduction of PAHs and alkyl-cyclohexanes were also significant when blending biodiesel fuels, even at -7˚C conditions. Some PAHs and alkyl-cyclohexanes were not found in the particles obtained when using biodiesel due to the special functional groups in biodiesel molecules. Triacetin largely existed in the PM emissions when using winter diesel. The use of biodiesel blends reduced the oxygenated compounds at the 20˚C condition, but produced 3-10 times of the dodecyl acrylate, methyl stearate, hexanedioic acid and dioctyl ester than those observed in the other cases at the -7˚C condition, due to the incomplete combustion.

9.2. FUTURE WORK AND RECOMMENDATIONS

Informed by the experimental work in this thesis, the author recommends several areas for future study:

1. Broaden the smoke index for application in various engines, engine conditions and fuels. The smoke index was only verified on one engine. Other engines with different compression ratios may have different effects. Meanwhile, different split injection strategies may affect the smoke index as well.
2. Create a smoke index for cold start and transient conditions. The engine performance and emissions are quite different at cold start and transient conditions. Due to the large difference of engine temperature between the cold start and the warmed up steady condition, the trends of engine emissions are totally different. A new index might be useful for particle prediction.
3. Validate other models to predict the NO_x and THC emissions. The NO_x and THC emissions were confirmed to correlate to some of the fuel properties. Models to predict the two emissions should be created as well.
4. At cold start, especially when the ambient temperature is very low, the EGR valve is closed. Considering that the exhaust gas of first several compression cycles has a higher temperature, introducing the compression gas or even gas from the first several combustion cycles back into combustion chamber might benefit the engine performance and emissions at cold start.
5. Try other biofuels with higher GHV of combustion in low temperature cold start. Biodiesel with lower GHV of combustion could not improve the performance and

emissions. Hence, another diesel-like fuel with higher GHV of combustion and lower viscosity might be good for engine cold start.

6. Analyse the particle emissions in hot engine tests and investigate the mechanism of particle formation in a more in-situ environment.
7. Comparing the fuel and lubricant oil compositions with those of particles emission and find out the quantity of the fuel-derived particles, lubricant oil-derived particles and particles from combustion. According to the results of the comparisons, try to find out one or two molecules which might play an important role in particulate formation and confirm it in experimental work.

APPENDIX

Table A0.1 The fuel properties of all the tested fuels

	Cetane Number	Density	Carbon content	Hydrogen	Oxygen content	Gross heat of combustion	Net heat of combustion	viscosity	surface tension
		Kg/m3	%	%		MJ/kg	MJ/kg	10-3Pa.s	
TME-10	54.3	836.7	86	13.5	0.5	45.36	42.48	3.83	26.1
TME-30	56.5	843.7	82.7	13.1	4.2	44.34	41.56	4.37	26.8
TME-60	59.1	857.4	80.2	13	6.8	42.2	39.44	5.36	27.2
HVO-10	56.8	827	86	13.6	0.4	45.7	42.8	3.58	26
HVO-30	58.8	815.5	85.5	14	0.5	45.74	42.76	3.49	25.6
HVO-60	64.3	798.7	85.1	14.4	0.5	46.72	43.66	3.43	25
RME2-10	55.1	837.8	84.4	13	2.6	44.84	42.1	nd	nd
RME2-30	57.1	848.3	83	12.8	4.2	43.54	40.82	nd	nd
JME-10	58.9	837.6	84.2	13.1	2.7	45.2	42.42	3.81	26.3
JME-30	57.4	847	82.4	12.7	4.9	43.78	41.08	4.3	26.9
RME-10	55.7	837.8	84.9	12.8	2.3	44.78	42.06	3.81	26
RME-30	57.8	847.9	82.7	12.7	4.6	43.44	40.76	4.3	26.5
RME-60	60.3	863.3	79.9	12.3	7.8	41.6	38.98	5.27	27.1
SME-10	52.9	837.7	85.4	12.9	1.7	45.08	42.36	nd	nd
SME-30	52.2	847.9	83.5	12.6	3.9	43.76	41.08	nd	nd
SME-60	52.8	863.6	81.5	12.3	6.2	41.86	39.24	nd	nd
UVOME-30	55.54	849	83.4	13.3	3.3	43.92	41.08	nd	nd
UVOME-60	57.23	865.5	80.6	12.7	6.7	42.2	39.5	5.75	27.4
Mineral Diesel	56.7	832.7	85.9	13.6	0.5	45.62	42.72	3.6	25.8

All data were provided by Shell Ltd.

'nd' means the property of this fuel was not measured in lab.

Table A0.2 EGR swept test conditions.

RPM	750	1250	1500	2250	1500	2280
Torque	35.95	48.4	72.025	94.925	142.8	196.125
BMEP	1.5 Bar	2 Bar	3 Bar	4 Bar	6 Bar	8.2 Bar
	0%	0%	0%	0%	0%	0%
	5%	5%	5%	5%	5%	5%
	10%	10%	10%	10%	10%	10%
	15%	15%	15%	15%	15%	15%
	20%	20%	20%	20%	17%	20%
	25%	25%	25%	25%	20%	22%
	30%	30%	30%	29%	22%	24%
	35%	35%	35%	31%	25%	27%
	40%	40%	37%	33%		
	45%	45%	39%	36%		
	47%	47%	41%			
	49%	48%	43%			
	51%	51%	46%			
	54%	54%				

Table A0.3 The injection strategies for each engine conditions

BMEP	pilot 2	pilot 1	main	post
1.5 Bar	ON	ON	ON	OFF
2 Bar	ON	ON	ON	OFF
3 Bar	ON	ON	ON	OFF
4 Bar	ON	ON	ON	ON
6 Bar	ON	ON	ON	ON
8.2 Bar	ON	ON	ON	ON

Table A4 Chemical compositions of mineral diesel, HVO and UVOME

	Chemical formula samples	Mineral Diesel (%)	HVO (%)	UVOME (%)
Normal (linear) Paraffins	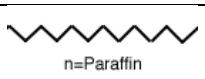	17.62	13.08	-
Iso (branched) Paraffins		21.09	86.45	-
Naphthenics	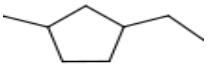	24.49	0.35	-
Di-Naphthenics	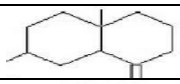	11.73	0.03	-
Mono-Aromatics		8.86	0.02	-
Naphthenic-mono-Aromatics	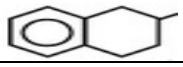	11.39	-	-
Di-Aromatics	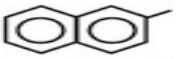	2.49	-	-
Naphthenic-di-Aromatics	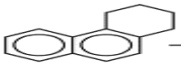	1.83	-	-
Tri-Aromatics	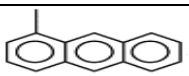	0.3	-	-
Methyl ester	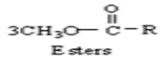	-	-	>98
Other		0.2	0.06	<2

Measured by Shell

REFERENCES

Aakko, Nylund, Westerholm, Marjamäki, Moisio, Hillamo, & Mäkelä. Emissions from heavy-duty engine with and without aftertreatment using selected biofuels..

Agarwal, 2013. Effect of fuel injection pressure on diesel particulate size and number distribution in a CRDI single cylinder research engine., 107, 84-89

Akihama, Takatori, Inagaki, & Sasaki. 2001. Mechanism of the Smokeless Rich Diesel Combustion by Reducing Temperature. *SAE Technical Paper 2001-01-0655*

Alt, Sonntag, Heuer, & Thiele 2005. Diesel Engine Cold Start Noise Improvement. *SAE paper*, 2005-01-2490,

Altiparmak, Keskin, Koca, & G¨¹r¨¹. 2007. Alternative fuel properties of tall oil fatty acid methyl ester-diesel fuel blends. *Bioresource Technology*, 98, (2) 241-246

André, Boehman, Song, & Alam 2005. Impact of biodiesel blending on diesel soot and the regeneration of particulate filters. *Energy Fuels*, 19, (5) 1857-1864

Andrews, Clarke, Rojas, Gregory, & Sale 2000. Particulate Mass Accumulation and Release in Practical Diesel Engine Exhaust Systems under Cold Start Conditions. *SAE paper*, 2000-10-16,

Armas, Arantzazu, & Ramos 2013. Comparative study of pollutant emissions from engine starting with animal fat biodiesel and GTL fuels. *Fuel*, 113, (560) 570

Armas, Hernández, & Cárdenas 2006. Reduction of diesel smoke opacity from vegetable oil methyl esters during transient operation. *Fuel*, 85, (17-18) 2427-2438

Assessment and Standards Division (Office of Transportation and Air Quality of the US Environmental Protection Agency) 2002, *A comprehensive analysis of biodiesel impacts on exhaust emissions* EPA420-P-02-001.

ATC(the Technical Committee of Petroleum Additive Manufacturers in Europe). Fuel additives and the environment. http://www.atc-europe.org/public/doc52.pdf . 2013.

Bagley, Gratz, Johnson, & McDonald 1998. Effects of an oxidation catalytic converter and a biodiesel fuel on the chemical, mutagenic, and particle size characteristics of emissions from a diesel engine. *Environ.Sci.Technol.*, 32, (9) 1183-1191

Ban-Weiss, Chen, Buchholz, & Dibble 2007. A numerical investigation into the anomalous slight NOx increase when burning biodiesel: a new (old) theory. *Fuel Processing Technology*, 88, (7) 659-667

Beatrice, Belardini, Bertoli, Lisbona & Sebastiano 2002. Diesel Combustion Control in Common Rail Engines by New Injection Strategies. *Int J Engine Research*, 3, 23-36

Beatrice, Capaldi, Del Giacomo, Guido, & Lazzaro The Effect of Clean and Cold EGR on the Improvement of Low Temperature Combustion Performance in a Single Cylinder Research Diesel Engine, *In 31st Meeting on Combustion*.

BEATRICE, RTOLI, & IACOMO, 1997. New Findings on Combustion Behavior of Oxygenated Synthetic Diesel Fuels. *Combustion Science and Technology*, 137, (1-6)

Benajes, Molina, García, & Novella, 2004. Influence of Boost Pressure and Injection Pressure on Combustion Process and Exhaust Emissions in a HD Diesel Engine. *SAE Technical Paper 2004-01-1842*

Benajes, Molina, Novella & DeRudder 2007. Influence of injection conditions and exhaust gas recirculation in a high-speed direct-injection diesel engine operating with a late split injection. *Proceedings of the Institution of Mechanical Engineers*, 222, 629-641

Bhusnoor, Babu, & Subrahmanyam. 2007. Studies on Performance and Exhaust Emissions of a CI Engine Operating on Diesel and Diesel Biodiesel Blends at Different Injection Pressures and Injection Timings. *SAE Technical Paper 2007-01-0613*

Bielaczyc & Merkisz 1998. Cold Start Emissions Investigation at Different Ambient Temperature Conditions. *SAE paper*, 980401,Accessed 1998.

Biodiesel 2020: A Global Market Survey, 2nd Edition, 2nd ed. Houston, TX, Emerging Markets Online, 2008.

Black & High. 1979. Methodology for Determining Particulate and Gaseous Diesel Hydrocarbon Emissions. *SAE Technical Paper 790422*

Blackwood, 1998. The Effect of an Oxidation Catalyst on Cold Start Diesel Emissions in the First 120 Seconds of Running., 980193,

Bowman. 1975. Kinetics of Pollutant Formation and Destruction in Combustion. *Prog.Energy Combst.Sci.*, 1, 33-45

BP. Changing diesel low temperature properties by using additives. http://www.bp.com/content/dam/bp-country/en_au/products-services/service-stations/downloads/Changing-Diesel-Fuel-Properties-Using-Additives.pdf . 2002. Ref Type: Electronic Citation

Brown, 2007. Investigations of fuel injection strategy for cold starting direct-injection diesel engines.

Buchholz, Mueller, Upatnieks & Martin. 2004. Using carbon-14 isotope tracing to investigate molecular structure effects of the oxygenate dibutyl maleate on soot emissions from a DI diesel engine. *SAE paper 2004-01-1849*

Buchwald, Brauer, Blechstein, & Sommer. 2004. Adaption of Injection System Parameters to Homogeneous Diesel Combustion. *SAE Technical Paper 2004-01-0936*

Canar, Tolga, Murat, & Can. 2004. Effects of injection pressure and intake CO2 concentration on performance and emission parameters of an IDI turbocharged diesel engine. *Applied Thermal Engineering*, 25, (11-12) 1854-1862

Can, Çelikten, & Usta 2004. Effects of ethanol addition on performance and emissions of a turbocharged indirect injection Diesel engine running at different injection pressures. *Energy Conversion and Management*, 45, (15-16) 2429-2440

Canakci 2005. Performance and emissions characteristics of biodiesel from soybean oil. *Proceedings of the Institution of Mechanical Engineers, Part D: Journal of Automobile Engineering*, 219, 915-922

Cardone, Prati, Rocco, Seggiani, Senatore & Vitoloi. 2002. Brassica Carinata as an alternative oil crop for the production of biodiesel in Italy: engine performance and regulated and unregulated exhaust emissions. *Environ Sci Technol.*, 36, (21) 4656-4662

Cetinkaya, Ulusoy, Tek¨¬n, & Karaosmano?lu 2005. Engine and winter road test performances of used cooking oil originated biodiesel. *Energy Conversion and Management*, 46, (7-8) 1279-1291

Chang & Van Gerpen 1998. Determination of particulate and unburned hydrocarbon emissions from diesel engines fueled with biodiesel. *SAE paper*, 982527,

Chang & Van Gerpen. 1997. Fuel properties and engine performance for biodiesel prepared from modified feedstocks. *SAE paper*, 971684,

Chapman & Boehman. Emissions characteristics of a light duty diesel engine fuelled with a hydrogenated biodiesel fuel, *In The 231st national meeting of the American Chemical Society*.

Chapman, Hile, Pague, Song, & Boehman 2003. Eliminating the NOx emissions increase associated with biodiesel. *Prepr.Pap.-Am.Chem.Soc., Div.Fuel Chem.*, 48, (2) 639-640

Chevron. Diesel Fuels Technical Review. https://www.chevronwithtechron.com/products/documents/Diesel_Fuel_Tech_Review.pdf . 2012. Ref Type: Electronic Citation

Choi & Bower. 1997. Effects of biodiesel blended fuels and multiple injections on D.I. diesel engines. *SAE paper*, 970218,

Choi & Reitz 1999. A Numerical Analysis of the Emissions Characteristics of Biodiesel Blended Fuels. *J.Eng.Gas Turbines Power*, 121, (1) 31-37

Chueng, Upatnieks, & Mueller 2005. Investigation of the impact of biodiesel fuelling on NOx emissions using an optical direct injection diesel engine. *International Journal of Engine Research*, 7, 297-318

Chuepeng, Tsolakis, Theinnoi & Xu. 2007. A Study of Quantitative Impact on Emissions of High Proportion RME-Based Biodiesel Blends. *SAE Technical Paper 2007-01-0072*

Chuepeng, Xu, solakis, Wyszynski & Philip 2011. Particulate Matter size distribution in the exhaust gas of a modern diesel Engine fuelled with a biodiesel blend. *Biomass and Bioenergy*, 35, (10) 4280-4289

Clerc 1986. Cetane Number Requirements of Light-Duty Diesel Engines at Low Temperatures. *SAE paper*, 1986-10-01,

Dec 1997. A Conceptual model of DI diesel combustion based on laser-sheet imaging. *SAE paper*, 970873,

Dennis, Garner & Taylor. 1999. The Effect of EGR on Diesel Engine Wear. *SAE Technical Paper 1999-01-0839*

Desantes, Arr¨¨gle, Molina & Lejeune. 2000. Influence of the EGR Rate, Oxygen Concentration and Equivalent Fuel/Air Ratio on the Combustion Behaviour and Pollutant Emissions of a Heavy-Duty Diesel Engine. *SAE Technical Paper 2000-01-1813*

Dhananjaya, Mohanan & Sudhir. 2008. EFFECT OF INJECTION PRESSURE AND INJECTION TIMING ON A SEMI-ADIABATIC CI ENGINE FUELED WITH BLENDS OF JATROPHA OIL METHYL ESTERS. *SAE Technical Paper 2008-28-0070*

Dober, Tullis, Greeves & Milovanovic. 2008. The Impact of Injection Strategies on Emissions Reduction and Power Output of Future Diesel Engines. *SAE Technical Paper 2008-01-0941*

Durán, Monteagudo, Armas, & Hernández. 2006. Scrubbing effect on diesel particulate matter from transesterified waste oils blends. *Fuel*, 85, (7-8) 923-928

Durbin & Norbeck. 2002. Effects of biodiesel blends and arco EC-diesel on emissions from light heavy-duty diesel vehicles. *Environ Sci Technol*, 36, (8) 1686-1691

Durbin, Collins, Norbeck, & Smith 2000. Effects of biodiesel, biodiesel blends, and a synthetic diesel on emissions from light heavy-duty diesel vehicles. *Environ Sci Technol*, 34, (3) 349-355

Eastwood. 2008. *Particulate Emissions from Vehicles* John Wiley & Sons Ltd.

Frijters & Baert, 2004 Oxygenated fuels for clean heavy-duty engines. In: Proceedings of VAFSEP2004.

Geller, Sardar, Phuleria, Fine, & Sioutas 2005. Measurements of Particle Number and Mass Concentrations and Size Distributions in a Tunnel Environment. *Environ.Sci.Technol.*, 39, (22) 8653-8663

Graboski & McCormick. 1998. Combustion of fat and vegetable oil derived fuels in diesel engines. *Progress in Energy and Combustion Science*, 24, 125-164

Graboski, McCormick, Alleman, & Herring 2003, *The effect of biodiesel composition on engine emissions from a DDC series 60 diesel engine*, National Renewable Energy Laboratory, NREL/SR-510-31461.
Graboski, Ross & McCormick 1996. Transient emissions from no. 2 diesel and biodiesel blends in a DDC series 60 engine. *SAE paper*, 961166,
Gumus 2009. Reducing cold-start emission from internal combustion engines by means of thermal energy storage system. *Applied Thermal Engineering*, 29, (4) 652-660
Haas, Scott, Alleman, & McCormick 2001. Engine performance of biodiesel fuel prepared from soybean soapstock: a high quality renewable fuel produced from a waste feedstock. *Energy Fuels*, 15, (5) 1207-1212
Hamasaki, Kinoshita, Tajima, Takasaki & Morita. Combustion characteristics of diesel engines with waste vegetable oil methyl ester.
Han, Henein, & Bryzik 2000. A New Ignition Delay Formulation Applied to Predict Misfiring During Cold Starting of Diesel Engines. *SAE paper*, 2000-01-1184,
Han, Henein, Nitu, & Bryzik 2001. Diesel Engine Cold Start Combustion Instability and Control Strategy. *SAE paper*, 2001-01-1237,
Hansen & Jensen. 1997. Chemical and biological characteristics of exhaust emissions from a DI diesel engine fuelled with rapeseed oil methyl ester (RME). *SAE paper*, 971689,
Hara, Itoh, Henein & Bryzik 1999. Effect of Cetane Number with and without Additive on Cold Startability and White Smoke Emissions in a Diesel Engine. *SAE paper*, 1999-01-1476,
Henein, Zahdeh, Yassine, & Bryzik 1992. Diesel Engine Cold Starting: Combustion Instability. *SAE paper*, 920005,
Henein. 1992. Diesel Engine Cold Starting: Combustion Instability., 920005,
Hengqing Liu, N.A.Henein, & Walter Bryzik 2003. Simulation of Diesel Engines Cold-Start. *SAE paper*, 2003-03-03,
Hess, Haas, Foglia, & Marmer 2005. Effect of antioxidant addition on NOx emissions from biodiesel. *Energy Fuels*, 19, (4) 1749-1754
Heywood. 1998. *Internal Combustion Engine Fundamentals* McGraw-Hill Book Co.
Hoekman, Broch, Robbins, Ceniceros, & Natarajan 2012. Review of biodiesel composition, properties, and specifications. *Renewable and Sustainable Energy Reviews*, 16, (1) 143-169
Horibe & Ishiyama. 2009. Relations among NOx, Pressure Rise Rate, HC and CO in LTC Operation of a Diesel Engine. *SAE Technical Paper 2009-01-1443*
Horibe, Harada, Ishiyama & Shioji 2009. Improvement of premixed charge compression ignition-based combustion by two-stage injection. *International Journal of Engine Research*, 10, (2) 71-80
Horn, Egnell, Johansson & Andersson. 2007. Detailed Heat Release Analyses with Regard to Combustion of RME and Oxygenated Fuels in an HSDI Diesel Engine. *SAE Technical Paper 2007-01-0627*
Ishiki, Oshida, Takiguchi & Urabe. 2000. A Study of Abnormal Wear in Power Cylinder of Diesel Engine with EGR - Wear Mechanism of Soot Contaminated in Lubricating Oil. *SAE Technical Paper 2000-01-0925*
Jacobs, Assanis, & Filipi. 2003. The Impact of Exhaust Gas Recirculation on Performance and Emissions of a Heavy-Duty Diesel Engine. *SAE Technical Paper 2003-01-1068*
Jean-Marc & Joumard 2005, *MODELLING OF COLD START EXCESS EMISSIONS FOR PASSENGER CARS*, INRETS, LTE 0509.

Jung, Kittelson, & Zachariah. 2006. Characteristics of SME Biodiesel-Fueled Diesel Particle Emissions and the Kinetics of Oxidation. *Environ Sci Technol.*, 40, (16) 4949-4955

Kado & Kuzmicky 2003, *Bioassay Analyses of Particulate Matter From a Diesel Bus Engine Using Various Biodiesel Feedstock Fuels*, National Renewable Energy Laboratory, NREL/SR-510-31463.

Kado, Okamoto, & Kuzmicky. 1996, *Chemical and bioassay analyses of diesel and biodiesel particulate matter: pilot study*, The Montana State Department of Environmental Quality and U.S. Department of Energy.

Kalam & Masjuki. 2005. Emissions and deposits characteristics of a small diesel engine when operated on preheated crude palm oil. *SAE paper*, 1999-01-3564,

Kaplan, Arslan, & Surmen 2006. Performance Characteristics of Sunflower Methyl Esters as Biodiesel. *Energy Sources, Part A: Recovery, Utilization, and Environmental Effects*, 28, (8) 751-755

Kawano, Ishii, Goto & Noda. 2007. Effect of Exhaust Gas Recirculation on Exhaust Emissions from Diesel Engines Fuelled with Biodiesel. *SAE Technical Paper 2007-24-0128*

Kheira & Atta 2009 Response of Jatropha curcas L. to water deficits: Yield, water use efficiency and oilseed characteristics. *Biomass and Bioenergy*, 33, (10) 1343-1350

Kimura, Aoki, Kitahara, & Aiyoshizawa. 2001. Ultra-Clean Combustion Technology Combining a Low-Temperature and Premixed Combustion Concept for Meeting Future Emission Standards. *SAE Technical Paper 2001-01-0200*

Kitamura, Ito, Senda & Fujimoto. 2001. Extraction of the suppression effects of oxygenated fuels on soot formation using a detailed chemical kinetic model. *JSAE Review*, 22, (2) 139-145

Kitanon, Sakata & Clark. 2006. Effects of Fuel Properties to the Cold Starting Performance of a Low-Compression-Ratio DI Diesel Engine. *SAE paper*, **2006-01-165**,

Knothe, Sharp, & Thomas W.Ryan 2005. Exhaust emissions of biodiesel, petrodiesel, neat methyl esters, and alkanes in a new technology engine. *Energy & Fuels*, 20, (1) 403-408

Kook, Bae, Miles & Choi. 2005. The Influence of Charge Dilution and Injection Timing on Low-Temperature Diesel Combustion and EmissionsKook, S. *SAE Technical Paper 2005-01-3837*

Kook, Bae, Miles & Choi. 2006. The Effect of Swirl Ratio and Fuel Injection Parameters on CO Emission and Fuel Conversion Efficiency for High-Dilution, Low-Temperature Combustion in an Automotive Diesel Engine. *SAE Technical Paper 2006-01-0197*

Krahl, Munack, Bahadir, Schumacher, & Elser 1996. Review: utilization of rapeseed oil, rapeseed oil methyl ester or diesel fuel: exhaust gas emissions and estimation of environmental effects. *SAE paper*, 962096,

Krahl, Munack, Schröder, & Stein. 2003. Influence of biodiesel and different designed diesel fuels on the exhaust gas emissions and health effects. *SAE paper*, 2003-01-3199,

Krahl, Munack, Schröder, Stein & Bünger. Comparison of biodiesel with different diesel fuels regarding exhaust gas emissions and health effects. 2004. Ref Type: Online Source

Krahl, Munack, Schroder, Stein, Herbst, Kaufmann & Bunger. 2005. Fuel design as constructional element with the example of biogenic and fossil diesel fuels. *Agricultural Engineering International: the CIGR Ejournal.Vol.VII.Manuscript EE 04 008.*

Labeckas & Slavinskas 2006. The effect of rapeseed oil methyl ester on direct injection diesel engine performance and exhaust emissions. *Energy Conversion and Management*, 47, (13-14) 1954-1967

Ladommatos, Abdelhalim, Zhao & Hu. 1998. The effects of carbon dioxide in exhaust gas recirculation on diesel engine emissions. *Proceedings of the Institution of Mechanical Engineers*, 212, (25) 42

Lapuerta & Agudelo 2008. Diesel particulate emissions from used cooking oil biodiesel. *Bioresource Technology*, 99, (4) 731-740

Lapuerta, Armas, & Ballesteros 2002. Diesel particulate emissions from biofuels derived from Spanish vegetable oils. *SAE paper*, 2002-01-1657,

Lapuerta, Armas, Ballesteros, & Fern¨¢ndez 2005. Diesel emissions from biofuels derived from Spanish potential vegetable oils. *Fuel*, 84, (6) 773-780

Last, Houben, Rottner, Stotz, & Ludwigsburg 2008, *Influence of modern diesel cold start systems on the cold start, warm-up and emissions of diesel engines*.

Last, Michael & Manfred. 1995. Emissions and performance characteristics of a 4-stroke, direct injected diesel engine fueled with blends of biodiesel and low sulfur diesel fuel. *SAE paper*, 950054,

Lavoie, Heywood & Keck. 1970. Experimental and Theoretical Investigation of Nitric Oxide Formation in Internal Combustion Engines. *Combust.Sci.Technol.*, 1, 313-326

Lea-Langton, Li & Andrews. 2009. Investigation of Aldehyde and VOC Emissions during Cold Start and Hot Engine Operations using 100% Biofuels for a DI Engine. *SAE Technical Paper 2009-01-1515*

Lea-Langton, Ross, Bartle, Andrews, Jones, Li, Pourkashanian & Williams. 2012. Low temperature PAH formation in diesel combustion. *Journal of Analytical and Applied Pyrolysis*, 103, 119-125

Leung, Luo, & Chan 2006. Optimization of exhaust emissions of a diesel engine fuelled with biodiesel. *Energy Fuels*, 20, (3) 1015-1023

Li, Csontos, Gable & Passut. 2002. Wear in Cummins M-11/EGR Test Engines. *SAE Technical Paper 2002-01-1672*

Lidstone, Harris, Gu & Ball 2007. An Experimental Study of NOx Emissions for the Development of an Emission Analysis Tool. *SAE Technical Paper 2007-01-0065*

Lin & Shiou-An Lin 2007. Effects of emulsification variables on fuel properties of two-three-phase biodiesel emulsions. *Fuel*, 86, (1-2) 210-217

Lin, Lee, Wu, & Wang 2006. Comparison of PAH and regulated harmful matter emissions from biodiesel blends and paraffinic fuel blends on engine accumulated mileage test. *Fuel*, 85, (17-18) 2516-2523

Mann. 1999. Fuel Effects on The Low Temperature Performance of Two Generations of Mercedes-Benz Heavy-Duty Diesel Engines., 1999-01-3594,

Marinov. 1997. Aromatic and polycyclic aromatic hydrocarbon formation in a premixed propane flame. *Combust.Sci.Technol.*, 128, 295-342

Marques, Monteiro, Moreira & Malheiro. 2007. NOx Emissions Reduction in a Biodiesel Engine by Means of EGR Technology. *SAE Technical Paper 2007-01-0078*

Marshall, Schumacher, & Howell, 1995 Engine exhaust emissions evaluation of a cummins L10E when fuelled with a biodiesel blend, *In SAE Technical Paper 952363*, SAE International.

McCormick, Alvarez, & Graboski 2003, *NOx solutions for biodiesel*, National Renewable Energy Laboratory, NREL/SR-510-31465.

Merryman & Levy. Nitrogen Oxide Formation in Flames: The Roles of NO2 and fuel nitrogen, the Combustion Institute.

Mitchell. 1993. The Cold Performance of Diesel Engines. *SAE paper*, 932768,

Mohr &Urlaub 1994. Improvement of the Cold Start Qualities of Diesel Engines with Swirl Chambers. *SAE paper*, 940075,

Moldanová, Fridell, Popovicheva, Demirdjian, Tishkova, Faccinetto & Focsa 2009. Characterisation of particulate matter and gaseous emissions from a large ship diesel engine. *Atmospheric Environment*, 43, (16) 2632-2641

Monyem & Van Gerpen 2001. The effect of biodiesel oxidation on engine performance and emissions. *Biomass and Bioenergy*, 20, (4) 317-325

Mueller, Pitz, Pickett, Martin, Siebers & Westbrook. 2003. Effects of oxygenates on soot processes in DI diesel engines: experiments and numerical simulations. *SAE paper*, 2003-01-1791,

Munack, Schröder, Krahl, & Bünger 2001. Comparison of relevant gas emissions from biodiesel and fossil diesel fuel. *Agricultural Engineering International: the CIGR Journal of Scientific Research and Development.Manuscript EE 01 001.Vol.III*

Murillo, M¨ªguez, Porteiro, Granada, & Mor¨¢n 2007. Performance and exhaust emissions in the use of biodiesel in outboard diesel engines. *Fuel*, 86, (12-13) 1765-1771

Myung-whan, Jung-ho, & Kazuo. 2000. The Characteristics of Wear in Diesel Engines with Scrubber EGR System. *SAE Technical Paper 2000-06-12*

Nabi, Akhter, &l Shahadat 2006. Improvement of engine emissions with conventional diesel fuel and diesel-biodiesel blends. *Bioresource Technology*, 97, (3) 372-378

Nabi, Shahadat, Rahman, & Beg 2004. Behavior of diesel combustion and exhaust emission with neat diesel fuel and diesel-biodiesel blends. *SAE paper*, 2004-01-3034,

Nikolic & Iida. 2007. Effects of intake CO2 concentrations on fuel spray flame temperatures and soot formations. *Proceedings of the Institution of Mechanical Engineers*, 221, (12) 1567-1573

Norinaga, Deutschmann, Saegusa, & Hayashi. 2009. Analysis of pyrolysis products from light hydrocarbons and kinetic modeling for growth of polycyclic aromatic hydrocarbons with detailed chemistry. *Journal of Analytical and Applied Pyrolysis*, 86, (1) 148-160

Opat, Ra, Gonzalez & Krieger. 2007. Investigation of Mixing and Temperature Effects on HC/CO Emissions for Highly Dilute Low Temperature Combustion in a Light Duty Diesel Engine. *SAE Technical Paper 2007-01-0193*

Owen, Coley, & Weaver 1995. *Automotive fuels reference book*, 2 ed. Society of Automotive Engineers.

Peng, Cui, Shi, & Deng 2008. Effects of exhaust gas recirculation (EGR) on combustion and emissions during cold start of direct injection (DI) diesel engine. *Energy*, 33, (3) 471-479

Pereyra-Irujo, Izquierdo, Covi, Nolasco, Quiroz, & Luis.Aguirrez¨¢bal 2009. variability in sunflower oil quality for biodiesel production: a simulation study. *Biomass and Bioenergy*, 33, (3) 459-468

Peterson & Reece 1996. Emissions testing with blends of esters of rapeseed oil fuel with and without a catalytic converter. *SAE paper*, 961114,

Peterson, Taberski, Thompson, & Chase 2002. The effect of biodiesel feedstock on regulated emissions in chassis dynamometer tests of a pickup truck. *Transactions of the ASABE.*, 43, (6) 1371-1381

Pflaum, Hofmann, Geringer, & Weissel. 2010. Potential of Hydrogenated Vegetable Oil (HVO) in a Modern Diesel Engine. *SAE Technical Paper 2010-32-0081*

Pierson & Brachaczek 1982. Particulate Matter Associated with Vehicles on the Road. II. *Aerosol Science and Technology*, 2, (1)

Pinto, Guarieiro, Rezende, Ribeiro, Torres, & Lopes et al 2005. Biodiesel: an overview. *Journal of the Brazilian Chemical Society*, 16, (6B) 1313-1330

Rakopoulos, Rakopoulos, Hountalas, Giakoumis, & Andritsakis 2007. Performance and emissions of bus engine using blends of diesel fuel with bio-diesel of sunflower or cottonseed oils derived from Greek feedstocks. *Fuel*, 87, (2) 147-157

Ramadhas 2011. *Alternative fuels for transportation* CPC press.

Ramadhas, Muraleedharan, & Jayara 2005. Performance and emission evaluation of a diesel engine fueled with methyl esters of rubber seed oil. *Renewable Energy*, 30, (12) 1789-1800. Ref Type: Electronic Citation

Randall von Wedel. Technical Handbook for Marine Biodiesel In Recreational Boats. http://www.cytoculture.com/Biodiesel%20Handbook.htm . 1999. Ref Type: Online Source

Robbins, Hoekman, Gertler, & Broch 2009, *Investigation of biodistillates as potential blendstocks for transportation fuels* CRC AVFL-17. Final Report.

Schauer, Kleeman, Cass, & Simoneit 1999. Measurement of Emissions from Air Pollution Sources. 2. C1 through C30 Organic Compounds from Medium Duty Diesel Trucks. *Environ.Sci.Technol.*, 33, (10) 1578-1587

Schmidt & Van Gerpen 1996. The effect of biodiesel fuel composition on diesel combustion and emissions. *SAE paper*, 961086,

Scholl & Sonrenson 1993. Combustion of soybean oil methyl ester in a direct injection diesel engine. *SAE paper*, 930934,

Schumacher, Borgelt, Hires, Fosseen & Goetz. 1994 Fueling diesel engines with blends of methyl ester soybean oil and diesel fuel. http://web.missouri.edu/~schumacherl/ASAED94.htm . 1994. 6-4-2014. Ref Type: Electronic Citation

Senatore, Cardone, Rocco & Prati 2000. A Comparative Analysis of Combustion Process in D.I. Diesel Engine Fueled with Biodiesel and Diesel Fuel. *SAE paper*, 2000-01-0691,

Shaheed & Swain 1999. Combustion analysis of coconut oil and its methyl esters in a diesel engine. *Proceedings of the Institution of Mechanical Engineers Part A Journal of Power and Energy*, 213, (5) 417-425

Sharp 1994, *Transient emissions testing of biodiesel and other additives in a DDC Series 60 engine*, Southwest Research Institute Report for National Biodiesel Board.

Sharp, Howell, & Jobe 2000. The effect of biodiesel fuels on transient emissions from modern diesel engines, part II: unregulated emissions and chemical characterization. *SAE paper*, 2000-01-1968,

Shi, Mark, & Harrison 2000. Characterization of Particles from a Current Technology Heavy-Duty Diesel Engine. *Environ.Sci.Technol.*, 34, (5) 748-755

Shi, Yu, He, Shuai, Wang, & Li 2005. Emission characteristics using methyl soyate-ethanol-diesel fuel blends on a diesel engine. *Fuel*, 84, (12-13) 1543-1549

Silva, Prata, & Teixeira 2003. Technical feasibility assessment of oleic sunflower methyl ester utilization in diesel bus engines. *Energy Conversion and Management*, 44, (18) 2857-2878

Soloiu, Duggan, Ochieng, Williams, Molina, & Vlcek 2013. Investigation of Low Temperature Combustion Regimes of Biodiesel With N-Butanol Injected in the Intake Manifold of a Compression Ignition Engine. *Journal of Energy Resources Technology*, 135, (4)

Song, Alam, Boehman, & Kim 2006. Examination of the oxidation behavior of biodiesel soot. *Combustion and Flame*, 146, (4) 589-604

Staat & Gateau 1995. The effects of rapeseed oil methyl ester on diesel engine performance, exhaust emissions and long term behaviour—a summary of three years of experimentation. *SAE paper*, 950053,

Starck. 2010. Cold Start on Diesel Engines: Effect of Fuel characteristics., 2010-01-1506,

Storey, Lewis, West, Huff, Slucer, & Wagner. 2005, *Hydrocarbon species in the exhaust of diesel engines equipped with advanced emissions control devices* AVFL-10b-2.

Sutton 1986. Investigation into Diesel Operation with Changing Fuel Property. *SAE paper*, 1986-02-01,

Szybist, Boehman, Taylor, & McCormick 2005a. Evaluation of formulation strategies to eliminate the biodiesel NOx effect. *Fuel Processing Technology*, 86, (10) 1109-1126

Szybist, Kirby, & Boehman 2005b. NOx Emissions of alternative diesel fuels: a comparative analysis of biodiesel and FT diesel. *Energy Fuels*, 19, (4) 1484-1492

Tanaka, Ando, & Ishizaka 2002. Study on pilot injection of DI diesel engine using common-rail injection system. *JSAE Review*, 23, (3) 297-302

Tat &Van Gerpen 2003, *Measurement of biodiesel speed of sound and its impact on injection timing*, National Renewable Energy Laboratory, NREL/SR-510-31462.

Tat 2003. *Investigation of oxides of nitrogen emissions from biodiesel-fueled engines.* Iowa State University.

Tritthart & Zelenka 1990. Vegetable oils and alcohols: additive fuels for diesel engines. *SAE paper*, 905112,

Tsolakis 2006. Effects on particle size distribution from the diesel engine operating on RME-biodiesel with EGR. *Energy Fuels*, 20, (4) 1418-1424

Turrio-Baldassarri, Battistelli, Conti, Crebelli, Berardis, Iamiceli & Gambino. 2004. Emission comparison of urban bus engine fuelled with diesel oil and biodiesel blend. *Science of The Total Environment*, 327, (1-3) 147-162

Twigg 2009. Cleaning the Air We Breathe – Controlling Diesel Particulate Emissions from Passenger Cars. *Platinum Metals Rev.*, 53, (1) 27-34

Ueki & Miura 1999. Effect of difference of high pressure fuel injection systems on exhaust emissions from HDDI diesel engine. *JSAE Review*, 20, (4) 555-557

Ullman, Spreen, & Mason 1994. Effects of cetane number, cetane improver, aromatics, and oxygenates on 1994 heavy-duty diesel engine emissions. *SAE paper*, 941020,

UNECE 2009, *Guidelines for handling and blending FAME*, CONCAWE Fuels Quality and Emissions Management Group, 9/09.

Wagner, Green, Dam, & Edwards. 2003. Simultaneous Low Engine-Out NOx and Particulate Matter with Highly Diluted Diesel Combustion. *SAE Technical Paper 2003-01-0262*

Wang, Lyons, Clark, & Gautam 2000. Emissions from nine heavy trucks fuelled by diesel and biodiesel blend without engine modificationEmissions from nine heavy trucks fuelled by diesel and biodiesel blend without engine modification. *Environ.Sci.Technol.*, 34, (6) 933-939

Westerholm & Li. 1994. A multivariate statistical analysis of fuel-related polycyclic aromatic hydrocarbon emissions from heavy-duty diesel vehiclesWesterholm. *Environ.Sci.Technol.*, 28, (5) 965-972

Wong & Steere 1982. The effect of diesel fuel properties and engine operating conditions on ignition delay. *SAE paper*, 1982-02-01,

Yamane, Ueta & Shimamoto 2001. Influence of physical and chemical properties of biodiesel fuels on injection, combustion and exhaust emission characteristics in a direct injection compression ignition engine. *International Journal of Engine Research*, 2, (4) 249-261

Yuan, Hansen, Tat, Van Gerpen, & Tan 2005. Spray, ignition and combustion modeling of biodiesel fuels for investigating NOx emissions. *American Society of Agricultural Engineers*, 48, (3) 933-939

Zhang, Rezaei, Xu, & Shuai 2014. Experimental Investigation of Different Blends of Diesel and Gasoline (Dieseline) in a CI Engine. *SAE Technical Paper 2014-01-2686*

Zhang. 1999. A Study of Pilot Injection in a DI Diesel Engine. *SAE Technical Paper 1999-01-3493*

Zielinska, Sagebiel, Arnott, Rogers, Kelly, Wagner, Lighty, Sarofim, & Palmer 2004. Phase and Size Distribution of Polycyclic Aromatic Hydrocarbons in Diesel and Gasoline Vehicle Emissions. *Environmental Science & Technology*, 38, (9) 2557-2567